

CRANFIELD UNIVERSITY

Rebecca L. Whetton

Multi-sensor and data fusion approach for determining yield limiting factors and for *in-situ* measurement of yellow rust and fusarium head blight in cereals

School of Energy Environment and Agrifood

This thesis is submitted in partial fulfilment of the requirements for the degree of Doctor of Philosophy

PhD

23rd December 2016

Supervisor: Prof. Abdul Mounem Mouazen

Co-Supervisor: Dr Toby Waine



CRANFIELD UNIVERSITY

School of Energy Environment and Agrifood

PhD

Academic Year 2013 - 2016

Rebecca L. Whetton

Multi-sensor and data fusion approach for determining yield limiting factors and for *in-situ* measurement of yellow rust and fusarium head blight in cereals

Supervisor: Prof. Abdul Mounem Mouazen

Co-Supervisor: Dr Toby Waine

This thesis is submitted in partial fulfilment of the requirements for the degree of Doctor of Philosophy

© Cranfield University 2016. All rights reserved. No part of this publication may be reproduced without the written permission of the copyright owner.



"If we do not change our direction, we are likely to end up where we are headed."



## **ABSTRACT**

The world's population is increasing and along with it, the demand for food. A novel parametric model (Volterra Non-linear Regressive with eXogenous inputs (VNRX)) is introduced for quantifying influences of individual and multiple soil properties on crop yield and normalised difference vegetation Index. The performance was compared to a random forest method over two consecutive years, with the best results of 55.6% and 52%, respectively. The VNRX was then implemented using high sampling resolution soil data collected with an on-line visible and near infrared (vis-NIR) spectroscopy sensor predicting yield variation of 23.21%.

A hyperspectral imager coupled with partial least squares regression was successfully applied in the detection of fusarium head blight and yellow rust infection in winter wheat and barley canopies, under laboratory and on-line measurement conditions. Maps of the two diseases were developed for four fields. Spectral indices of the standard deviation between 500 to 650 nm, and the squared difference between 650 and 700 nm, were found to be useful in differentiating between the two diseases, in the two crops, under variable water stress. The optimisation of the hyperspectral imager for field measurement was based on signal-to-noise ratio, and considered; camera angle and distance, integration time, and light source angle and distance from the crop canopy.

The study summarises in the proposal of a new method of disease management through suggested selective harvest and fungicide applications, for winter wheat and barley which theoretically reduced fungicide rate by an average of 24% and offers a combined saving of the two methods of £83 per hectare.

## **Keywords**

Yellow rust, Fusarium head blight, PLSR regressions, yield limiting factors, on-line, precision agriculture.



## **ACKNOWLEDGEMENTS**

I would like to acknowledge the Farm FUSE project from the ICT-AGRI under the European Commission's ERA-NET scheme under the 7th Framework Programme, and the UK Department of Environment, Food and Rural Affairs (contract no: IF0208), for providing funding which made this PhD possible.

To my supervisors, Abdul Mouazen and Toby Waine, firstly thank you for giving me the opportunity to undertake this PhD research. Abdul your guidance, and expertise in the area has been invaluable, and your patience and drive with the project has been greatly appreciated. Toby I'm very grateful for your guidance, suggestions and constructive comments on the project. Without the knowledge and direction from both of my supervisors, this project and the papers would not have been possible. Furthermore, for having made the last three years (...3 months... and 3 weeks) at Cranfield thoroughly rewarding and enjoyable. Involving me with other projects, collaborations, and your support for attending conferences, has been of great use in the thesis, and I'm sure will continue to be highly valuable, and for that I can't express my gratitude enough. I'd also like to acknowledge and thank Kim Blackburn for his guidance. To both Yifan and Said, it's been a great pleasure to work with you on the papers, and your insights and persistence towards publishing have been greatly encouraging. To Dimitrios' team at Aristotle University and Boyan at Cranfield thank you, you really helped me get started with the project. I would also like to say a big thank you to my examiners Jon and Paul. Your knowledge in the area, and detailed attention to improving the thesis has been greatly appreciated. To you all, I'm much obliged.

To my thesis committee, including my subject advisor, Naresh Magan and independent chairman, Ahmed Al-Ashaab, the guidance and constructive comments that you provided throughout the course of this PhD were invaluable. Furthermore, to all the Cranfield staff, both in the lab and in the office, who have helped me in my PhD studies, many thanks to you all. I'd like to say a particular thankyou to Bob Walker without whom I don't think this project would ever have gotten to the field, and to Mr Maskell for giving me access to "play" with the sensors in those fields.

Matt and Olly thank you for all your time and patience with the various software and coding. And thankyou to Scott for always being a reference of BASIS knowledge. To all my fellow students and friends at Cranfield, past and present, thanks for all of the distractions, coffee breaks, great times and support. To all of my other friends, despite asking "aren't you done yet?" you have been there all the way. You have helped to balance out my life, reminding me there is more to life than work, and many of you have gone out of your ways to ensure I have eaten and slept (when I had often forgotten to).

I would like to say a big thankyou to my parents and family who throughout my PhD, (and despite thinking I play with soil all day) have always given me their utmost support (emotional, financial, and in cake).

And thank you to you, the reader, even if you stop here.

# TABLE OF CONTENTS

ABSTRACT.....	vii
ACKNOWLEDGEMENTS.....	ix
TABLE OF CONTENTS.....	xi
LIST OF FIGURES .....	xv
LIST OF TABLES.....	xx
LIST OF ABBREVIATIONS.....	xxiv
1 Introduction.....	1
1.1 Background and Context.....	1
1.2 Research objectives.....	8
Hypothesis .....	8
Aim .....	8
Objectives .....	9
1.3 Thesis structure .....	10
1.4 Disclosure .....	11
2 Literature review.....	14
2.1 Fungal diseases .....	14
2.1.1 Yellow rust.....	14
2.1.2 Fusarium head blight .....	15
2.1.3 Fungal disease resistance .....	19
2.1.4 Disease distribution and spread .....	20
2.1.5 Current approach in fungal disease control .....	26
2.1.6 Timings of fungicide applications .....	26
2.2 Techniques for disease detection .....	27
2.2.1 Review of optical imaging techniques of crop canopies .....	30
2.2.2 Application of visible and infrared spectroscopy in disease detection.....	32
2.2.3 Application of fluorescence spectroscopy in disease detection.....	34
2.2.4 Alternative spectral methods .....	36
2.2.5 Hyperspectral and multispectral imaging .....	36
2.2.6 Optical imaging summary.....	39
2.3 Variability and yield limiting factors.....	42
2.4 On-line measurement of soil properties.....	43
2.5 Literature conclusions; research gaps .....	44
3 Quantification of yield limiting factors.....	46
3.1 A new non-linear parametric modelling method to quantify influence of soil properties on crop yields: Methodology .....	47
Abstract.....	47
3.1.1 Introduction.....	48
3.1.2 Material and methods.....	50
3.1.3 Results and discussion .....	58

3.2 A new non-linear parametric modelling method to quantify influence of soil properties on crop yields: Application to on-line soil data .....	74
Abstract .....	74
3.2.1 Introduction.....	75
3.2.2 Materials and Methods.....	78
3.2.3 Results and discussion .....	85
3.3 Summary conclusions .....	103
4 Optimising the configuration of a hyperspectral imager for on-line measurement of wheat canopies .....	105
Abstract .....	105
4.1 Introduction.....	106
4.2 Materials and methods .....	109
4.2.1 Hyperspectral configuration in the laboratory .....	109
4.2.2 On-line soil and crop measurements in the field .....	113
4.2.3 Data analyses .....	116
4.2.4 Mapping .....	121
4.3 Results and Discussion .....	121
4.3.1 Spectral quality in the laboratory.....	121
4.3.2 Hyperspectral image configuration parameters; laboratory.....	123
4.3.3 Hyperspectral imager; on-line measurement .....	129
4.4 Influence of soil properties on signal-to-noise ratio during the on-line measurement .....	131
4.5 Conclusions.....	134
5 Hyperspectral measurements of yellow rust and fusarium head blight in cereal crops:	
Part 1: Laboratory study.....	136
Abstract.....	136
5.1 Introduction.....	137
5.2 Materials and methods .....	140
5.2.1 Wheat and Barley cultivation and inoculation.....	140
5.2.2 Disease assessments.....	143
5.2.3 Hyperspectral data capture.....	146
5.2.4 Data pre-processing and modelling .....	148
5.3 Results.....	153
5.3.1 Crop canopy spectra.....	153
5.3.2 Model performance for yellow rust and fusarium head blight detection.....	159
5.4 Discussion .....	163
5.4.1 Crop canopy spectra.....	163
5.4.2 Model performance for yellow rust and fusarium head blight detection.....	168
5.5 Summary conclusions .....	171
6 Hyperspectral measurements of yellow rust and fusarium head blight in cereal crops:	
Part 2: on-line field measurement .....	173
Abstract.....	173

6.1 Introduction.....	174
6.2 Materials and methods .....	177
6.2.1 Field sites .....	177
6.2.2 Hyperspectral on-line data capture .....	179
6.2.3 Moisture content measurement .....	181
6.2.4 Disease recognition in the field.....	182
6.3 Data analyses. ....	185
6.3.1 Crop canopy spectral data pre-processing .....	185
6.3.2 Evaluation of model performance.....	186
6.3.3 Mapping .....	192
6.4 Results.....	193
6.4.1 Crop canopy spectra analysis.....	193
6.4.2 Evaluation of model performance.....	195
6.4.3 Maps.....	199
6.5 Discussion .....	208
6.5.1 Crop canopy spectra analysis.....	208
6.5.2 Evaluation of model performance.....	210
6.5.3 Maps.....	213
6.6 Summary conclusions .....	217
7 Management zone maps for variable fungicide application and selective harvest....	218
Abstract.....	218
7.1 Introduction.....	219
7.2 Materials and methods .....	222
7.2.1 Field site.....	222
7.2.2 Disease and canopy property data collection.....	224
7.2.3 On-line soil measurement .....	226
7.2.4 Spectral modelling of disease and soil properties.....	226
7.2.5 Mapping .....	228
7.2.6 Management zone maps.....	228
7.2.7 Eventual calculation of cost-benefit analysis.....	229
7.3 Results and discussion .....	231
7.3.1 Spatial variability of different properties.....	231
7.3.2 K-means clusters.....	237
7.3.3 Treatment maps.....	242
7.3.4 Economic benefits.....	247
7.4 Summary conclusions .....	254
8 Conclusions and further work.....	255
8.1 Recent publications .....	255
8.2 Objectives and chapter conclusions .....	256
8.2.1 Objective 1:.....	257
8.2.2 Objective 2:.....	259
8.2.3 Objective 3:.....	262

8.2.4 Objective 4: .....	264
8.2.5 Objective 5: .....	266
8.3 Hypothesis consideration .....	268
8.4 Contributions to knowledge .....	269
8.5 Further work.....	270
8.5.1 Yield limiting factors .....	270
8.5.2 Hyperspectral imaging of disease .....	271
8.5.3 Management zones .....	271
8.6 Concluding remarks .....	271
REFERENCES .....	273
APPENDICES .....	295

## LIST OF FIGURES

Figure 1: Example of yellow rust ( <i>Puccinia striiformis</i> ) disease on winter wheat. ....	15
Figure 2: Example of Fusarium head blight (FHB) disease on winter wheat.....	16
Figure 3: Zadok’s scale of the main growth stages of wheat, (consistent across other small cereal crops) (OMAFRA, 2009).....	18
Figure 4: Field location in Premslin near Rostock in Germany, where soil samples and yield data were recorded in 2013 and 2014.....	51
Figure 5: Yield maps of oilseed rape and barley measured in 2013 (a) and 2014 (b), respectively, and developed with ordinary kriging based on spherical model (shown by the line). Semi-variograms fit to the lag points which are distance classes into which pairs of locations are grouped (shown by the small circles), with a sum of square error (SSE) value of 0.0001 and 0.0001 for (c) and (d), respectively. Figure also shows position of 140 soil samples used in this study. ....	62
Figure 6: Illustrated image of the tractor mounted on-line visible and near infrared spectroscopy (vis-NIRS) sensor (Mouazen, 2006).....	79
Figure 7: Examples of the raw on-line soil visible and near infrared (vis-NIR) spectra, collected with the on-line sensor. Showing slight deviations in relative absorbance, across the wavelengths, which is dependent on the soil properties.....	80
Figure 8: Interpolated yield map (a) and exponential semi-variogram of 0.036, 0.817 and 20.358, representing, nugget, sill and range, respectively. Semi-variograms fit to the lag points which are distance classes, into which pairs of locations are grouped (shown by the small circles) (b) based on the 2013 harvest of wheat grain in tons per hectare. Lighter areas representing lower yield. ....	86
Figure 9: Measured transects (a), map of the soil moisture content (MC) measured with the on-line visible and near infrared spectroscopy (vis-NIRS) sensor after crop harvest in August, 2012 (b) respectively. ....	87
Figure 10: Soil property maps of the study field in Bedfordshire, UK; magnesium (Mg) magnesium in mg/l, organic carbon (OC) in % of dry matter, phosphorus (P) in mg/l, CEC in meq/100g, calcium (Ca) in mg/l, total nitrogen (TN) in % of dry matter, pH the log measurement of acidity. On-line spectral data was collected and applied to PLSR models developed by Kuang and Mouazen (2013) and Marin-González <i>et al.</i> (2013). ..	89
Figure 11: Schematic illustration of the laboratory (simulated field) configurations used and the variables implemented to obtain the hyperspectral data with the highest signal-to-noise ratio (SNR). The hyperspectral imager is a passive sensor, but has been applied with an external halogen light source. The Laser pointers allow to precisely position the hyperspectral imager over the target. ....	113
Figure 12: Illustrates the on-line field hyperspectral measurement using hyperspectral measurement configuration. ....	115
Figure 13: Example of the overcast sky at on-line hyperspectral imaging collection. ....	116

Figure 14: Schematic illustration outlining how mean, standard deviation and signal-to-noise ratio for wavelength ( $M_w$ , $SD_w$ , $SNR_w$ , respectively) and a spectrum ( $M_s$ , $SD_s$ , $SNR_s$ , respectively) were calculated. ....	119
Figure 15: Examples of smooth (the grey line with 1.6 signal-to-noise ratio (SNR), noisy (the black line with 1.2 SNR), and saturated (the dotted line with 1.8 SNR) spectra of wheat canopy. The saturated spectrum flattens off at 680-750 nm and important information is lost on the peak around 700 nm that is otherwise illustrated by the clear spectra. ....	123
Figure 16: Principal component analysis similarity maps developed for principal components 1 and 2 (a) and for principal components 1 and 3 (b). Input variables are camera and light height, light distance, camera angle, integration time and signal-to-noise ratio (SNR).....	126
Figure 17: Comparison of canopy spectra of water stressed wheat crop obtained in the laboratory (the dashed line) and on-line in the field (the dotted and grey lines). The crop was of the same variety and at comparable growth stages. Laboratory and field scans were collected under the suggested optimal configurations. The on-line field scans are: 1) field scan (the grey line) is of a more water stressed plant and 2) field scan (the dotted line) is of a less water stressed plant. ....	131
Figure 18: Maps of on-line measured soil moisture content (MC) (a) total nitrogen (TN) (b), and the average signal-to-noise ratio (SNR) per scan (c).....	133
Figure 19: Schematic of tray replicates and treatments, showing winter barley and winter wheat, with yellow rust and fusarium head blight (FHB) diseases, and healthy crop, both rain fed and water stressed, in replicates of three.....	142
Figure 20: Fusarium inoculation of wheat and barley trays in the laboratory. Inoculation took place at the anthesis crop growth stage. ....	143
Figure 21: Illustrating influence of foliar health on yield (HGCA, 2008).....	145
Figure 22: Schematic illustration of the laboratory configurations of hyperspectral camera and light source (Whetton <i>et al.</i> , 2016b).....	148
Figure 23: Example spectra of wheat and barley canopy at growth stage 72, after white and dark corrections. Arrows highlight areas of interest for indices to distinguish the health of the crop.....	153
Figure 24: Comparison of an average wheat crop canopy spectra between watered (-) and water-stressed (----) treatments for a) healthy, b) yellow rust infected and c) fusarium head blight (FHB) infected crop canopy. Plot (d) compares canopy spectra under watered conditions of healthy (---), yellow rust (---) and FHB (-).....	155
Figure 25: Comparison of an average barley crop canopy spectra between watered (-) and water-stressed (----) treatments for a) healthy, b) yellow rust infected and c) fusarium head blight (FHB) infected crop canopy. Plot (d) compares canopy spectra under watered conditions of healthy (---), yellow rust (---) and FHB (-).....	156
Figure 26: Scatter plots of predicted versus reference measured (based on 20% prediction set) yellow rust coverage in wheat (a), yellow rust coverage in barley (b), yellow rust scale in wheat (c), yellow rust scale in barley (d), fusarium head blight (FHB) severity in wheat	



(e), FHB severity in barley (f), wheat yellow rust logit (g), barley yellow rust logit (h). The R <sup>2</sup> report significance level of <0.01 for each regression. ....	162
Figure 27: Hyperspectral imagery system mounted on a metal frame attached to the side of a tractor, ready for on-line canopy measurement.....	179
Figure 28: Schematic of work flow from data capture to production of PLSR models, validation, and on-line prediction for production of maps.....	180
Figure 29: on-line hyperspectral measurement lines and position of ground truth plots, collected at five samples per ha, in the four fields. Fields 1 and 4 were validated at the same locations at two time intervals.....	183
Figure 30: Example of photo interpretation to assess yellow rust and fusarium head blight (FHB) coverage based on a 100-point grid. ....	185
Figure 31: Indicative spectra of wheat canopy collected at early (booting) and late (milk) growth stages, comparing on-line and non-mobile (off-line ground truth) spectra as: (-) late non-mobile (---) early non-mobile (...) early on-line, and ( _ _ ) late on-line. ....	194
Figure 32: Indicative spectra of barley canopy collected at anthesis growth stage, comparing between on-line (--) and non-mobile (-) spectra. ....	194
Figure 33: Scatter plots for the on-line predicted versus reference assessed diseases. On-line predictions was based on partial least squares regression model developed, based on visual yellow rust coverage in wheat (a), visual yellow rust coverage in barley (b), visual yellow rust scale in wheat (c), visual yellow rust scale in barley (d), image fusarium head blight (FHB) scale in wheat (e) and image FHB scale in barley (f).....	198
Figure 34: Maps of % disease cover of fusarium head blight (FHB) of ground truth data obtained with photo interpretation at a 10 by 10 m resolution. Maps are shown for the four experimental fields; Field 1 with wheat (a) (4 ha anthesis), field 2 with barley (b) (10 ha anthesis), field 3 with wheat (c) (12 ha Milk), and field 4 with wheat (d) (7 ha Milk).....	201
Figure 35: Maps of yellow rust classed in the 0-5 scale of ground truth data at a 10 by 10 m resolution. Maps are shown in the four experimental fields: (a and b) refer to maps of early stage scans in field 1 with wheat (4 ha booting) and field 3 with wheat (12 ha booting), respectively. Maps of late stage scans are shown by (c) for field 3 with wheat (12 ha Milk), (d) for field 4 with wheat (7 ha Milk) (e) for field 1 with wheat (4 ha anthesis) and (f) field 2 with barley (10 ha anthesis). ....	202
Figure 36: On-line measured % infection of fusarium head blight (FHB) maps using photo interpretation in the four experimental fields; Field 1 with wheat (a) (4 ha anthesis), field 2 with barley (b) (10 ha anthesis), field 3 with wheat (c) (12 ha Milk), and field 4 with wheat (d) (7 ha Milk).....	205
Figure 37: On-line measured yellow rust maps, classed in the 0-5 scale (0 is given when no disease is present, 1 for up to 5% cover, 2 for up to 10%, 3 for up to 30%, 4 for up to 50% and 5 for >50%) in the four experimental fields: (a and b) refer to maps of early stage scans in field 1 with wheat (4 ha booting) and field 3 with wheat (12 ha booting), respectively. Maps of late stage scans are shown by (c) for field 3 with wheat (12 ha	

Milk), (d) for field 4 with wheat (7 ha Milk) (e) for field 1 with wheat (4 ha anthesis) and (f) field 2 with barley (10 ha anthesis). .....	206
Figure 38: Soil moisture content map and images of measured with the on-line visible and near infrared spectroscopy sensor (Mouazen, 2006) in field 4. ....	208
Figure 39: Images of wheat crop at the field site in Bedfordshire, UK. Wheat was at growth stage 72 (Milk). Part A) Fusarium head blight infection (FHB), and part B) Yellow rust infection.....	213
Figure 40: Map of the experimental field where ground sample locations (5 per hectare, n=60) are shown. ....	225
Figure 41: Disease severity; On-line predicted maps of fusarium head blight (FHB) measured at milk growth stage 72 (july 2015), early yellow rust measured at booting growth stage 43 (may 2015), and late yellow rust measured at milk growth stage 72 (july 2015). The disease is classified on a 0 to 5 scale, where 0 indicates low disease presence and 5 indicates high disease. ....	234
Figure 42: Properties attributed to the canopy; On-line measured normalised difference vegetation index (NDVI), along with the 60 samples based developed maps for leaf area index (LAI), canopy air temperature and humidity. These data were all collected at the booting growth stage 43, in May 2015.....	235
Figure 43: Soil properties; On-line predicted soil cation exchange capacity (CEC in Cmol/kg), total nitrogen (TN in %), moisture content (MC in %) and organic carbon (OC in %). The soil properties were collected before the seed was drilled in September 2014. ....	236
Figure 44: Yield map of wheat measured in September 2015.....	237
Figure 45: K-means cluster analysis based on the on-line predicted late yellow rust and fusarium head blight (FHB) showing two classes to be adopted for the selective harvest (SH). ....	239
Figure 46: K-means cluster analysis for variable rate fungicide application (VRFA) at the T1 and T2 growing stages. Input data were measured normalised difference vegetation index (NDVI), air temperature, air humidity, leaf area index (LAI), on-line predicted soil organic carbon (OC), total nitrogen (TN), moisture content (MC) and cation exchange capacity (CEC), and on-line predicted early yellow rust disease. ....	240
Figure 47: K-means cluster analysis for variable rate fungicide application (VRFA) at the T3 growing stage. Input data were measured normalised difference vegetation index (NDVI), air temperature, air humidity, leaf area index (LAI), on-line predicted soil organic carbon (OC), total nitrogen (TN), moisture content (MC) and cation exchange capacity (CEC), and on-line predicted fusarium head blight (FHB) disease. ....	242
Figure 48: Management zone (MZ) maps for selective harvest (SH), The map on the left shows high disease infection (MZ 1) and low disease infection (MZ 2) which is obtained by k-means clustering that included on-line predicted fusarium head blight (FHB) and late yellow rust. With the right map showing high and low infection zones on the right,	

with the field being split into plots of 12 m (due to the combine harvest cutting head).  
.....244

Figure 49: Management zone (MZ) maps for variable rate fungicide application (VRFA) at the T1 and T2 growing stages. The map on the left show low yellow rust (MZ 1) and high yellow rust (MZ 2), which is obtained by k-means clustering that included, measured canopy properties (normalised difference vegetation index (NDVI), air temperature, air humidity, and leaf area index (LAI)), on-line predicted soil (organic carbon (OC), total nitrogen (TN), moisture content (MC) and cation exchange capacity (CEC)), and on-line predicted early yellow rust disease. With the right map showing high and low infection zones on the right, with the field being split into plots of 24 m (due to the boom width). .....245

Figure 50: Management zone (MZ) maps for variable rate fungicide application (VRFA) at the T3 growing stages, The map on the left show high fusarium head blight (FHB) (MZ 1) and medium FHB (MZ 2), and high FHB (MZ3), which is obtained by k-means clustering that included, measured canopy properties (normalised difference vegetation index (NDVI), air temperature, air humidity, and leaf area index (LAI)), on-line predicted soil (organic carbon (OC), total nitrogen (TN), moisture content (MC) and cation exchange capacity (CEC)), and on-line predicted FHB. With the right map showing high and low infection zones on the right, with the field being split into plots of 24 m (due to the boom width). .....246

## LIST OF TABLES

Table 1: Pathogen infection and influence. The economic impact, and environmental conditions conducive to yellow rust, fusarium head blight (FHB) infection and associated mycotoxins. The growth stages are in reference to Zadoks scale (Zadoks et al., 1974; De Vallavieille-Pope et al., 1995; Gilbert and Tekauz, 2000; Rossi et al., 2001; Bravo et al., 2003; Xu, 2003; Del Ponte et al., 2007) .....	23
Table 2: summary of different spectral applications to recognition of crop diseases and associated observations and accuracies .....	41
Table 3: Statistics of measured soil properties of the 140 soil samples used as input data into the three models. TN, OC, MC in %, P, K, Mg Na, Ca in mg/l and CEC meq/100g60	
Table 4: Semi-variogram model parameters of yield maps. The best fit was achieved with spherical models for each, showing nugget ( $c_0$ ), sill $c$ , range ( $r$ m), proportion ( $C_0/C$ %), and the sum of square error (SSE).....	60
Table 5: Pearson correlation ( $r$ ) between soil properties and yield of 2013 and 2014. ..	64
Table 6: Calculated variable importance score (MSE) of yield prediction obtained with the random forest (RF) model, indicating contribution of each soil property to crop yield in 2013 and 2014. ....	65
Table 7: Calculated individual contribution (ERRC) of each soil property and sum of contribution (SERR) to crop yield in 2013 and 2014 cropping seasons, obtained with Volterra Non-linear Regressive with eXogenous inputs (VNRX), accounting for both linear and non-linear relationships (VNRX-LN).....	69
Table 8: Calculated individual contribution (ERRC) of each soil property and sum of contribution (SERR) to crop yield in 2013 and 2014 cropping seasons, obtained with Volterra Non-linear Regressive with eXogenous inputs (VNRX), accounting for linear relationship only (VNRX-L). ....	71
Table 9: Summaries of the statistics for the soil properties predicted in the field and the reliabilities of the models they were predicted from. The models were developed in Kuang and Mouazen (2013) and Marin-González et al. (2013).....	90
Table 10: Pearson correlation ( $r$ ) between on-line measured soil properties in 2012 and wheat yield harvested in 2013.....	92
Table 11: The correspondence between inputs variables in Volterra Non-linear Regressive with eXogenous inputs (VNRX) model and soil properties .....	93
Table 12: The first 10 terms with corresponding error reduction ratio contribution (ERRC) values and coefficients based on the shortest distance approximation (SDA) re-sampling technique with a 3 m radius.....	95
Table 13: Error reduction ratio contribution (ERRC) contribution of each soil property (input) to the crop yield (system output) with corresponding significance threshold based on the shortest distance approximation (SDA) re-sampling technique with a 3 m radius. ....	97

Table 14: Contribution of the top three significant soil properties in terms of the sum of error reduction ratio (SERR) on the crop yield, based on shortest distance approximation (SDA) and (CAA) sampling techniques calculated for different radius values. ...	102
Table 15: Factors included in configuring the hyperspectral imager measured in meters (m), degrees (°) and micro seconds (ms) (multiple configurations considered).....	111
Table 16: Average and standard deviation (SD) values of the highest signal-to-noise-ratios (SNR) obtained with different integration times, camera settings and light source settings when scanning a wheat canopy. Theoretical forward distance travelled (and captured to a single data line) if applied on a moving platform at field scale. ....	124
Table 17: Statistics of samples used in the partial least squares regression (PLSR) models, with 80% and 20% of samples were considered for cross validation and prediction, respectively. The data has a normal distribution. Yellow rust % refers to the percent cover of yellow rust on the leaves (used for both % and the logit transformation). Yellow rust scale refers to classes of disease infection levels with 0 being non and 5 being >50%. Fusarium head blight (FHB) refers to number of infected ears compared to number of healthy ears with 0 being healthy and 2 being >50%. ....	151
Table 18: Classes of the ratio of prediction deviation (RPD) and their suitability for predicting yellow rust and fusarium head blight (FHB) in cereal crops, and is based on the classifications from Rossel et al. (2006).....	152
Table 19: Spectral differences indicated as standard deviation of the 500-650 nm range and squared difference of 650 and 700 nm, calculated for healthy, yellow rust and fusarium head blight (FHB) infected wheat and barley canopy under watered and water-stressed conditions, averaged from spectra captured at growth stage 70. One average spectra were produced per line scan, with 9 line scans being considered for each class. ....	158
Table 20: Analysis of Variance (ANOVA) table for the analysis of transformed spectral indices over the different treatments. Analysis of the index the squared difference of 650 and 700 nm (sqDiff) was done on the square root scale, whilst analysis of the index standard deviation (SD) is done on of the range 500-650 nm.....	159
Table 21: Summary of model prediction performance of yellow rust and barley in cross-validation and prediction showing the R <sup>2</sup> , root mean square error of the prediction (RMSEP) and cross validation (RMSECV), and the ratio of prediction deviation (RPD). The three models for each are shown; yellow rust coverage (which is in two formats a % coverage of the yellow rust disease on the leaves, and the LOGIT transformation), yellow rust scale (which is a class of 0 to 5 with 0 being healthy and 5 being >50% yellow rust covered leaf area), and fusarium head blight (FHB) severity (severity and ratio of infected ears to healthy, 0 being healthy and 2 being >50%). ....	161
Table 22: Experimental fields, scanning time and growth stage identified according to the Zadok's scale (Zadoks et al., 1974). The soil type is presented for northern (N), southern (S) or eastern (E) and western (W) parts of a field. ....	178
Table 23: Explanation of validation sets, cross, non-mobile and on-line, along with the datasets included and the methods for each. ....	187

Table 24: Summary of the models produced for the yellow rust and fusarium head blight (FHB) models. Showing the datasets used, the achieved outcomes and validations.	188
Table 25: Statistics of samples for the assessment of yellow rust in wheat used in the validation techniques of the partial least squares (PLSR) regression analysis (which at creation undergoes cross validation), and non-mobile and on-line predictions. Demonstrating the number of samples (Nr), standard deviation (SD), and the max, mean, and min of the samples considered in each model. Visual cover analysis in %, i photo interpretation in %, and visual scale analysis on a 0-5 scale.....	190
Table 26: Statistics of samples for the assessment of fusarium head blight (FHB) in wheat used in the partial least squares (PLSR) regression analysis and non-mobile and on-line predictions. Demonstrating the number of samples (Nr), standard deviation (SD), and the max, mean, and min of the samples considered in each model. Visual cover analysis in %, photo interpretation in %.....	191
Table 27: Statistics of samples used for on-line prediction of yellow rust and fusarium head blight (FHB) in barley. Visual cover analysis in %, photo interpretation in %, and visual scale analysis on a 0-5 scale .....	191
Table 28: Ranges of the ratio of prediction deviation (RPD) and their suitability for predicting yellow rust and fusarium head blight (FHB) in cereal crops, proposed by which was proposed in Whetton et al. (2016c), and is based on the classifications from Rossel et al. (2006). .....	192
Table 29: Summary of model prediction performance of yellow rust and fusarium head blight (FHB) in wheat in cross-validation and non-mobile independent validation. Models were developed with the five on-line scanning occasions in three wheat fields. The five models are presented below; FHB visual cover analysis (%), FHB photo interpretation (%), Yellow rust visual coverage analysis (%), Yellow rust visual scale analysis (0-5) Yellow rust photo interpretation (%). .....	196
Table 30: on-line validation based on-line spectral data collected from three wheat fields and one barley field. The five models are presented below; Fusarium head blight (FHB) visual cover analysis (%), FHB photo interpretation (%), Yellow rust visual coverage analysis (%), Yellow rust visual scale analysis(0-5) Yellow rust photo interpretation (%). .....	199
Table 31: shows the summary statistics of the ground truth values for fusarium head blight (FHB) early and late yellow rust, for each field for the two models selected for on-line application. ....	200
Table 32: Semi-variogram model parameters of each mapped disease in the four fields. The best fit was achieved with spherical models. Yellow rust early and late and fusarium head blight (FHB).....	203
Table 33: Date of different measurement as related to crop growth stages according to the zadok's scale (Zadoks et al., 1974). .....	223
Table 34: Properties of the spherical semi-variogram obtained for yellow rust early (YR early) and late (YR late) scans, fusarium head blight (FHB), soil moisture content (MC), organic carbon (OC), total nitrogen (TN), cation exchange capacity (CEC), leaf area	

index (LAI) and normalised difference vegetation index (NDVI), crop humidity and temperature.....	232
Table 35: Statistics of yield and disease pressure (fusarium head blight (FHB), early and late yellow rust (YR)) of each management zone (MZ), for the variable rate fungicide applications (VRFA) at growing stage T1 and T2 (which consider soil properties, canopy properties and early yellow rust), and growing stage T3 (which consider soil properties, canopy properties, and FHB), and for the selective harvest (SH) (late yellow rust and FHB). For the VR T1 and T2 applications two MZ are considered; MZ1 (high yellow rust disease) and MZ2 (low yellow rust disease). For the VR T3 applications three MZ are considered; MZ1 (high FHB disease) and MZ2 (medium FHB disease) MZ3 (low FHB disease). SH considers two MZ; MZ1 (lower quality crop) and MZ2 (higher quality crop).....	248
Table 36: Cost-benefit analysis results comparing the selective harvest (SH) with the homogeneous harvest (HH), based on on-line available prices of grain (FWI, 2016). Management zone (MZ) 2 being of high quality grain (low fusarium head blight (FHB) spread and low mycotoxin concentration) and MZ1 being of low quality grain (high FHB spread and high mycotoxin concentration).....	249
Table 37: Cost-benefit analysis results for variable rate fungicide application (VRFA) at T1 and T2 growth stages, and at T3 growth stage, as compared to homogeneous application (HA). Management zones (MZs) 1, 2 and 3 refer to high dosage rate, medium rate and low rate, respectively. Fungicide used is Proline 275 (£34 per litre) for T1 and T2 application and Adexar (£55 per litre) for T3 application.....	251

## **LIST OF ABBREVIATIONS**

AFOLS	Adaptive-forward-orthogonal least squares
ANOVA	Analysis of variance
Ca	Calcium
CAA	Circle-based average approximation
CEC	Cation exchange capacity
DGPS	Differential global positioning system
DON	Deoxynivalenol
ERR	Error reduction ratio
ERRC	Error reduction ratio contribution
FAO	Food and Agriculture Organisation
FHB	Fusarium head blight
FOV	Field of view
GS	Growth stage
HH	homogenous harvest
HI	Hyper spectral imager
HRFA	Homogeneous rate fungicide application
HS	Hyperspectral
IF	Immunofluorescence
IR	Infrared
K	Potassium
LAI	Leaf area index
MC	Moisture content
Mg	Magnesium
Ms	Mean reflectance of spectrum
MSE	Mean square error (Variable importance scores)
Mw	Mean reflectance of wavelength
MZ	Management zones
N	Nitrogen



Na	Sodium
NARMAX	Non-linear auto-regressive moving model with exogenous inputs
NDVI	Normalised differential vegetation index
NFIR	Non-linear finite impulse response
NIR	Near infrared
OC	Organic carbon
OLS	Orthogonal least squares
OOB	Out-of-bag
P	Phosphorus
PC	Principal component
PCA	Principal component analysis
PCR	Polymerase chain reaction
pH	potential of hydrogen
PLS	Partial least squares regression
PLSR	Partial least squares regression
QDA	Quadratic discriminant analysis
RF	Random forest model
RMSE	Root mean square error
RMSECV	Root mean square error of cross validation
RMSEP	Root mean square error of prediction
RPD	Ratio of prediction deviation
SD	Standard deviation
SDA	Shortest distance approximation
SDs	Standard deviation of spectrum
SDw	Standard deviation of wavelengths
SEER	Sum of error reduction ratio
SH	selective harvest
SNR	Signal-to-noise ratio
SNRs	Signal-to-noise ratio of spectrum
SNRw	Signal-to-noise ratio of wavelengths

SSE	Sum of square error
STB	Septoria tritici blotch
SWIR	Short wavelength infrared
T0	Timing 0
T1	Timing 1
T2	Timing 2
T3	Timing3
TN	Total Nitrogen
UTM	Universal transverse Mercator
Vis	Visible
Vis-NIR	Visible near infrared
VNIR	Visible and near infrared
VNRX	Volterra non-linear regressive with exogenous inputs
VNRX-l	Linear variability
VNRX-LN	Non-linear variability
VOCIT	Volatile organic compound
VOCs	Volatile organic carbons
VRFA	variable rate fungicide application

# **1 Introduction**

## **Chapter Synopsis;**

This chapter sets the background and scope of the research in this thesis, which is focused towards spectral recognition of crop disease. The research presented here has been conducted as part of the larger Farm FUSE project, which aimed to fuse a set of data on soil and crop together with auxiliary data on topography, land use and weather to delineate management zones for site specific, land and crop management including site specific agro-chemical applications. The specific aims and objectives of the thesis are provided below, which are targeted towards the recognised gaps in knowledge from literature. The thesis structure is outlined, and a full disclosure of contribution to work in each section is given here.

## **1.1 Background and Context**

Conventional farming relies upon the unsustainable management of external inputs, and high-yield varieties susceptible to disease, to achieve higher yields. However, crop diseases cause significant reductions in harvest and further financial losses from reduced quality (Hole *et al.*, 2005; Godfray *et al.*, 2010). The homogenous application of inorganic, chemical, disease control products, started more than a century ago (Oerke 2006). With the world's population estimated to reach 9 billion by 2050, sustainable approaches to increase crop yield are a necessity (Hole *et al.*, 2005). One way to achieve this is by site specific management of farm resources. Among these, fungicide applications may well be reduced by targeted site specific spraying. Accurate measurement of fungal diseases is a main requirement for sustainable application of fungicides and expected to contribute to the reduction and prevention of the spread of crop disease and the quantity and quality losses incurred from them. The thesis will focus on the detection of crop diseases (specifically yellow rust and fusarium head blight

(FHB)), and consider the potential of variably applying fungicides at field scale, in response to their severity.

Soil variability within agricultural fields differs in spatial scale, from small scales of 0.30 m by 0.30 m grids (Raun *et al.*, 1998), to larger scales of 2 m by 2 m grids (Dhillon *et al.*, 1994). Borlaug and Doswell (1994) stated that soil fertility is the single most important factor that limits crop yields in developing countries. However, an area such as 0.30 m by 0.30 m would only effect a few plants (depending on drill rate). From a management perspective, soil variability on small scales (e.g. less than a few meters) cannot be variably managed on a commercial scale, due to practicality issues and technology limitations. As much as 50% of the increase in crop yields worldwide during the 20th century is due to the use of chemical fertilizers (Baligar *et al.*, 2001). Conventional farming in the UK relies on unsustainable applications of external inputs, based on homogeneous applications of micro- and macro-nutrients to obtain higher crop yields. These applications are made based on an average sample collected per field or per 1-3 ha in the best scenario. Plant resistance to diseases and pests are linked to balanced crop nutrition. A lack of different nutrients will increase the crop's vulnerability to specific diseases. However, an abundance of nutrients (such as available nitrogen) are of particular interest in linking a crop's susceptibility to various fungal diseases, through prolonged, and denser canopies, and nitrogen availability (Huber, 1980; Engelhard, 1989; Agrios, 1997; Fageria and Baligar, 1997; Graham and Webb, 1991; Snoeijers *et al.*, 2000). However, nitrogen is needed to support plants in growth and repair and resistance from disease injury. A lack of nitrogen can leave a plant susceptible to pathogens that are specialised in infecting weak plants (Agrios, 1997; McElhaney *et al.*, 1998).

The spatial and temporal variability of soil physical and chemical properties affect agricultural quantitative and qualitative production (Mzuku *et al.*, 2005). Assessment of field variability can help identify limiting factors of crop growth and optimise agrochemical inputs (Vrindts *et al.*, 2003). Assessing the contribution of disease, in comparison to nutrient factors, as a yield limiting factor has not yet been approached in the literature, and would require a high sampling resolution of environmental parameters, crop disease, and yield mapping.

Fungal plant diseases and stressful environmental conditions can result in a significant agronomic impact. Diseases can potentially spread over large areas through vectors and infected plant materials (López *et al.*, 2003; Sankaran *et al.*, 2010). Streams can spread the fungal spores through locations and rain through the crop canopy. Certain pathogens require a moist leaf surface for successful infection (Bisby 1943; HGCA 2010). Through wind dispersal, it is possible for fungal spores to be spread across and between continents (Brown and Hovmøller, 2002). Crop diseases cause major economic and agricultural losses worldwide by reducing both production quantity and quality (Roberts and Paul, 2006). A greater occurrence of fungal diseases is observed in denser canopies, although a conclusive regression through multiple years and fields has not been obtained, potentially due to the strong influence of weather conditions (Sentelhas *et al.*, 1993; Rozalski *et al.*, 1998). Cunniffe *et al.* (2015) have recently summarised the issues in modelling of crop epidemiology, and the parameters considered. Therefore, the monitoring and detection of stress and diseases in plants is vital for sustainable agriculture practice.

Fungal disease control is a large task for successful production of cereals worldwide. For example, yellow rust (*Puccinia striiformis*) is a foliar disease, which can reduce crop yields by up to 7 t ha<sup>-1</sup> in severe epidemics (Bravo *et al.*, 2003). A virulent strain of yellow rust developed during 2009 which attacked several widely grown genetically resistant cereal crop varieties, including Solstice (Milus *et al.*, 2009). Another important fungal disease that attacks cereal crops is FHB with the most aggressive and prevalent species (*Fusarium graminearum*), being highly pathogenic and produces mycotoxins (Rotter *et al.*, 1996; Brennan *et al.*, 2005; Desjardin, 2006; Leslie and Summerell, 2006). FHB predominantly affects the ear of the crop and has become one of the most important pre-harvest diseases worldwide. Similar to yellow rust, fusarium also causes a reduction in yield quantity and quality, and when producing mycotoxins, it becomes a significant threat to both humans and animals. Fusarium is a sporadic disease, dependent on warm and humid weather conditions, which causes variability of disease presence and level of infection across regions, and years (Jelinek *et al.*, 1989; Rossi *et al.*, 2001; Xu, 2003). Yellow rust and FHB were selected for the thesis focus, as they have been reliably seen at the field site over numerous years. However, diseases such as Septoria also have a high geographic distribution and are economically important, causing significant losses of up to 50% in wheat each year (Moss, 2013; Quaedvlieg *et al.*, 2013).

Although azole fungicides are currently widely used in wheat production, there is a risk that these fungicides may not be available in the future (Chandler, 2008). The European and Mediterranean Plant Protection Organization (EPPO, 2010) conclude that a diverse availability of azoles are the major contributing factor in the successful management of fungal pathogens. Agronomists are currently taking preventative measures not to compromise azoles, by rotating their usage and combining them with other active ingredient based

fungicides (Mielecki, 2011). The potential consequences of changes in the EU Pesticide Directive (91/414/EEC) will have considerable impacts on crop production in complying countries, requiring the withdrawal of 20% of the active ingredients (Hillocks, 2012). Consequently, this will result in more food having to be produced with fewer fungicides. In the next few decades, average crop yields are predicted to continue levelling off or to decline across many regions. Even in the most managed and irrigated cropping systems, the yield is currently ~80% of its expected potential (at best), hence, reducing the gap between actual and potential yields is of importance. However, no evidence exists suggesting that yields have ever achieved >80% of their potential (Lobell *et al.*, 2009; Fischer *et al.*, 2014). Therefore, it is necessary to measure and map the spatial distribution of these two diseases aiming at optimising variable rate application of relevant fungicide for sustainable increase in crop yield.

Limited measurement techniques of crop diseases are available at research or commercial scales. Some of these methods provide direct quantification of crop disease spread, whereas others rely on the measurement of a parameter linked with disease spread. A CROP-meter (Ehlert *et al.*, 2003) is currently sold as agricultural equipment, which can vary the application rate of fungicide in accordance to the measurement of crop density. The CROP-meter's application is relevant to plant density. Plant density affects microclimates and its conduciveness to diseases (Park *et al.*, 1992; Murray *et al.*, 1994; Dammer and Ehlert, 2006). The financial benefit of the CROP-meter method is attributed to a reduction in application rate in sparser areas. The crop density could be a reflection of multi-stresses occurring at the same time e.g., water, nutrients, temperature, disease etc. Crop density is also dependent upon the climatic conditions each year and associated crop variety (Cuculeanu *et al.*, 2002). Therefore, there is a big question mark of the applicability of the CROP-meter for disease

monitoring and control. Reports showed that the CROP-meter optimizes fungicide control by reducing fungicide input, but does not increase crop quality or quantity, highlighting an unmet demand where quality and quantity of yield is improved by taking into account environmental parameters.

A few optical devices for crop health are available commercially. Handheld devices for assessing parameter such as chlorophyll levels (correlated to nitrogen status) are used, by measuring leaf reflectance in the visible and infrared wavebands of the fluorescence like PocketPEA (Hansatech, Norfolk, UK). Tractor mounted sensors, which measure crop canopy reflectance in the visible and infrared are commercially available and most frequently used for normalized difference vegetation index (NDVI) calculations across the field, such as those from GreenSeeker (Trimble, California, USA), and Crop Circle (Holland Scientific, Lincoln, NE USA).

Spectroscopy and imaging techniques are currently used as direct tools for disease and stress monitoring (Hahn, 2009). Non-mobile (off-line) field and laboratory methods for disease classification and plant growing conditions have been studied and demonstrated (Roggo *et al.*, 2003; Wu *et al.*, 2008). Moshou *et al.* (2005) have shown that hyperspectral imaging for the recognition of *in-situ* disease can provide identification with a high degree of accuracy. However, their use in the field as mobile (also known as on-line) applications, for mapping crop disease has got rather limited attention by research (Lenk *et al.*, 2007; Sankaran *et al.*, 2010). It was recognised in 2003 (West *et al.*, 2003) that although optical technologies are available for development into suitable disease detection systems, many challenges are still needed to be overcome, and this is still arguably the case. No sensor-based technologies for disease detection commercially exist, that take into account the dispersion dynamics of pathogens within a field (West *et al.*, 2003; Dammer and Ehlert 2006; Mahlein 2016). Whilst



progress has been made in disease recognition in the field, there are only a few yellow rust specific identification systems and none for FHB. Commonly the attempts of disease recognition using hyperspectral and multispectral imagery, are targeted to individual leaves rather than the canopy (Bock *et al.*, 2010a).

Although on-line applications are still rather limited, optical techniques have the potential to be integrated with agricultural vehicles. Optical methods provide non-invasive and high sampling resolution data necessary for monitoring and mapping of crop diseases. Among optical sensing methods, hyperspectral and multispectral imaging techniques are the best candidates as they have been used in disease and stress monitoring (Hahn, 2009). Hyperspectral imaging takes near simultaneous spectral measurements along a series of spatial positions, providing spectral features at high resolutions and with an improved understanding of the target than multispectral imagery (Gilchrist 2006).

Spectral reflectance in vegetation canopies is dependent on several factors including the illumination angle, the canopy architecture and the radiative properties of the plants (Pinter and Jackson, 1985; Asner, 1998). Other factors affecting this are the integration time, light source, and camera distance and angle. Therefore, optimising the measurement configuration is essential before on-line field measurements using a hyperspectral imager can be successfully carried out, which is the main target of this thesis.

## **1.2 Research objectives**

There is a necessity for on-line recognition of crop disease, being both disease specific and capable of quantifying disease presence, for site specific management and evaluation of yield limiting factors.

### **Hypothesis**

The project will consider the following hypotheses;

1. Proximal hyperspectral imagery is capable of detecting specific crop diseases (e.g., FHB and yellow rust), and can be applied for on-line detection and mapping of their spatial distribution in cereal crops.
2. Multi-sensor and data fusion of crop disease, canopy and soil properties collected at high sampling resolutions, can be successfully used for the quantification of the yield limiting factors.

### **Aim**

The aim of the thesis is;

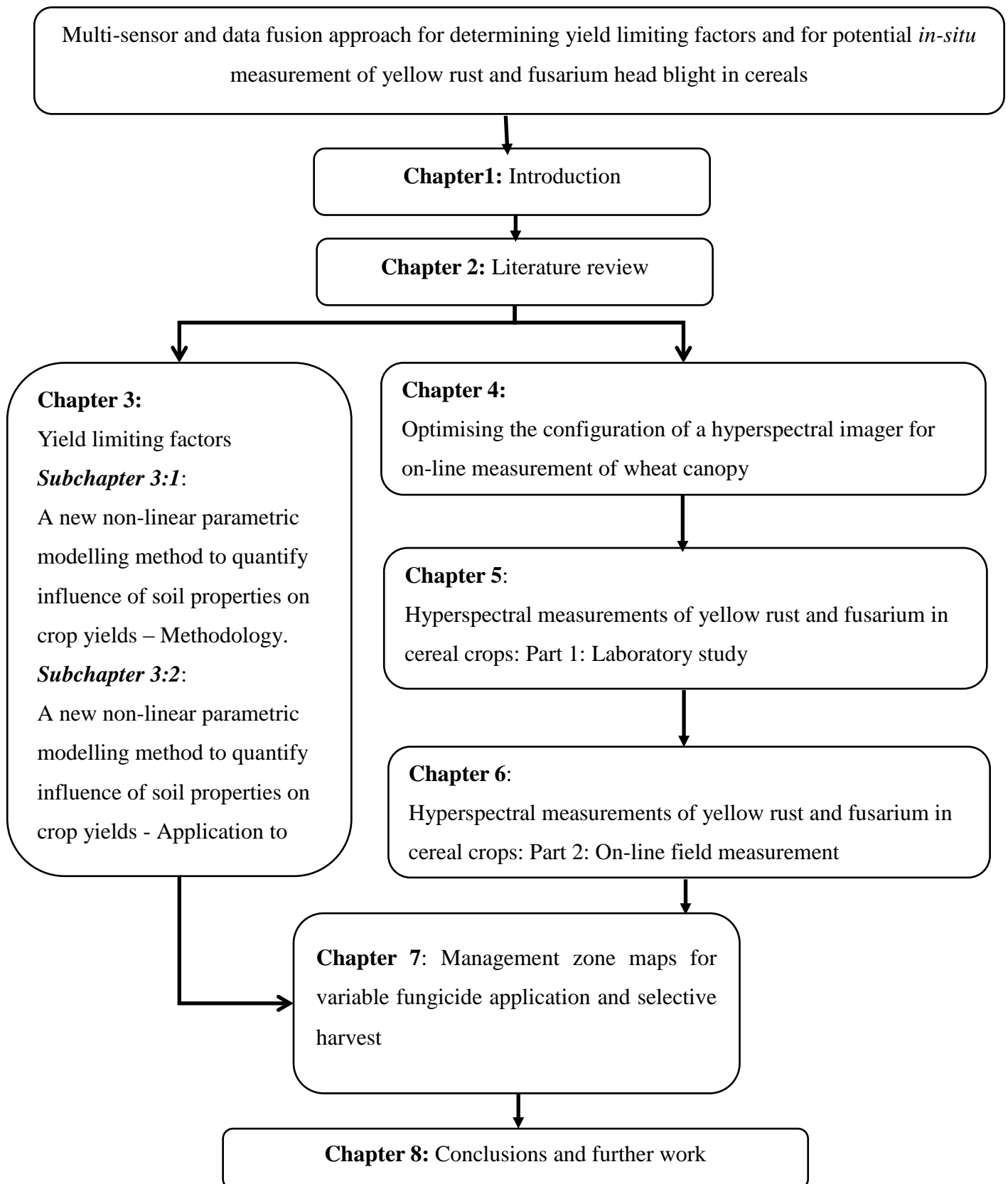
To apply a hyperspectral imager on-line application to cereal crop disease recognition, critically appraising the existing technology. It also investigates a novel modelling approach for quantifying the crop yield limiting factors. The key aim is to produce management zone maps for variable rate fungicide application and selective harvest, in response to crop disease pressures, soil characteristics and micro-climatic conditions.

## Objectives

The objectives of the thesis are;

1. To critically appraise different approaches, and identify the best configuration for the hyperspectral imaging systems for *in-situ* and on-line field measurement of crop disease.
2. To evaluate the individual and interaction effects of parameters limiting crop growth and yield.
3. To create a spectral library using hyperspectral data to identify and quantify specific crop diseases (yellow rust and fusarium head blight) independent from water stresses.
4. To implement the hyperspectral imager for on-line detection and mapping of the spatial distribution of yellow rust and fusarium head blight in winter wheat and barley.
5. To adopt a data-fusion approach for delineation of management zones for variable rate fungicide application and selective harvest.

### 1.3 Thesis structure



## 1.4 Disclosure

The thesis consists of 8 Chapters. Apart from Chapter 1 (Introduction), Chapter 2 (Literature review) and Chapter 8 (Conclusions and Further work), the remaining chapters are presented as papers (accepted or under review) and are detailed below;

**Chapter 3 part 1:** A new non-linear parametric modelling method to quantify influence of soil properties on crop yields - Methodology

The study was collaborative work with Dr. Yifan Zhao and Dr. Said Nawar. The paper is submitted to the *European journal of Agronomy*. The paper is presented as part 1 of chapter 3. My contribution to this work was being the lead author, and conducting all the field work data collection, soil processing and property analysis. The majority of NARMARX modelling was produced by Dr. Yifan Zhao, and random forest analysis By Dr. Said Nawar.

*Whetton, R.L., Zhao, Y., Nawar, S., and Mouazen, A.M. (2016). A new non-linear parametric modelling method to quantify influence of soil properties on crop yields - Methodology. European journal of Agronomy (under review).*

**Chapter 3 part 2:** A new non-linear parametric modelling method to quantify influence of soil properties on crop yields - Application to on-line soil data

The study was collaborative work with Dr. Yifan Zhao, and the paper is submitted to *Soil Research*. The paper presented as part 2 of chapter 3. My contribution to this work was being the lead author, and conducting all the field work data collection, soil processing and property analysis. I have also prepared the data layers through interpolation (kriging) and raster analysis. The methodology and results for NARMARX modelling were produced by Dr. Yifan Zhao.

Whetton, R.L., Zhao, Y. and Mouazen, A.M. (2016). *A new non-linear parametric modelling method to quantify influence of soil properties on crop yields - Application to on-line soil data. Soil research (under review).*

**Chapter 4:** Optimising the configuration of a hyperspectral imager for on-line field measurement of wheat canopy

The study was first presented at ATIA, with a short paper included in the proceedings. A more elaborated version of the work (provided in the thesis) was accepted for publication in *Biosystem Engineering*. All work was my own with supervision and guidance from my supervisors.

Whetton R.L., Waine T.W. and Mouazen, A.M. (2016). *Optimising configuration of a hyperspectral imager for on-line field measurement of wheat canopy. Biosystems Engineering (accepted on 9<sup>th</sup> December 2016).*

10.1016/j.biosystemseng.2016.12.006.

**Chapter 5:** Hyperspectral measurements of yellow rust and fusarium head blight in cereal crops: Part 1: Laboratory study.

This work was submitted to *Biosystems Engineering* and the work is currently in review. All work was my own with supervision and guidance from my supervisors.

Whetton, R.L., Waine, T.W. and Mouazen, A.M. (2016). *Hyperspectral measurements of yellow rust and fusarium head blight in cereal crops: Part 1: Laboratory study. Biosystems Engineering (under review).*

**Chapter 6:** Hyperspectral measurements of yellow rust and fusarium head blight in cereal crops: Part 2: on-line field measurement.

The study was first presented at CIGAR in June 2016, with the abstract provided in the proceedings. A full paper was prepared and submitted to *Biosystems Engineering*. All work was my own with supervision and guidance from my supervisors.

*Whetton, R.L., Waine, T.W. and Mouazen, A.M. (2016). Hyperspectral measurements of yellow rust and fusarium head blight in cereal crops: Part 2: on-line field measurement. Biosystems Engineering (under review).*

**Chapter 7:** Management zone maps for variable fungicide application and selective harvest

All work was my own with supervision and guidance from my supervisors.

*Whetton, R.L., Waine, T.W. and Mouazen, A.M. (2016). Yellow rust and fusarium head blight disease in winter wheat; proposed Management zones European Journal of Agronomy (under review).*

## **2 Literature review**

### **Chapter Synopsis;**

This chapter undertakes a critical review of the literature, with particular focus on cereal crop yield limiting factors, fungal disease, soil properties, nutrient status, water stress, climate and infection. It will also review measurement and monitoring techniques used for disease detection.

### **2.1 Fungal diseases**

Fungal diseases result in significant yield losses of cereal crops worldwide. Yellow rust, a foliar disease, and fusarium, which affects the head of the crop, are two fungal infections common on the small cereal crops, wheat and barley. Over 200 million hectares of farmland worldwide is used to grow wheat (*Triticum aestivum*), which contributes to about 21% of the world's food according to the food and agriculture organization (FAO) (Gustavsson *et al.*, 2011).

#### **2.1.1 Yellow rust**

Yellow rust, *Puccinia striiformis*, is a plant pathogen (Figure 1), causing yellow rust (commonly in patches through a field) alternatively known as stripe rust, which produces yellow uredo spores on the leaves. Yellow rust, is one of the most widely destructive plant diseases in winter cereal crops (Wellings, 2011). The spores are predominantly dispersed by the wind, and require damp or very humid conditions to infect the crop's leaves. Disease symptoms start with chlorosis, occurring parallel to leaf veins in a narrow 2mm wide stripe, which develop into multiple yellow coloured rust pustules (De Vallavieille-Pope *et al.*, 1995). Disease presence can vary considerably between plants. In severe epidemics, the yields can be reduced by up to 7 tonne ha<sup>-1</sup> (Bravo *et al.*, 2003). A virulent strain of yellow rust that



developed during 2009, attacked several widely grown genetically resistant cereal crop varieties, including Solstice (Milus *et al.*, 2009). A broad-spectrum seed dressing and appropriate fungicide treatments should be used in areas at-risk and those with historic infection (Blake *et al.*, 2011).



**Figure 1:** Example of yellow rust (*Puccinia striiformis*) disease on winter wheat.

### **2.1.2 Fusarium head blight**

Fusarium head blight (FHB) infection (Figure 2) is a major fungal disease, affecting several hosts including wheat and barley (Parry *et al.*, 1995). The disease occurs throughout most of the world and is caused by the genus, *Fusarium*. FHB is prevalent as several species, including; *F. avenaceum*, *F. culmorum*, *F. graminearum*, *F. poae*, *F. sporotrichoides*, *M. nivale* and *M. Majus* (Parry *et al.*, 1995; Xu *et al.*, 2005). *Fusarium* fungi survive over winter on plant residues (as mycelium), which can produce ascospores that infect the flag shoot (Sutton, 1982; Oberti *et al.*, 2014). FHB is a sporadic disease, severity is dependent on warm humid weather (Rossi *et al.*, 2001; Xu, 2003), causing variability of disease presence and level of infection across regions and years (Jelinek *et al.*, 1989). FHB symptoms in wheat and

barley appear in the head and peduncle tissues, causing discolouration and early senescence. Early visual symptoms consist of a characteristic purple/pink discolouration. Seed from a FHB affected crop is often shrunken, with a bleached appearance (Andersen, 1948; Parry *et al.*, 1995; McMullen *et al.*, 1997; Goswami and Kistler, 2004). FHB can result in yield losses, reduced grain, seed quality and size, causing direct economic losses. Mycotoxin contamination (a secondary metabolite of the fusarium mould) in the grain, results in indirect economic losses, due to market rejection or downgrading of grain quality (Sutton, 1982; Gilbert and Tekauz, 1995; Parry *et al.*, 1995; Goswami and Kistler, 2004). Due to legal limits imposed by the European commission, for the fusarium mycotoxins deoxynivalenol (DON), and zearalenone (ZON) high levels of mycotoxins in cereal grain mean that it cannot be sold for human consumption (1250ppb for DON and 100ppb for ZON in wheat crop) but the crop can be downgraded to cattle feed (ruminants are more resistant to mycotoxins) but at a reduced price (HGCA 2014).



**Figure 2:** Example of Fusarium head blight (FHB) disease on winter wheat.

FHB has become one of the most important pre-harvest diseases worldwide (Magan *et al.* 2002). Control of fusarium and high mycotoxin contaminations are required to prevent toxic contamination reaching the food chain either in milling grain (for human consumption) or as cattle feed (Magan *et al.*, 2002). *F. graminearum* is regarded as the most prevalent fusarium pathogen in the UK, as it is highly pathogenic (when considering mycotoxins) with a high genetic variation due to being a species complex (Rotter *et al.*, 1996; Brennan *et al.*, 2005; Desjardin, 2006; Leslie and Summerell, 2006). Ear development is a critical growth stage for cereal pathogen infection. Cereals are highly susceptible to fusarium infection during anthesis (growth stage 60, Figure 3), as the anthers provide nutrients to fungal growth (Andersen, 1948; Parry *et al.*, 1995; Lacey *et al.*, 1999; Xu, 2003; Del Ponte *et al.*, 2007). Imathiu *et al.* (2008) found that fusarium DNA can be detected in the ‘panicle’ of the crop at the end of anthesis (growth stage 60 – 69 illustrated in Figure 3). If the crop is infected later during grain development, visual symptoms may not develop, though mycotoxins can still be produced in the grain (Salas *et al.*, 1999; Osborne and Stein, 2007).

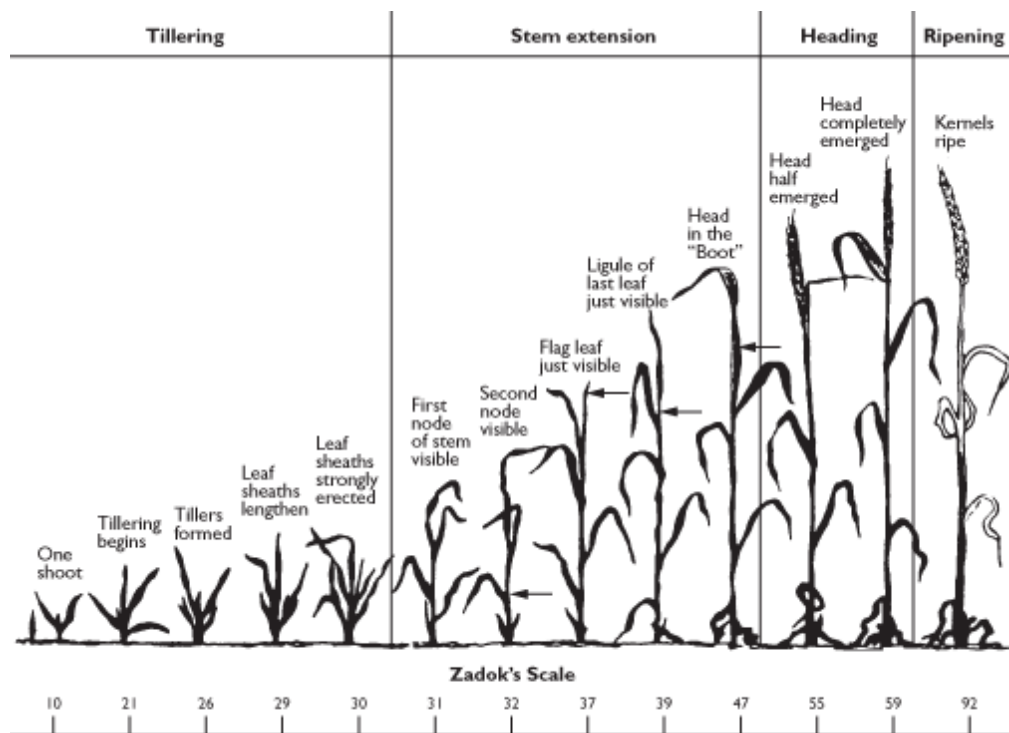


**Figure 3:** Zadok's scale of the main growth stages of wheat, (consistent across other small cereal crops) (OMAFRA, 2009).

Impey (2012) confirmed the presence of fusarium leaf lesions in Herefordshire. This study was based on leaf analysis from five sites by the Agricultural and Environmental Consultancy. Fusarium leaf lesions found on the top two leaves is unusual but indicates the disease's establishment in the ear (Impey, 2012). The addition of leaf lesions reduces photosynthesising green leaf area, contributing to a reduction in yield.

Early detection of cereal disease, which may lack obvious visual symptoms, allows for a more effective fungicide treatment, preventing losses to crop yield and quality. Optical sensing provides non-destructive measurements, allowing repeated data acquisition throughout the growing season (Oberti *et al.*, 2014). Among these optical techniques, hyperspectral imagers show the potential for such system and are discussed later on.

### **2.1.3 Fungal disease resistance**

Significant increases in cereal crop yields have been achieved over the last half-century through changes in agronomic practice, synthetic fertilizers, pesticides, resistant and high yielding cultivars (Bilsborrow *et al.*, 2013). The most economical approach is to cultivate varieties with a genetic resistance to fungal diseases. Genetically modified plants with an increased resistance to fungal diseases are part of active research aiming to aid the reduction of the use of chemical fungicides (Bliffeld *et al.*, 1999; Clausen, 2000; Bieri *et al.*, 2003). However, resistant crops are susceptible to being overcome by fungal pathogens, due to many resistant plant varieties relying on a few key resistance genes. Fungicide resistance has also developed to many of the available fungicide classes (Mielecki, 2011).

Cultivating varieties with resistance genes to FHB infection can be complicated due to the nature of the disease and the necessity to check 'resistant' plants at maturity for disease expression and distinguishing them under varying and complex environmental effects as well as the cost and time implications required for phenotyping (Bai and Shaner, 1994; Yang, 1994; Campbell and Lipps, 1998). There are varying types of resistance genes for FHB infection in wheat and small cereal crops (Bai and Shaner, 1994; Yang, 1994; McMullen *et al.*, 1997). Genetic resistance to FHB is generally expressed as a quantitative trait, due to its resistance relying on only a few genes, and their wide variation in response to environmental conditions. Fungicide resistant pathogens, and pathogens overcoming crop genetic resistance are both cause for concern (Wolfe 1985). With approaches to fungal disease control becoming less effective there is pressure for new disease management strategies to be developed. Improving disease control and the timings of application of fungicides, could prolong certain fungicides' effectiveness, and keep them available as a reliable method for longer, due to reducing the chance of resistant mutants establishing (FRAC, 2010).

## **2.1.4 Disease distribution and spread**

There are multiple environmental factors in addition to those of crop resistance, which contributes to disease distribution. These include climate, humidity, weather, sources of inoculation, and environmental stresses. Balanced nutrition has an important role in determining plant resistance or susceptibility to diseases.

### **2.1.4.1 Sources of fungal disease inoculation**

Theoretically, a higher disease pressure is expected to occur in fields of minimum or no tillage (Edwards, 2007; Parikka *et al.*, 2007; Imathiu, 2008). A regular practice in conventional farming is to grow a wheat crop for 2 successional years without rotation, which commonly results in a yield loss and a higher demand for fungicide (Bilborrow *et al.*, 2013). Yellow rust and FHB species can survive in soil and weeds occurring in the hedgerows and borders of a field, acting as a source of inoculum (Jenkinson and Parry, 1994; Champeil *et al.*, 2004; Imathiu *et al.*, 2013). Initial infections of soil-borne pathogens, commonly result from infected plant residues left over from the previous year's harvest. *Fusarium* species survive over winter on plant tissues and residues as mycelium (Sutton, 1982), infecting the ear of the crop as conidia and ascospores (Osborne and Stein, 2007), even after two years on the soil surface (Pereyra *et al.*, 2004). Crop residue is considered a major factor for inoculation levels (Teich and Hamilton, 1985; Dill Macky and Jones, 2000). Pathogen survival is expected to be reduced in ploughed systems, as tillage buries residue, speeds decomposition and reduces pathogen reproduction and survival (Khonga and Sutton, 1988; Pereyra *et al.*, 2004). However, stubble can have a significant impact on other fungal diseases as well, such as *Septoria tritici* Blotch (STB). *Zymoseptoria tritici* causes STB on wheat. STB is a highly significant disease reducing wheat yields by up to 50% in severe epidemics on susceptible varieties (Eyal *et al.*, 1973; Eyal *et al.*, 1987; Fones and Gurr 2015).

Annual losses in the UK are around 20% of harvest (HGCA, 2012). STB poses a threat in temperate climates around the world. *Septoria* shows symptoms only in the later stages of infection, as the fungus can grow between leaf cells without causing visible damage. However, once established, visible symptoms can occur throughout infected crops, rapidly creating oval pale brown lesions, containing black spots (pycnidia). Lesions can form from a single spore. In high severity, these lesions can join together, covering a large surface area of the leaf. Airborne ascospores, rain splashed pycnidiospores (from infected plant debris), and seed-borne infections are the main causes of STB.

There is a trade-off between preserving top soil and increasing disease presence. Stubble can help the survival of stubble-borne pathogens, for example, *Z. tritici* populations can survive between growing seasons and release spores to infect the next crop. This increased survival can increase potential mutations, and the rate of evolution. Traditionally crop rotations and burying infected crop residues (tillage) reduces levels of early inoculation within a field. However, there is a large airborne source of inoculum from ascospores from neighbouring fields (Schuh 1990). This means that tillage has little impact on STB levels later in the season (Schuh 1990; Suffert and Sache 2011). STB control is the focus of about 70% of fungicide applications in Europe (Eyal *et al.*, 1973; Eyal *et al.*, 1987). Whilst STB is not considered further in the thesis, it would be a suitable disease for further work. The adaptability of STB supports studies into early disease recognition, as a method of control.

The fusarium conidial spores are usually transported by rain drop splashes from the infected tissue to plant leaves and ears, though wind and insects are also sources for its distribution. Yellow rust infection is caused by uredospores and are predominantly dispersed by the wind and require damp or high humid conditions to infect the crop's leaves (De Vallavieille-Pope

*et al.*, 1995; Parry *et al.*, 1995; Sache 2000; Paul *et al.*, 2004). This method of pathogen transportation is more effective in sparse canopies, though in low precipitation levels, a dense crop stand will be more infected due to higher humidity (Broscious *et al.*, 1985; Sentelhas *et al.*, 1993). Cultivation practices, environmental factors such as crop density and climate variations are important factors to consider when modelling the spread of disease. Influence of environment on disease distribution

Epidemics of fungal diseases are strongly influenced by the local environment, persistence and adaption of the pathogen, and the crop's variety and physiological condition (Dammer, 2003). The climate and local weather conditions are considered a highly influential factor regarding the distribution and severity of fungal infections in a crop stand. Warm, humid conditions are ideal for FHB infection in crops (Rossi *et al.*, 2001; Xu, 2003), particularly if occurring during anthesis and early stages of kernel development (Gilbert and Tekauz, 2000). Yellow rust infections are closely correlated with temperature, ideally between 10°C and 15°C with little infection occurring <2°C and above >23°C (Murray *et al.*, 1994; Park *et al.*, 1992). Environmental conditions and the economic impact of yellow rust, FHB infection and associated mycotoxins are highlighted in Table 1.



**Table 1:** Pathogen infection and influence. The economic impact, and environmental conditions conducive to yellow rust, fusarium head blight (FHB) infection and associated mycotoxins. The growth stages are in reference to Zadoks scale (Zadoks *et al.*, 1974; De Vallavieille-Pope *et al.*, 1995; Gilbert and Tekauz, 2000; Rossi *et al.*, 2001; Bravo *et al.*, 2003; Xu, 2003; Del Ponte *et al.*, 2007)

	<b>Pathogens</b>	<b>Growth stage</b>	<b>Weather conditions promoting infection</b>	<b>Effect on yield</b>
<b>Yellow rust</b>	<i>Puccinia striiformis</i> .	Usually at stem elongation and onwards (growth stage 30 shown in Figure 3.	Infection pressures correlated with temperature, wind to spread, moisture to inoculate, cool moist summers.	Reduced quality and 40-50% reductions in yield. The reduction can reach up to 7 tonne ha <sup>-1</sup> .
<b>FHB</b>	Several fusarium and Microdochium species.	Usually at anthesis and onwards (growth stage 60 shown in Figure 3.	Variety of species suited to varying conditions, predominantly ideal if warm and humid.	40% reduction in quantity and reduction in quality by size, weight, shape, and toxins. Reduced quality; potentially toxic.

There is unequivocal evidence that the climate is changing at an increasing, and alarming rate (Change 2007; Parry 2007). Due to the impact of climate on crop disease pressure, there is a recognised need for a suitable crop monitoring system. *F. graminearum* is a dominant cause of FHB with a broader adaption to environmental variability and climatic conditions, compared to other species. The incidence of the disease can occur over varying temperatures and moisture conditions, either through different regions, or from within field variability due to e.g., soil type and moisture, and the impact of crop density on humidity and temperature (Dammer, 2003; Backhouse 2014). Climate change could cause a population change in the

pathogen, allowing for a wider distribution of aggressive and virulent strains, which again supports a need for optimisation of disease monitoring and control (Sung and Cook, 1981; Dufault *et al.*, 2006; Rossi *et al.*, 2001).

#### **2.1.4.2 Influence of canopy density on microclimate and disease spread**

Under clear weather conditions in spring and summer, areas of the field with a low crop density will warm up and cool down faster than those with dense canopies. Differences in a wheat field's microclimate could have an inter-canopy variation of up to 7.5°C (Dammer, 2003). Considering the influence of canopy density on environmental conditions and thus disease distribution, the impact of crop density variation should be considered when monitoring crop health.

#### **2.1.4.3 Influence of rainfall on disease distribution**

Imathiu *et al.* (2008) concluded that the closer the plant part is to the soil surface, the higher the infection with fusarium species. It also showed a dilution effect of the inoculum away from the soil surface and potential sources of inoculum, possibly resulting from splash dispersal or from earlier inoculation where the disease concentration increases between inoculation and sampling. Moisture is often required for disease infection (De Vallavieille-Pope *et al.*, 1995; Rossi *et al.*, 2001; Xu, 2003). Therefore, when assessing the regional distribution of fungal disease, the impacts of local weather conditions should be a consideration.

#### **2.1.4.4 Influence of soil characteristics**

Balanced nutrition has an important role in determining plant resistance to diseases. Soil properties can have an indirect effect on disease pressure. For example, variable soil moisture will affect the crop microclimate, and an increase in nitrogen will increase the duration and green area index of the canopy (Stokes *et al.*, 1997; Sylvester-Bradley and Kindred, 2009).

Both macro (specifically nitrogen, potassium and phosphorus) and micro nutrients have an impact on the severity of fungal diseases. A lack of different nutrients will increase the crop's vulnerability to specific diseases. Nutrients provide building blocks for the synthesis of plant components (e.g., additional amino acids, proteins, chlorophyll), supporting growth, repair, and resistance from disease (Huber, 1980; Engelhard, 1989; Graham and Webb, 1991; Fageria and Baligar, 1997; McElhaney *et al.*, 1998). Plant growth promoting bacteria in the rhizosphere, can also increase the crops nutrient uptake (Amule *et al.*, 2017). When considering a method of disease control, it is important to acknowledge its interaction with nitrogen. A lack of nitrogen can leave a plant susceptible to pathogens that are specialised in infecting weak plants (Agrios, 1997; Snoeijers *et al.*, 2000). However, increases in nitrogen will increase the green area index and duration of the canopy (Stokes *et al.*, 1997; Sylvester-Bradley and Kindred, 2009). This subsequently affects the microclimate of the crop and the effect of suitable disease control (by fungicides or genetic resistance) and prolongs the canopy duration (Bryson *et al.*, 1997).

Studies observed that a high increase in nitrogen application within a wheat crop led to an increase in the disease severity due to prolonged green canopy (Leitch and Jenkins, 1995; von Tiedemann, 1996). Ishikawa *et al.* (2012) argue that there is an optimum N concentration for fungal infections to develop in wheat. The quality and nutritional content of whole grain

wheat stay the same between organic and conventional farming practices though a drop in yield may be seen under organic practices (Shier *et al.*, 1984; Mader *et al.*, 2002).

### **2.1.5 Current approach in fungal disease control**

Multiple fungal pathogens commonly co-exist within a cereal field. Fungicide treatments are often ‘*broad-band*’, and applied homogenously to the field, in an attempt to control the various established plant diseases, and pre-emptively protect plants from later occurring ones (Dammer and Ehlert, 2006). The recommended dosages of fungicide products given on the product labels usually have a high efficacy even when subjected to environmental conditions conducive to disease spread (FRAC, 2010). However, if there is a low disease pressure at the time of spraying, a lower dosage is often sufficient to get the same efficacy of disease control (Burth *et al.*, 1990). However, crop pathogens under conditions conducive to disease can spread very quickly, particularly if already established in the crop stand. A variable rate could be applied to the crop stand in response to areas of high and low disease pressure. In this instance, a sensing system of crop intensity would be valuable in optimising fungicide application.

### **2.1.6 Timings of fungicide applications**

Typically there are up to four timings of fungicide application to control yellow rust. T0 (Timing 0) is applied between growth stage 25 and 30 (Zadoks scale). Its application is usually a preventative in historically problematic fields, or if an early disease is observed. T1 (GS 31-33) and T2 (GS 37-39) are applied to keep the third, second and flag leaves healthy, as these heavily influence yield in wheat. The T3 application (GS 52-60) is usually an “ear wash”, usually to preserve the quality of the grain. T2 is commonly considered the most crucial application, and is the most frequently followed, due to the importance of maintaining

flag leaf health. T1 is considered secondary in importance followed by T3 and then T0 (HGCA 2008; Clark, 2016).

## **2.2 Techniques for disease detection**

There are several techniques applied for disease detection. The main methods currently used for disease recognition are based on visual assessments conducted by expert knowledge, molecular techniques, spectroscopy, volatile organic compounds (VOC's). There are direct and indirect methods of fungal disease detection. Direct methods include molecular techniques such as immunology-based methods and Polymerase chain reactions, whilst indirect methods rely on stress based symptom detection (through imaging and spectroscopy) and biomarker based detection (through plant metabolites, and volatile organic compound profiling) (Ray *et al.*, 2017).

Biosensors have been utilised for environmental monitoring. They are analytical devices, which incorporate a biological material for recognition of a concentration of an analyte and produce an electrical signal for the output (Tothill, 2001). In recent years, biosensors have been used for rapid detection in quantifying and diagnosing plant diseases in the field, detecting pathogens and aiding management decisions for the reduction of disease spread (Ray *et al.*, 2017). A few electrical biosensors are available, but have been advancing through research, for example, air sampling coupled with PCR (West *et al.*, 2008).

Molecular techniques are commonly used to confirm the presence of a disease pathogen within a crop stand. In 2004 there were approximately 100 commercially available test kits for the methods described above (Alvarez, 2004). These techniques are commonly based on liquid chromatography, Polymerase Chain Reaction (PCR) and Enzyme Linked Immunosorbent Assay (ELISA). Liquid chromatography separates a complex sample into

individual components through solid and liquid stages, while PCR detects a specific sequence of DNA, and ELISA is an immunological response to detect antigenic protein. As techniques have continued to develop in increasing the accuracy and the process speed, the number of commercially available molecular tests have continued to grow. Next-generation sequencing was introduced in 2005 and has rapidly developed in the area. DNA sequencing, such as that based on nanopores, is a rapidly growing industry, which is currently making advances in agricultural research. However, it still requires extensive sample preparation (Thate *et al.*, 2007). Moreover, PCR and real-time PCR detect and multiply a specific sequence of DNA (Schaad and Frederick, 2002; and Henson and French, 1993). Other techniques available and have applied in the field of crop disease detection include; immunofluorescence (IF), fluorescence *in-situ* hybridization (FISH), flow cytometry, and DNA microarrays, loop-mediated isothermal amplification (LAMP) assays and real-time Lamp assays (Prithiviraj *et al.*, 2004; Das, 2004; Saponari *et al.*, 2008; Ruiz-Ruiz *et al.*, 2009; Yvon *et al.*, 2009; Bekele *et al.*, 2011). Molecular techniques provide a reliable and thorough evaluation of plant pathogen presence. However, their application is generally limited due to them being time consuming, labour-intensive, expensive and require experienced operators. Commonly, they require preparation involving intricate procedures, equipment, and consumable pathogen specific reagents. Therefore, they cannot realistically be used in preliminary screening of a large quantity of samples (Sankaran *et al.*, 2010).

An alternative approach to the molecular techniques is the recognition and distinguishing of VOC's. Metabolic activities within plant components (e.g. leaves, stem, and seed) release VOC's. Species, physiological condition and stress, age and development stage, environmental conditions, disease pressure and any pest stress all dictate the VOC profile. A distinct volatile biomarker identifying a specific plant and disease from that of a nutrient or

environmental stress is necessary to overcome the natural variation in the VOC profile within a plant species, which can otherwise conceal the presence of stress and disease (Sankaran *et al.*, 2010). Potential exists for distinguishing between species of fungi based on characteristic volatile patterns (Magan and Evans, 2000). Indirect detection methods are where disease occurrence is predicted based on other factors, such as the density of the crop. Currently, the market offers a method, for fungal control, which is based on crop density measurement for optimising the application of a variable rate of fungicide (Dammer and Ehlert, 2006). This method contributes towards real-time control of fungicide application. Spatial information about crop density can be obtained by a CROP-Meter (Ehlert *et al.*, 2003). The CROP-Meter provides an indirect measurement of leaf area index (LAI) and plant mass using a pendulum, which passes through the plant matter. Authors reported an increase in savings from CROP-meter between 7% and 38% of fungicide costs depending on the heterogeneity of the field and the variability and extent of the LAI, which is attributed to a reduction in application rate in sparser areas. This success suggests an influence of LAI on the microclimate conditions within the crop. Studies have shown a correlation of leaf rust infection with temperature (Park *et al.*, 1992; Murray *et al.*, 1994; Dammer and Ehlert, 2006). However, LAI could be a reflection of multiple stresses at the same time e.g. water, nutrients, temperature, and diseases. Although Dammer and Ehlert (2006) report that variable-rate fungicide application based on plant biomass is fiscally successful, it did not improve grain quality or quantity. A direct method of specific disease detection could result in not only an economic benefit, from reduced fungicide input (like the biomass based CROP-meter), but also lead to an increase in yield, by reducing losses caused by disease presence.

The direct detection methods of crop diseases refer to those methods based on proximal sensors. These include classical imaging, visible and infrared spectroscopy, fluorescence

spectroscopy, and hyperspectral imaging. Optical sensing performs non-destructive measurements, allowing for repeated data acquisitions throughout the growing season without interfering with crop growth. The capability of two commercially available optical devices, the GreenSeeker RT100™ (Trimble, California, USA) and Crop Circle™ (Holland Scientific, Lincoln, NE USA), which are both active sensors for measuring relative greenness of crop, were used to discriminate levels of downy mildew (*Plasmopara viticola*) infection on detached grapevine leaves. A linear relationship between disease severity and output optical data was found from both sensors (Calcante *et al.*, 2012). Since optical methods based on a hyperspectral imager were used in this study, a detailed literature review on optical methods is provided in the following section.

### **2.2.1 Review of optical imaging techniques of crop canopies**

Originally, spectral images were sequentially taken, through a series of wavelength band pass filters; an image is collected at one wavelength at a time in a fixed field of view (FOV). If an object is moving or spectrally unstable, the results would be questionable. Integral spectral images require all the wavelengths to be recorded near simultaneously. Spectroscopy (based on the measurement of electromagnetic radiation reflectance of a targeted object) both passive (using an external light source), and active (using its own light source e.g., a halogen lamp), and conventional analyses have traditionally been used in the past to analyse individual samples under off-line (non-mobile) measurement conditions, which is time and resource consuming. Recent applications have been developing towards real-time (on-line, mobile) measurements for use *in-situ* and monitoring (Gilchrist, 2006). Spectroscopic technology has been successfully applied for plant stress detection such as water-stress and nutrient-stress detection (Sankaran *et al.*, 2010). Crop disease would ideally be identified in



spectroscopy by a wavelength range or index that is specific to a plant disease and is little affected by environmental conditions (Griffin and Burke, 2003).

Spectral reflectance in vegetation canopies is dependent on the illumination angle of the canopies' architecture and the radiative properties of the plants. The most important plant characteristics that determine reflectance are LAI and leaf pigmentation. Cell structure in the leaves reflects near-infrared light (from 700 to 1000 nm), greater foliage has a greater effect, and chlorophyll in plant leaves, absorbs visible light, particularly blue and red, (from 400 to 700 nm) (Campbell and Norman, 1998). Normalized Difference Vegetation Index (NDVI) measures the visible and near-infrared sunlight reflected by the crop. For the most effective method for measuring LAI, it can be first scanned by a proximal NDVI scanner and calibrated for LAI, which is conducted as a commercial practice. Canopy reflectance is dependent upon the structure and changes of the solar angle. Moreover, wind direction can also influence reflectance due to the orientation of the leaf (Rauner, 1976). A common approach is to include leaf angle and its effect on reflectance to derive an average leaf angle, developing it into a conical distribution and substituting it into a radiation transfer calculation (Monteith and Unsworth, 2008). In a homogenous canopy, the absorption of light is evenly distributed, making an ellipsoidal distribution adequate for use in many canopy types (Jones and Vaughan, 2010). Crop density through the use of a LAI measure is a traditional approach to calculate how much radiation is absorbed by the canopy. The overall reflectance in a dense canopy is less than a less-dense canopy, which is attributed to the light having passed through more than one reflection, due to a greater capacity for absorption and light scattering (Jones and Vaughan, 2010). The occurrences of sparse or irregular clouds affect the quality of light incidence, so that each spectral measurement should include a sunlight irradiance measurement (Jones and Vaughan 2010). Soil moisture can have a strong influence on

reflectance, related to an increase in absorption from wet soil, particularly in a sparse crop (Jones and Vaughan, 2010).

### **2.2.2 Application of visible and infrared spectroscopy in disease detection**

Visible and infrared (350-2500 nm) spectroscopy has been used as a rapid, non-destructive tool for detection of plant diseases. It is cost effective and a fast developing technology (Ramon *et al.*, 2002; Delwiche and Graybosch, 2002; Pontius *et al.*, 2005; Gomez *et al.*, 2006; Zhang *et al.*, 2008a,b; Guo *et al.*, 2009; Sundaram *et al.*, 2009). Visible and infrared spectroscopy can be applied to detect plant stress, damage and disease, and when applied to plant disease detection it is commonly used in combination (Malthus and Madeira, 1993; Polischuk *et al.*, 1997; Bravo *et al.*, 2003; Huang *et al.*, 2004; Spinelli *et al.*, 2006; Larsolle and Muhammed, 2007; Naidu *et al.*, 2009). The visible and infrared wavelengths of the electromagnetic spectrum provide maximum information on the plant's physiological stress state (Muhammed, 2002, 2005; Xu *et al.*, 2007). When specific wavebands indicative of a disease are known, they can be applied to detect the plant disease in a crop field (West *et al.*, 2003). It is even feasible to detect the presence of a pathogen before visible disease symptoms appear (Sankaran *et al.*, 2010).

Within the visible spectrum, the radiation reflectance from an environmentally stressed plant will increase. This is due to an increase in the incident light reflection from the leaf of a stressed plant (Cibula and Carter, 1992). Using leaf spectral reflectance at 500, 600 and 650 nm wavelengths, Sasaki *et al.* (1998) classified to 90% accuracy, diseased and healthy cucumber plants. Polischuk *et al.* (1997) used spectral reflectance measurements in making an early diagnosis of Tomato mosaic tobamovirus (ToMV) infection in Debney's tobacco (*Nicotiana debneyi*). Significant visual symptoms were noted three weeks after inoculation,

whilst a reduction in chlorophyll was detected by leaf reflectance after ten days. Similar results were also found on barley leaves with powdery mildew (Lorenzen and Jensen, 1989).

Spinelli *et al.* (2006) used a NIR-based technique under greenhouse conditions for detecting fire blight disease in pear plants. Results showed that the NIR technique alone was unable to detect and therefore, classify the infected and healthy plants. This was attributed to the small leaf scan area, which in this study was 2mm<sup>2</sup>. Spinelli *et al.* (2006) highlighted the importance of field of view, recommending that a large area of both the diseased and healthy plants should be considered.

Under field conditions, Naidu *et al.* (2009) used leaf spectral reflectance to identify viral infections causing leaf roll disease in grapevines (*Vitis vinifera L.*). To assess the ability and use of spectral reflectance in identifying a disease, discriminant analysis was performed to classify leaves into infected and non-infected leaves. The accuracy was reached a maximum of 75% for classifying leaf disease categories, when both the vegetative indices and individual reflectance bands (from the green, mid infrared and near infrared spectral regions) were used. The many successful studies on using the visible near infrared (vis-NIR) spectroscopy for disease detection confirm the possibilities of using this technology for early detection of diseases in field conditions. Moshou *et al.* (2011) introduced a prototype of an on-line and automated multi-spectral camera (using the 495, 747 and 837 nm wavebands) for the detection of early stages of disease in wheat crop, for both yellow rust and septoria. A review by Mahlein (2016), discusses the use of optical sensors for the recognition of crop disease, and the development process they must continue to undergo. Thomas *et al.* (2017) recorded both reflectance and transmittance imagery in barley crop inoculated with powdery mildew, finding that reflectance data outperformed transmission data in early disease

detection. They also highlight the significance of reflectance in the 580 to 650nm wavelengths, for disease detection.

Mahlein *et al.* (2010) studied the potential of three spectral indices (NDVI, Anthocyanin Reflectance Index (ARI) and modified Chlorophyll Absorption Integral (mCAI) between 400–1050 nm wavelengths, in early disease detection of sugar beets, concluding that multiple indices would be required for an accurate distinction of diseases. Results suggested that a distinctive differentiation of the three sugar beet diseases using spectral vegetation indices is possible using two or more indices in combination. Rumpf *et al.* (2010) used nine spectral vegetation indices (collected with hyperspectral reflectance) relating to physiological parameters in a support vector machine learning for the classification of specific diseases between healthy and inoculated sugar beet plants. Discrimination between healthy and diseased leaves was successfully done with an accuracy of 97%. These studies highlighted the potential accuracy of spectral indices in disease recognition.

Whilst previous research has studied spectral data collected in the field and from mobile systems, limited studies on on-line (mobile, and attached to a vehicle) captured spectral data, for crop disease detection could be found in the literature, which is a key gap for research to justify the novelty of this thesis.

### **2.2.3 Application of fluorescence spectroscopy in disease detection**

Fluorescence characteristics have been used for the last twenty years in vegetation studies. It is a method, where fluorescence is measured during excitation (Sankaran *et al.*, 2010). Excitation is where fluorescence occurs when a molecule absorbs light photons from the ultra violet visible light spectrum (200-900 nm). The molecule then rapidly emits light photons and

returns to its previous state. A small quantity of energy is lost in heat or movement within the molecule, so excitation energy is greater than the emitted energy. Belasque *et al.* (2008) commented on how the change in blue-green fluorescence and chlorophyll fluorescence of plants at excitation could be used not only to encompass the monitoring of stress on the physiological condition of the plant, but potentially be applied in detecting and discriminating disease stress from mechanical one (physical damage such as broken stems and damaged leaves).

A further advancement of fluorescence spectroscopy is fluorescence imaging. Instead of using a UV (10-400 nm) or halogen (320-1100 nm) light source for fluorescence excitation, a xenon (240-1100 nm with strong peaks at 750-1000 nm) light source is becoming more common. Fluorescence images are collected using a camera instead of a single spectrum, and at specified wavelengths the fluorescence is recorded with use of a charge coupled device (CCD) camera based system (Bravo *et al.*, 2004; Lenk and Buschmann, 2006; Chaerle *et al.*, 2007; Lenk *et al.*, 2007, Sankaran *et al.*, 2010). In fluorescence imaging, the commonly used regions of the electromagnetic spectra are blue (440 nm), green (520–550 nm), red (690 nm), far red (740 nm), and near infrared (800 nm) (Lenk and Buschmann, 2006; Chaerle *et al.*, 2007). Lenk *et al.* (2007) described multispectral fluorescence and its possible application in monitoring disease symptoms in plants, as well as use in fruit quality, leaf structure and photosynthesis.

In 2007, Poutaraud *et al.* (2007) measured the distribution of downy mildew (*P. viticola*) from grapevine stress induced secondary metabolites (stilbenic phytoalexins) using *in vivo* fluorescence measurements, finding that the high intensity of blue and violet fluorescence (near 390 nm) emitted by the metabolite could be used as a strong indicator for early onset of disease. Also using fluorescence measurements B elanger *et al.* (2008) showed that disease

could be quantified on detached leaves. Authors reported that the ratio between blue (near 440 nm) and green (near 520 nm) intensity between the healthy and diseased tissue was significantly different shortly after inoculation.

#### **2.2.4 Alternative spectral methods**

There are other imaging techniques that can be applied in the detection of plant diseases, such as x-ray imaging, terahertz spectroscopy, NMR spectroscopy and infrared thermography. These techniques are generally not applied to plant pathology as they are expensive to run, and so are not cost effective when compared to the potential of crop quality and yield increase (Sankaran *et al.*, 2010). However, Masri *et al.* (2017) using thermography, found that air temperature and fusarium infected ears were negatively correlated 6 days after inoculation.

#### **2.2.5 Hyperspectral and multispectral imaging**

Hyperspectral imaging has been developed dramatically from large, aircraft-based systems, to a more compact (UAV connected), economic tool that can be applied in monitoring, inspecting and diagnosing crop disease. A hyperspectral imaging instrument takes simultaneous (or near-simultaneous) spectral measurements along a series of spatial positions, giving both the shape and features of the spectral curve. The more spectral wavelengths observed (resolution of wavelength nm collected), the greater is the understanding of the sample quality (Gilchrist, 2006). Hyperspectral imaging is similar to multispectral imaging, but differs on having a broader range of wavelengths and spectral bands. One spectrum of different wavelengths per pixel, to form the hyperspectral image (Sankaran *et al.*, 2010). These wavelengths can include the visible (Vis), near infrared (NIR) and infrared (IR) regions. Each spectral region provides information about the plant. The reflectance at visible wavelengths is attributed to leaf pigmentation, with a low reflectance

indicating larger absorption of the light due to darker coloured leaves. This is attributed to the photosynthetic pigments of the plants leaves, governed by the abundance of chlorophyll, absorbing most of the light radiation (Gates *et al.*, 1965; Thomas and Gausman, 1977). Leaf reflectance in the NIR range is affected by the structure of the plant leaves (Gates *et al.*, 1965), and can be related to the leaf wax coating (Cameron 1970). The infrared wavelength reflectance provides information on the physiological condition of the plant. The wavelength measurement for the return of light intensity in hyperspectral imaging adds the multiple wavelengths (spectrum) with its spatial position to the brightness information of the spectral image, providing a rapid image-contrast, which would not be present in a conventional image approach (Huang *et al.*, 2007). Mahlein *et al.* (2013) used spectral vegetation indices to differentiate between diseases on sugar beet plants and three leaf diseases. Hyperspectral signatures of healthy and diseased sugar beet leaves were assessed, finding a single wavelength and normalised wavelength difference between 450 to 950 nm to be most relevant, with classification accuracies being between 85 and 92%.

In addition, the proximal applications of hyperspectral imaging have been successfully adapted to use in remote sensing (air and satellite) applications for a range of control, monitoring, and scientific applications. Remote-sensing based monitoring has also been used in agriculture for detecting invasive species (Sankaran *et al.*, 2010). Application of remote hyperspectral sensing techniques have been aimed at supporting real-time monitoring and inspection, in the identification, quantification and quality control (Gilchrist 2006; Sankaran *et al.*, 2010). Hyperspectral imaging is commonly used for monitoring food product quality and pharmaceuticals (Mehl *et al.*, 2004; Lee *et al.*, 2005; Yao *et al.*, 2005; Tallada *et al.*, 2006; Gowen *et al.*, 2007; Mahesh *et al.*, 2008; Sighicelli *et al.*, 2009). The application of the

technology for use in precision agriculture and plant disease detection has been gaining popularity (Okamoto *et al.*, 2009).

The use of hyperspectral imaging techniques for disease identification was reported by several researchers under non-mobile measurement conditions (Roggo *et al.*, 2003; Wu *et al.*, 2008). The early success in field studies for hyperspectral detection of yellow rust focused on detecting the presence of yellow rust (Bravo *et al.*, 2003; Moshou *et al.*, 2004). Bravo *et al.* (2003) detected early symptoms of yellow rust (*P. striiformis*) on winter wheat, using a quadratic discriminant model with an accurate classification accuracy of 92–98%. Moshou *et al.* (2004) successfully detected yellow rust disease in winter wheat by using spectral wavelengths of 460 to 900 nm, classifying individual plants into healthy and infected with accuracies between 92.0% and 99.4%. Moshou *et al.* (2005) combined hyperspectral reflectance and multispectral fluorescence imaging for the detection of yellow rust in winter wheat, through sensory and data fusion approach. The hyperspectral imaging data collection was obtained under ambient light conditions in winter wheat plots, whereas data for fluorescence images was obtained through UV excitation. Moshou *et al.* (2005) demonstrated that when sensory imagery was combined with quadratic discriminant analysis (QDA) based classification, the accuracy of healthy plants improved considerably to 97% from a prior 71–90%. Similarly, the classification accuracy of the diseased plants increased to 99.4% and healthy plants' classification further improved to 98.7% accuracy, when the self-organizing map (SOM)-based neural network was used for the plant classification. More recent attempts with hyperspectral and multispectral imagery are targeted to leaves rather than the canopy (Bock *et al.*, 2010). Huang *et al.* (2015) successfully provided quantitative assessment of yellow rust in winter wheat, through hyperspectral measurement of individual infected leaves. This research shows the potential application for hyperspectral imaging in the



application of disease recognition *in-situ* with resultant high accuracies. Whilst the use of hyperspectral imaging techniques for offline disease identification has been reported by several researchers there are few on-line (Roggo *et al.*, 2003; Wu *et al.*, 2008; Bock *et al.*, 2010).

Soil and canopy properties can vary on different scales and a greater resolution in data collection could be more sensitive to detecting the smaller scale changes (Raun *et al.*, 1998; Dhillon *et al.*, 1994; Rossi *et al.*, 2001; Dammer, 2003; Xu, 2003). Proximal spectral data can have a high resolution, an example of this is the on-line soil measurement platform created by Mouazen (2006), where a spectrophotometer (Tec5 Technology for Spectroscopy, Oberursel, Germany) was applied to a tractor travelling at a speed of 3 km h<sup>-1</sup> and collecting spectral soil data every second at 10 m parallel intervals. The resolution of data acquired, of course, depends on the method of application and the make and model of the camera. Satellite data, for example from Landsat 8, has a spatial resolution of 30 meters for the visible and NIR, which may not detect finer spatial changes. However, the benefit of the spatial and temporal coverage of satellite data may outweigh the negatives for certain applications (Lobell, 2013).

### **2.2.6 Optical imaging summary**

Optical imaging techniques don't require direct contact with samples, hence, they can be operated at a wide range of distances. Measurements are very rapid and can be performed at normal field vehicle operation speeds. Moshou *et al.* (2011) developed a prototype, tractor mounted, hyperspectral imager demonstrating the practicality towards field-scale disease detection of yellow rust.

Studies have considered proximal detection of diseased and healthy crops, by using sampled leaves/ears, a summary of which can be found in Table 2. They commonly found the most

discriminant wavelength intervals to be at green (near 500 nm) and near infrared (900 nm and 1600 – 2200 nm) (Naidu *et al.*, 2009). Polder *et al.* (2005) reported successful detection of fusarium in single kernels, by using both spectroscopy and imaging. Bauriegel *et al.* (2011) successfully recognised FHB infection at growth stages 71–85, using spectral ranges of 400–1000 nm, 500–533 nm (green), 560–675 nm (yellow), 682–733 nm (red) and 927–931 nm (red edge). Similarly, Delwiche and Kim (2000) successfully detected FHB in wheat kernels using a hyperspectral imager at 435 – 860 nm spectral range based on machine learning. Oerke and Steiner (2010) detected significantly higher temperature in fusarium infected ears, by means of an infrared thermography method for *in-situ* measurement of crop canopy.

Although certain nm wavelengths can be associated to disease recognition in the spectra, the use of a full spectral range generally produces a more reliable prediction model, due to interactions of different properties on the spectrum. This was confirmed for the Vis-NIR spectral analysis for the prediction of soil properties (Mouazen *et al.*, 2005). Therefore, the analysis of the full spectral range obtained in this study will be considered rather than focusing on specific wavebands.

Although many studies of the use of optical methods for the recognition of crop disease can be found in the literature, very limited research was published on the use of these optical techniques for on-line measurements.

**Table 2:** summary of different spectral applications to recognition of crop diseases and associated observations and accuracies

<b>Spectrum</b>	<b>Observations and success</b>	<b>Reference</b>
Visible spectrum	90% accuracy for detection of environmentally stressed plant due to an increased radiation reflectance.	Sasaki <i>et al.</i> (1998)
Hyperspectral wavelengths at 704, 1423 and 1926 nm	Quantitative assessment of yellow rust in winter wheat, through individual infected leaves with an R <sup>2</sup> of 0.88.	Huang <i>et al.</i> (2015)
Spectroscopy and imaging.	Successful detection of fusarium in single wheat kernels,	Polder <i>et al.</i> (2005)
Flourescence spectrum	The method could be applied in detecting and discriminating disease stress from environmentally attributed stress.	Belasque <i>et al.</i> (2008)
hyperspectral wavelength range of 435 to 860 nm	Fusarium head blight in wheat kernels through machine learning.	Delwiche and Kim (2000)
NIR spectrum	Unable to discriminate between infected and healthy plants. Recommend a larger area of view rather than a small one.	Spinelli <i>et al.</i> (2006)
NIR spectrum	Maximum of 75% accuracy for classifying leaf disease categories	Naidu <i>et al.</i> (2009)
Vis-NIR spectral range of 400–1000 nm	Discrimination of fusarium infected from healthy plants at growth stages 71–85 using principal component analysis (PCA)	Bauriegel <i>et al.</i> (2011)
NIR along with mid infrared spectrum	Noticed it was more reliable than NIR spectroscopy alone for earlier disease detection and identification	Sankaran <i>et al.</i> (2010).
Vis-NIR spectrum	Detecting early symptoms of yellow rust on winter wheat, with a discrimination accuracy of 92–98% between infected and healthy plants.	Bravo <i>et al.</i> (2003)
Vis- NIR spectrum	Discriminating healthy from infected individual plants with classifications accuracies ranged between 92.0% and 99.4%.	Moshou <i>et al.</i> (2004)
Infrared thermography	Detected significantly higher temperature in fusarium infected ears.	Oerke and Steiner (2010)
Hyperspectral imaging	Classification accuracy of the infected and healthy plants ranged between 98.7% and 71–90%.	Moshou <i>et al.</i> (2005)
Hyperspectral imaging and fluorescence	When sensory imagery was combined with quadratic discriminant analysis (QDA) based classification, the accuracy improved to 97% and 99.4% for healthy and infected plants.	Moshou <i>et al.</i> (2005)

### **2.3 Variability and yield limiting factors**

The spatial variability that exists in the majority of agricultural fields requires careful management with the aim to increase yield at reduced input cost and related environmental impacts. Conventional management of fields relies on homogeneous applications of external inputs. For example, current fertiliser applications are made based on an average soil sample collected per field or 1-3 per ha in the best scenario, which ignores within field variability. But, soil commonly varies within an agricultural field (Raun *et al.*, 1998; Dhillon *et al.*, 1994). Therefore, an alternative scenario of the conventional homogeneous application is required, namely, variable rate applications, by which the required amount of input (e.g., fungicide, fertilizer, etc) is applied in the right place where needed. Variable rate applications have seen a surge of innovative technologies in recent years, relying on input data from normalised difference vegetation index (NDVI), leaf area index (LAI), soil properties or a combination of these (Lowenberg-DeBoer and Aghib, 1999; Maleki *et al.*, 2008; Halcro *et al.*, 2013). Although precision management of farm external inputs is growing due to its economically beneficial results (Halcro *et al.*, 2013), quantifying the yield limiting factors is still a crucial question to be answered, before variable rate applications can be optimised to meet the exact crop needs.

One way to analyse and quantify the yield limiting factor is by adopting an input-output model that describes the relationship of the inputs (e.g. crop and soil properties, topography and terrain attributes, disease and weather conditions) and output (crop yield) of a system. This can be achieved for example by the implementation of machine learning, multivariate statistical analyses, random forest and others. Wang and Shen (2015) used classification and regression tree analysis to relate soil characteristics to yield. They classified low yield areas and could detect them based on just a few soil properties to an accuracy of 61.8%. Volterra

Non-linear Regressive with eXogenous inputs (VNRX) is a non-linear parametric model (Zhao *et al.*, 2013), which will be applied for quantifying the individual and collective influences of soil properties on yield variability, for the first time in this thesis.

Parametric models have attracted more and more interest recently due to their limited reliance on field calibration, less requirement of sample size and their transparent assessment of model performance. Parametric modelling in agriculture was used to assess soil erosion as correlated to landslide events (Pradhan *et al.*, 2012), to assess land size for a maximum crop output (Färe *et al.*, 1997), water retention (Timlin *et al.*, 2004) and soil respiration (Chen *et al.*, 2011). However, very few studies on the use of parametric modelling to predict yield can be found in literature. The first successful application of parametric modelling to predict crop yield was reported by Mkhabela *et al.* (2011), where NDVI was the sole input. Authors reported difficulties associated with removing non-target crop NDVI obtained from the earth observation satellite imagery (with a resolution of 250m). Huang *et al.* (2013) developed a regression model to predict rice yield based on a direct empirical relationship established between NDVI and rice yields, achieving some success. Whilst the relationship between nutrients in soil and yield is widely understood, there are areas of interest where high sampling resolution data (obtained with advanced remote and proximal sensing technologies) could be applied.

## **2.4 On-line measurement of soil properties**

In addition to crop disease and crop NDVI measurements, soil property data was also collected using on-line measurement systems. Kuang *et al.* (2012) stated that among the different sensing techniques for soil properties, the most applicable one for the field under both non-mobile and on-line mobile conditions is vis-NIR spectroscopy. It has the potential to provide a rapid, cost effective and accurate analysis of multiple soil properties. The

technology can be mounted on a tractor for on-line sensing, capable of collecting high sampling resolution data e.g., >500 readings per ha (Mouazen, 2006; Maleki *et al.*, 2008; Kuang and Mouazen, 2011a; 2011b). The Mouazen (2006) internationally patented system was proven by many publications to enable the measurement of key soil properties with appreciable accuracy (Mouazen *et al.*, 2005; Kuang and Mouazen, 2012; Kuang *et al.*, 2015). By utilising such a system, a greater understanding of the spatial distribution of soil properties and their impact and correlation on crop growth and yield will be possible. This on-line soil sensor will be a key contributor for the delineation of management zones for selective harvest and fungicide application to be investigated in this thesis.

## **2.5 Literature conclusions; research gaps**

The literature review confirmed that there is a need to develop and test a proximal sensor for on-line measurement of crop diseases, e.g., yellow rust and FHB. The sensor should enable the collection of high sampling resolution data on these diseases to enable site specific application of fungicide or selective harvest.

The literature review has highlighted the impact of soil, canopy properties, and microclimate conditions, on the risk of infection. It is more effective to know the location and severity of the disease, rather than estimating the overall average for the field (Dammer, 1999; Fleischer *et al.*, 1999). On-line soil and crop data and micro-climatic conditions when fused with quantitative data on crop disease may not only be beneficial for variable rate fungicide application and selective harvest, but predicting future infection patterns.

There is a need for high sampling resolution data on soil characteristics, crop growth, diseases, and microclimate conditions to enable understanding for managing variability that exists in most agricultural fields. These layers could be applied to a non-linear model to

explore the yield limiting factors, by quantifying the individual and collective influences of these layers on the yield variability within a field.

## **3 Quantification of yield limiting factors**

### **Chapter Synopsis;**

This chapter discusses the implementation of a new non-linear parametric modelling approach for quantifying the yield limiting factors, by estimating the individual contributions and interactions of soil properties to NDVI and yield.

Chapter 3 is split into two subchapters;

3.1 A new non-linear parametric modelling method to quantify influence of soil properties on crop yields – Methodology.

3.2 A new non-linear parametric modelling method to quantify influence of soil properties on crop yields - Application to on-line soil data.

This modelling approach is further explored with the inclusion of disease data (e.g., fusarium head blight (FHB) and late yellow rust) with some key soil properties (TN, OC, MC, and CEC). Results of this further analysis can be found in Appendix A.



### **3.1 A new non-linear parametric modelling method to quantify influence of soil properties on crop yields: Methodology**

#### **Abstract**

This paper aims at introducing a new non-linear parametric modelling technique based on a Volterra Non-linear Regressive with eXogenous inputs (VNRX) model to study and quantify the effect of soil properties on crop yield. Two versions of VNRX were implemented, namely, VNRX-LN, accounting for both the linear and non-linear variability in the system, and VNRX-L, accounting for linear variability only. The performance was compared with a non-linear random forest (RF) model to predict oilseed rape (2013) and barley (2014) yields in one field in Germany. Soil samples were collected in 2013 and analysed in the laboratory for ten properties. These were used as system inputs for the three models and crop yield data of 2013 (oilseed rape) and 2014 (wheat) were used as the system outputs. Results demonstrated the individual and total contribution of soil properties on crop yield to vary throughout different cropping seasons. Both VNRX-LN and RF models outperformed the VNRX-L model (attributed to the ability of these models to account for non-linearity) and explained up to 55.6% (2013) and 45.8% (2014) of yield variation for the RF model and 52.2% (2013) and 50.6% (2014) of yield variation for the VNRX-LN model. Although VNRX-LN and RF models almost equally performed for yield prediction, the RF models were more consistent with the soil properties ranking for describing the yield variability, indicating a greater stability. The VNRX-LN accounted for slightly more variability over the two years, though the ranking of properties was more variable, which could be attributed to other parameters that have not been involved in this study.

## **Keywords**

Yield prediction; yield limiting factors; soil fertility; random forest, VNRX.

### **3.1.1 Introduction**

Quantification of soil related yield limiting factors is essential for site specific management of farm resources and for crop yield forecast. However, the estimation of these limiting factors is not a straightforward process, as many affecting parameters exist in a very complex system, consisting of soil and associated micro- and macro-variability, microclimate, topography, land use and others. Whilst the relationship between nutrients in soil and yield is widely understood, there is little work using high sampling resolution data obtained with advanced on-line proximal sensing technologies. Modelling approaches to predict crop yield have been introduced (Hole *et al.*, 2005), which included statistical, process-based numerical, machine learning and parametric modelling approaches. Although statistical models are more suitable for large spatio-temporal scales, they can hardly extrapolate beyond historical extremes (Hahn, 2009). Process-based models (Fourcaud *et al.*, 2008; Thorp *et al.*, 2014) emulate the main processes of crop growth and development. These models are typically developed and tested using experimental trials, and thus offer the distinct advantage of leveraging decades of research on crop physiology and reproduction, agronomy, and soil science, among other disciplines. These models also require extensive input data on cultivar, management, and soil conditions that are unavailable in many parts of the world. Apart from overfitting issues, machine learning modelling techniques were successfully implemented recently to predict wheat yield using proximal sensors (Pantazi *et al.*, 2016).

Parametric models have attracted more and more interest recently due to their limited reliance on field calibration, less requirement of sample size and their transparent assessment of model performance. Very few studies on the use of parametric modelling to predict yield can be found in literature. Assuming that regression analysis falls under parametric modelling, the number of studies on prediction of crop yield suddenly increases. Palm (1997) produced the simplest form of parametric modelling to estimate crop yield, in the form of a regression of yield against rainfall. In areas where water is a limiting parameter, about 46% of yield variability was attributed to rainfall. A simple parametric simulation of maize yields using the standard Food and Agriculture Organisation (FAO) methodology was produced by Rijks *et al.* (2003), where 73.75% of the yield variability between separate years was attributed to evapotranspiration.

The non-linear auto-regressive moving average model with eXogenous inputs (NARMAX) is a parametric modelling method introduced by Billings *et al.* (1989) and one of the most popular classes of non-linear system identification methods for a complex system, where the inner structure of the underlying system is unknown but only input and output observational data are available. Comparing with machine learning methods, one of the advantages of the NARMAX model is transparency, which means that it can be written down, can be related to known and existing models in the literature, and also can be analysed in frequency and other domains. This characteristic is attractive for a studying brain, climatic change or an agriculture system that is a typical input-output system with an unknown inner structure, because it not only allows further frequency analysis or statistical analysis based the identified model, but also is easily understood and interpreted. A Volterra non-linear regressive with eXogenous inputs (VNRX) is a special case of NARMAX that has been recently introduced. Although it has been successfully applied in brain signal analysis (Zhao

*et al.*, 2012; Sarrigiannis *et al.*, 2014), climate change (Bigg *et al.*, 2014; Zhao *et al.*, 2016a) and non-destructive tests (Zhao *et al.*, 2017), its application in agriculture is novel. This non-linear model has potential to understand how soil properties and other factors affecting the crop yield due to its capability to reveal non-linear information whilst linear modelling methods cannot, or would produce misleading results.

This paper aims at (1) exploring the potential of the new proposed VNRX models to quantify soil related yield limiting factors and understand the dependence among crop yield and soil properties within a field, (2) comparing between VNRX with random forest (RF) models for identifying and quantifying the most influencing soil properties that affect yield variability. All methods were tested in one arable field in Germany, throughout two cropping seasons in 2013 and 2014 with oilseed rape and wheat grown, respectively.

### **3.1.2 Material and methods**

#### **3.1.2.1 Study site and data collection**

The study site was an arable field located in Premslin near Rostock in Germany (Figure 4), with 11°46'2.00" E latitude and 53°6'58.00" N longitude according to the Universal transverse Mercator (UTM) system. The field is about 33 ha in area, with an average annual rainfall of 591 mm, an average temperature of 16.5 °C from May through to August in the 2013 and 2014 cropping seasons. The soil type according to FAO soil classes is a homogenous Dystric Cambisol with humic loam texture, on a sandstone rock (FAO code Bd67-2b). Oilseed rape and barley were cultivated during the experiment in 2013 and 2014 cropping seasons, respectively.

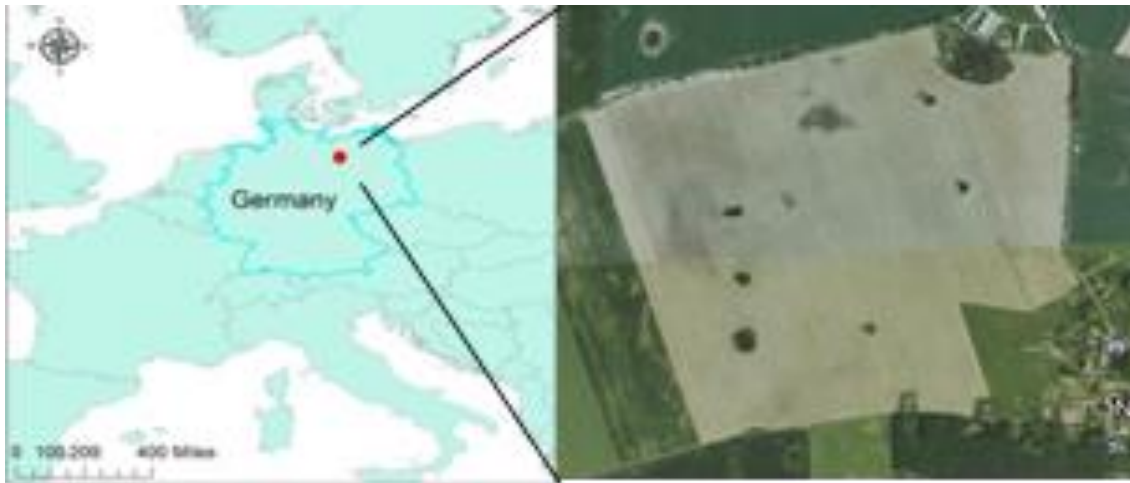


**Figure 4:** Field location in Premslin near Rostock in Germany, where soil samples and yield data were recorded in 2013 and 2014.

A total of 140 soil samples were collected after the harvest of the previous crop in 2013 (Figure 4). About 700 g of each soil sample was prepared as a mixture of soil collected over 1.5 m distance at about 0.15 m depth. An equal gap between neighbouring sampling lines of 12 m was selected. A differential global positioning system (DGPS) (EZ-Guide 250, Trimble, California, USA) with sub-metre accuracy was used to record the position of each soil sample. Soil samples were placed into tightly sealed plastic bags to hold field moisture, and stored in a refrigerator at 4 °C, until laboratory analysis. Yield data were collected in 2013 and 2014, at different spatial resolutions to that of the soil samples using the on-board yield sensor of the farmer's combine harvester (New Holland, CX8070 model).

### **3.1.2.2 Laboratory analysis and development of calibration models of soil properties**

Each sample was air dried at a temperature not greater than 30 °C, grinded and sieved with a 2 mm sieve. Samples were then subjected to chemical analyses to determine selected soil parameters that were likely to be limiting the yield of the oilseed rape and barley. These parameters are pH, soil moisture content (MC), cation exchange capacity (CEC), organic

carbon (OC), total nitrogen (TN), and the available cations sodium (Na), potassium (K), calcium (Ca), magnesium (Mg), and available phosphorous (P). pH was measured potentiometrically on a suspension of soil to water ratio (1:2.5) under a controlled temperature environment (DEFRA, 2010). MC was determined by oven drying of soil samples at 105 °C for 24 h. To determine CEC, soil was saturated with Sodium Acetate (pH 7.0), and the excess acetate removed by washing with water and ethanol. The sodium ions absorbed onto the cation exchange sites of the soil were displaced with 1.0M Ammonium Acetate, and their concentration was determined using a Flame Photometer (Chapman 1965). OC was determined according to the British Standard BS 7755 Section 3.8:1995 using a combustion method, which is identical to ISO 10694:1995. TN was determined by the Dumas method, where soil samples are heated to 900 °C in the presence of oxygen gas as described by British Standard BS EN 13654-2:2001. Exchangeable K, Na, Ca and Mg were extracted with 1.0 molar Ammonium Nitrate (MAFF/ADAS, 1986), and their concentrations in the extract were determined by Agilent 240 FS AA atomic absorption spectrophotometry (Agilent Technologies, Inc. USA). Available P was determined by extraction from the soil at 20 °C by shaking with 0.5 M sodium bicarbonate solution at pH 8.5 and the concentration was determined by an ascorbic acid method (Olsen, 1954).

### **3.1.2.3 Data processing**

Yield and ten soil data layers were first fitted to semi-variograms using Vesper software developed by the Australian Centre of Precision Agriculture (Sydney, Australia) to typify the spatial variation. After satisfactory semi-variogram selection, semi-variogram parameters were transferred into ArcGIS (Esri, USA) software to perform ordinary kriging to predict values of un-sampled positions. The interpolated (through kriging) data layers were then converted into a common 5 m<sup>2</sup> raster grid in ArcGIS (Esri, USA) in order to assist data fusion

(Frogbrook and Oliver, 2007). The resulting 5 m<sup>2</sup> raster squares of the layers were converted into a common grid of points by extracting the value at the midpoint of each raster square. These steps ensured that all layers consisted of common sets of 5 m<sup>2</sup> grid points, which is essential for running different spatial analyses. This method allowed data from a diverse range of soil and yield surveys, measured at different resolutions, to be merged (Khosla *et al.*, 2008). However, it is worth to mention that transferring information of 5 m<sup>2</sup> raster to a point would introduce unavoidable error to the spatial distribution of data. The different soil and crop data were subjected to the linear and non-linear VNRX, and RF modelling methods, detailed in the following sections.

#### 3.1.2.4 Random forest method

Random forest is a non-linear classification and regression algorithm developed first by Breiman (2001), which can be described as follows:

Suppose we have a calibration set  $C = \{C_1, \dots, C_n\}$  with  $C_i \equiv (x_i, y_i)$  and an independent test case  $C_0$  with predictor  $x_0$ , the following steps can be carried out:

- 1) Sample the calibration set  $C$  with replacement to generate bootstrap resamples  $B_1, \dots, B_M$
- 2) For each resample  $B_m, m = 1, \dots, M$ , grow a regression tree  $T_m$ .
- 3) For predicting the test case  $C_0$  with covariate  $x_0$ , the predicted value by the whole RF is obtained by combining the results given by individual trees. Let  $\hat{f}_m^*(x_0)$  denote the prediction of  $C_0$  by  $m^{\text{th}}$  tree, the RF prediction for regression problems can then be written as:

### Equation 1

$$\frac{1}{M} \sum_{m=1}^M \hat{f}_m^*(x_0)$$

- 4) Parallel to the calibration step, RF performs an internal cross-validation by dividing the calibration set into in-bag and out-of-bag (OOB) sets (2/3 as in-bag set and the remaining as OOB). The number of variable per level ( $mtry = 1$ ), size of nodes ( $nodesize = 20$ ) and number of trees ( $ntree = 500$ ) parameters are optimized by minimizing the aggregate error rate of the OOB set (RMSE\_OOB) (Breiman, 2001; Xin *et al.*, 2012). The accuracy of a random forest's prediction can be estimated from these OOB data, by using the following equation:

### Equation 2

$$OOB - MSE = \frac{1}{n} \sum_{i=1}^n (y_i - \overline{\hat{y}_{OOB}})^2$$

Where  $\overline{\hat{y}_{OOB}}$  is the average prediction for the  $i^{\text{th}}$  observation from all trees, for which this observation has been OOB (Grömping, 2009).

Breiman (2002) suggested reduction in mean square error (MSE) (known as variable importance scores) when permuting a variable  $X_j$  called “MSE reduction, and decrease in classification accuracy after permuting  $X_j$  over all trees”. Permutation-based MSE reduction has been adopted as the state-of-the-art approach for measuring the importance of a variable by various authors (Ishwaran, 2007; Genuer *et al.*, 2008; Strobl *et al.*, 2008). According to Grömping (2009), this is determined as follows: for tree  $t$ , the OOB mean squared error is calculated as the average of the squared deviations of OOB responses from their respective predictions:



### Equation 3

$$\text{OOB} - \text{MSE}_t = \frac{1}{n_{\text{OOB},t}} \sum_{\substack{i=1: \\ i \in \text{OOB}_t}}^n (y_i - \hat{y}_{i,t})^2$$

where the  $\hat{y}$  indicates predictions,  $\text{OOB}_t = \{i : \text{observation } i \text{ is OOB for tree } t\}$ , that is, summation is over OOB observations only, and  $n_{\text{OOB},t}$  is the number of OOB observations in tree  $t$ . If regressor  $X_j$  does not have predictive value for the response, it should not make a difference if the values for  $X_j$  are randomly permuted in the OOB data before the predictions are generated. The  $\text{OOBMSE}_t(X_j \text{ permuted})$  can be calculated using;

### Equation 4

$$\text{OOBMSE}_t(X_j \text{ permuted}) = \frac{1}{n_{\text{OOB},t}} \sum_{\substack{i=1: \\ i \in \text{OOB}_t}}^n (y_i - \hat{y}_{i,t}(X_j \text{ permuted}))^2$$

Then, the difference  $\text{OOBMSE}_t(X_j \text{ permuted}) - \text{OOBMSE}_t$  is calculated for each variable  $X_j$  in each tree  $t$ , based on one permutation of the variable's out-of-bag data for the tree. For the complete forest, the MSE reduction according to regressor  $X_j$  can be calculated as the average over all  $n_{\text{tree}}$  trees of these differences (Grömping, 2009). The values of calculated MSE should be always between 0% and 100%. All RF models were performed within R program using the software package Random Forest Version 4.6-12 (Liaw and Wiener, 2015), based on Breiman and Cutler's Fortran code (Breiman, 2001). Results were evaluated by calculating the MSE reduction in RF to indicate the contribution of each soil property on crop yield in 2013 and 2014. Values of EMS range always from 0% to 100%. The larger EMS is, the higher dependence is between this term and the output.

### 3.1.2.5 Parametric modelling

In this study, a simplified VNRX model, also known as non-linear finite impulse response (NFIR) model, is proposed to understand and quantify the correlation between soil properties and crop yield. This model has been commonly used to represent a multi-inputs and single-output system, and can be expressed as:

#### Equation 5

$$y = f(u_1, u_2, \dots, u_r) + \varepsilon$$

where  $r$  is the number of the system inputs,  $f$  is some unknown linear or non-linear mapping, which links the system output  $y$  to the system inputs  $u_1, u_2, \dots, u_r$ ;  $\varepsilon$  denotes the model residual.

A commonly employed model type to specify the function  $f$  in Eq. (5) is a polynomial function (Chen and Billings, 1989; Wei *et al.*, 2004), which can be expressed as follows:

#### Equation 6

$$y = \theta_0 + \sum_{m=1}^N \theta_m \phi_m + \varepsilon$$

where  $\phi_m$  is the  $m^{th}$  model term generated from all input vectors;  $\theta_m$  is the corresponding unknown parameters;  $N$  is the total number of potential model terms. Note that  $\phi_m$  is, in general, non-linear. Considering a system with two inputs  $u_1$  and  $u_2$ , a second order polynomial function can be written as:

#### Equation 7

$$y = \theta_0 + \theta_1 u_1 + \theta_2 u_2 + \theta_3 u_1^2 + \theta_4 + \theta_5 u_1 u_2 + \varepsilon$$

Comparing with existing linear parametric methods, the proposed method accommodates the non-linear relationship between the inputs and the output by introducing terms  $\{u_1^2, u_2^2, u_1 u_2\}$ . Note that the candidate term  $\phi_m$  in Eq. (6) can be any linear or non-linear relationship among inputs. This paper will compare the performance of a model accounting only for linear terms, designated as VNRX-L, with a model accounting for both linear and non-linear terms, named VNRX-LN throughout this paper.

The next step is to estimate the parameters  $\theta_m (m = 0, 1, \dots, 5)$  based on the observations  $\{y, u_1, u_2\}$ . The procedure begins by determining the structure, or the important model terms, using the orthogonal least squares (OLS) estimation procedures. It determines which dynamics and non-linear terms should be included in the model by computing the contribution that each potential model term makes to the variation of the system output. The model is to be built up term by term in a manner that exposes the significance of each new term that is added. Once the structure of the model has been determined, the unknown parameters can be estimated, and the procedure of model validation can ensure the model is adequate. In this paper, a routine called adaptive-forward-orthogonal least squares (AFOLS) was employed not only to determine the model structure but also to estimate the unknown parameters. More detailed explanation of this method can be found in Zhao *et al.* (2012).

Finally, the performance of the VNRX models in the prediction of yield was evaluated. This was done by considering the value of error reduction ratio (ERR) for each selected term calculated from AFOLS that measures the percentage this term contributes to the system output (Zhao *et al.*, 2013). Values of ERR range always from 0% to 100%. The larger ERR is, the higher dependence is between this term and the output. It is, therefore, a very important index to indicate the importance of each term to the output.

To calculate the contribution of each input variable to the output, the sum of ERR values of all selected terms, denoted as  $SERR$ , is calculated by

**Equation 8**

$$SERR = \sum_{i=1}^N [err]_i$$

to describe the percentage explained by the identified model to the system output, where  $N$  denotes the number of the selected terms. If the considered inputs can fully explain the variation of system output, the value of  $SERR$  is equal to 100%. It is an indicator of model performance and uncertainty. The contribution of the  $i^{th}$  input variable to the variation of the system output, denoted as  $ERRC_i$ , is defined as the sum of ERR values of the terms that include this input variable. Because some selected terms may involve more than one input variable due to non-linearity, the sum of  $ERRC_i$  for all input variables can be greater than  $SERR$ . To overcome this problem, the value of  $ERRC_i$  is written as:

**Equation 9**

$$ERRC_i = \frac{\sum_{j=1}^N ([err]_j | u_i \in \phi_j)}{\sum_{p=1}^r \sum_{j=1}^N ([err]_j | u_p \in \phi_j)} \times SERR$$

The value of  $ERRC_i$  should be always between 0% and 100%.

### 3.1.3 Results and discussion

In this work, the ten laboratory measured soil properties (i.e., TN, OC, Ca, CEC, Na, Mg, K, pH, P and MC) were normalised and used as inputs to the VNRX and RF models' establishments, whereas the model output was crop yield. The aim was to investigate the contribution of each soil property on crop yield through two different cropping seasons. Whilst the soil properties were collected only in 2013 the yield was collected in 2013 and

2014, it is assumed that soil properties may have decreased or increased in the time. The methods used are not process based, and do not consider any temporal patterns or outline any expected behaviours as input parameters, so the outputs cannot be considered interpretable to other circumstances. However, they were applied in this study to understand yield variability within a field at a given time. The knowledge gained is limited to its application in this field and year. The study was designed to assess the models potential to explain yield variability, particularly in non-homogenous fields.

### **3.1.3.1 Soil and yield data analysis**

Results of the descriptive statistical analyses for soil properties are shown in Table 3, where soil data were collected in 2013. The experimental soil ranges from strongly acidic to slightly alkaline (pH = 5.4 to 7.7), with a mean neutral pH value of 6.63. The pH and OM conditions were appropriate for the growth of oilseed rape and wheat (DEFRA, 2010), with a potential pH effect on the P and Mg availability for smaller pH ranges than 6.5 (Truog, 1946, Murrmann and Peech, 1969; Murrmann *et al.*, 2005). Exchangeable K, Mg, Na, and Ca were considered low for both crops, with mean values of  $0.5 \text{ mg l}^{-1}$ ,  $0.29 \text{ mg l}^{-1}$ ,  $0.06 \text{ mg l}^{-1}$  and  $2.86 \text{ mg l}^{-1}$ , respectively. Available P, CEC and TN were of low concentrations for oilseed rape and wheat growth (DEFRA, 2010). P was consistently one of the largest contributors to yield variation, this could be due to it being present in low concentrations, compared to the crops ideal requirement (e.g., for oilseed rape the target soil index is 16-25 mg/l). However, it was variable through the field from 9.54 mg/l to 1.34 mg/l (HGCA, 2014). These low concentrations indicate these soil properties to be limiting of crop growth and yield.

**Table 3:** Statistics of measured soil properties of the 140 soil samples used as input data into the three models.

	TN	pH	P	OC	MC	K	Mg	Na	Ca	CEC
Max	0.141	7.7	9.54	1.29	12.5	1.33	0.63	0.13	5.17	11.7
Min	0.058	5.4	1.34	0.59	6.15	0.14	0.13	0.025	1.47	6.3
Mean	0.08	6.63	2.69	0.83	8.19	0.5	0.29	0.06	2.86	8.45
SD	0.014	0.467	0.93	0.15	1.12	0.23	0.089	0.016	0.665	1.04

TN is total nitrogen, OC is organic carbon, and MC is moisture content which are all in % of dry matter; K is exchangeable potassium in mg/l; P is extractable phosphorous in mg l<sup>-1</sup>; CEC is cation exchange capacity in mg100g<sup>-1</sup>; Ca is calcium in mg l<sup>-1</sup>; Na is sodium in mg l<sup>-1</sup>; Mg is magnesium in mg l<sup>-1</sup>; and pH the log measurement of acidity.

The semi-variogram analysis of yield 2013 and 2014 shows the best fit of yield data to be obtained with spherical models with negligible sums of squares error (SSE) values (Table 4). Spherical models were selected as they best fit the empirical data. Spherical models are most suitable for data with a progressive decrease in spatial autocorrelation. Selection of a suitable model fit is important as the steepness of the curve (fitted to the empirical data) will impact the influence of the closer data points.

**Table 4:** Semi-variogram model parameters of yield maps. The best fit was achieved with spherical models for each, showing nugget ( $c_0$ ), sill ( $c$ ), range ( $r$  m), proportion ( $C_0/ C$  %), and the sum of square error (SSE)

Variable	$c_0$	$c$	$r$ (m)	$(c_0/ c)$ (%)	(SSE)
Yield 2013	0.0021	0.007	24.38	30.0%	0.0001
Yield 2014	0.0039	0.009	40.98	43.1%	0.0001

$c_0$  is nugget variance,  $c$  is sill,  $r$  is range and SSE is sum of squared error.

The ratio of nugget variance to sill variance is an important parameter to quantify short-distance autocorrelation or the degree of spatial dependency for a variable (Cambardella *et al.*, 1994; Chang *et al.*, 2014). Cambardella *et al.*,(1994) defined three categories of spatial dependency of high, moderate, and weak with ratios of less than 25%, between 25% and 75%, and greater than 75%, respectively. In this study, variations of the ratio of nugget variance to sill variance of yield 2013 and 2014 are of moderate spatial dependence, with ratios of 30.0% and 43.1%, respectively. Ranges of spatial dependence vary from 19.49 m (yield 2013) to 0.98 m (yield 2014), which in 2013 is wider than the sampling interval of 12 m and confirming the effectiveness of geostatistical analysis adopted in this study (Chang *et al.*, 2014). Although the yield data in 2014 demonstrates smaller spatial variability than that in 2013, which can be attributed to different crops and agricultural inputs (fertilisers, pesticides and seeding rate), a different spatial distribution pattern across the study area can be observed (Figure 5).

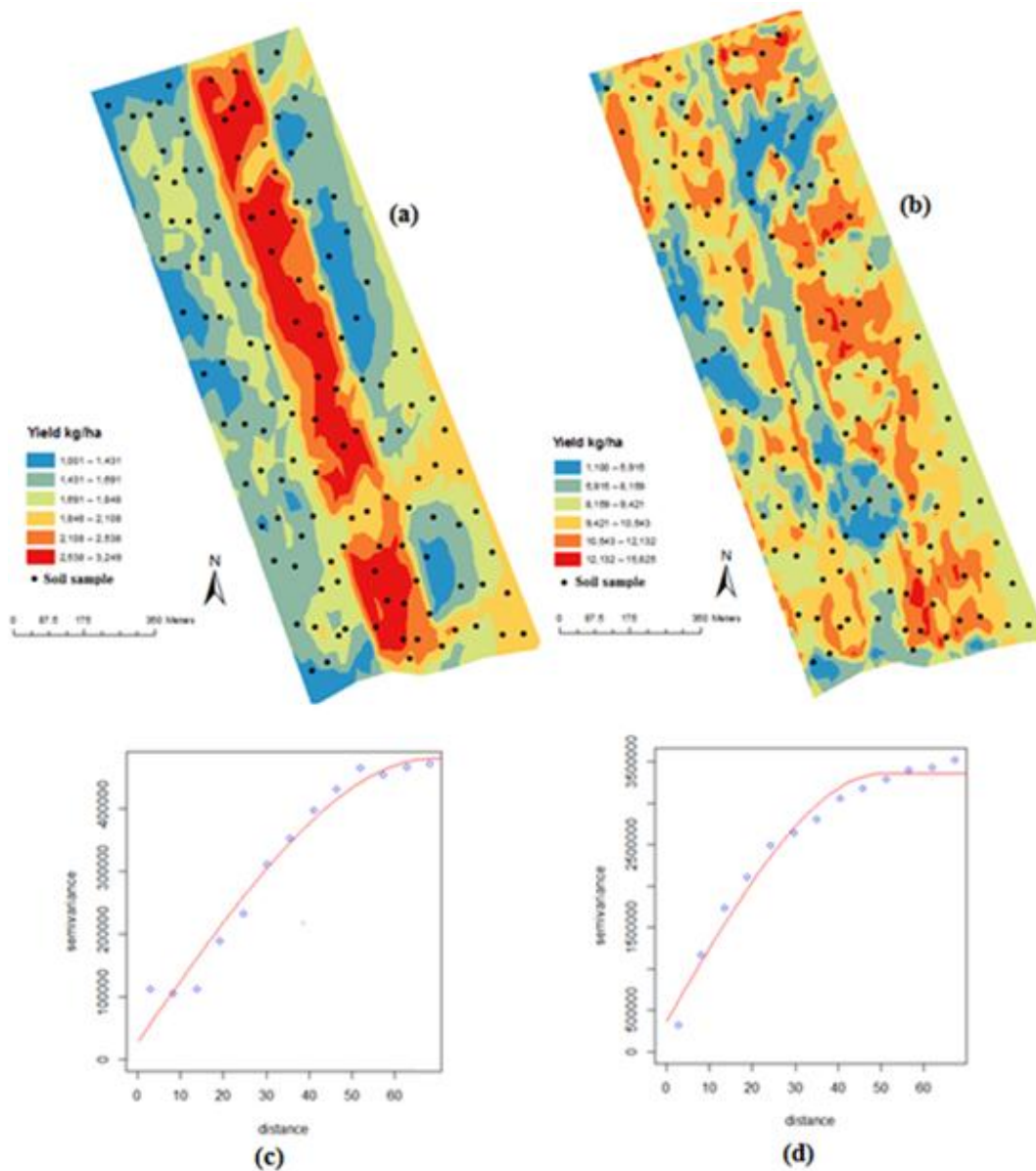


**Figure 5:** Yield maps of oilseed rape and barley measured in 2013 (a) and 2014 (b), respectively, and developed with ordinary kriging based on spherical model (shown by the line). Semi-variograms fit to the lag points which are distance classes into which pairs of locations are grouped (shown by the small circles), with a sum of square error (SSE) value of 0.0001 and 0.0001 for (c) and (d), respectively. Figure also shows position of 140 soil samples used in this study.



### 3.1.3.2 Linear correlation

Examining Pearson's correlation coefficient ( $r$ ) values between pairs of soil properties reveals few linear correlations, with the strongest correlation unsurprisingly recorded between OC and TN ( $r = 0.945$ ), which is in line with other reports (Carlyle, 1993; Kuang and Mouazen, 2011). Other reasonable correlations can be observed between Ca and pH ( $r = 0.716$ ), although those calculated between OC and MC, TN and Ca, TN and MC are of smaller  $r$  values ranging between 0.507 and 0.559. Another interesting but negative linear correlation ( $r = -0.656$ ) is calculated between pH and CEC, explaining that pH decreases with increasing CEC, which is true as CEC represents the soil's ability to hold positively charged ions e.g., exchangeable cations (Hazelton and Murphy, 2007).

The  $r$  values indicate no linear correlation could be observed between the ten soil properties and yield in 2013 and 2014 (Table 5). The highest correlation of 0.239 is calculated between OC and yield of 2013, which makes P the second highest correlated at 0.192, which for single properties is very reasonable, as they are both influential soil fertility parameters (Tiessen *et al.*, 1994; Baligar *et al.*, 2001; Agegnehu *et al.*, 2016; Zhang *et al.*, 2016). TN, Na, and pH also make a slight correlation to yield estimation in the two years. However, collectively the contribution is very limited and does not offer much explanation to yield variability, in either of the years. This indicates the system complexity and non-linearity that cannot be explored or quantified by simple linear relationships.

**Table 5:** Pearson correlation (*r*) between soil properties and yield of 2013 and 2014.

	Ca	CEC	K	MC	Mg	Na	OC	P	pH	TN	Yield13	Yield14
Ca	1.000											
CEC	-0.018	1.000										
K	-0.096	0.187	1.000									
MC	0.442	0.101	0.192	1.000								
Mg	-0.040	0.197	0.111	0.168	1.000							
Na	0.103	-0.052	0.350	0.235	-0.023	1.000						
OC	<b>0.507</b>	0.150	0.004	<b>0.510</b>	0.189	-0.033	1.000					
P	-0.238	0.180	0.074	-0.360	-0.219	0.004	-0.131	1.000				
pH	<b>0.716</b>	<b>-0.656</b>	-0.076	0.285	-0.124	0.140	0.297	-0.300	1.000			
TN	<b>0.564</b>	0.216	0.079	<b>0.559</b>	0.217	0.006	<b>0.945</b>	-0.130	0.305	1.000		
Yield13	-0.058	-0.010	-0.037	-0.030	0.059	-0.002	0.239	0.192	-0.043	0.160	1.000	
Yield14	0.092	-0.092	-0.071	0.054	-0.011	0.109	-0.043	0.141	0.127	-0.084	0.190	1.000

TN is total nitrogen, OC is organic carbon, MC is moisture content are all in % of dry biomass; K is exchangeable potassium in mg/l; P is extractable phosphorous in mg/l; CEC is cation exchange capacity in meq/100g; Ca is calcium in mg/l; Na is sodium in mg/l; Mg is magnesium in mg/l; and pH the log measurement of acidity.

### 3.1.3.3 Random forest model

To analyse the contribution of soil variables to the yield prediction, we fit two separate RF models for the dataset of 2013 and 2014. Since the RF algorithm automatically considered interactions among the explanatory variables, the two separate RF models provided quite similar prediction results for yield with  $R^2$  of 0.83 and 0.81 for 2013 and 2014, respectively, with both being significant at  $<0.01$ . Permuting the predictor's values over the dataset showed

a negative influence on prediction. The MSE with the original dataset were compared with the 'permuted' dataset results and the final results are shown in Table 6.

**Table 6:** Calculated variable importance score (MSE) of yield prediction obtained with the random forest (RF) model, indicating contribution of each soil property to crop yield in 2013 and 2014.

Rank	2013		2014	
	Input	MSE (%)	Input	MSE (%)
1	OC	12.84	TN	11.44
2	TN	11.01	OC	7.43
3	Ca	9.43	P	6.41
4	P	6.22	Ca	5.20
5	CEC	4.73	pH	5.12
6	pH	3.91	CEC	3.23
7	Na	3.72	Mg	2.82
8	Mg	1.94	MC	2.33
9	MC	1.35	Na	2.03
10	K	0.82	K	0.11
<b>Total</b>		<b>55.62</b>	<b>45.81</b>	

TN is total nitrogen, OC is organic carbon, MC is moisture content are all in % of dry biomass; K is exchangeable potassium in mg/l; P is extractable phosphorous in mg/l; CEC is cation exchange capacity in meq/100g; Ca is calcium in mg/l; Na is sodium in mg/l; Mg is magnesium in mg/l; and pH the log measurement of acidity.

The results show that according to MSE values, soil properties' contribution to the yield are 55.62% and 45.81% for models of years 2013 and 2014, respectively. Some of 44.38 and

54.19% variation in the yield was left unexplained by both models. This result may be explained by the fact that there are some factors could not be measured or included in the models, such as weather conditions (Roberts *et al.*, 2012; Lobell *et al.*, 2014), and crop disease (Paveley *et al.*, 2012). The OC, TN and Ca were the top three highest contributors to oilseed rape yield in 2013, whereas TN, OC, and P were the top three highest contributors to barley yield in 2014. The OC has the highest variable importance score (12.84%) in 2013, meanwhile it was the second highest variable importance score (7.43%) in 2014. This result is expected and supported by the fact that OC can play a vital role in increasing crop yield (Agegnehu *et al.*, 2016), improving soil fertility (Tiessen *et al.*, 1994; Zhang *et al.*, 2016), improving soil structure (Lorenz *et al.*, 2007; Lal, 2011), and water retention (Fan *et al.*, 2013). Furthermore, soils with low OC contents have low crop yield and low use efficiency of added nutrients (Agegnehu *et al.*, 2016). Similarly, TN was the highest contributor to yield prediction after OC in 2014 with a MSE value of 11.44%, whereas TN was the second highest contributor in 2013 (MSE = 11.01%). Agegnehu *et al.* (2016) found that nitrogen supply appeared to be a much greater factor limiting yield, which was related to the soil TN content before planting and uptake rate by plants during the growing season. Interestingly, they found that increases in yield and yield components were more pronounced when organic amendments and N fertilizer were both applied, in comparison to one or the other. Surprisingly, K had the lowest variable importance score for both RF 2013 and 2014 models with contributions of 0.82%, and 0.11%, respectively. There was a gradual decline in soil K levels, however, cereals remove less K compared to other crops (Malo *et al.*, 2008). Both P and Ca exchange the third and fourth places on the list. CEC is ranked the fifth and the sixth in 2013 and 2014 with MSE values of 4.73% and 3.23%, respectively, whereas pH on contrary to CEC, is ranked the sixth (3.91%) and the fifth (5.12%) on the list for 2013 and

2014, respectively. The remaining soil properties e.g., Na, Mg, and MC collectively contributed to the yield of 7.01% and 7.18% for 2013 and 2014, respectively.

### 3.1.3.4 Parametric models

Based on Eq. (6), the following VNRX-LN model with quadratic terms was established to relate the ten soil input variables with yield:

#### Equation 10

$$y = \theta_0 + \sum_{i=1}^{10} \theta_i u_i + \sum_{i=1}^{10} \sum_{j=i}^{10} \theta_{ij} u_i u_j + \varepsilon$$

This model included 66 terms consisting of 11 linear terms  $\{\theta_0, \theta_i u_i | i = 1, 2, \dots, 10\}$  and 55 non-linear terms  $\{\theta_{ij} u_i u_j | i = 1, 2, \dots, 10; j = i, i + 1, \dots, 10\}$ . The VNRX-L model can be written as:

#### Equation 11

$$y = \theta_0 + \sum_{i=1}^{10} \theta_i u_i + \varepsilon$$

The contributions of each soil property to crop yield variation were listed in Table 7 and Table 8 for the VNRX-LN model and VNRX-L model, respectively. The VNRX-LN model accounted for both linear and non-linear interactions, whilst the VNRX-L only considered linear interaction. The non-linear aspect of the VNRX-LN model, permitted far more of the yield variation to be understood, which is shown in the SERR values for 2013 and 2014 being 52.23% and 50.66%, respectively for the VNRX-LN and 19.15% and 8.5% for the VNRX-L. This is supported by the negligible linear correlations calculated with  $r$  (Table 5). The variation of SERR contribution between the years can be attributed to varying weather conditions (Renouf *et al.*, 2010; Boone *et al.*, 2016), pests (Eberhart and Russell, 1966;

Paveley *et al.*, 2012) and finally, the different crops grown, e.g., oilseed rape in 2013 and wheat in 2014.

The output of the VNRX-LN model indicated as ERRC shows P, CEC and OC to be the top three contributors to oilseed rape yield variability in 2013, whereas P, Na and OC were the top three contributors to wheat in 2014. This seems logical from the soil fertility point of view, as these (apart from Na) are all key nutrients to crop growth and development (Baligar *et al.*, 2001). As indicated above, OC can improve soil fertility, soil structure and water retention, hence improve soil productivity. Na is a minor nutrient, which can have negative effects on moisture uptake and can inhibit enzyme activities at high levels. The high yield variability attributed to Na from the VNRX models is thus unexpected. Though there is an optimal K:Na ratio for plant growth and yield development (Wakeel 2013). High amounts of K have been found to reduce the occurrence of crop disease. High quantities of Na can reduce the availability of K to plants (Perrenoud 1990; Prabhu *et al.*, 2007). Within the studied field, levels of K were more variable through the field than Na, the interaction between K and Na may help explain the higher Na impact on yield variation, particularly in the non-linear VNRX model (Baligar *et al.*, 2001; Wakeel 2013). CEC is often used as a measurement of soil fertility, but is not nutrient specific, whereas P is a main soil nutrient (with N and K) for crop growth and development. CEC is also related to K content and clay particles, which all affect available water content (Bergaya and Vayer, 1997).

Surprisingly, TN (Table 7) had a small contribution to yield variation in 2013 (ERRC = 1.23%), which may well be attributed to the small variation in nitrogen in this field (Table 3), or to the smaller sensitivity of oilseed rape to nitrogen as compared to barley, as TN demonstrates a higher contribution (ERRC = 5.01%) in 2014's calculations. Both pH and Mg

were quite consistent contributors to 2013 and 2014 yield variability with calculated ERRC values of 4.915 and 5.05%, respectively.

**Table 7:** Calculated individual contribution (ERRC) of each soil property and sum of contribution (SERR) to crop yield in 2013 and 2014 cropping seasons, obtained with Volterra Non-linear Regressive with eXogenous inputs (VNRX), accounting for both linear and non-linear relationships (VNRX-LN).

Rank	2013		2014	
	Input	ERRC (%)	Input	ERRC (%)
1	P	12.74	P	8.30
2	CEC	12.47	Na	6.77
3	OC	6.44	OC	6.71
4	pH	4.91	K	5.89
5	Ca	3.87	pH	5.05
6	Na	3.82	TN	5.01
7	Mg	3.41	MC	5.00
8	K	1.75	Mg	4.06
9	MC	1.59	CEC	2.79
10	TN	1.23	Ca	1.08
	<b>SERR</b>	<b>52.23</b>		<b>50.66</b>

TN is total nitrogen, OC is organic carbon, MC is moisture content are all in % of dry biomass; K is exchangeable potassium in mg/l; P is extractable phosphorous in mg/l; CEC is cation exchange capacity in meq/100g; Ca is calcium in mg/l; Na is sodium in mg/l; Mg is magnesium in mg/l; and pH the log measurement of acidity.

The range of soil pH in this field is between moderately basic to moderately acidic (Table 3). Furthermore, it is interesting to see that MC has a low contribution to yield variation in 2013 (ERRC = 1.59%), with a higher contribution calculated in 2014 (ERRC = 5.0%), which may be attributed to different crop or weather conditions across the two cropping seasons. Reasonable contributions of K to the yield variability are calculated with the best contribution observed in 2014. Ca was the lowest contributor in 2014 only.

The VNRX-L model (Table 8) shows different ranking results and different contributions of individual soil properties as compared to the VNRX-LN model. With the VNRX-L model both P and OC are the top two contributors to yield variability in both 2013 and 2014 years. Contrary to the VNRX-LN model, TN obtained with the VNRX-L model in 2013 was of more significant influence and got the same ranking in 2014, although the ERRC with the VNRX-L model is smaller (e.g., 0.88) compared to the VNRX-LN model (e.g., 5.01%), which is attributed to the larger SERR of the latter than the former approach. Ca has a remarkably similar contribution in both 2013 and 2014, being the fourth most significant parameter. Na was a larger contributor to yield variability in 2014 than in 2013, which is in line with the VNRX-LN model predictions. pH varied in contribution between the two years significantly, this could be due to the availability of nutrients detailed in Table 3, and being reasonably neutral in acidity. Mg and MC are both insignificant contributors, which is in line with the VNRX-LN model that accounts for both the linear and non-linear variability. K holds a similar position in 2013 and 2014 for both parametric models investigated. CEC most interestingly had no effect in 2013 in the VNRX-L model, opposed to the VNRX-LN model predictions.



**Table 8:** Calculated individual contribution (ERRC) of each soil property and sum of contribution (SERR) to crop yield in 2013 and 2014 cropping seasons, obtained with Volterra Non-linear Regressive with eXogenous inputs (VNRX), accounting for linear relationship only (VNRX-L).

Rank	2013		2014	
	Input	ERRC (%)	Input	ERRC (%)
1	P	6.18	P	2.01
2	OC	5.73	OC	1.46
3	TN	3.94	Na	1.21
4	Ca	1.23	Ca	1.20
5	pH	1.09	K	1.13
6	Mg	0.53	TN	0.88
7	K	0.17	CEC	0.33
8	Na	0.15	MC	0.18
9	MC	0.13	Mg	0.07
10	CEC	0	pH	0.03
	<b>SERR</b>	<b>19.15</b>		<b>8.50</b>

TN is total nitrogen, OC is organic carbon, MC is moisture content are all in % of dry biomass; K is exchangeable potassium in mg/l; P is extractable phosphorous in mg/l; CEC is cation exchange capacity in meq/100g; Ca is calcium in mg/l; Na is sodium in mg/l; Mg is magnesium in mg/l; and pH the log measurement of acidity.

### 3.1.3.5 Parametric models versus random forest models

Based on results discussed above, it seems that OC always retained a high contribution to yield variability through both years. This is true for all three models investigated in this study. Soil OC arguably was the best single indicator of soil quality and function because of its impact on soil physical, chemical and biological properties (Reeves, 1997; Shukla *et al.*, Ebinger, 2006; D'Hose *et al.*, 2014). Furthermore, OC is a source of plant nutrients in soils and is vital in maintaining and improving soil structure, promoting water retention, and reducing erosion (D'Hose *et al.*, 2014). Therefore, it is not surprising to observe that soil OC is a high contributor to yield variability.

P has a direct link with yield and so is expected to be a high contributor to yield variability (Harmsen *et al.*, 2001). P was the highest contributor to yield variability in both VNRX models. However, with the RF model, P consistently contributed around 6% to yield variability, being ranked as the third contributor to yield variability in 2014, and fourth in 2013. VNRX-LN presents TN as a moderate contributor, whereas the highest contribution for TN is obtained with RF models. Since N is a key indicator for soil quality and plays a vital role in crop production, this is an advantage of RF over VNRX (Sharma *et al.*, 2008).

Although VNRX-LN and RF models allow the prediction of yield variability to be around 50%, with the input data from ten on-line soil properties, there is a remaining 50% of the contribution that has not been accounted for. Kravchenko and Bullock (2000) stated that yield variability is caused by a host of factors in addition to topographical and soil characteristics. Therefore, it's suggested that there are other external factors (such as diseases, pests, and compaction) that need to be incorporated along with soil properties to allow for more accurate assessment of the yield limiting factors and for improving the accuracy of prediction of yield. Phosphorus along with Nitrogen are commonly added as fertilisers, and are the main

soil macro nutrients, affecting the severity of fungal diseases (Huber, 1980; Engelhard, 1989; Fageria and Baligar, 1997; Graham and Webb, 1991). Whilst fungal diseases have not been considered in this study, it would be interesting to involve them in further work, particularly with the yield variation attributed to Na by the VNRX models.

The total contributions of the RF model to crop yield variability were 55.6% and 45.8% in 2013 and 2014 cropping seasons, respectively. The VNRX-LN model that was more successful than the VNRX-L model in yield prediction contributed with similar percentages (52.23% and 50.66% for years 2013 and 2014 respectively) to those of the RF models. The total contribution of VNRX-LN models provides a greater consistency for high contribution to yield variation. However, the RF model was more consistent on the ranking of influencing soil properties of the yield variability. The consistency of the contribution of regression models to predict yield was an issue raised by Kravchenko and Bullock (2000). Their findings suggested that the capability of models to predict yield based on input soil properties is heavily variable. Whilst successful in explaining a substantial portion of the yield in some years, it is only capable of explaining a small portion of the yield variability in others. Consistency of model predictions is highly valued. Each of the models demonstrated some consistency between the two years, with RF being more consistent in ranking the influencing soil properties on yield variability. VNRX-LN predicted a much larger contribution of K to yield variation than the RF model, particularly in 2014. K is correlated to disease pressure, making the VNRX-LN model an interesting concept for further work, if disease data could be included. This study using parametric models, which could draw an understanding of ~50% of the variabilities affecting yield in this field, in the two studied years. However, for universal conclusions to be drawn, process based models, which consider climate data, crop specific input parameters, and temporal patterns of parameters would be required

### **3.2 A new non-linear parametric modelling method to quantify influence of soil properties on crop yields: Application to on-line soil data**

#### **Abstract**

There is a limited understanding of soil factors limiting crop yield, due to the complexity and variability of the system. High spatial sampling resolution data on soil properties, may contribute towards this, though soil properties are not the only factor affecting crop yield. This study attempts to use a novel data mining approach, based on non-linear parametric modelling, to study the effects of high resolution data of multiple soil properties on wheat yield in a 22 ha field in Bedfordshire, UK. A Volterra Non-linear Regressive with eXogenous inputs (VNRX-LN) model was introduced and tested in Part 1 of this study, where a limited number of soil data were considered in the analysis. In Part 2, moisture content (MC) along with the seven soil properties; total nitrogen (TN), organic carbon (OC), pH, available phosphorous (P), magnesium (Mg), calcium (Ca), and cation exchange capacity (CEC) were collected with an on-line (tractor mounted) visible and near infrared spectroscopy (vis-NIR) sensor and used as multiple-input to the VNRX-LN model, while crop yield represented the single-output in the system.

Results showed that the largest contributors to wheat yield were CEC, Mg and TN, with error reduction ratio contribution (ERRC) values of 14.6%, 4.69% and 1%, respectively. The overall contribution (SEER) of the soil properties considered in this study totals a value of 23.21%, which was surprisingly low as compared to 50-52% obtained in Part 1 with a limited number of soil samples analysed with laboratory standard methods. This was attributed to a large area of the studied field having been waterlogged, which masked the effect of soil nutrient properties on crop yield. The study recommends further validation on a greater

number of fields where additional crop yield affecting parameters are taken into account e.g., crop disease, pests, drainage, topography, and microclimate conditions.

## **Keywords**

Yield limiting factors; proximal soil sensing; VNRX; NARMAX; non-linear parametric modelling.

### **3.2.1 Introduction**

The world's population is expected to rise to 9 billion by 2050, hence, there is an increasing demand for land for the use of biofuels, and there is already a food shortage. An increase in yield of 60% will be required to match these requirements (Hole *et al.*, 2005; Godfray *et al.*, 2010). One way to increase yield may be through precision management of farm resources. The spatial variability in agricultural fields exists at different scales (Raun 1998; Dhillon *et al.*, 1994), which requires careful management with the aim to increase yield at reduced input cost and related environmental impacts. This is hardly achievable by conventional agriculture that relies on homogeneous applications of external inputs. For example, current fertiliser applications are made based on an average soil sample collected per field or 1-3 ha in the best scenario, which ignore within field variability as the fertilisers are spread homogeneously. This may result in over-application in rich zones, and under-application in poor zones in the field (i.e., nitrogen rich areas receiving high rates of nitrogen fertiliser, due to the field having nitrogen poor areas). In this context, recent years have seen a surge of variable-rate application technologies where external farm inputs are applied in response to input data from normalised difference vegetation index (NDVI), leaf area index (LAI), high resolution soil properties or a combination of these (Lowenberg-DeBoer and Aghib, 1999; Maleki *et al.*, 2008; Mouazen *et al.*, 2009; Halcro *et al.*, 2013; Mouazen and Kuang, 2016). Commercial fertiliser commonly contains nitrogen (N), phosphorus (P), and potassium (K). Other

nutrients such as, magnesium (Mg) and Calcium (Ca), are applied with less frequency. Mg and Ca, N, P, K are used in the structural component of proteins, energy conversion, chemical reactions in the plants, building components of the chlorophyll, respiration, and cell membrane permeability. In non-homogenous fields, precision management of fertilisers is the obvious way forward to increase crop yield. Understanding and quantifying the yield limiting factors is still a crucial research question to be answered, before variable rate applications can be optimised.

Since spatial variability in the majority of agricultural fields exist, proximal sensor technologies are necessary to measure this variability accurately. This will require robust and reliable sensing platforms of crop and soil. Proximal (e.g., Crop Circle ACS 470, Holland Scientific, Lincoln, NE USA) and remote sensing (e.g., satellite imagery, unmanned aerial vehicles or aircrafts) both can provide high resolution data on crop canopy characteristics indicated e.g., as NDVI or LAI (Mulla, 2013; Kipp, Mistele, and Schmidhalter, 2014) and they are commercially available. However, remote sensing methods provide data on the top millimetres of soil and require a bare soil surface. Furthermore, due to the complex nature and vast variability of agricultural soils, the majority of proximal soil sensors are still premature to fulfil this requirement. Kuang *et al.* (2012) concluded in an extensive review that the most promising proximal sensing technologies for quantifying soil properties are electrochemical techniques and optical visible and near infrared (vis-NIR) spectroscopy. Although they are limited to particular research groups worldwide, on-line vis-NIR sensors (Shibusawa *et al.*, 2001; Mouazen, De Baerdemaeker, and Ramon, 2006; Christy, 2008) enable the prediction of high sampling resolution (e.g. >500 samples per ha) of key soil properties (Kuang *et al.*, 2012; Kodaira and Shibusawa, 2013; Kuang and Mouazen, 2013;

Kweon, Lund, and Maxton, 2013 Marin-González *et al.*, 2013;), which are valuable sources of information to be utilised for the analysis of soil related crop yield limiting factors.

The use of a simplified volterra non-linear regressive with eXogenous inputs (VNRX) model, also known as non-linear finite impulse response (NFIR) model, was proposed and implemented to understand the correlation between laboratory measured soil properties and crop yield in Part 1 of this study (Whetton *et al.*, 2016a), where on-line soil data was not included in the analysis. In Part 1 of this study, VNRX accounting for both the linear and non-linear (VNRX-LN) variability was compared to random forest (RF) models, and results revealed VNRX-LN performed almost equally as good as RF in quantifying the total contribution of soil properties on yield variation. The VNRX-LN reported interesting results for field application. To our best knowledge, no literature about the use of a VNRX-LN model to predict crop yield based on on-line measured soil properties can be found in the literature. This is important to investigate, since on-line soil sensors provide high sampling resolution data (>500 samples per ha) to enable accounting for variability that exists within small scales (few meters), which cannot be obtained with the traditional soil sampling and laboratory analytical methods.

The aim of this work is to explore the potential of the VNRX-LN model to quantify the individual, interaction and collective contribution of high sampling resolution data of eight selected soil properties collected with an on-line soil sensor on wheat yield Variability in one site in Bedfordshire, UK. It will be based on multiple input data of soil properties (e.g., total nitrogen (TN), organic carbon (OC), pH, available phosphorous (P), magnesium (Mg), calcium (Ca), moisture content (MC), and cation exchange capacity (CEC), and wheat yield used as the model output.

## **3.2.2 Materials and Methods**

### **3.2.2.1 Study site**

The study site was one field designated as Horns End, and located at a commercial farm, called Duck end farm, in Wilstead, Bedfordshire UK ( $52^{\circ}5'52.087''$ W latitude and  $0^{\circ}27'19.76''$ N longitude, according to the Universal Transverse Mercator (UTM). The field is about 22 ha area, with an average annual rainfall of 598 mm. The farm has a crop rotation of wheat, barley, and oilseed rape. The soil texture over the field down to 0.20 m is non-homogeneous, including three textures of sandy loam, loam, and sandy clay loam according to the United State Department of Agriculture (USDA) texture classification system. Wheat was cultivated during the experiment in 2013, with Oilseed rape being previously cultivated.

### **3.2.2.2 On-line collected data**

The on-line vis-NIR sensor (Mouazen, BE Patent No. WO/2006/015463, 2006) was used (Figure 6) to carry out the field measurement. It consists of a subsoiler that penetrates the soil to the required depth, making a smooth trench to the subsoiler (Mouazen, De Baerdemaeker, and Ramon, 2005).



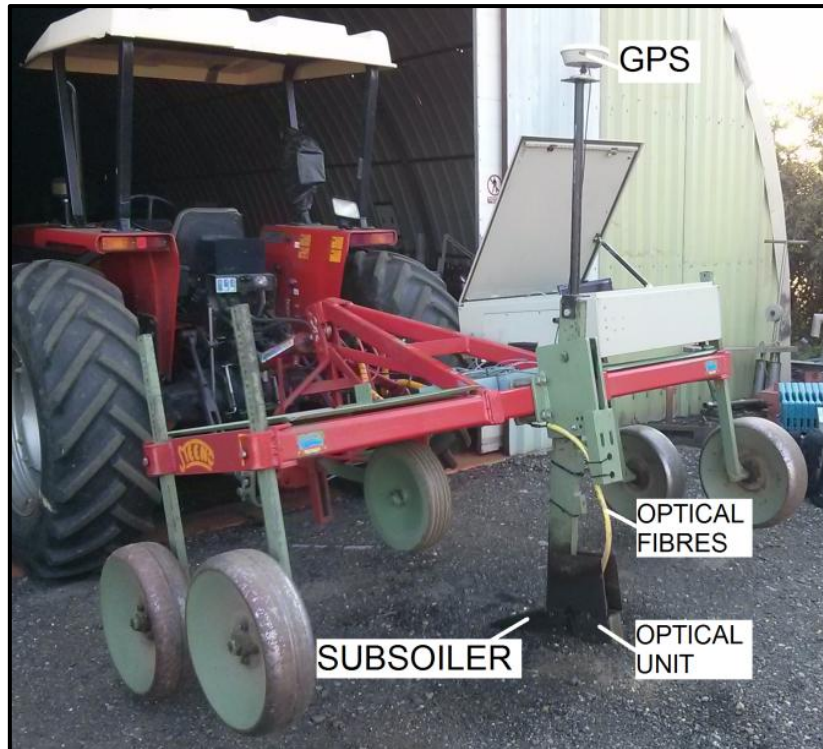


**Figure 6:** Illustrated image of the tractor mounted on-line visible and near infrared spectroscopy (vis-NIRS) sensor (Mouazen, 2006).

The optical probe, housed in a steel lens holder, was attached to the rear of the subsoiler chisel to acquire soil spectra in reflectance mode from the smooth bottom of the trench. The subsoiler, retrofitted with the optical unit, was attached to a frame that was mounted onto the three point hitch of the tractor. An AgroSpec mobile, fibre type, vis-NIR spectrophotometer (tec5 Technology for Spectroscopy, Germany) which is an active sensor, with a measurement range of 305-2200 nm was used to measure soil spectra in diffuse reflectance mode. A differential global positioning system (DGPS) (EZ-Guide 250, Trimble, California, USA) was used to record the position of the on-line measured spectra with sub-metre accuracy. A Panasonic semi-rugged laptop was used for data logging and communication. The spectrometer system, laptop and DGPS were powered by the tractor battery. A New Holland

T5000 tractor with 100 Ah battery was used. The total power consumption for all electrical parts of the on-line vis-NIR sensor was around 60 W.

On-line soil measurement occurred in summer 2012 after the harvest of the previous crop, at parallel transects with an average forward speed of the tractor of 2 km h<sup>-1</sup> and the measurement depth set at 150 mm. A few on-line collected vis-NIRS spectra are shown in Figure 7, as an example.

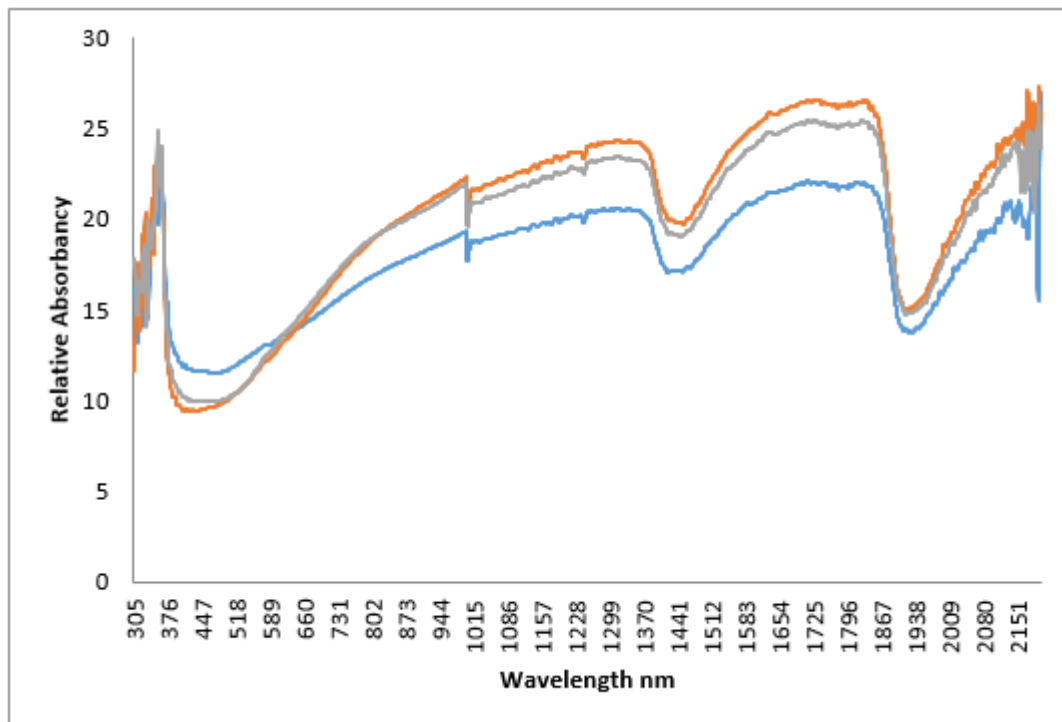


**Figure 7:** Examples of the raw on-line soil visible and near infrared (vis-NIR) spectra, collected with the on-line sensor. Showing slight deviations in relative absorbance, across the wavelengths, which is dependent on the soil properties.

During each line measurement, two or three soil samples were collected from the bottom of a trench and the sampling positions were carefully recorded with the DGPS. Samples collected during the on-line measurement were analysed for calcium (Ca), cation exchange capacity (CEC), magnesium (Mg), phosphorous (P), pH, moisture content (MC), organic carbon (OC) and total nitrogen (TN). These samples were subjected to the same laboratory methods of soil analysis mentioned in Part 1 of this study. The laboratory measurement techniques varied for each value and the units they are presented in are in relation to this. MC, OC, and TN are given in % (ISO 10694:1995; British Standard BS EN 13654-2:2001). P, Ca, and Mg is given in mg/l (MAFF/ADAS, 198; Agilent Technologies, Inc. USA; Olsen, 1954). CEC is given in meq/100g (Chapman 1965). pH is given in log measure (DEFRA, 2010).

Partial least squares regression (PLSR) based calibration models, developed with Unscrambler V9.8 software (Camo Software, Norway) were used to predict all eight soil properties using the on-line collected soil spectra (>500 samples per ha). More details about the on-line vis-NIR sensor and accuracy of measurement can be found in Kuang and Mouazen (2013) and Marin-González *et al.* (2013).

Wheat yield data was collected in August, 2013 by the on-board yield sensor and GPS system of the farmer's combine harvester (New Holland, CX8070 model), with a header width of 7.25 m commonly used for barley and wheat harvest. In addition, the harvest was optimised to: I) record wheat yield when the machine header was full for the full length of the study area, and II) avoid the bare soil in the tramlines (by collecting harvest data only from a full header). Total yield was calculated from the mean yield (tonnes per hectare) of an area, multiplied by the size of the area (m<sup>2</sup>), which was derived using ArcGIS (Esri, USA).

### **3.2.2.3 Data processing**

Features in the environment, are the product of many interacting processes, including physical, chemical and biological. They are determined with exceedingly complex interactions. To overcome the difficulty of predicting this intricate distribution, it is required to treat the variation as if it is random (Matheron, 1963). The measurement points from the on-line soil sensor and yield sensor required a method of interpolation, to provide a continuous data set across the locations. Kriging was selected as a non-biased approach to predict the values between the sample points, where semi-variograms were first produced and then applied in Kriging interpolation calculations. The interpolated data were then converted into a common 5 m raster grid in ArcGIS (Esri, USA) in order to assist data fusion (Frogbrook and Oliver, 2007). The raster squares of the layers were converted into this common grid of points by extracting the value at the midpoint of each raster square. A smaller resolution has no practical implementation, due to the limitations of the size and response time of the precision farming equipment. The 5 m grid size provided a balance between adequately characterising the spatial variation and practical farm management. These steps ensured that all layers consisted of a common set of 5 m grid point-values, to allow the application of parametric modelling to be carried out. This method allowed data from a diverse range of soil and crop property surveys, measured at different resolutions, to be merged (Khosla R. *et al.*, 2008). The different soil and crop layers of a 5 by 5 m grid were subjected to the VNRX-LN detailed in the following section.

### **3.2.2.4 Volterra Non-linear Regressive with eXogenous Model**

In this study, the simplified VNRX-LN model, also known as NFIR model, introduced in Part 1 of this study was used, to represent a multi-inputs and single-output system:

## Equation 12

$$y(k) = f(u_1^{[k-1]}, u_2^{[k-1]}, \dots, u_r^{[k-1]}) + \varepsilon(k)$$

was considered to represent a multi-inputs and single-output system, where  $k(k = 1, 2, \dots)$  is a time index,  $r$  is the number of the system inputs,  $f$  is some unknown linear or non-linear mapping, which links the system output  $y$  to the system inputs  $u_1, u_2, \dots, u_r$ ;  $\varepsilon(k)$  denotes the model residual.

The on-line measured soil properties (i.e., TN, OC, pH, P, Mg, Ca, MC, and CEC) were normalised and used as inputs to the VNRX-LN model, whereas the model output was wheat yield. The analysis also included the interaction between pairs of soil properties and their contribution to crop yield. The aim was to investigate the contribution of each soil property and their pairwise interaction on crop yield variability.

Parameters are estimated based on the observations, and these are determined by the structure, using the orthogonal least squares (OLS) estimation procedures. Adaptive-forward-orthogonal least squares (AFOLS) was employed not only to determine the model structure but also to estimate the unknown parameters. More detailed description of this method can be found in Zhao *et al.*, (2012). More details about the VNRX-LN model is described in the Part 1 of this study (Whetton *et al.*, 2016a).

Performance of VNRX-LN model output was evaluated by considering the value of error reduction ratio (ERR) for each parameter to the prediction of yield (system outputs). Values of ERR always range from 0% to 100%. The larger the ERR is, the higher the dependence is between this term and the output. It is, therefore, a very important index to indicate the

contribution of each term to the output. To calculate the contribution of each input variable to the output, the sum of ERR values (SERR) of all selected terms is used to describe the percentage explained by the identified model to the system output. If the considered inputs can fully explain the variation of system output, the value of SERR is equal to 100%. It is an indicator of model performance and uncertainty. The contribution of the  $i^{th}$  input variable to the variation of the system output, denoted as  $ERRC_i$ , is defined as the sum of ERR values of the terms that include this input variable. The value of  $ERRC_i$  should be always between 0% and 100%.

### **3.2.2.5 Significance Test**

To determine the statistical significance of the contribution from each input to the system output, a threshold  $\tau_i$ , representing the level of contribution, above which value had less than a 5% probability of occurring by chance, requires being determined. The conventional 95% (0.05 significance level) confidence interval is not suitable for this study because the distribution of ERRC value is unknown, as the condition to use 95% confidence interval is that the value must follow the Gaussian distribution. As the distribution of ERRC value is unknown, a 95% confidence may produce biased conclusions. For this purpose, the following surrogate data technique was used.

Assuming the signal  $Y$  is a function of the signal  $X$ , this sort of dependence is destroyed when  $Y$  is ordered randomly in some way while  $X$  keeps the same order. For this purpose, the order of the data in  $Y$  was randomised by a shuffle procedure that saves the distribution properties of the  $Y$  signal, but destroys the spatial relationship between  $X$  and  $Y$ . This procedure was repeated 100 times and then the 95% quantile was determined as the threshold. A

significance threshold for each term is firstly calculated, and then the significance threshold for each input can then be derived by the same way to calculate  $ERRC_i$ .

### **3.2.2.6 Optimal spatial resolution of soil properties versus yield**

Since the spatial sampling resolutions of soil properties and crop yield are different, before applying the proposed VNRX-LN modelling method, the data must be re-sampled to establish the correspondence between the inputs and the output. Two re-sampling techniques have been used in this study. In the first technique, for each crop yield data  $y(e_i, w_i)$  on a location  $(e_i, w_i)$ , the corresponding soil properties were approximated by the properties on the location that has the shortest distance to  $(e_i, w_i)$ , which must be smaller than a radius  $r$ . It is possible that some crop yield data cannot find corresponding soil properties if  $r$  is too small, for which scenario this yield data will be discarded. In the second technique, for each crop yield data  $y(e_i, w_i)$ , each corresponding soil property was approximated by the averaging value of all values of this soil property inside a circle with a radius  $r$ . A small value of  $r$  leads to more accurate correspondence between yield and properties, but a lower number of samples included in the analysis. The former method of re-sampling is designated here as ‘shortest distance approximation (SDA)’, whereas the latter method is designated as ‘circle-based average approximation (CAA)’.

### **3.2.3 Results and discussion**

The yield data from the 2013 harvest is given in Figure 8, along with the semi-variogram used for the interpolation. The yield data shows a consistently higher yield in the centre of the field compared to the E and W edge. This variability is partially due to the field being on reclaimed land, consisting of variable soil types as discussed earlier, but there is also an influence from the hedgerow surrounding the field. The impact from the hedgerow was not

observed in Part 1 of this study, which used a field in Germany (Whetton *et al.*, 2016a), due to the field there having no hedgerow boundaries, as it was an area within a large continuous field (with multiple crop varieties). However, anomalies in yield data can occur, particularly towards the boundaries of the field (crop varieties) due to a decrease in combine speed, turning, and headers being cut separately. The noise and influence of these areas were removed from the yield data, but it is possible that there is still an artefact of this.

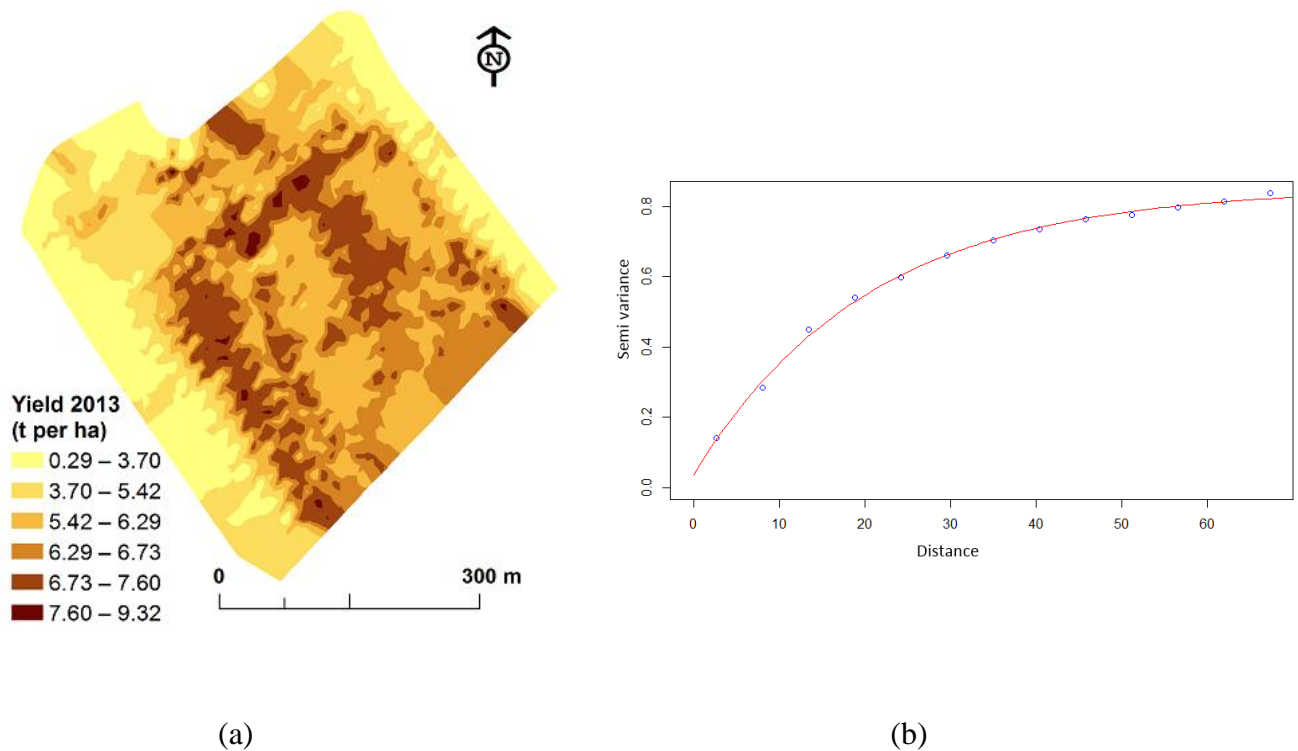


**Figure 8:** Interpolated yield map (a) and exponential semi-variogram of 0.036, 0.817 and 20.358, representing, nugget, sill and range, respectively. Semi-variograms fit to the lag points which are distance classes, into which pairs of locations are grouped (shown by the small circles) (b) based on the 2013 harvest of wheat grain in tons per hectare. Lighter areas representing lower yield.

The on-line collected soil properties (shown in Figure 9 for moisture content, and in Figure 10 for Mg, OC, P, CEC, Ca, TN, and pH) were achieved through applying PLSR models. A summary of the statistics and model accuracy can be found in Table 9. Further details about the development of these models can be found in Kuang and Mouazen (2013) and Marin-



González *et al.* (2013). The moisture content map is shown along with the measurement transects (Figure 9), where the spectral data was collected. Whilst MC is involved in the VNRX model this is sampled at the beginning of the growing season. The MC map highlights the moisture distribution spatial pattern in a field although the levels will vary in short periods of time (Vachaud *et al.*, 1985). The studied field site has different soil property types, as areas of the field are on reclaimed land. It was noted through the growing season that there was a waterlogging problem on the west side of the field.

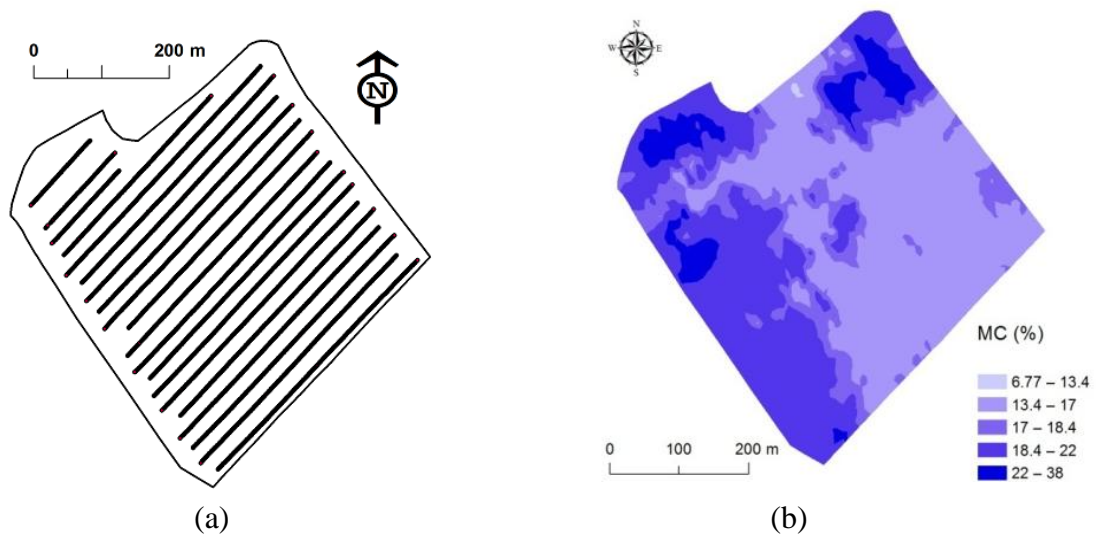


**Figure 9:** Measured transects (a), map of the soil moisture content (MC) measured with the on-line visible and near infrared spectroscopy (vis-NIRS) sensor after crop harvest in August, 2012 (b) respectively.

Figure 10 shows the on-line predicted soil properties (i.e., Mg, OC, P, CEC, Ca, TN, and pH), the semi-variogram results for the interpolated maps can be found in Table 9. General trends can be seen between the soil properties, with a low strip running through the centre of the field. The highest correlation seen is between moisture content and yield. However, Ca and Mg (Figure 10) show this same trend, being higher in nutrients in the areas of higher moisture

content, associated with low yield. Total nitrogen is in the highest concentrations in the NW of the field with a high band running through the S of the field, and phosphorus mimics this pattern. The lowest yield and highest moisture content are found in the NW of the field. Organic carbon appears to be homogenous through the field apart from a band in the centre, which is notably lower, with the NE and SW edge being slightly higher. PH is the lowest in the NW, with a low strip through the centre, but otherwise quite homogenous. A general trend can be seen between pH and CEC. Whilst an inverted pattern can be seen between pH and P. CEC is the highest on the SW and NE of the field. The most obvious spatial similarity is between yield and MC, where low yield (Figure 8) was seen in areas of higher moisture (Figure 9), suggesting a waterlogging problem effect on crop yield, which was confirmed by the farmer.

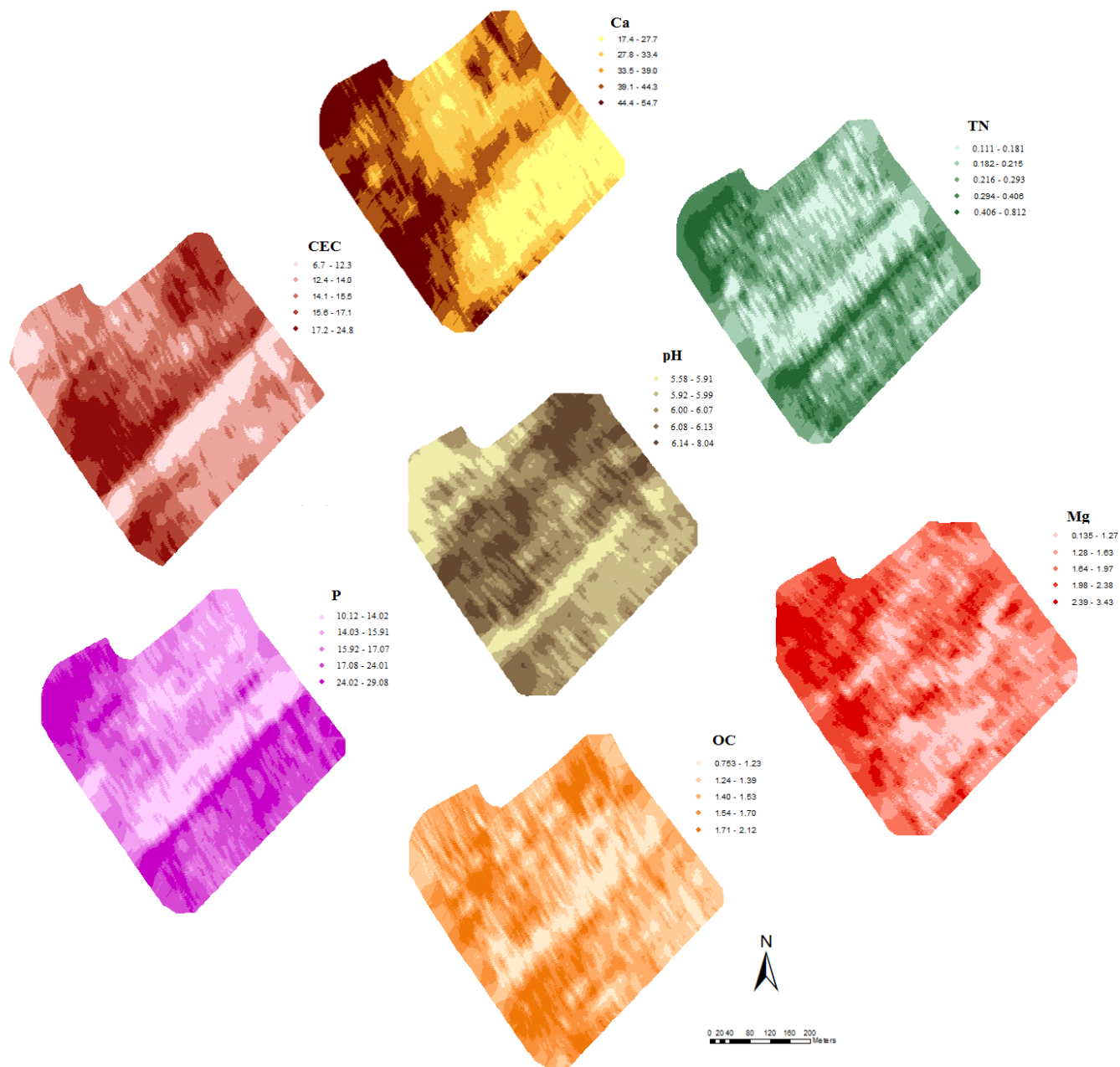


**Figure 10:** Soil property maps of the study field in Bedfordshire, UK; magnesium (Mg) magnesium in mg/l, organic carbon (OC) in % of dry matter, phosphorus (P) in mg/l, CEC in meq/100g, calcium (Ca) in mg/l, total nitrogen (TN) in % of dry matter, pH the log measurement of acidity. On-line spectral data was collected and applied to PLSR models developed by Kuang and Mouazen (2013) and Marin-González *et al.* (2013).

**Table 9:** Summaries of the statistics for the yield and on-line soil properties predicted in the field and the prediction results. The models were developed by Kuang and Mouazen (2013) and Marin-González *et al.* (2013). The semi-variogram results are also presented for each property  $c_0$  is nugget variance,  $c$  is sill,  $r$  is range,  $c_0/c$  is proportion, and SSE is sum of squared error.

Statistics	pH	P	TN	OC	Mg	Ca	MC	CEC	Yield
Max	8.04	29.08	0.81	2.12	3.43	54.7	35.47	24.83	9.32
Min	5.58	10.12	0.11	0.75	0.13	17.4	5.60	6.74	0.29
Mean	6.04	16.98	0.26	1.75	1.05	33.1	16.55	13.5	6.13
SD	0.49	3.46	0.07	0.33	0.44	9.36	3.29	2.69	2.12
RMSEP	0.33	8.61	0.013	3.34	0.31	7.34	1.45	1.47	NA
R <sup>2</sup>	0.86	0.69	0.72	0.75	0.88	0.76	0.56	0.72	NA
RPD	2.37	1.77	1.85	2.36	2.55	1.87	1.49	1.70	NA
$c_0$	0.51	0.22	0.05	0.02	1.03	0.55	3.62	0.56	0.01
$r(m)$	25.7	32.4	28.2	12.57	58.1	67.8	18.74	36.1	67.3
$c$	1.09	0.77	0.09	0.04	1.39	0.78	5.28	1.57	0.81
$c_0/c$ (%)	0.47	0.29	0.55	0.5	0.74	0.71	0.69	0.36	0.01
SSE	2.11	1.79	2.89	2.46	3.00	0.67	5.21	4.30	1.59

OC is organic carbon, MC is moisture content, and TN is total nitrogen and are all in % of dry matter; P is extractable phosphorous in mg/l; CEC is cation exchange capacity in meq/100g; Ca is calcium in mg/l; Mg is magnesium in mg/l; and pH the log measurement of acidity. RMSEP: Root mean square error of prediction, RPD is ratio of prediction deviation = standard deviation / RMSEP,  $c_0$  is nugget variance,  $c$  is sill,  $r$  is range,  $c_0/c$  is proportion, and SSE is sum of squared error.

### 3.2.3.1 Pearson correlations

Pearson coefficient ( $r$ ) values between pairs of soil properties suggest collective (positive) linear relationships to exist between Ca and CEC, MC, Mg, OC, pH and TN ( $r = 0.747 - 0.519$ ) and between CEC and Ca, Mg, MC and pH ( $r = 0.590 - 0.748$ ). This may indicate that although Ca has no direct spectral response in the NIR range, it is measured with vis-NIR spectroscopy through covariation with MC and OC, both having direct spectral response (Stenberg *et al.*, 2010; Kuang *et al.*, 2012). However, CEC is measured through covariation with MC only. As expected, TN correlated with OC, which is in line with the reports (Carlyle, 1993; Kuang and Mouazen, 2011; Whetton *et al.*, 2016a).

Examining  $r$  values between the eight on-line measured soil properties and yield, reveals negligible (negative) relationships (Table 10), which is in-line with results of Part 1 of this study (Whetton *et al.*, 2016a), based on the correlation between laboratory measured soil properties and yield. If the relationship between variables is not linear, then the correlation is not strongly presented. The correlation could be affected by a third variable. The negative correlations of the soil properties to the yield could be explained due to the non-linearity of a soil system (Evans, 1996). The highest linear correlation is calculated between CEC and yield ( $r = -0.349$ ). This again proves the complexity of the system and supports the interest in modelling techniques that account for both linear and non-linear interactions. As mentioned earlier, the interactions of soil properties that lead to their distribution are intricate and complex (Matheron, 1963). Ines *et al.* (2013) applied a simulation model where remotely sensed soil moisture, and LAI data were used to update the model variables for yield prediction of maize crop. Ines *et al.* (2013) model were process based which allowed the consideration of a large area, over multiple years. They found that in very wet conditions, a better accuracy was achieved with LAI parameters alone, and concluded that the water stress influence later in the season was negligible. Involving a process model in this study could have allowed a greater understanding and interpretation of the results, and would be interesting to involve in further modelling studies.

**Table 10:** Pearson correlation ( $r$ ) between on-line measured soil properties in 2012 and wheat yield harvested in 2013.

	Ca	CEC	MC	Mg	OC	P	pH	TN	Yield
Ca	1.000								
CEC	<b>0.733</b>	1.000							
MC	<b>0.519</b>	<b>0.748</b>	1.000						
Mg	<b>0.628</b>	<b>0.586</b>	0.476	1.000					
OC	<b>0.650</b>	0.441	0.436	0.176	1.000				
P	0.163	0.216	0.019	0.042	0.027	1.000			
pH	<b>0.747</b>	<b>0.590</b>	0.492	0.348	0.432	-0.013	1.000		
TN	<b>0.596</b>	0.411	0.269	0.167	<b>0.543</b>	<b>0.556</b>	0.307	1.000	
Yield	-0.321	-0.349	-0.209	-0.320	-0.199	-0.000	-0.152	-0.057	1.000

TN is total nitrogen, OC is organic carbon, MC is moisture content are all in % of dry; P is extractable phosphorous in mg/l; CEC is cation exchange capacity in meq/100g; Ca is calcium in mg/l; Mg is magnesium in mg/l; and pH the log measurement of acidity.

### 3.2.3.2 Model output

The detailed correspondence between inputs variables and soil properties are described in Table 11.

**Table 11:** The correspondence between inputs variables in Volterra Non-linear Regressive with eXogenous inputs (VNRX) model and soil properties

Input	Property	Input	Property	Input	Property	Input	Property
$u_1$	Ca	$u_2$	CEC	$u_3$	MC	$u_4$	Mg
$u_5$	OC	$u_6$	P	$u_7$	pH	$u_8$	TN

TN is total nitrogen, OC is organic carbon, MC is moisture content are all in % of dry; P is extractable phosphorous in mg/l; CEC is cation exchange capacity in meq/100g; Ca is calcium in mg/l; Mg is magnesium in mg/l; and pH the log measurement of acidity.

The initial full model, based on quadratic terms, was chosen in this paper, which can be written as follows:

**Equation 13**

$$y = \theta_0 + \sum_{i=1}^8 \theta_i u_i + \sum_{i=1}^8 \sum_{j=i}^8 \theta_{ij} u_i u_j + \varepsilon$$

This model has 45 terms. All inputs and output were normalised (through maximum normalisation) before being applied to the model. The proposed method was then applied to calculate the ERRC of each term. Table 12 lists the first 10 terms selected using the SDA re-sampling technique with a radius of 3 m. From this calculation it was observed that the contribution of CEC to the wheat yield variability was the largest (e.g. ERRC = 15.68%) among the 45 terms, including all soil properties and their interactions. This was followed successively by Mg (ERRC = 3.57%) and Ca \* CEC (ERRC = 1.13%) terms. This is explained by the fact that although CEC is not a nutrient, it is a widely accepted measure to assess the fertility of the soil. In fact, CEC represents the soil ability to hold positively

charged ions e.g., exchangeable cations, which is directly linked to nutrients, hence, it is an important indicator of the availability of nutrients (Hazelton and Murphy, 2007). Its significant contribution to crop yield could be due to the quantity of nutrients being variable through the field (Table 9), with Ca, P, MC and CEC having the highest standard deviations successively. Mg was variable through the field with very low concentrations in some areas. Mg contributed highly in explaining yield variability, which is understood as Mg is the central part of a chlorophyll molecule and its availability can be limited by high availability of other nutrients (i.e., potassium) (Holmes 1962). Whilst Mg has been influential in this study to explaining yield variability in the field, it is not the most crucial nutrient to crop growth (Engelhard, 1989). The high influence of Mg on yield variability observed in this study could be attributed to it being a limiting factor in the field, rather than an essential nutrient for crop growth. Mg influence on yield variation may also be due to its interactions with Ca on the soil structure (with a recommended Ca:Mg ratio of around 5:1) (Rengasamy *et al.*, 1986; Tiwari *et al.*, 2010).



**Table 12:** The first 10 terms with corresponding error reduction ratio contribution (ERRC) values and coefficients based on the shortest distance approximation (SDA) re-sampling technique with a 3 m radius.

Rank	Term	ERRC	Coefficient $\theta_i$
1	CEC	15.68%	-0.0948
2	Mg	3.57%	-0.4840
3	Ca*CEC	1.13%	-0.0025
4	MC*Mg	0.72%	-0.0558
5	OC	0.78%	-0.2056
6	Mg*P	0.34%	-0.9615
7	Mg*TN	0.78%	5.0750
8	pH*pH	0.39%	-0.0670
9	constant	0.82%	0.1917
10	TN*TN	0.37%	-8.5096

TN is total nitrogen, OC is organic carbon, MC is moisture content are all in % of dry; P is extractable phosphorous in mg/l; CEC is cation exchange capacity in meq/100g; Ca is calcium in mg/l; Mg is magnesium in mg/l; and pH the log measurement of acidity.

Furthermore, CEC is an important indicator influencing soil structure stability, nutrient availability, soil pH and the soil's reaction to fertilisers and other ameliorants (Hazelton and Murphy, 2007), which as a result will have a positive influence of crop growth and yield. Furthermore, CEC is also related to clay particles, which affect available water content (Bergaya and Vayer, 1997), hence, influencing crop growth and development.

By comparing the contribution of each soil property to the wheat yield with the corresponding significance threshold, the soil properties having significant contribution to the crop yield variability can then be highlighted as shown in Table 13. It can be clearly observed that among the eight studied soil properties, the following six soil properties e.g., CEC, Mg, TN, Ca, OC and MC have all significant influence on the crop yield variability, with declining order. However, the largest influence was attributed to CEC, followed successively by Mg and TN.

It is worth noting that pH is normally associated with soil fertility (and CEC) but pH has one of the lowest influence on yield variation (Hazelton and Murphy, 2007). But, pH level directly affects nutrient availability and crop nutrient uptake (HGCA, 2014). With acidic soils (soil pH is smaller than 5), the pH would have negative influence on nutrient uptake. It is commonly stated in farmer's guides that the optimum pH for soils under continuous arable cropping of cereal crops is between 6 and 7 with 6.5 being the ideal. However, in the Horns End experimental field, the pH value of the majority of the field area ranged between 5.6 and 8, with the average being 6.04 and a SD of 0.49, which may explain the low contribution of pH to yield variability prediction (Bruulsema, 2015). However, all measured soil properties were included in the model, even those with low variability across the field. The model is not process based and does not produce universal truths, but reports the influence of influencing factors on the yield variability for this field, in this cropping season. Similar observation can be made for P. Although P is a key nutrient for crop growth and development, no significant contribution to wheat yield variability was observed. Mg, Ca, N, P, and K are used in the structural component of proteins, energy conversion, chemical reactions in the plants, building components of the chlorophyll, respiration, and cell membrane permeability (Epstein, 1972).

**Table 13:** Error reduction ratio contribution (ERRC) contribution of each soil property (input) to the crop yield (system output) with corresponding significance threshold based on the shortest distance approximation (SDA) re-sampling technique with a 3 m radius.

Rank	Input	ERRC (%)	Significance threshold (%)	Significant
1	CEC	14.60	0.60	Yes
2	Mg	4.69	0.52	Yes
3	TN	1.00	0.50	Yes
4	Ca	0.98	0.43	Yes
5	OC	0.68	0.49	Yes
6	MC	0.62	0.47	Yes
7	pH	0.34	0.46	No
8	P	0.30	0.56	No
Total		23.21	4.03	

OC is organic carbon in % of dry matter; P is extractable phosphorous in mg/l; MC is moisture content in %; TN is total nitrogen in % of dry matter, CEC is cation exchange capacity in meq/100g; Ca is calcium in mg/l; Mg is magnesium in mg/l; and pH the log measurement of acidity.

This is a contradictory result to that achieved in Part 1, where the VNRX model was applied to soil samples from a field in Germany, where P was the largest contribution soil parameter to crop yield across the two cropping seasons studied. P is not a limiting property in the Bedfordshire field, as manure is being frequently applied (Table 9) (Mouazen and Kuang, 2016). Another reason might that a part of the field i.e., the NW part, experienced a water

lodging problem associated with a poor drainage system for many years. Whilst MC was mapped for the field prior to crop growth, the level of water will change throughout the growing season, though the distribution pattern will stay relatively constant, so issues which occur (such as waterlogging) after the data collection were not considered by the model. The low yield and high moisture content is demonstrated in Figures 8 and 9 respectively). This impact could have been negated by establishing plot areas through the field, using a factorial approach with different quantities of soil properties. This should be considered in further work, as it could not be applied in this study, due to restrictions with it being a commercial farm.

A multiple linear regression analyses with least square estimation conducted by Kravchenko and Bullock (2000) found OC as the main and most consistent, positively correlated parameter with corn and soybean yield. Interestingly, they found that the contribution from K, CEC and P was mostly negligible, and this was attributed to K and P being ample in abundance in the soils. This finding is in line with those of the current work regarding the observed P values (as K was not considered in the work) However, Kravchenko and Bullock (2000) stated that the performance of crop prediction models varies from field to field across different cropping seasons. They could on average explain about 30% of yield variability (results from 5 to 71%), whereas the model presented in this study explained 23.21% of the yield variability.

TN ranked as the third largest contributor to wheat yield variability. A high influence of TN to a field's variability is supported by previous research. It is known that nitrogen supply is a highly influential factor to crop yield (Agegnehu *et al.*, 2016). The high contribution of TN to yield variability in this study, suggests nitrogen supply was not homogenous through the field. TN large variation is also shown by the soil maps in Figure 10.

MC had only a minor influence on crop yield as it is ranked sixth among the eight soil properties included in the analysis. However, the yield was thought to be considerably impacted by the waterlogging problem associated with the poor drainage system in the NW part of the field (Figure 9), Ines *et al.*(2013) found a similar issue in very wet conditions. MC may be ranked low because it doesn't capture the impact of water logging, and some of the crop nutrients (such as Mg and Ca), closely mimic MC spatial distribution. This may also explain the surprising high influence of Mg on the yield variability, which was ranked the second most influential property for yield variance. The ratio of Mg and Ca can affect soil conductivity (with a recommended Ca:Mg ratio of around 5:1). If Mg concentrations are high it can cause high Flocculation in clay particles, resulting in ponding in wet conditions (Rengasamy *et al.*, 1986; Tiwari *et al.*, 2010). Mg had particularly low values in some areas of the field, with the high areas correlating well with the high areas of moisture content. However, the high Ca areas were generally reflected in the high Mg areas, however this is not true throughout the field, and this could have potentially contributed to Mg high impact on yield variability.

There is an optimum for soil moisture (varying with crop growth stage) being beneficial to crop yield. As MC increases it may become a hindrance to crop yield after reaching a threshold. The waterlogged areas are of high MC and nutrient concentrations but low in yield due to the water stress, which affects crop growth and yield. Waterlogged crop roots are unable to respire, as there is too little oxygen in the soil pores (Boyer, 1982). Water logging at grain filling stages can cause a significant loss in grain yield (Condon and Giunta, 2003).

Kravchenko and Bullock (2000) commented that the capability of models to predict yield is heavily variable spatially and across different cropping seasons. Whilst successful in explaining a substantial portion of the yield variability in some years, they are only capable of

explaining a small portion of the yield variability in others. This could be due to not using process based models, whilst suitable in explaining the contribution of a properties variability to the yield variability in a specific field, it does not provide universal truths. Low variability of properties in a field, could reduce the amount of explainable yield variability.

Along with the waterlogging issue in Horns End field encountered in Part 2 of this study, this goes further to suggest a reason why results in the Part 1 of this study (Whetton *et al.*, 2016a) were more successful (e.g., SERR reaching 52%). Regression analyses between cotton yield and soil properties collected by a traditional soil sampling method (Corwin *et al.*, 2003) suggested that issues surrounding moisture content, salinity and pH were the most significant influence on the yield outcome, which support the finding of the current work regarding the water logging problem.

### **3.2.3.3 Model sensitivity**

All results discussed above are based on the SDA re-sampling technique with a 3m radius. To evaluate the sensitivity of the results to the selection of re-sampling technique and the size of radius, more tests where been performed, whose results are shown in Table 14, in which only the top 3 significant soil properties are presented. Inspection of Table 14 reveals that the top two soil properties (e.g., CEC and Mg) showed exactly same response for all tests, appearing at first and second factors affecting yield, respectively, whereas TN appears three times and Ca appears once in the third position. Additionally, the CAA re-sampling technique consistently had a larger total contribution (SERR = 22.97% for 3 m radius) to wheat yield than that of the SDA re-sampling technique (SERR = 20.29% for 3 m radius), which indicates the CAA technique may be more suitable for the high resolution soil and yield data, because the identified model explains more of the system output. Also, the total contribution to variability decreases, following the increase of the re-sampling radius, which is expected

because more samples in an area, should be more sensitive and indicate more spatial variations of the underlying rule (Billings 2013).

**Table 14:** Contribution of the top three significant soil properties in terms of the sum of error reduction ratio (SERR) on the crop yield, based on shortest distance approximation (SDA) and (CAA) sampling techniques calculated for different radius values.

Re-sampling technique	Re-sampling radius	Sampled number	Top three inputs		Total Contribution (SERR)
			Inputs	Contribution	
SDA	3	1377	CEC	14.60%	20.29%
			Mg	4.69%	
			TN	1.00%	
CAA	3	1377	CEC	16.54%	22.97%
			Mg	4.00%	
			TN	2.43%	
SDA	5	3605	CEC	9.20%	13.61%
			Mg	2.45%	
			TN	1.96%	
CAA	5	3605	CEC	12.90%	15.87%
			Mg	3.02%	
			Ca	2.65%	

OC is organic carbon in % of dry matter; P is extractable phosphorous in mg/l; MC is moisture content in %; TN is total nitrogen in % of dry matter, CEC is cation exchange capacity in meq/100g; Ca is calcium in mg/l; Mg is magnesium in mg/l; and pH the log measurement of acidity.



Results showed that the overall contribution of the eight soil properties to wheat yield variability is 23.21%. One would expect that the contribution of soil properties to yield should be larger than the overall calculated contribution in the current work. Nutrients are required for healthy plants. This study has assessed the impact of the variabilities of eight soil properties through a field. It does not report the necessity of these nutrients, but has attempted to assess the variability of yield, attributed to the soil properties spatial variability. However, the results obtained confirmed this to be a significant contribution, but also shows that there is variability still at play, influencing the crop yield (e.g., crop disease, pests, topography, micro-climatic conditions etc.). For example, whilst TN and OC should have significant effects, and both are required by the crop for healthy growth and grain production, they can also increase and prolong the leaf area index of the crop, which in turn increases humidity, making the plant more susceptible to disease, hence, crop yield is negatively affected (Bryson *et al.*, 1997). In wheat, epidemics can cause significant crop losses, pest damage, including weeds, and disease can result in global loss of around 50% (Bravo *et al.*, 2003; Oerke 2006; Moss, 2013). Further work should expand by including additional variables, to account for more yield variability.

### **3.3 Summary conclusions**

In part one of this study;

The results showed that over the two years the VNRX-L models produced the poorest results for yield variability of 19.15% and 8.5% in 2013 and 2014, respectively. VNRX-LN model accounting for both linear and non-linear interactions, which was the reason why this model has explained 52.2% and 50.7% of yield variation in 2013 and 2014 respectively. The RF model produced the highest contribution of 55.6% in 2013, which dropped down considerably to 45.8% in 2014. Authors encourage further studies into the novel VNRX

modelling approach, for quantifying the individual and collective influences of soil properties on yield variability.

In part two of this study;

Results showed that the overall contribution of the eight soil properties (collected at high resolution) to wheat yield variability using a VNRX-LN model is 23.21%. There is a need for a future work to expand on the current data mining approach to quantify yield limiting factors, based on a greater number of fields with different crops and different agricultural systems. The study should also account for the other affecting factors of crop yield including crop disease, pests, topography, micro-climatic conditions etc., which was highlighted in work by Shearman *et al.* (2005) and Sylvester-Bradley *et al.* (1999).

## **4 Optimising the configuration of a hyperspectral imager for on-line measurement of wheat canopies**

### **Chapter Synopsis;**

This chapter concerns the laboratory-based optimisation of measurement configuration of a hyperspectral imager for cereal crop canopy measurements. The optimal configurations are later applied in the recognition of yellow rust and fusarium head blight (FHB) at canopy level, under laboratory and field on-line measurement conditions to be discussed in chapters 5 and 6, respectively.

### **Abstract**

There is a lack of information on optimal measurement configuration of hyperspectral imagers for on-line measurement of a wheat canopy. This paper aims to identify this configuration using a passive sensor (400-750 nm). The individual and interaction effects of camera height (above the canopy) and angle, sensor integration time and light source distance and height on the spectra's signal-to-noise ratio (SNR) were evaluated under laboratory scanning conditions, from which an optimal configuration was defined and tested under on-line field measurement conditions. The influences of soil total nitrogen (TN) and moisture content (MC), measured with an on-line visible and near infrared (vis-NIR) spectroscopy sensor, on SNR were also studied. Analysis of variance and principal component analysis (PCA) were applied to understand the effects of the laboratory considered factors and to identify the most influencing components on SNR.

Results showed that integration time and camera height and angle are highly influential factors affecting SNR. Among integration times of 10, 20 and 50 ms, the highest SNR was obtained with 1.2 m, 1.2 m and 10° values of light height, light distance and camera angle,

respectively. The optimum integration time for on-line field measurement was 50 ms, obtained at an optimal camera height of 0.3 m. On-line measured soil TN and MC were found to have significant effects on the SNR with Kappa values of 0.56 and 0.75, respectively. In conclusion, an optimal configuration for a tractor mounted hyperspectral imager was established for the best quality of on-line spectra collected for wheat canopy.

## **Keywords**

Hyperspectral imager, signal-to-noise ratio, wheat canopy, principal component analysis, soil properties.

## **4.1 Introduction**

Advanced methods for early disease detection in crops is vital for improving the efficacy of treatment, reducing infection and minimising losses to yield and quality. Traditionally, disease detection is carried out manually, which is costly, time consuming and requires special expertise (Schmale and Bergstrom, 2003; Bock *et al.*, 2010). Developments in agricultural technology have led to demands for a non-destructive, automated approach for crop disease detection that should be ideally rapid, disease specific, and sensitive to early symptoms (López *et al.*, 2003). Optical sensing methods are non-destructive, allowing repeated data acquisition throughout the growing season without inhibiting crop growth. Spectroscopy and imaging techniques have been used in disease and stress monitoring (Hahn, 2009). However, their *in-situ* application although established in other industries (e.g. health services, pharmacology and food safety) is still rather limited. Both Lenk *et al.* (2007) and Sankaran *et al.* (2010) focused on implementing the technology in the field, as a mobile (on-line) application for mapping crop disease. Yuan *et al.* (2016) have used high spatial satellite imagery in the detection of powdery mildew. Remote spectral sensing for identification of

weeds in wheat fields has been tested by means of ground collected data (Gómez-Casero *et al.*, 2009). Herrmann *et al.* (2013) have applied proximal hyperspectral imagery in the field for weed detection (e.g., both broadleaf and grass weeds), reporting 85% accuracy. Okamoto and Lee (2009) collected *in-situ* hyperspectral images for the detection of green citrus fruits, reporting promising results for identification of citrus fruits from background objects. In contrast, non-mobile (off-line) and laboratory methods for disease classification and plant growing conditions have been studied and demonstrated (Roggo *et al.*, 2003; Wu *et al.*, 2008).

A UAV mounted with a multi-spectral camera was successfully applied in the detection of leaf stripe disease in grapevines when monitored with ground assessments (Di Gennaro *et al.*, 2016). Calderón *et al.* (2014) claimed accurate detection of downy mildew in opium poppy using unmanned aerial vehicles (UAV) technology and a combination of thermal and multi-spectral cameras. With the inclusion of fluorescence indices, Calderón *et al.* (2013) could successfully detect *verticillium* wilt in olive trees.

Hahn (2009) claims that spectroscopic and imaging techniques could be integrated with agricultural vehicles, providing non-invasive and reliable systems for the monitoring and mapping of crop diseases, with further potential for early disease detection. Moshou *et al.* (2005) have shown that hyperspectral imaging for the recognition of *in-situ* disease can provide identification with a high degree of accuracy. Depending on the method of analysis and data fusion, an error between 1 - 16.5% was reported.

Spectral reflectance in vegetation canopies is dependent on several factors including the illumination angle, the canopy architecture and the radiative properties of the plants. The reflectance of crop canopies is non-lambertian scattering, varying with the sun position, view

positions and meteorological conditions including cloud cover (Pinter and Jackson, 1985; Asner, 1998). Plant species, maturity, phenology, level of foliage and nutrient status are plant properties affecting reflectance (Asner, 1998; Coops *et al.*, 2003; Gnyp *et al.*, 2014). Geometrical arrangement of objects can affect the spectral reflectance such as leaf orientation, which cannot be controlled during on-line measurements (Asner, 1998; Coops *et al.*, 2003). This creates problems associated with reduced reflection from light scattering. Shadows at small scale can be reduced by additional light sources. Barbedo *et al.* (2015) found that opposing lighting can help reduce shadows. Oberti *et al.* (2014) argued that the angle between the canopy and camera in the range between 0° to 60° affects the sensitivity of a mounted on-line (mobile) sensor due to light backscattering, suggesting the potential of an oblique camera angle, to reduce the impact on signal-to-noise ratio (SNR) variation.

A tractor mounted hyperspectral imager allows for on-line field crop canopy sensing and mapping, however, an optimal configuration of the camera, light source and integration time needs to be established for optimal quality of imagery and spectra to be collected. Spectral quality is predominantly affected by sensor integration time, camera orientation, and light height and angle from the object (leaf or canopy). Integration time is the period over which the detector collects photons of light. The greater the integration time and light intensity, the more reflected light is expected to be captured by the detector, providing a higher SNR and pronunciation of the spectral peaks. Though when relying on sun light, the intensity can be variable. Ideally the system could be run at night to exclude external variabilities, however this solution is not practical. When applying a spectral technique to a forward moving platform (on-line measurement) longer integration times result in an average spectrum over a larger area, reducing the sensitivity. Furthermore, the greater the distance between the camera and its subject, the larger the area observed and captured by a single pixel, reducing spatial

resolution. Therefore, optimising the measurement configuration is essential before on-line field measurements can be successfully carried out. Furthermore, background soil influences canopy spectra, and efforts have been made to remove this influence (Huete, 1988). Based on remote sensing data of the surface soil, Demetriades-Shah *et al.* (1990) suggested using a second order derivative to remove deviations caused by the soil background. However, none of these studies have investigated the influences of on-line measured (at a depth of 15-20 cm) soil properties [e.g., moisture content (MC) and total nitrogen (TN)] on the quality of crop canopy spectra.

This paper evaluates, under laboratory conditions, the individual and interaction effects of camera height and angle, integration time and light distance and height on the spectral SNR of a wheat plant canopy captured with a hyperspectral line imager. Furthermore, the influence of on-line measured soil MC and TN on SNR of plant spectra collected on-line in the field is also assessed. This was essential to inform optimal configuration and operational conditions for on-line field measurement of crop canopy and diseases.

## **4.2 Materials and methods**

### **4.2.1 Hyperspectral configuration in the laboratory**

Winter wheat *Triticum sativum* (Solstice variety) was grown outdoors in 600 x 400 mm trays (depth of 120 mm) with 100 seeds evenly sown and spaced in 5 parallel lines. After seeding, the trays were predominantly rain fed, to reduce input of excess salts from treated tap water. As the crops were grown outside no artificial vernalisation was given. Three grams of Nitrogen (34%) fertiliser were added to each tray, the same composition as that applied during the field experiment (discussed below). A push broom hyperspectral imager (spectrograph) (HS spectral camera model from Gilden Photonics Ltd., UK) was used to capture high-resolution-line images with a resolution of 1,608 pixels over 1 second, using a

diode array detector. It is a 12 bit Basler piA 1600-35 gm camera, with Schneider-Kreuznach XNP1.4/23 lens and has a pixel pitch of 7.4  $\mu\text{m}$  interpolated/averaged to 0.6 nm readings with a spectral range of 400 - 750 nm. The reflected light from the target travels through the lens, past an entrance slit through a series of inspector optics in the spectrograph and is then split by the prism dispersing element into different wavelengths. This sensor was chosen for its potential for being applied to crop canopy measurements, and was of low price compared to comparable sensors, commercially available in the market.

The data captured is in the form of a line array, with each pixel containing a spectrum and one detector per pixel across the swath. In order to compile a full image, every line across a target must be captured (Gilden Photonics Ltd, Glasgow, UK). When configured on a consistent moving platform, the imager sweeps across an area to build up an image. Due to practical restraints of applying a consistent moving platform, the spectraSENS v3.3 (Gilden Photonics Ltd, Glasgow, UK) software was adapted to record a single line array, which required an additional RGB photo taken by a 5 megapixel camera with a 3.85 mm f/2.8 lens at the same time of image capture, so that the scanned area could be comprehended. Two laser pointers were added at each side of the hyperspectral imager to indicate the area of the canopy to be scanned. The laser pointers were shut off when the spectral image was captured to remove any interference. Before data analysis, the collected scans were corrected by means of a dark and white reference, which were collected just before spectral capture, and at 10 minute intervals until scanning was completed. The white reference used was a commercially available Spectralon Teflon white calibration panel with 99.9% white reflectance value. The distance of the camera was set at variable heights from the top of the canopy, so crop height information was not included in the study.



Factorial analysis was undertaken to understand and quantify the influence of configuration parameters on SNR. The wheat was at growth stage 47 according to Zadoks scale (Zadoks *et al.*, 1974) (whilst the head was booting, and the canopy had closed) at the time of scanning. The studied configuration parameters are shown in Table 15.

**Table 15:** Factors included in configuring the hyperspectral imager measured in meters (m), degrees (°) and micro seconds (ms) (multiple configurations considered)

Camera angle, deg °	Light height, m	Light distance, m	Camera height, m	Integration time, ms
0	0.90	0.60	0.15	10
5	1.2	0.90	0.30	20
10	-	1.2	0.45	50
-	-	-	0.60	1000

The same area was scanned in triplicate for the different combination of configurations. The laboratory (simulated-field) measurement configuration is shown in Figure 11. For the indoor environment, two 500 watt diffused broad spectrum halogen lamps were positioned at either end of the crop sample tray with an average Lux measurement of 1650. The additional illumination used in the current work was shown by experience to reduce the influence of shadow within the complex and non-homogenous canopy structure. Imagery data was then captured at different camera and light heights, light distances, camera angles and integration times (measured in milliseconds (ms)), as illustrated in Table 15. Light angle was kept

constant at 45°, which is debated as the optimal angle to provide the strongest response (Huadong, 2001). Additional opposing lighting was used to reduce shadows (Barbedo *et al.*, 2015). Four integration times of 10, 20, 50 and 1000 ms were adopted as these cover the most practical ranges. The 1000 ms integration time illustrates the highest potential time, during which the system will absorb the reflected light hence; this is expected to give the smoothest spectra.

Having determined a suitable configuration in the laboratory, the next experiments were designed to apply the configurations to a field environment and assess the impact of the environmental factors; e.g., soil moisture and total nitrogen, on SNR. Field measurements were conducted in a 9 ha field at Duck End farm, Wilstead, Bedfordshire, UK (52°05'46.3"N 0°26'41.4"W), with an average annual rainfall of 598 mm. The farm has a crop rotation of barley, wheat and oilseed rape. Wheat was cultivated during the experiment in the 2013 cropping season (drilled in September 2013) with canopy measurements being taken in April 2014. The dominant soil type in the field is a clay loam, but has a sand fraction due to underlying gravel deposits.

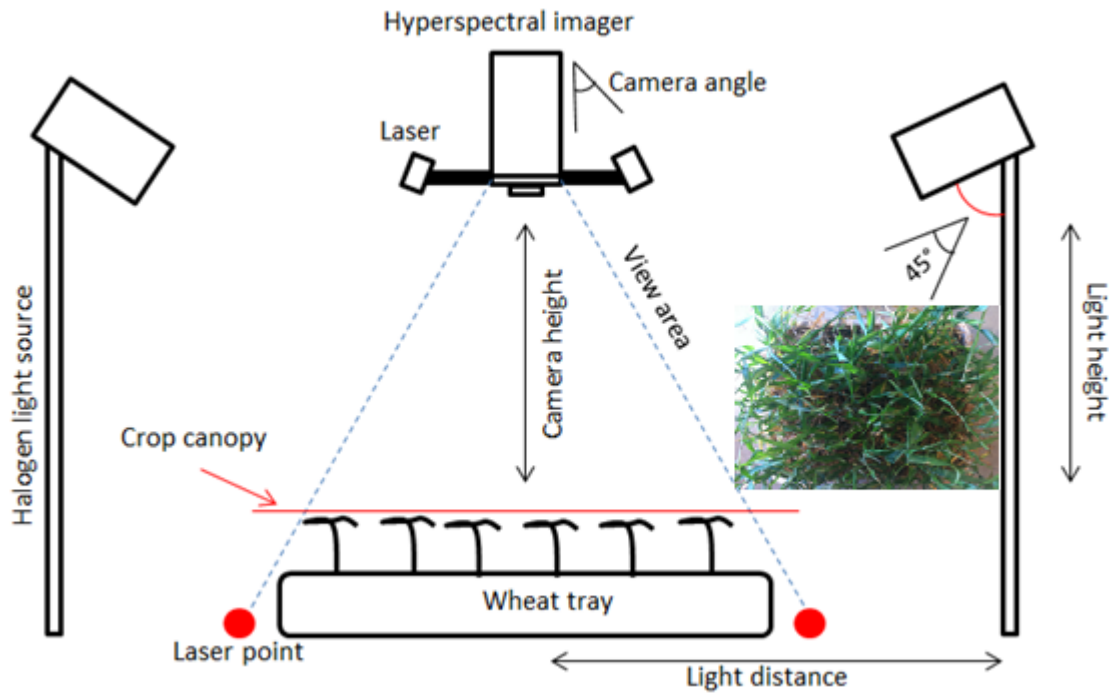


**Figure 11:** Schematic illustration of the laboratory (simulated field) configurations used and the variables implemented to obtain the hyperspectral data with the highest signal-to-noise ratio (SNR). The hyperspectral imager is a passive sensor, but has been applied with an external halogen light source. The Laser pointers allow to precisely position the hyperspectral imager over the target.

#### 4.2.2 On-line soil and crop measurements in the field

The on-line field measurements included crop spectra and soil MC and TN. The reason why MC and TN were the selected soil properties, is that the former affects the soil physical and mechanical conditions, influencing the soil dynamic behaviour below the tractor tyres during the on-line measurement, whereas both may well be linked with crop growth (assuming that TN is directly linked to mineral nitrogen). It is worth mentioning that mineral nitrogen (e.g. nitrate and ammonia) cannot be measured with visible (400-780 nm) and near infrared (780-2200 nm) (vis-NIR) spectroscopy, however analytical tests could be applied (Kuang *et al.*, 2012). Furthermore, the literature confirmed the potential of the vis-NIR to measure MC and TN, which is attributed to the direct spectral response of these properties in the NIR range

(Stenberg *et al.*, 2010; Kuang *et al.*, 2012). The SNR values from the canopy's hyperspectral data was compared against the on-line measured soil properties at the same location via Kappa statistics and visual comparisons. This was essential to evaluate whether or not the optimal measurement configuration established in the laboratory was applicable in the field, and whether modifications should be considered.

An on-line vis-NIR soil sensor developed by Mouazen (2006) was used in this study to measure soil MC and TN, with the objective of mapping the spatial variability of these two selected soil properties. The system consists of a subsoiler, opening a smooth trench at 15 cm depth (Mouazen *et al.*, 2005). The sensor was mounted on a three-point linkage of a tractor travelling at a speed of 3 km h<sup>-1</sup> and collecting spectral soil data at 10 m parallel intervals. In order to measure soil spectra, an AgroSpec mobile, fibre type, vis-NIR spectrophotometer (Tec5 Technology for Spectroscopy, Oberursel, Germany), with a measurement range of 305–2200 nm and a light source of 20W tungsten halogen lamp were used (Kuang and Mouazen, 2013). A differential global positioning system (DGPS) (EZ-Guide 250, Trimble, California, USA) recorded the position of the on-line spectra with sub-meter accuracy. The collection of soil spectra and DGPS readings took place at 1 sec sampling resolution using AgroSpec software (Tec5 Technology for Spectroscopy, Oberursel, Germany).

The same hyperspectral imager (Gilden Photonics Ltd, Glasgow, UK) as that used in the laboratory to optimise measurement configuration was used for on-line measurement of the wheat canopy in the field. The following hyperspectral measurement configuration was considered: an integration time of 50 ms, a camera height of 0.3 m and light height and distance of 1.2 m and a camera angle of 10°. The hyperspectral imager was mounted on a tractor boom (Figure 12) traveling at approximately 4 km h<sup>-1</sup>. The direction and angle of the imager was kept consistent, and a day with uniformly overcast weather (complete cloud

cover) was selected (Figure 13), which helped prevent issues of moving shadows from lateral sun movement on the data (West *et al.*, 2003). Nevertheless, a handheld LUX meter (RS 180 – 7133, RS Components and Controls, India) was utilized to check the sunlight and readings ranged between 1950 and 2000 LUX, indicating no significant difference. Alternatively, to overcome sunlight issues the data collection could be conducted at night with the use of broad spectrum artificial lighting. The hyperspectral camera was mounted to the side of the tractor. It captures images of 1608 pixels per line, over a one-second interval, which is subsequently logged and geo-located using a DGPS. The collected scans were corrected by means of a dark and a white reference (spectralon 99% white reflectance panel). The latter was used before spectral capture, and at a maximum of 30 minute intervals until scanning was completed.

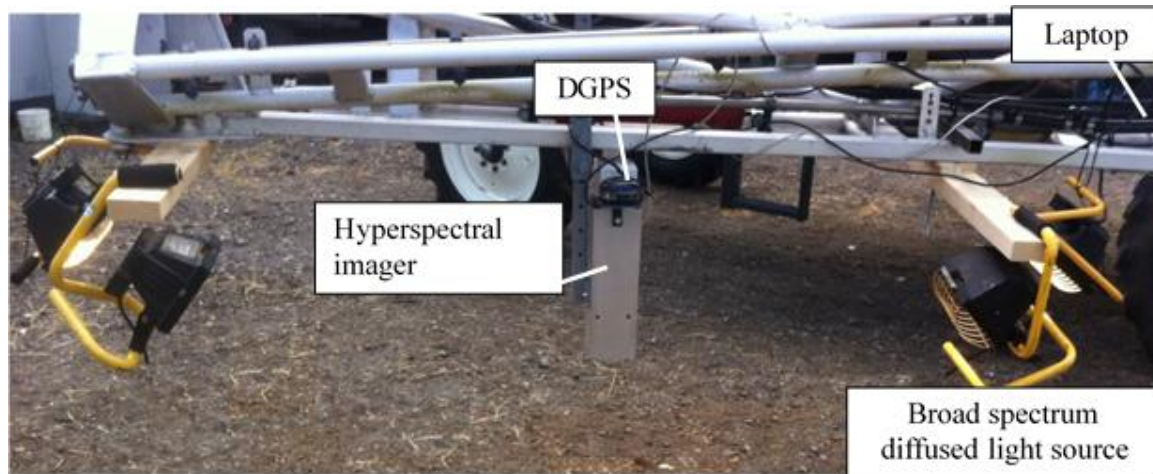


**Figure 12:** Illustrates the on-line field hyperspectral measurement using hyperspectral measurement configuration.



**Figure 13:** Example of the overcast sky at on-line hyperspectral imaging collection.

### **4.2.3 Data analyses**

#### **4.2.3.1 Spectrograph spectral data processing and evaluation**

Quality of the wheat canopy spectra (measured both in the laboratory and field) was evaluated by analysing SNR. The SNR is defined here as a ratio of the signal strength to that of unwanted interference. A strong signal devoid of interference is the desired outcome in measurements. If the data is too noisy it can hide key features of the spectrum, and data pre-processing such as smoothing can result in them being removed (Dasu and Johnson, 2003). A noisy spectrum can result in poor calibration models, due to noise being considered as a feature. There are many applications for estimating the SNR from sources such as electrical, chemical, and spectral. Different methods are often applied to estimate the SNR value,

depending on the data input. Curran and Dungan (1989) used a bright homogenous surface to estimate the SNR and produced a method termed the geostatistical method for removal of periodic noise in images. Van der Meer (2000) used a method outlined by Lee *et al.* (1990) for remote spectral sensing, to assess SNR of Landsat Thematic imagery. Analysis of image SNR has also been conducted through production of histograms of an image (Ramamurthy *et al.*, 2004). A similar approach was outlined earlier by Smith (1999), where spectra were collected from grayscale images. Smith (1999) exemplified a SNR range between 0.5 and 2.0, stating that there is only an issue if the SNR value drops below 1.0. We have used a crop canopy in this study instead of a white or grey reference panel to calculate SNR, since the intention was to use the optimal configuration for on-line measurement of crop canopy in the field, where variations in canopy architecture and leaf orientation are foreseen. The same area of the canopy was used for all individual scans. In this case, whilst uniform intensity cannot be achieved across the spectrum in one scan, each pixel has almost the same target object throughout all the scans. Similar to the measurements carried out in the current work, Daumard *et al.* (2010) relied on crop canopy spectra to maximise SNR, although details of the calculation of SNR were not provided. However, they considered central pixels only in their calculations, whilst we have considered all pixels in a line image after removing non-crop canopy spectra. The following assumptions were made in the current study to justify the selection of a crop canopy for achieving an optimal measurement configuration:

- 1- Non-crop contaminated spectra including soil and soil-plant, etc. can be excluded from the analysis. This was done by calculating normalised differential vegetation index (NDVI) of all pixels. Spectra of pixels with NDVI values smaller than 0.3 were removed from the calculation of SNR. This method is used by Bravo *et al.* (2004) and Huete (1988).

2- Spectra of remaining pixels contain both residual noise and canopy signal, the intensity of which depends on the pixel position within a complex canopy structure of the crop. This will represent the measurement of a homogenous canopy (without soil spectra).

3- Variation in position of pixels for a series of scans can be minimised by fixing the position of crop trays, so that line images are collected from the same target area for different measurement configurations. In this case, whilst uniform intensity cannot be achieved across the spectrum in one scan, each pixel has almost the same target object throughout all the scans.

The calculation of the SNR was done in this study following a similar approach adopted by Ramamurthy *et al.* (2014) and described earlier by Smith (1999). As the data collected is single line 2-dimensional captures, the data was assessed as spectra rather than images. This method of SNR was selected as it could be used as a basis of comparison between individual spectral data captures. We calculated the SNR of individual wavelength ( $SNR_w$ ) as follows:

**Equation 14**

$$SNR_w = M_w / SD_w$$

Where:  $M_w$  is the mean reflectance value of individual wavelengths through all the pixels, and  $SD_w$  is the standard deviation of mean reflectance of individual wavelengths of all pixels explained in a schematic in Figure 14. It is worth noting that all pixels were considered important in the current work to calculate SNR. An alternative approach to this method would have been to select central pixels only to calculate SNR, a method applied by Daumard *et al.* (2010).

The mean spectral signal describes what is being measured, whereas the standard deviation represents noise and other interference for each pixel (Smith, 1999).  $M_w$  values for different



wavelengths were calculated on the remaining 583 wavebands, after removing the spectral range outside of the 400 to 750 nm range, since they were found to be noisy. Once  $M_w$  and  $SD_w$  are calculated for each individual wavelength, the SNR for a spectrum ( $SNR_s$ ) was calculated as follows (see Figure 14):

**Equation 15**

$$SNR_s = M_s / SD_s$$

Where:  $M_s$  is mean reflectance of all wavelengths in a spectrum (a scan) and  $SD_s$  is mean standard deviation of the reflectance of all wavelengths in a spectrum. The SNRs was used in this study to evaluate the strength of scans, hence, the quality of spectral signal. It is worth noting that SD is not important in itself, but only in comparison to the mean. Therefore, a strong SNR with pronounced absorption peaks provides increased recognition for the association of spectral signatures to a subject.

		Wavelength (nm)							
		W 400	W 400.6 ...	...	W 749.4	W 750			
<b>Pixels</b>	P 321	↓	↓			↓	↓	<b>Per Scan (spectrum)</b>	
	P 322								
	...								
	...								
	P 1287								
	P 1288								
<b>Per Wavelength</b>									
	$M_w$	0.196	0.15		0.12	0.192		$M_s$	0.1645
	$SD_w$	0.14	0.1		0.08	0.12		$SD_s$	0.11
	$SNR_w$	<b>1.4</b>	<b>1.5</b>		<b>1.5</b>	<b>1.6</b>		$SNR_s$	<b>1.5</b>

**Figure 14:** Schematic illustration outlining how mean, standard deviation and signal-to-noise ratio for wavelength ( $M_w$ ,  $SD_w$ ,  $SNR_w$ , respectively) and a spectrum ( $M_s$ ,  $SD_s$ ,  $SNR_s$ , respectively) were calculated.

A principal component analysis (PCA) was also undertaken on laboratory measured hyperspectral data only using Statistica software (StatSoft inc., Oklahoma USA) to identify parameters with the greatest impact on SNR. PCA is a statistical method, which analyses the distribution of data in multidimensional space (principal components) or similarity maps, where similarities (within groups of a variable) and differences between groups can be evaluated (Dytham, 2011). In this instance, SNR, integration time, light height and distance, and camera angle and height were used as input variables for the PCA analysis. Additionally, a two-way analysis of variance (ANOVA) was carried out with RStudio software (RStudio Boston, MA) to estimate significant influences of individual variables and interaction between variables on SNR (Webster, 2007; Dytham, 2011).

#### **4.2.3.2 On-line soil sensor calibration**

Laboratory measurements of MC and TN were carried out using a standard reference method. Soil MC was measured with oven drying of samples at 105°C for 24 h, whereas TN was measured with a TrusSpecCNS spectrometer (LECO Corporation, St. Joseph, MI, USA), using the Dumas combustion method (Dumas, 1826 as cited by Buckee, 1994). The on-line collected soil spectra were subjected to pre-processing before modelling. Pre-processing included noise cut by removing wavelengths smaller than 400 nm and larger than 1900 nm. Noise cut was followed successively by maximum normalisation, and Savitzky-Golay first derivative and smoothing was applied. The smoothing reduces noise in the spectrum, and the first derivative was used to eliminate the effect of the roughness of soil surface on the spectrums absorption (Shibusawa *et al.*, 2000; Waiser *et al.*, 2007), Partial least squares regression (PLSR) analysis with leave-one-out full cross-validation was carried out to establish correlations between soil spectra and laboratory measured MC and TN. Spectra pre-

processing and PLSR analysis were carried out using Unscrambler 7.8 software (Camo Inc.; Oslo, Norway).

#### **4.2.4 Mapping**

Maps for on-line vis-NIR predicted MC and TN and on-line spectrograph measured wheat canopy reflectance were developed using ArcGIS 10 (ESRI, California, USA) software. Kriging was used to develop maps, assuming that the distance or direction between sample points reflects a spatial correlation that can be used to explain spatial variations. The advanced parameters option in ArcGIS 10 software (ESRI, California, USA) allowed control of the semi-variogram used for kriging, with spherical selected as the best fit. The semi-variogram values were calculated in RStudio (RStudio, Boston, MA).

The similarity assessment between maps can be performed by visual inspection and statistical tests (Tekin *et al.*, 2013). The simplest way of comparing between maps is by visual inspection, to conclude whether similarities may exist or not. However, this is insufficient, as quantitative estimation of similarity is a more robust approach to adopt. To compare the statistical relationship of pairs of maps, Kappa statistics (Cohen, 1960) analyses were performed to calculate the Kappa value ( $\kappa$ ), using SPSS (Statistical Package for the Social Sciences, IBM, Armonk, New York, USA). However, before running Kappa statistics, data was subjected to raster analyses to have the same 5 m by 5 m grid size for all maps, after which the data underwent maximum normalisation.

### **4.3 Results and Discussion**

#### **4.3.1 Spectral quality in the laboratory**

Typical wheat crop canopy spectra can be observed in Figure 15, which shows clear, noisy and saturated spectra. The clear and saturated spectra can be observed to be more pronounced, whereas a weak absorption in the spectral signature and interference in the noisy

spectrum leads to reduced quality, low SNR, masking detail in the signature and causing a loss of important spectral information through the entire spectral range studied. The clear spectrum is the best quality, and the target to be obtained. The noisy spectrum is caused by the low integration times, and greater distance of the Halogen light source. A strong SNR with pronounced absorption peaks would allow for a greater success in analysis of crop assessments and disease presence. Although, pre-processing of spectral data includes techniques such as smoothing, if the process of cleaning the data is intensive due to noisy spectra it can lead to the loss of important spectral features, and thus impact on the success of analysis (Dasu and Johnson, 2003).

Saturation predominantly occurs within the central pixels associated with the highest reflectance, causing data in the peaks of the electromagnetic spectrum to be lost (starting around 650 nm). Leaf reflectance in the NIR range is affected by the structure of the plant leaves (Gates *et al.*, 1965), and can be related to the leaf wax coating (Cameron 1970). In the case of spectral saturation the data becomes unusable. In the remaining parts of the spectrum, however, particularly the visible range (400–700 nm), there is a lower reflectance due to a larger absorption of the light, which is attributed to the photosynthetic pigments of the plants leaves, (Gates *et al.*, 1965).

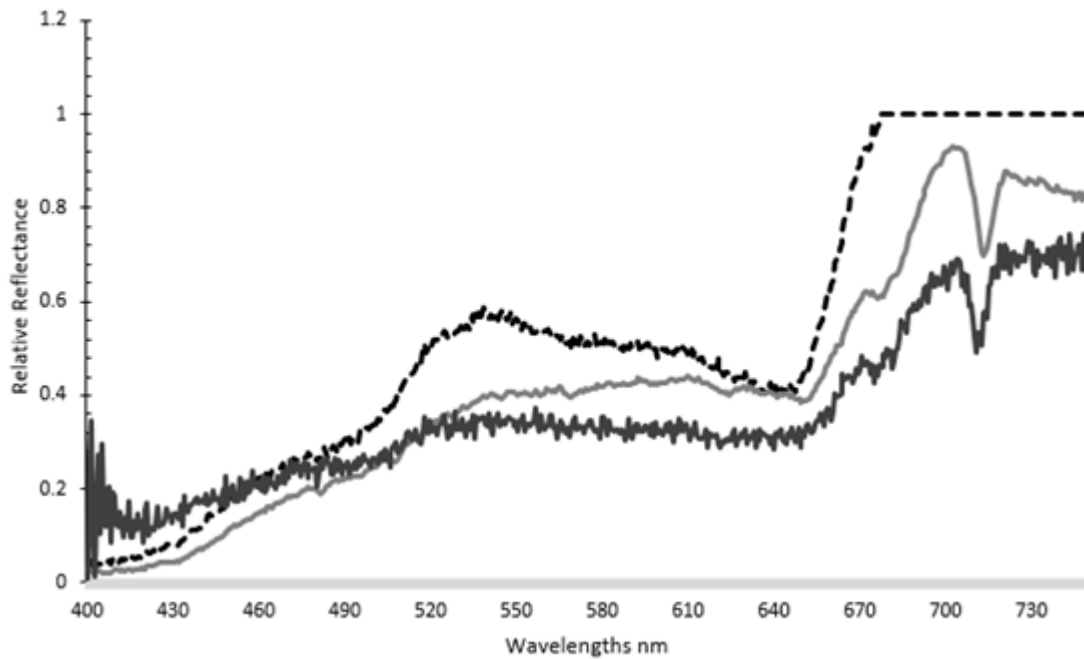


**Figure 15:** Examples of smooth (the grey line with 1.6 signal-to-noise ratio (SNR), noisy (the black line with 1.2 SNR), and saturated (the dotted line with 1.8 SNR) spectra of wheat canopy. The saturated spectrum flattens off at 680-750 nm and important information is lost on the peak around 700 nm that is otherwise illustrated by the clear spectra.

When analysing the entire spectral signature, saturation causes a reduction in sensitivity. Therefore, sensor configurations leading to saturated spectral data were removed from the analysis of SNR. All saturated data were obtained with integration time of 1000 ms, this is in line with the literature, where larger integration times can cause saturation of the data (Dell’Endice, 2008).

#### **4.3.2 Hyperspectral image configuration parameters; laboratory**

The integration time considerably affected the SNR, expressed as average and SD values (Eq. 1), as shown in Table 16.

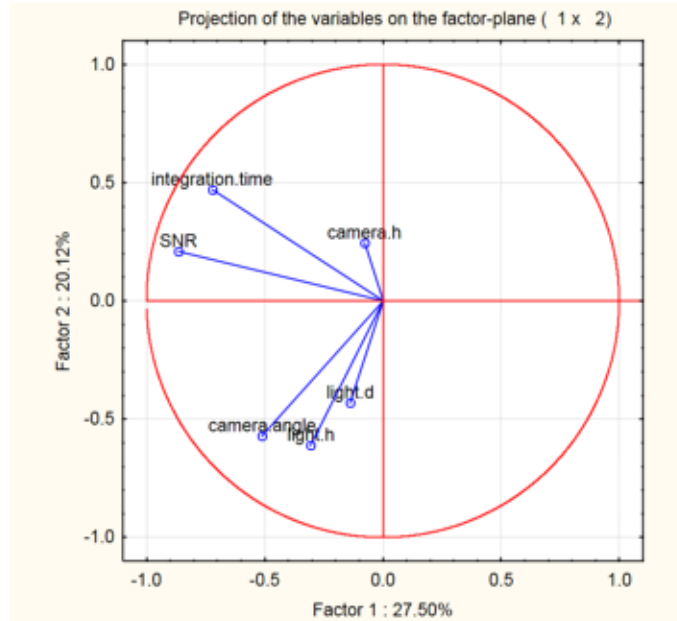
**Table 16:** Average and standard deviation (SD) values of the highest signal-to-noise-ratios (SNR) obtained with different integration times, camera settings and light source settings when scanning a wheat canopy. Theoretical forward distance travelled (and captured to a single data line) if applied on a moving platform at field scale.

<b>Average, SNR</b>	<b>SD</b>	<b>Integration time, ms</b>	<b>Light height, m</b>	<b>Light distance, m</b>	<b>Camera height, m</b>	<b>Camera angle, deg</b>	<b>Distance travelled, m</b>
<b>1.688</b>	0.102	1000	1.2	1.2	0.15	10	4
<b>1.669</b>	0.160	50	1.2	1.2	0.30	10	0.2
<b>1.471</b>	0.103	20	1.2	1.2	0.45	10	0.08
<b>1.386</b>	0.078	10	1.2	1.2	0.45	10	0.04

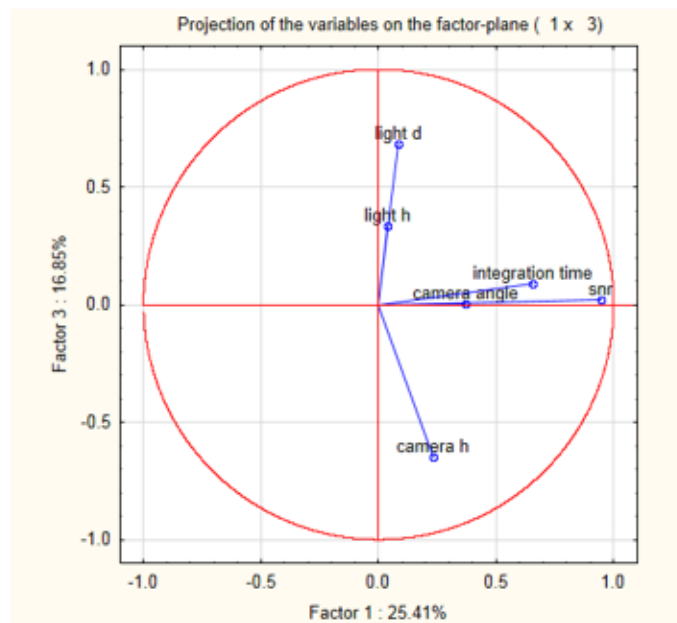
The longer the integration time, the greater the opportunity for more energy to be captured by the spectrograph. The 1000 ms configuration was the highest potential integration time and was trialled (under field simulations) to see the potential highest SNR, whilst the manufacturer recommended around 20 ms for laboratory use. The results from the 1000 ms integration time provided a high percentage of saturated results. The non-saturated recordings were of the same SNR values to that of the 50 ms integration times, so integration times higher than 50 ms were not trialled further. With varying the integration time, parameters had constant values apart from the camera height. The optimal camera height decreases with an increased integration time, the closer the camera to the object, the higher the integration time required. This may mean that the most influencing parameters on the SNR were the

integration time and camera height. Other studies demonstrated that the movement (adjustments, bounce or vibration) between the imager and the subject during integration time can cause a compiled image to be warped or noisy (Zhong *et al.*, 2011). For on-line measurements, the easiest variable to control is integration time, as angle and height can alter slightly as ground is uneven, crop stands vary and unavoidable movement occurs in mountings. It becomes necessary to have the optimal configurations set initially but to understand there would be slight deviations. A NADIR camera angle was selected, due to reports from Oberti *et al.* (2014) and Van Beek *et al.* (2013).

ANOVA (appendix B) showed that all individual variables and interactions of variables had significant influences on SNR at the (0.05) 5% probability level, except for the interactions of light distance and integration time (0.01), and light distance, camera height and integration time (0.01) (Appendix B). Therefore, the null hypothesis 'that variables and subsequent interactions of variables will have no significant effect on SNR' can be rejected.



(a)



(b)

**Figure 16:** Principal component analysis similarity maps developed for principal components 1 and 2 (a) and for principal components 1 and 3 (b). Input variables are camera and light height, light distance, camera angle, integration time and signal-to-noise ratio (SNR)



Principal component analysis, allows for a simpler visual understanding of a dataset as it emphasise patterns and variations, by expressing the variation in a minimal number of observations (Wold *et al.*, 1987). Figure 16 illustrates the similarity maps of principal component (PC) 1 and 2 (a), and PC1 and 3 (b) accounting for 47.62% and 42.26% of variance, respectively. Examining the plot of PC1 vs PC2 one can observe that the integration time, SNR and camera height are gathered in one group, which explains these to be closely related. Integration time showed the strongest influence and correlation with SNR, whereas, camera height demonstrated the second closest corresponding variable on SNR with the latter having a weaker influence (Figure 16a). Light distance, light height and camera angle seem to have a smaller influence on SNR (compared to integration time and camera height), as they make a separate group associated with PC2 with minor variance associated with PC1. Disregarding other variables, it becomes clear that a longer integration time and a smaller camera height result in a higher SNR.

Although the light distance and height are strongly associated in the PCA similarity maps (Figure 16 a and b), they have a negligible influence on the SNR. This does not mean that the absence of light would have no effect. As long as there was ample diffused light, in order for the detector to collect photons, light variables appeared to have little impact. Although the influence of camera height was the second largest in the PC1-PC2 similarity map, in the PC1-PC3 similarity map, the camera height had little influence on SNR, similarly to the light variables. Furthermore, the close correlation between camera height and integration time shown in the PC1-PC2 similarity map is not observed in the PC1-PC3 similarity map. In the latter similarity map (Figure 16 b), the camera angle has the second largest influence on SNR after the integration time. This means that both camera height and angle have strong influences on the SNR. Under laboratory measurement conditions, larger camera angles were

reported to be beneficial for powdery mildew recognition in leaves of grape vines by Oberti *et al.* (2014). Smaller view angles are discussed by Pisek *et al.* (2009) to theoretically be better due to observing a larger area. Rautiainen *et al.* (2008) concluded greater nadir angles are more suitable for viewing the top canopy and had a very limited view of the understory. This is supported by the finding that 80% of the crop yield is calculated from the health of the top 3 leaves (HGCA, 2008). The correlation between green leaf retention and yield has been observed in a number of trials (Reynolds *et al.*, 2009; Ali *et al.*, 2010; Hunt and Poole, 2010) and can be observed with reference to trial work in barley conducted by the authors in 2009, where every 1% reduction in green leaf area on flag-1 at GS80 correlated to a 20 kg/ha loss in yield. This is true when applying a camera angle. But when assessing light conditions, an off-nadir angle can create more lighting variability, due to shady and illuminated areas of the crop. Van Beek *et al.* (2013) found that for smaller off-nadir viewing angles ( $<20^\circ$ ) of the sensor, the sun orientation was found not to be important. This, along with issues of shadow from the infield mountings, is why small angles for the configurations were selected.

To make a decision on an optimal configuration that would result in the highest SNR, was not a straightforward process. However, when SNR values are arranged according to the integration time (Table 16), a clear trend is observed. For example, SNR increased with integration time, where the highest values of SNR were obtained with an integration time of 1000 ms, however, they were only marginally higher than the SNR values at 50ms. Since several variable combinations resulted in similar SNR values, it is perhaps premature to suggest the optimal configuration as the single highest, so configurations with SNR variability of less than 5% from the highest reading (of each integration time) were considered for further evaluation. The further analysis confirms that the highest SNR occurs with the same configurations of 1.2 m, 1.2 m, and  $10^\circ$  of light height, light distance and

camera angle, respectively. As stated earlier, the camera height is negatively correlated with the integration time (Table 16). A possible theory for reoccurrence of these configurations could be that they allow for the greatest amount of reflected light to be captured by the detector. Among the integration time steps of 10, 20, 50 and 1000 ms selected, a practical range for on-line measurement is between 10 ms and 50 ms, a range which is suggested by the manufacturers. Assuming that the best integration time for practical on-line (mobile) measurement in the field is 50 ms, the optimal configuration parameters of 1.2 m, 1.2 m, 0.3 m and  $10^\circ$  are recommended for light height, light distance, camera height, and camera angle, respectively. The average SNR for this integration time is 1.669 (seen in Table 16), which in reference to Smith (1999) we believe is a strong signal for a crop canopy. These optimal configuration parameters were adopted for the on-line measurement of wheat canopy measurement in this study.

#### **4.3.3 Hyperspectral imager; on-line measurement**

During the on-line measurement, it was noticed that there was an unavoidable bounce in the boom observed to be at  $\pm 0.2$  m of the original height of the mounting (set at 0.3 m above the crop canopy). On inspection of the data, the camera height from the object affected the uniformity of light intensity measured across the pixels, (particularly at the beginning and end of the captured line). Therefore, for calibrating the on-line hyperspectral scans, it is recommended to overcome this fluctuation by removing the first and last 320 pixels from the spectral data. This is specific to this hyperspectral imager but is an interesting factor for consideration.

Comparing the laboratory with on-line field measured canopy spectra, one can observe that the laboratory reflectance scans are of a higher relative reflectance than the on-line scans, specifically between 500nm and 700nm (Figure 17). The laboratory spectra are from tray grown crops, whilst the on-line scans highlight different spatial areas of a field. The reflectance difference between the laboratory and field scans could be also due to other influencing factors such as water stress. The laboratory spectra shown is an average spectrum from multiple trays. Although trays are reasonably deep (120 mm), they do not necessarily hold as much water as in the field and this is believed to be reflected by the laboratory spectra (Wang *et al.*, 2014). Initially, the on-line spectra showed variation throughout the field, which appeared to be in response to different crop spatial conditions. For example, the field scan 1, refers to the canopy of water stressed wheat plants, whereas field scan 2 refers to healthier wheat plants. Crops start to show yellow colour as a symptom of water stress, which leads to reduce light absorption and increased reflectance as shown in field scan 1 (Figure 17). More detailed analysis of crop and soil properties needs to be assessed to understand differences in quality of canopy spectra collected in the field.

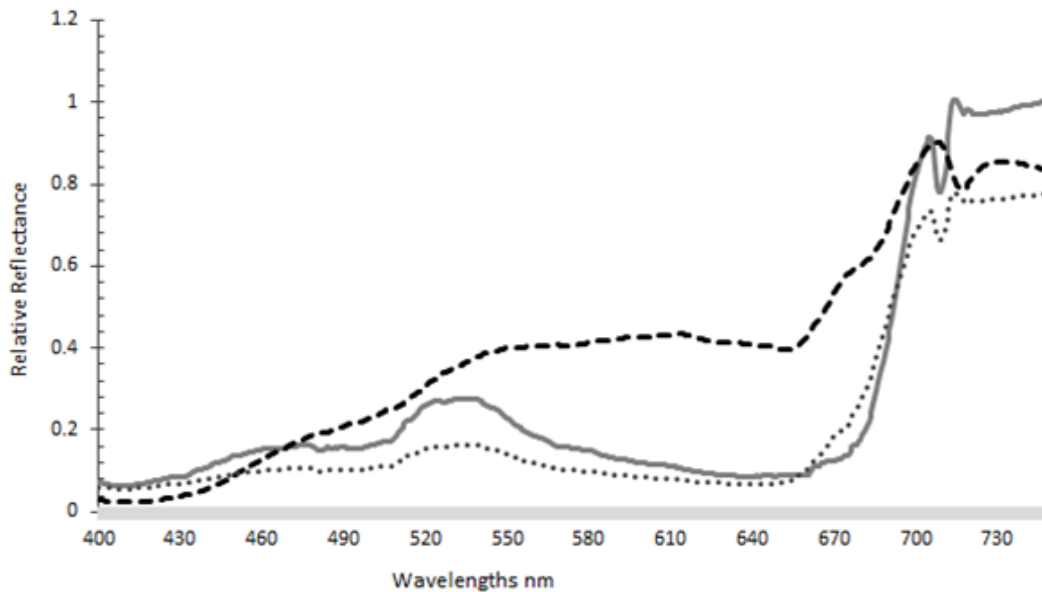


**Figure 17:** Comparison of canopy spectra of water stressed wheat crop obtained in the laboratory (the dashed line) and on-line in the field (the dotted and grey lines). The crop was of the same variety and at comparable growth stages. Laboratory and field scans were collected under the suggested optimal configurations. The on-line field scans are: 1) field scan (the grey line) is of a more water stressed plant and 2) field scan (the dotted line) is of a less water stressed plant.

#### **4.4 Influence of soil properties on signal-to-noise ratio during the on-line measurement**

The on-line measured soil MC and TN maps of the field provided a visual explanation (Figure 18) for a drop in reflectance within certain areas of the field. Comparing the MC map with the SNR map, one can draw a general conclusion that areas of low MC correspond with areas of high SNR, and vice versa (areas of high MC being of low SNR). This can be explained by the fact that soil deformation under the tractor tyre in wet soils is larger than that in drier soil conditions. A larger soil deformation should result in a larger fluctuation in camera height and angle, compared to the baseline setup, which may lead to reducing the

SNR. Work carried out by Söhne (1958) showed that an increase in the MC of a soil and the increase in payload on a tyre both increase the depth of soil deformation.

Both on-line measured MC and TN were found to have significant effects on the SNR of the wheat canopy spectra at 95% confidence. The kappa values between the SNR map and TN and MC maps confirm spatial similarities within the field. Landis and Koch (1977) classified Kappa values into different categories: 0–0.20, 0.21–0.40, 0.41–0.60, 0.61–0.80, and 0.81–1, which indicate slight, fair, moderate, substantial, and almost perfect agreement, respectively. Results show that the Kappa value between TN and SNR is rather small (kappa = 0.56), indicating moderate similarity between these two maps. Since TN is the main source of mineral nitrogen essential for crop growth and development, it can be influential on the quality of the crop canopy and SNR.

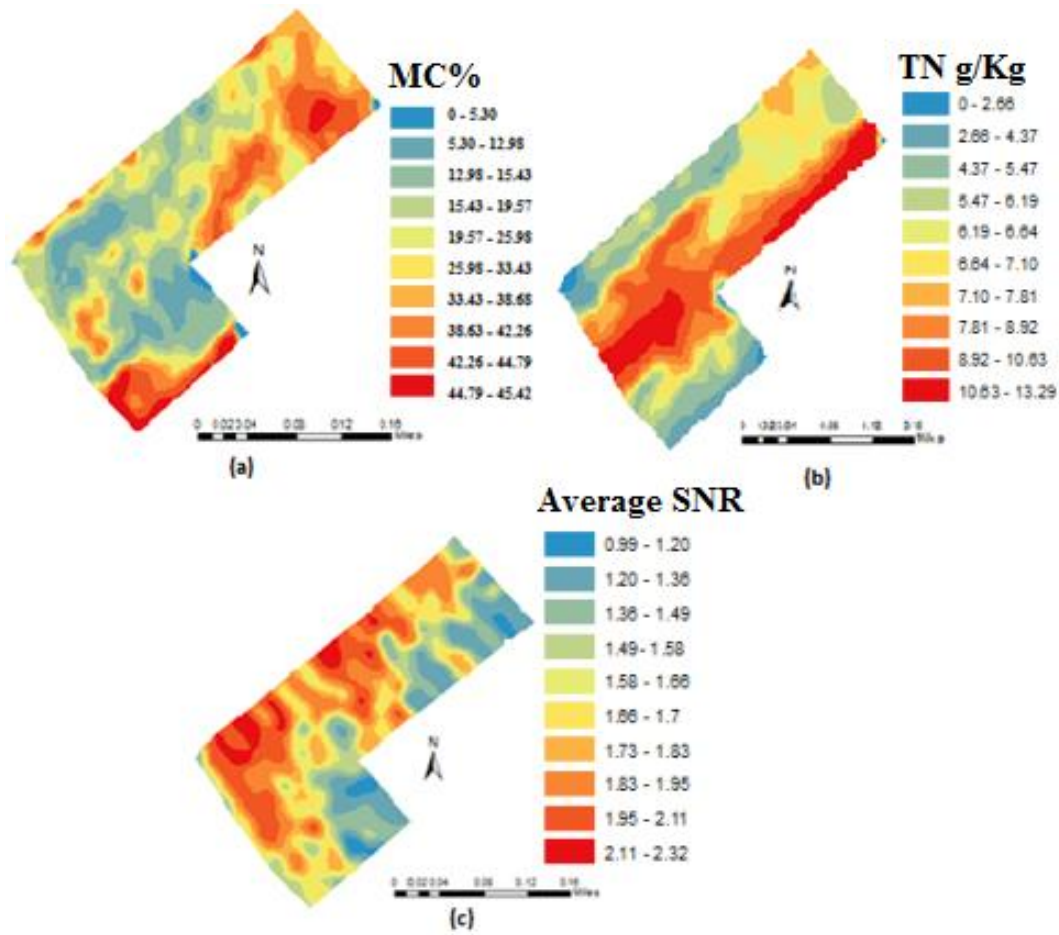


**Figure 18:** Maps of on-line measured soil moisture content (MC) (a) total nitrogen (TN) (b), and the average signal-to-noise ratio (SNR) per scan (c).

The kappa value between MC and SNR was much higher ( $\kappa = 0.75$ ) than that between TN and SNR map, confirming substantial similarity between the two maps. This supports the earlier suggestion about the influence of MC on soil deformation that changes the initial (optimal) hyperspectral measurement configuration obtained in the laboratory and implemented for on-line measurement in the field. To reduce the negative influence of soil deformation on SNR due to high soil MC during on-line scanning, proper spectra pre-processing is recommended e.g., normalisation, derivation, and multiplicative scatter corrections. Further research is required to confirm this assumption, as when measuring on-

line, deviations from the optimum configuration (due to tractor vibration, bounce in the boom and soil deformation) were unavoidable.

## **4.5 Conclusions**

This study was undertaken to determine an optimal measurement configuration of a hyperspectral line imager (400-750 nm). The SNR was calculated on the hyperspectral measurement of a wheat canopy, under laboratory scanning conditions. The individual and interaction effects of the systems configurations were evaluated for the impact on the SNR. Optimal configuration was determined and implemented for on-line field measurement. The influence of on-line measured soil moisture content (MC) and total nitrogen (TN) on SNR was evaluated. Results allowed the following conclusions to be drawn:

1- The integration time followed by the camera height and camera angle appeared to have the largest influence of the SNR. A long integration time (>50 ms) was of a negligible influence and only slightly increased the SNR, but resulted in spectral saturation, hence should be avoided.

2- The PCA similarity map showed that the light height and distance have a strong correlation with each other but a minimal influence on SNR.

3- Both on-line measured MC and TN were found to have significant effects on the SNR of the wheat canopy spectra at 95% confidence. The on-line soil measurements revealed stronger spatial similarity between the hyperspectral SNR and MC maps (kappa value = 0.75), which was attributed to soil deformation below the tractor tyre.

4- The variable reflected light intensity captured by the different pixels across the line imagery is an interesting factor to consider, due to the impact of varying camera height



during the on-line measurement. Whilst the solution suggested here is appropriate, it is camera specific.

Further work is planned to overcome variation in SNR associated with camera height changes (vibration, bounce in the boom, and soil deformation during the on-line measurement) by the implementation of a proper spectra pre-processing. It is also planned to implement these hyperspectral measurement configurations for on-line measurements of crop canopy for detection of crop health and disease presence.

## **5 Hyperspectral measurements of yellow rust and fusarium head blight in cereal crops: Part 1: Laboratory study**

### **Chapter Synopsis;**

This chapter focuses on the application of the hyperspectral imager with the optimised configurations achieved in Chapter 4 for the detection of yellow rust and fusarium head blight (FHB) in wheat and barley canopies. This was done based on PLSR models developed for yellow rust and FHB quantitative prediction. The methods developed in this chapter will be applied in the following chapter (6) using on-line data.

### **Abstract**

The aim of this study was to assess the potential use of a hyperspectral camera for measurement of yellow rust and fusarium head blight (FHB) in wheat and barley canopy under laboratory conditions. The plants were grown in trays and inoculated with different spore concentrations of the two studied pathogens. In order to account for water stress, trays were water stressed at the crop growth stage 45. Visual assessment of disease was made at four levels, namely, at the head (when present), at the flag leaves, at 2<sup>nd</sup> and 3<sup>rd</sup> leaves (mid canopy), and at the lower canopy. Partial least squares regression (PLSR) was implemented to establish calibration models to predict the percentage coverage and scale of infection (0-5 for yellow rust and 0-2 for FHB). Results showed that a hyperspectral technique coupled with PLSR can be successfully used for the prediction of yellow rust in winter wheat and barley canopies. Ratio of prediction deviation (RPD) values of 2.25 (equivalent to an  $R^2= 0.8$ ) and 1.97 ( $R^2= 0.77$ ) were calculated for wheat and barley based on scale measurement and 2.04 ( $R^2=0.77$ ) and 1.80 ( $R^2=0.69$ ) for percentage coverage, respectively, which were classified as good accuracy in wheat and as moderately accurate in barley. For FHB detection, results were less successful (RPD = 1.5 in wheat and 1.36 in barley, equivalent to an  $R^2$  of 0.57 and

0.5, respectively). The standard deviation between 500 and 650 nm and squared difference between 650 and 700 nm can explain differences between healthy, yellow rust and FHB infected canopies. It is recommended to explore the potential of hyperspectral imaging for on-line measurement of studied diseases in cereals.

## **Keywords**

Yellow rust, fusarium head blight, wheat, barley, crop canopy, partial least squares regression.

## **5.1 Introduction**

With the world's population estimated to reach 9 billion by 2050, sustainable approaches to increase crop yield is a necessity (Hole *et al.*, 2005; Godfray *et al.*, 2010). The majority of current farming practices are based on unsustainable production systems, relying on external inputs and high-yield varieties susceptible to disease (Hole *et al.*, 2005). Advanced management (e.g., precision agriculture) of farm external resources such as fungicides, if applications were site specific, could result in increasing yield at a reduced amount of input and cost. This can be achieved by applying the full rate to areas of the field which would benefit from the resource, and by applying a reduced rate to areas of lower demand, which would reduce the quantity of input (Wittry and Mallarino 2004; Maleki *et al.*, 2007). Among these resources, fungicide application may well be reduced by targeted site specific spraying (FRAC, 2010). However, accurate measurement of fungal diseases is a main requirement for sustainable application of fungicides, and is expected to contribute to the reduction and prevention of the spread of crop disease and the losses of quantity and quality incurred from them.

Fungal disease control is a large task for the successful production of cereals worldwide. Both yellow rust and fusarium head blight (FHB) are fungal diseases which infect small cereal crops, and are responsible for causing severe yield losses (De Vallavieille-Pope *et al.*, 1995; Bravo *et al.*, 2003). Disease presence can vary considerably between plants. Yellow rust caused by *Puccinia striiformis* is a foliar disease, which can alone reduce crop yields by 40%. Bravo *et al.* (2003) stated that reductions in the yield can be as high as 7 t ha<sup>-1</sup> in severe epidemics. Alternatively known as stripe rust, yellow rust produces yellow uredo spores on the leaves. Following infection, the disease starts with chlorosis occurring parallel to leaf veins, in a narrow 2 mm wide stripe, which develops later into multiple yellow coloured rust pustules (De Vallavieille-Pope *et al.*, 1995). FHB is one of the most important pre-harvest diseases worldwide, reducing yield quantity and quality. The most aggressive and prevalent fusarium species is *Fusarium graminearum*, which is a highly pathogenic species. The pathogen can also produce mycotoxins, which can become a significant threat to both humans and animals. FHB symptoms in wheat and barley appear in the head and peduncle tissues, causing discolouration and early senescence. Lesions can occur on the leaves during heavy infection and fusarium can also cause fusarium foot rot. Disease presence can vary considerably between plants (Rotter *et al.*, 1996; Brennan *et al.*, 2005; Desjardin, 2006; Leslie and Summerell, 2006), hence, it is required to adopt site specific treatments of fungal diseases.

Advanced methods for disease detection in crops is vital for improving the efficacy of treatment, reducing infection and minimising the losses to yield and quality. Traditionally, disease detection is carried out manually, which is costly, time consuming and requires special expertise (Schmale and Bergstrom, 2003; Bock *et al.*, 2010). Alternative methods of detection are needed to enable mapping the spatial distribution of yellow rust and FHB.

Among those methods, optical sensing methods are recommended candidates since they are non-destructive and allow for fast and repeated data acquisition throughout the growing season without inhibiting crop growth. It was recognised by West *et al.* (2003) that although optical technologies are available for development into suitable disease detection systems, many challenges are still needed to be overcome, and this is still arguably the case.

Spectroscopy and imaging techniques have been used in disease and stress monitoring (Hahn, 2009). One of the optical methods reportedly used to measure disease in crops is hyperspectral imagery in the visible (vis) and/or the near infrared (NIR) spectral ranges. The reflectance in the visible wavelength range is relevant to leaf pigmentation whilst infrared wavelength range provides information on the physiological condition of the plant. The wavelength function for light intensity in hyperspectral imaging adds the wavelength and spectrum (with its spatial position) to the brightness information of the spectral image, providing a rapid image-contrast, which would not be present in a conventional image approach (Huang *et al.*, 2007). Within the visible spectrum, the radiation reflectance from an environmentally stressed plant will increase. This is due to an increase in the incidence reflection within the leaf of a stressed plant (Cibula and Carter, 1992). Bélanger *et al.* (2008) showed that disease could be quantified on detached leaves, finding that the ratio between blue (near 440 nm) and green (near 520 nm) intensity between the healthy and diseased tissue was significantly different shortly after inoculation. Using vis-NIR imaging, Bravo *et al.* (2003) detected early symptoms of yellow rust on winter wheat, with a quadratic discriminant model analysis, reporting a correct discrimination accuracy of 92–98%. To our knowledge none of the above studies incorporated water stress effects, in the prediction model of yellow rust and FHB intensity in cereal crops. Some studies have focused on bringing the technology to the field. However, the first step towards field application is to test the

accuracy of the methods under laboratory conditions (allowing more control and observation of the crop), where disease and water stress are accounted for in one experiment.

The aim of this paper is to assess the potential implementation and performance of a hyperspectral imager for recognition of yellow rust and FHB diseases in winter wheat and winter barley under laboratory conditions, with the intention to establish calibration models and spectral library for potential use under mobile on-line measurement conditions. Both diseases (yellow rust and FHB) and water stress were introduced and accounted for.

## **5.2 Materials and methods**

### **5.2.1 Wheat and Barley cultivation and inoculation**

Treated seeds of winter wheat *Triticum sativum* (Solstice variety) and winter barley *Hordeum vulgare* L. (Carat Variety) were grown outdoors in 600 x 400 mm trays (depth of 120 mm), with 100 seeds evenly sown and spaced in 5 parallel lines. After seeding, the trays were predominantly rain fed, to reduce input of excess salts from treated tap water. Three treatments were adopted, where each treatment was triplicated in three separate trays. A total of 18 trays of wheat, and 18 trays of barley were grown for each of the following three treatments (illustrated in Figure 19);

- 1) Treatment 1 – Naturally yellow rust infected: consisting of six trays that were not treated with fungicide, as these were to represent the more heavily infected yellow rust trays, and were not inoculated with fusarium.
- 2) Treatment 2 – Healthy: consisting of six trays of each that were kept healthy by applying a broad spectrum fungicide, namely, Rubric (epoxiconazole) at a rate of 1 lha<sup>-1</sup>.
- 3) Treatment 3 – Fusarium inoculated: consisting of six trays of each that were infected with fusarium as the crop reached anthesis growing stage (Figure 20).

When the crop growth reached 'booting' growth stage 45 on the Zadoks scale (Zadoks *et al.*, 1974), half of trays in each were water stressed using a transparent tarpaulin and water content was monitored throughout the growing season using a moisture-probe ML3 Thetakit (Delta-T Devices Ltd, Cambridge, UK).

Yellow rust occurred naturally in the crops as early as growth stage 30. Therefore, half of the crop trays were treated early with fungicide to fulfil treatments 2 and 3. This allowed for a difference in intensity of yellow rust disease. *Fusarium* inoculation was applied to trays in treatment 3 at the anthesis crop growth stage. The spores were first cultivated in the laboratory by using the following method. A 2% wheat agar was produced using 100 ml distilled water, with 2 g agar and 2 g milled wheat. This was autoclaved at 120°C. Plates were poured to a consistent depth, and inoculated with *Fusarium graminearum* BFE1006 isolated from infected wheat grain. The plates were grown for 5-7 days under near UV light as this was shown to help cause sporulation (Leach, 1967). The agar plates were subsequently agitated with distilled water to suspend the spores with the concentration increased as necessary by gentle use of the centrifuge. Spore concentrations were standardised at approximately  $10^6 \text{ ml}^{-1}$  using serial dilutions and a haemocytometer. Every  $1 \text{ m}^2$  of crop ear was inoculated with 100 ml of the suspension, which is an adapted method from Lacey (1999). These trays were then kept under a high humidity conditions for 24 hours.

Whilst it has been reported that fungicide has little to no effect on crop canopy reflectance, some azole fungicides can have a negative impact on crop growth and yield, when applied to small plants (Geis, 2014; AHDB, 2016). In this study, the epoxiconazole fungicide was applied at growth stage 32. Some symptoms of yellow rust disease were recorded in the fungicide treated trays. However, the fungicide treated trays remained healthier, and these were included in the PLSR models.

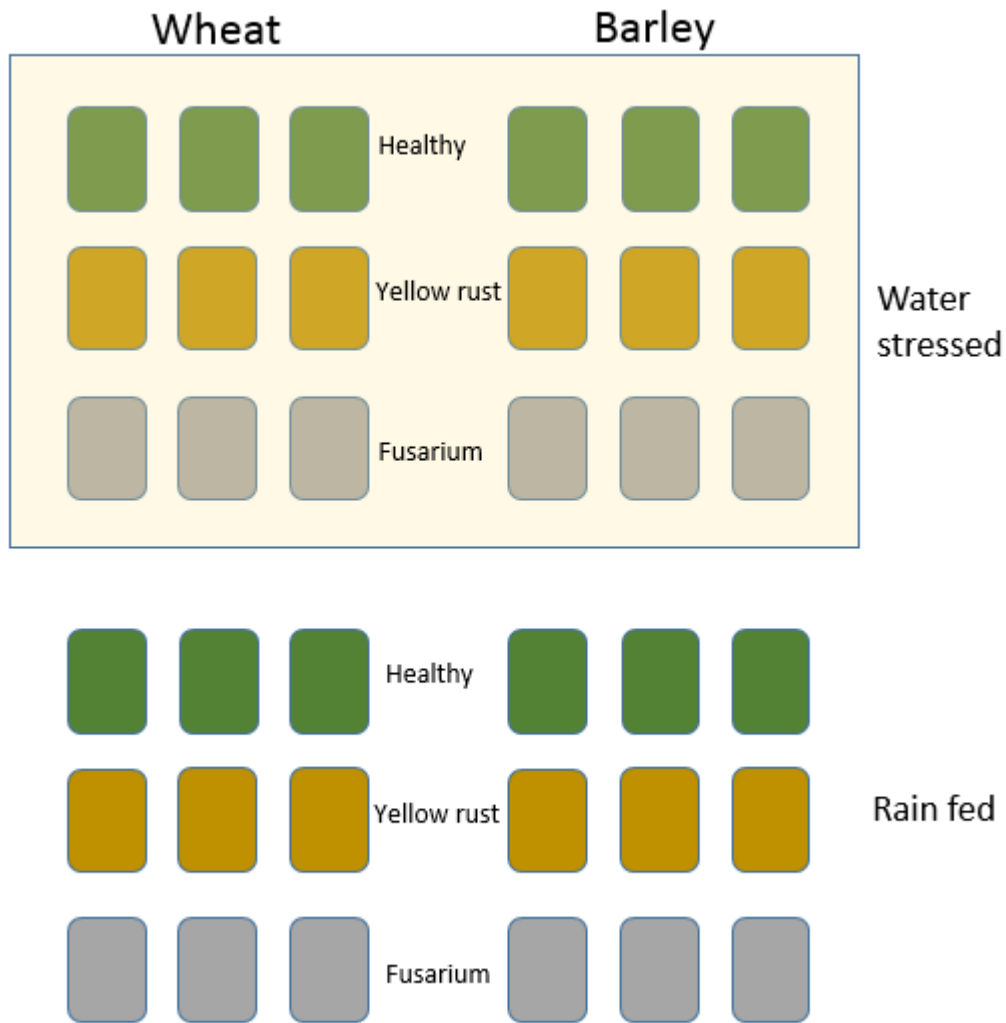


**Figure 19:** Schematic of tray replicates and treatments, showing winter barley and winter wheat, with yellow rust and fusarium head blight (FHB) diseases, and healthy crop, both rain fed and water stressed, in replicates of three.



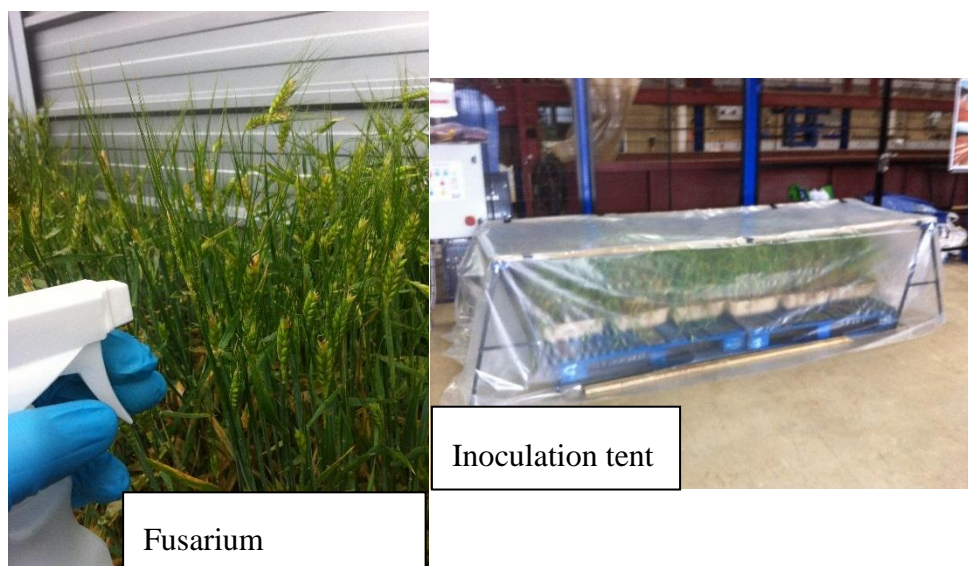


**Figure 20:** Fusarium inoculation of wheat and barley trays in the laboratory. Inoculation took place at the anthesis crop growth stage.

### 5.2.2 Disease assessments

A common approach for disease assessments and general crop health is by visual inspection, known as diagnosis (Oberti *et al.*, 2014). This is done based on both a percent coverage and a visual score, with a range between 0 and 5 (from less to more affected plots) where 0 is given when no disease is present, 1 for up to 5% cover, 2 for up to 10%, 3 for up to 30%, 4 for up to 50% and 5 for >50%. This visual score can eliminate most of the variability of judgment between plots, which is a commonly used technique (Eby, 1996; Zhou *et al.*, 2015). The scale groups of percentage classes were chosen due to bias in assessment of low infection. According to Parker *et al.* (1995), plants with smaller than 10% infection are the most misdiagnosed, and often estimated as having much higher disease infection.

Two assessment methods for yellow rust and one of FHB were used (detailed below) on both wheat and barley trays. These methods are defined by Chiarappa (1981), as two distinct quantitative disease measurements: 1) Disease incidence, which is the number of individual plants affected as a ratio or percentage of the total number, 2) Disease severity which is the

amount of expressed disease tissue of a plant. These disease parameters can be assessed with some objectivity, although they may well be subjected to some subjectivity. In the current work, each tray was assessed for both diseases at four levels, namely, at the head (when present), at the flag leaves, 2<sup>nd</sup> and 3<sup>rd</sup> leaves (mid canopy), and at the lower canopy explained as follows;

- 1) For fusarium infection, only the head of the crop was assessed as we were assessing for FHB, which appears in the head and peduncle tissues, causing discolouration and early senescence. Earlier visual symptoms consist of a characteristic purple/pink discolouration. The seeds from FHB affected crops are often shrunken, with a bleached appearance (Andersen, 1948; Parry *et al.*, 1995; McMullen *et al.*, 1997; Goswami and Kistler, 2004). Impey (2012) confirmed the presence of fusarium leaf lesions in Herefordshire, the leaf lesions are very unusual, and found only in heavy infections. The assessment considered both early and later symptoms, and were assessed as either a 0 for no infection, 1 for mild infection (describing FHB symptoms on up to 50 % of the ears, with the majority being symptoms of early infection), and a 2 for heavy infection (describing FHB infection in over 50% of the ears with the majority being early senescence), dependent on the ratio of occurrence of infected to healthy crops.
- 2) For yellow rust infection, the three foliar stages were assessed for percent coverage of yellow rust lesions. Disease starts with chlorosis occurring parallel to leaf veins, in a narrow 2 mm wide stripe, developing into multiple yellow coloured rust pustules (De Vallavieille-Pope *et al.*, 1995). Average disease coverage was given for all the plants in the assessment area at the 3 different stages, and a visual score was also given. As it's needed for each ground truth plot to have a singular assessment for the later analysis, the data from each stage was combined and weighted appropriately

according to HGCA (2008) recommendations; that 80% of a wheat yield can be calculated from the top 3 leaves (Figure 21). The weighting given in this study was as follows; flag leaf 55%, mid canopy 40%, and lower canopy 5%. This allowed a single yellow rust assessment to be associated to a tray. This was done for both wheat and barley crops. Barley has a much smaller flag leaf, representing about 4% of the leaf area. However, the health of the flag leaf is still considered to be significant in determining yield (Jebbouj and Yousfi 2006 and 2009), and due to the image being taken from above the canopy, the flag leaf will still be highly captured. Therefore, barley was also subjected to the same weighting. Two different quantitative assessments were recorded, one for the percent cover on the leaves and one recorded as a 0-5 scale, based on a similar approach to Bergamin Filho and Amorim (1996), Godoy *et al.*(2006) and Huang *et al.*(2007).

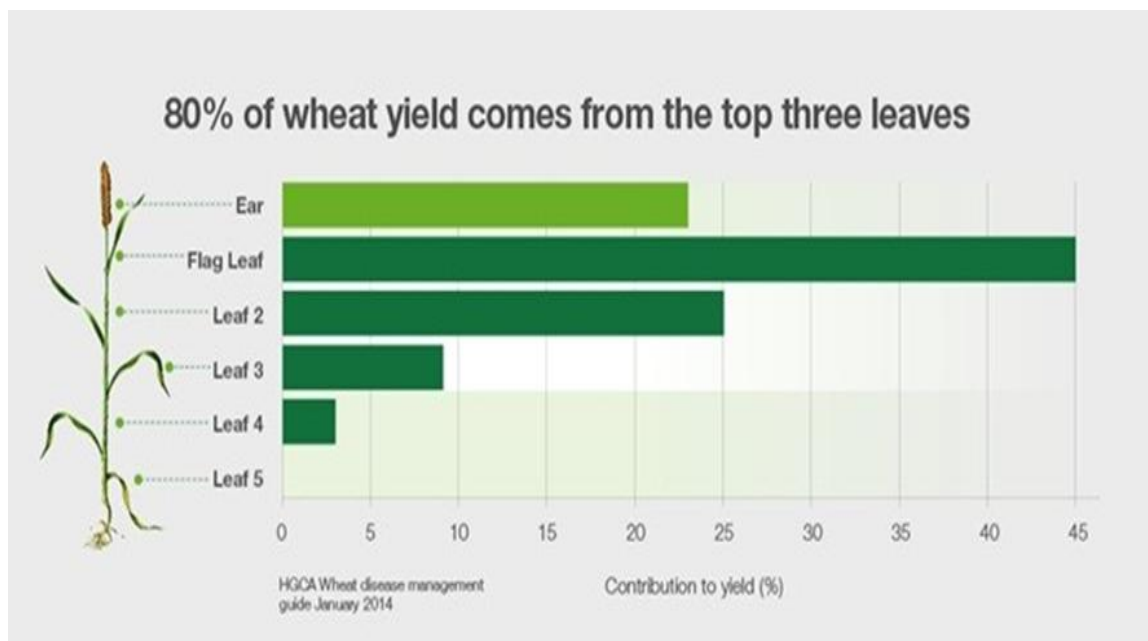


**Figure 21:** Illustrating influence of foliar health on yield (HGCA, 2008)

### 5.2.3 Hyperspectral data capture

A push broom hyperspectral imager (spectrograph) (HS spectral camera model from Gilden Photonics Ltd., UK) was used to capture high-resolution (1,608 pixels) line images over 1 second, using a diode array detector. It is a 12 bit Basler piA 1600-35 gm camera, with Schneider-Kreuznach XNP1.4/23 lens and has a pixel pitch of 7.4  $\mu\text{m}$  interpolated/averaged to 0.6 nm readings with a spectral range of 400 - 1000 nm. The reflected light from the target travels through the lens, past an entrance slit through a series of inspector optics in the spectrograph and is then split by the prism dispersing element into different wavelengths. This sensor was chosen for its potential for being applied to crop canopy measurements, and was of a lower price compared to comparable sensors, commercially available in the market. The spectral data was captured at three separate places along the crop tray at slightly different positions. Captured in the form of a line array, each pixel has a spectrum and one detector per pixel across the swath. In order to compile a full image, every line across a target must be captured (Gilden Photonics Ltd, Glasgow, UK). When configured on a consistent moving platform, the imager sweeps across an area to build up an image. Due to practical constraints of applying a consistent moving platform, the spectraSENS v3.3 (Gilden Photonics Ltd, Glasgow, UK) software was adapted to record a single line array, which required an additional RGB photo taken by a 5 megapixel camera with a 3.85 mm f/2.8 lens at the same time of image capture, so that the scanned area could be comprehended. Two laser pointers were added at each side of the hyperspectral imager to indicate the area of the canopy to be scanned (Figure 22). The laser pointers were shut off when the spectral image was captured to remove any interference. The collected scans were corrected by means of a dark and a white reference (spectralon 99% white reflectance panel) providing the relative reflectance.

The latter was used before spectral capture, and at 10 minute intervals until scanning was completed.

The optimal configuration of the push broom hyperspectral imager including light sources was optimised in the laboratory (Whetton *et al.*, 2016b). A schematic illustration of the configurations can be observed in Figure 22, where two 500 watt diffused broad spectrum halogen lamps were positioned at either end of the crop sample tray. Light angle was kept constant at 45°, which is debated as the optimal angle to provide the strongest response (Huadong, 2001). The optimal configuration adopted included integration time, light height, light distance, camera height, and camera angle, of 50 ms, 1.2 m, 1.2 m, 0.3 m and 10°, respectively (Whetton *et al.*, 2016b). These configurations were used in the current work, for crop canopy scanning that started at booting growth stage 43 on Zadoks scale and continued until reaching ripening at growth stage 90.

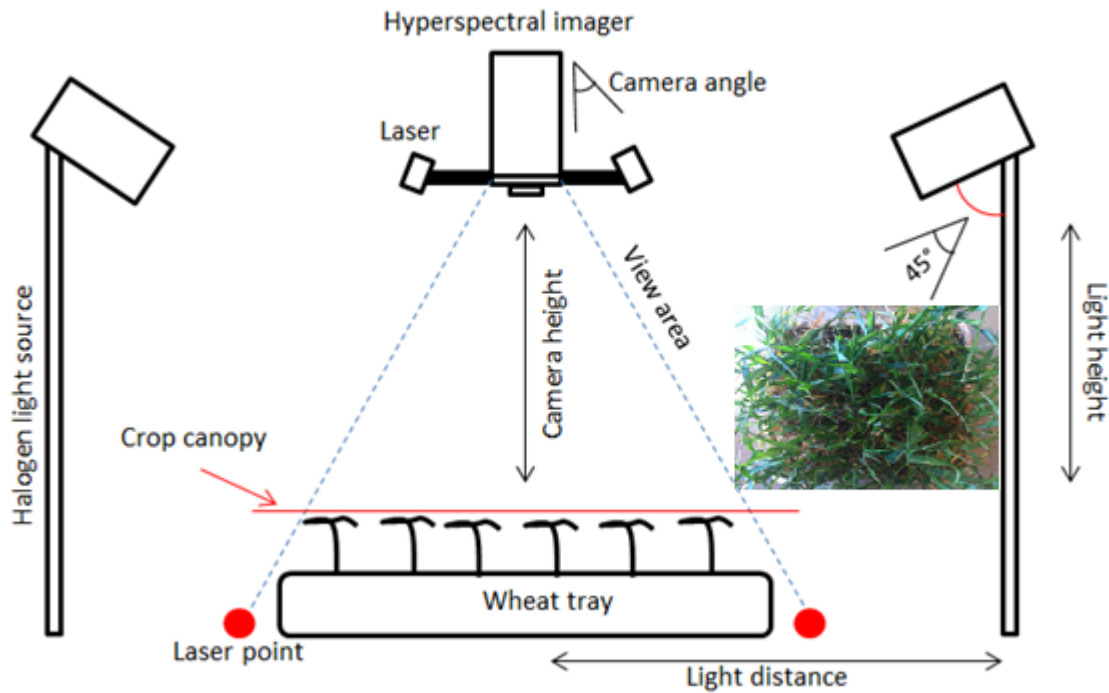


**Figure 22:** Schematic illustration of the laboratory configurations of hyperspectral camera and light source (Whetton *et al.*, 2016b).

#### 5.2.4 Data pre-processing and modelling

If the spectral data is too noisy, there is a risk that key features of the spectrum will be hidden, and data pre-processing such as smoothing is necessary to remove noise, but can remove significant features (Dasu and Johnson, 2003). Furthermore, a noisy spectrum can result in poor model performances, due to noise being considered as a feature. So the first step towards successful measurement should ensure obtaining a good quality spectrum, which was ensured in the current work by adopting the optimal configurations established in Whetton *et al.* (2016b).

The spectral data were averaged to reduce the number of wavelengths (variables), which was successively followed by maximum normalisation, Savitzky–Golay first derivative and smoothing (Mouazen *et al.*, 2006). Maximum normalisation is typically used to get all data to

approximately the same scale, or to get a more even distribution of the variances and the average values. The maximum normalisation is a normalisation that “polarizes” the spectra. The peaks of all spectra with positive values scale to +1, while spectra with negative values scale to -1. Since all soil spectra in this study have positive values, the peaks of these spectra scaled to +1. This scaled spectra between 0 and +1. Using the Savitzky–Golay first derivative enables the computation of the first or higher-order derivatives, including a smoothing factor, which determines how many adjacent variables will be used to estimate the polynomial approximation used for derivatives. A second order polynomial approximation was selected. A 2:2 smoothing was carried out after the first derivative to decrease noise from the measured spectra. All pre-processing steps were carried out using Unscrambler 10 software (Camo Inc.; Oslo, Norway).

Analysis of variance (ANOVA) was used to analyse two spectral indices captured at the growth stage 72. A factorial treatment structure was incorporated to test for differences between disease type (healthy, FHB, yellow rust), water treatment (watered, water-stressed) and crop type (barley, wheat). In addition, a contrast was used to test for differences between healthy and diseased trays and between the different diseases. Analysis of the index SD was done on a log scale, whilst analysis of SQdiff was done on a sqrt scale to ensure homoscedasticity of variance. GenStat 18<sup>th</sup> Edition (© VSN International Ltd, Hemel Hempstead, UK) was used to compute the ANOVA tables.

PLSR analyses were applied to the hyperspectral data (Table 17) to establish quantitative models to predict yellow rust and FHB infection. Before PLSR analysis, data were divided into two sets of 80% (e.g., 174 samples for yellow rust and 129 for FHB) and 20% (e.g., 43 samples for yellow rust and 32 for FHB), representing the calibration and prediction data sets (Tables 17), respectively. The pre-processed spectra and visual

assessments of yellow rust and FHB of the calibration dataset were subjected to PLSR with leave-one-out full cross-validation to establish calibration models. The performance of these models was evaluated by predicting crop disease using the prediction dataset. Separate models for wheat and barley were developed and evaluated for yellow rust and FHB. PLSR analysis was carried out using Unscrambler 10 software (Camo Inc.; Oslo, Norway). The following models were developed and validated:

- 1) Yellow rust prediction in wheat and barley, estimated as % of disease spread on the leaves. This was referred to as yellow rust in %.
- 2) Yellow rust prediction in wheat and barley, estimated at 0 to 5 scales of the amount of disease spread on the leaves. This was referred as yellow rust scale.
- 3) FHB prediction in wheat and barley estimated as either a 0 for no infection, 1 for mild infection and a 2 for heavy infection.

For yellow rust, a LOGIT transformation of the % coverage response was also trialed to ensure homoscedascity of variance. The inverse LOGIT function ( $\exp(p)/(1+\exp(p))$ ) was applied before assessment of the prediction results. PLSR analysis was carried out using Unscrambler 10 software (Camo Inc.; Oslo, Norway). Outliers were detected and removed to a maximum of 5% of the total input data. The model performance was evaluated in cross-validation and prediction by means of coefficient of determination ( $R^2$ ), root mean square error of prediction (RMSEP) and ratio of prediction deviation (RPD), which equals standard deviation divided by the RMSEP. In order to compare between the performances of different models developed, we proposed classifying RPD values into the classes mentioned in Table 18. The entire pre-processed spectrum was used in the PLSR analyses.



**Table 17:** Statistics of samples used in the partial least squares regression (PLSR) models, with 80% and 20% of samples were considered for cross validation and prediction, respectively. The data has a normal distribution. Yellow rust % refers to the percent cover of yellow rust on the leaves (used for both % and the logit transformation). Yellow rust scale refers to classes of disease infection levels with 0 being none and 5 being >50%. Fusarium head blight (FHB) refers to number of infected ears compared to number of healthy ears with 0 being healthy and 2 being >50%.

	Wheat			Barley		
	Yellow rust (%)	Yellow rust scale	FHB	Yellow rust (%)	Yellow rust scale	FHB
<b><i>Cross-validation</i></b>						
Sample Nr.	174	174	129	174	174	129
Maximum	70	5	2	60	5	2
Minimum	0	0	0	0	0	0
Mean	21	2.56	0.55	21.1	1.8	0.55
SD	15	1.5	0.83	12.75	1.05	0.83
<b><i>Prediction</i></b>						
Sample Nr.	43	43	32	43	43	32
Maximum	40	5	2	60	4	2
Minimum	1	1	0	10	0	0
Mean	12	3.09	0.87	34	1.8	0.61
SD	9.87	1.35	0.8	17	0.95	0.93

**Table 18:** Classes of the ratio of prediction deviation (RPD) and their suitability for predicting yellow rust and fusarium head blight (FHB) in cereal crops, and is based on the classifications from Rossel *et al.* (2006).

RPD range	Class and prediction capability
< 1	Poor model predictions - not useful.
1-1.5	Possibility to discriminate between low and high values
1.5-2.0	Moderate prediction capability
2.0-2.5	Good prediction capability
2.5-3.0	Very good prediction capability
>3.0	Excellent prediction capability

Outliers were detected, and removed to a maximum of 5% of the total input data. These outliers were recognised by being distant from the other observations, either due to variability in the measurements or an error in data capture (e.g. missed in data cleaning). The model performance was evaluated in cross-validation and prediction by means of  $R^2$  and root mean square error of prediction (RMSEP) and ratio of prediction deviation which equals standard deviation divided by the RMSEP. In order to compare between the performances of different models developed, we proposed classifying the ratio of prediction deviation (RPD) values into the classes mentioned in Table 17, calculated by dividing the RMSEP by the standard deviation of visually assessed infection. RPD values were used as they are more thorough in reporting the reliability of a model, than  $R^2$ . However,  $R^2$  has been referenced through the text for use as a comparison.

## 5.3 Results

### 5.3.1 Crop canopy spectra

Crop canopy spectra for wheat and barley are shown in Figure 23. The spectral signatures were selected to demonstrate clearly the variations in shape. Arrows have been added to highlight important wavelengths, where the spectrum shows the most visible variation between the two crops (500, 650 and 700 nm).

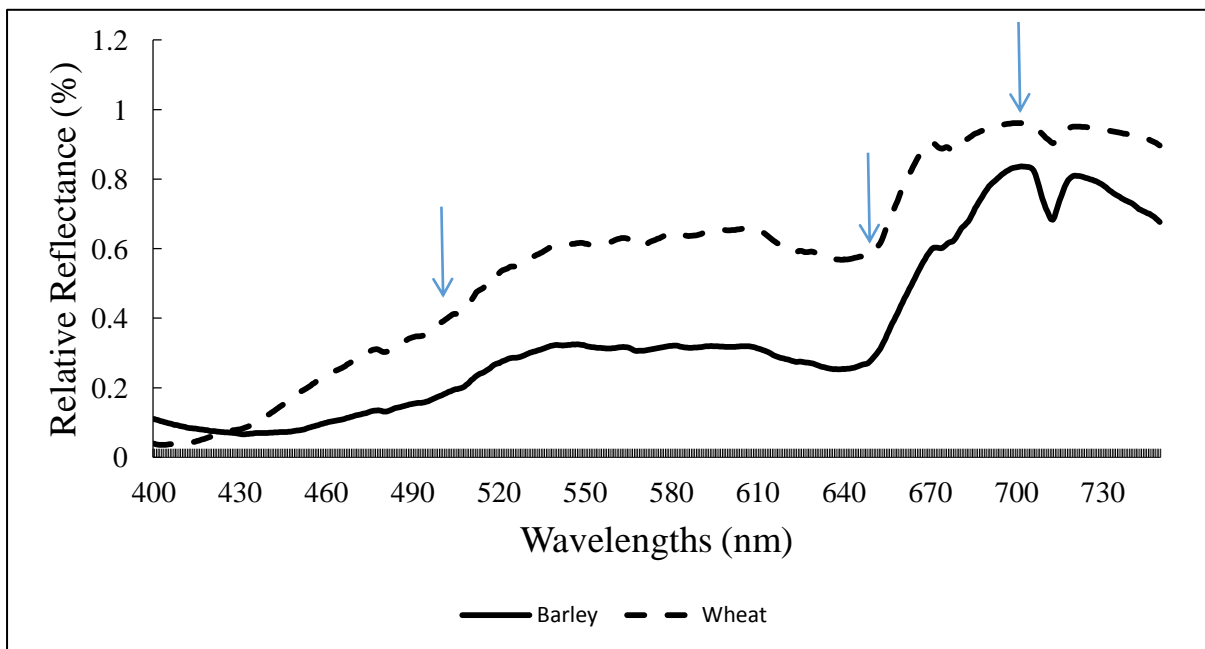


**Figure 23:** Example spectra of wheat and barley canopy at growth stage 72, after white and dark corrections. Arrows highlight areas of interest for indices to distinguish the health of the crop.

Average spectra of healthy, yellow rust and FHB infected wheat crop canopy at growth stage 72, are plotted in Figure 24, and for barley in Figure 25. While plots a, b and c compares between watered and water stressed spectra, plot d compares between healthy and infected canopies under watered conditions. Slight differences in the shape of the reflectance spectrum can be observed in the healthy canopy (Figure 24 a) than in the water-stressed canopy. However, in the healthy barley canopy, the water-stressed spectrum shows less absorption than the watered canopy (Figure 25 a). The water-stressed spectra are less reflective than watered spectra, particularly for the yellow rust in both wheat and barley (Figure 24 b and Figure 25 b, respectively). Only a negligible deviation is observed between FHB infected spectra in both wheat and barley (Figure 24 c and Figure 25 c, respectively), indicating a larger influence of yellow rust on crop canopy when combined with water stress, compared to FHB. A closer examination of Figure 24 and 25 (d) indicates differences in spectra between healthy, yellow rust and FHB infected crop canopy under watered conditions. Barley and wheat canopies show a similar high reflectance for yellow rust infected canopy, compared to those of FHB and healthy canopies.

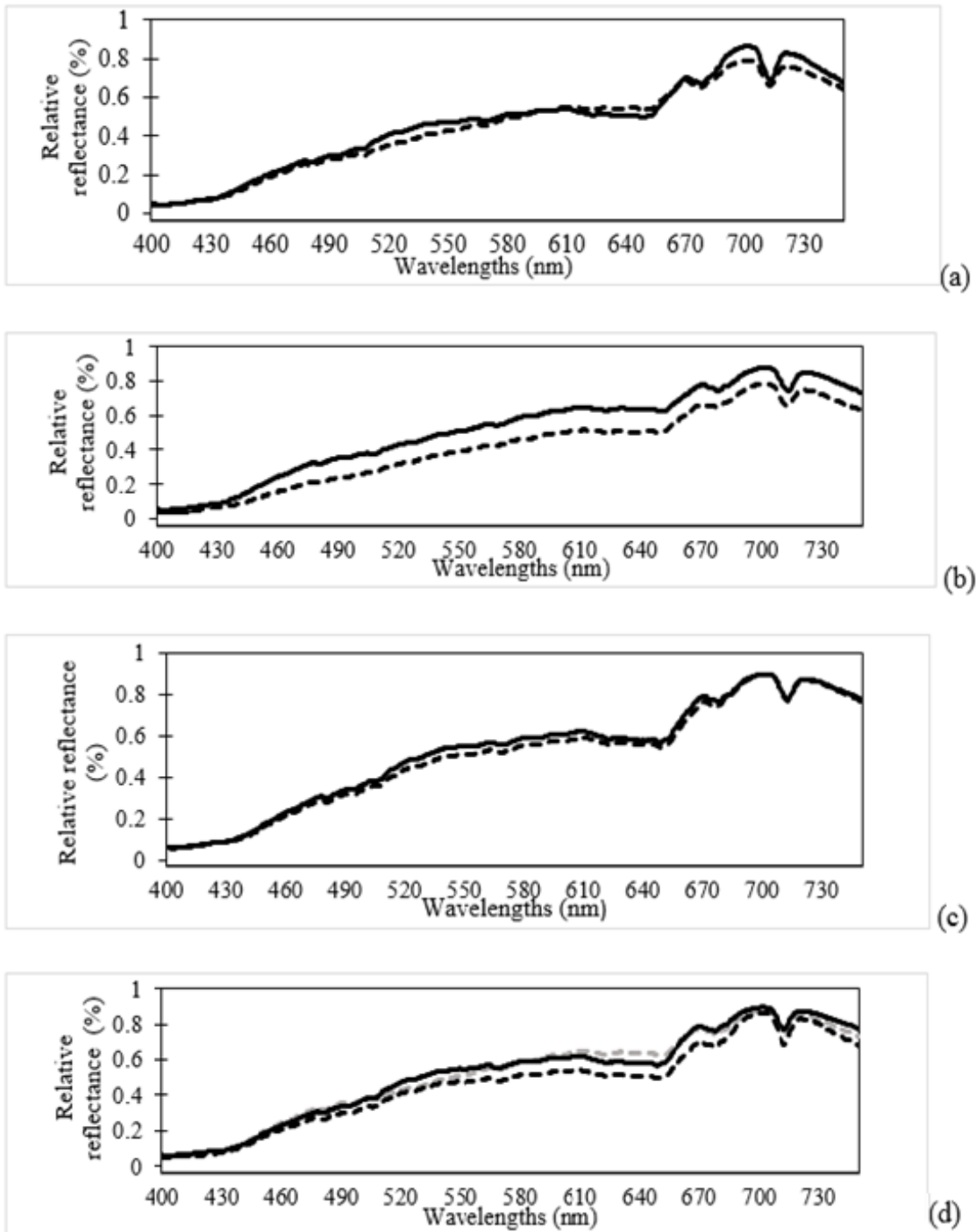


**Figure 24:** Comparison of an average wheat crop canopy spectra between watered (-) and water-stressed (----) treatments for a) healthy, b) yellow rust infected and c) fusarium head blight (FHB) infected crop canopy. Plot (d) compares canopy spectra under watered conditions of healthy (---), yellow rust (---) and FHB (-).

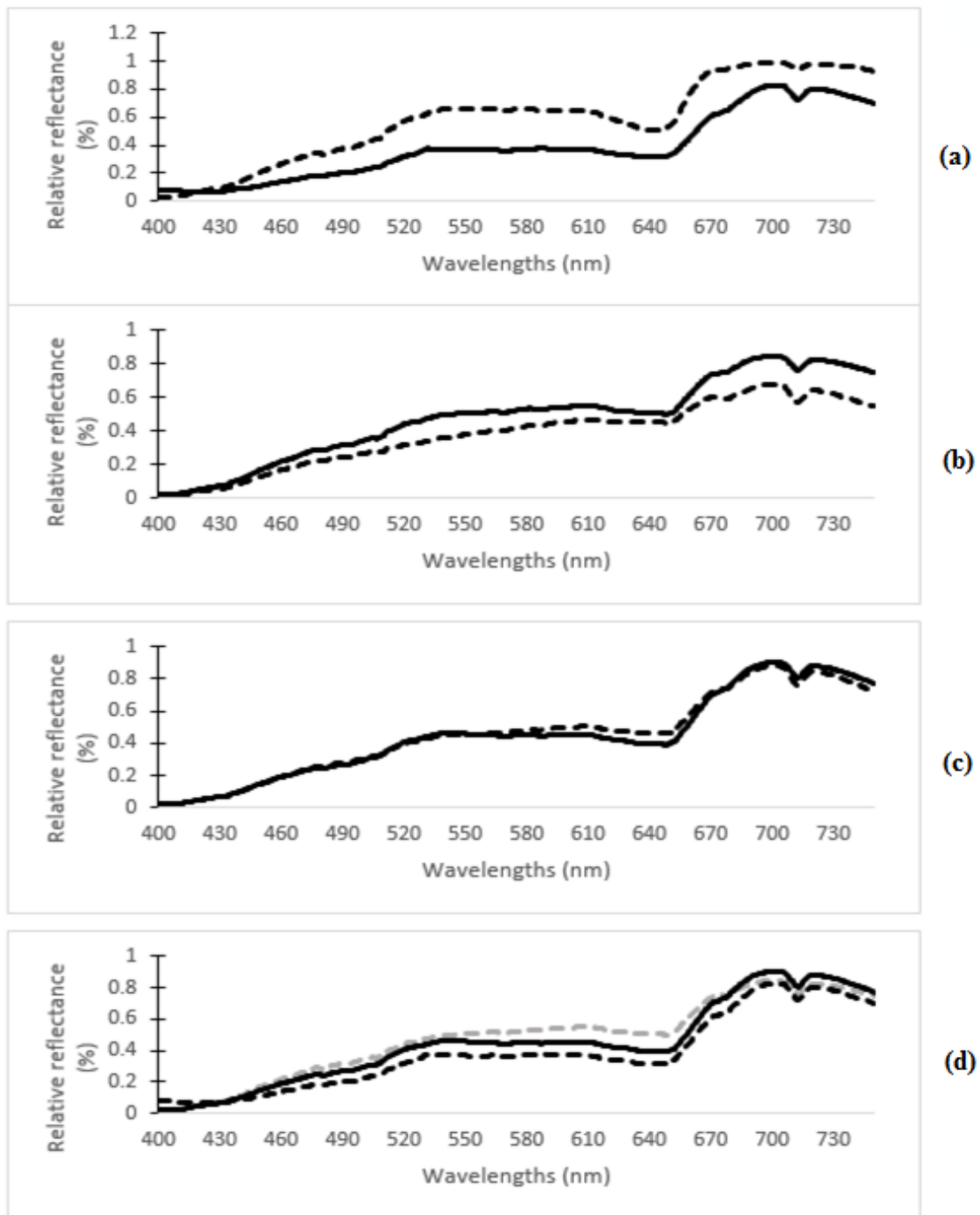


**Figure 25:** Comparison of an average barley crop canopy spectra between watered (-) and water-stressed (----) treatments for a) healthy, b) yellow rust infected and c) fusarium head blight (FHB) infected crop canopy. Plot (d) compares canopy spectra under watered conditions of healthy (---), yellow rust (-.-) and FHB (-).

To quantify differences between healthy, yellow rust and FHB infected spectra, two indices were considered in this study, namely, standard deviation of all wavelengths in the 500-650 nm range and squared difference of 650 and 700 nm, these areas are highlighted in Figure 23. In table 19, where spectral areas of interest (500 to 650 and 700nm) are assessed, and indices are created showing similar patterns in the watered and water stressed trays for each of the yellow rust infected, FHB infected, and healthy crop. This is supported by the statistical analysis of the indices through ANOVA. The ANOVA results are shown in Table 20, which shows a clear difference in response, both in the different crops and the different treatments. SD revealed significant differences in response in barley and wheat, whereas SD along with SQdiff showed a large difference between healthy and diseased trays. SD and SQdiff both showed no evidence of an effect of water stress.

**Table 19:** Spectral differences indicated as standard deviation of the 500-650 nm range and squared difference of 650 and 700 nm, calculated for healthy, yellow rust and fusarium head blight (FHB) infected wheat and barley canopy under watered and water-stressed conditions, averaged from spectra captured at growth stage 70. One average spectra were produced per line scan, with 9 line scans being considered for each class.

		SD 500-650 (nm)	SQdiff 650 and 700 (nm)
Wheat	Yellow rust watered	0.089	0.062
	Yellow rust water-stressed	0.081	0.076
	Healthy watered	0.057	0.15
	Healthy water-stressed	0.063	0.14
	FHB watered	0.16	0.1
	FHB water-stressed	0.15	0.11
Barley	Yellow rust watered	0.056	0.08
	Yellow rust water-stressed	0.061	0.077
	Healthy watered	0.051	0.15
	Healthy water-stressed	0.065	0.18
	FHB watered	0.15	0.25
	FHB water-stressed	0.13	0.18

SD is standard deviation



**Table 20:** Analysis of Variance (ANOVA) table for the analysis of transformed spectral indices over the different treatments. Analysis of the index the squared difference of 650 and 700 nm (sqDiff) was done on the square root scale, whilst analysis of the index standard deviation (SD) is done on of the range 500-650 nm.

		d.f.	s.s.	m.s.	v.r.	F pr.
log(SD)	Disease Status (Healthy vs Infected)	1	7.484	7.484	874.11	<.001
	Water (Watered vs Water stressed)	1	0.015	0.015	1.79	0.193
	Crop (Barley vs Wheat)	1	0.810	0.810	94.59	<.001
	Disease Status: Disease Class (Fusarium vs Yellow rust)	1	10.268	10.268	1199.23	<.001
	Disease Status:Water	1	0.274	0.274	31.98	<.001
	Disease Status:Crop	1	0.234	0.234	27.31	<.001
	Water:Crop	1	0.053	0.053	6.24	0.02
	Disease Status:Disease Class:Water	1	0.055	0.055	6.37	0.019
	Disease Status:Disease Class:Crop	1	0.324	0.324	37.8	<.001
	Disease Status:Water:Crop	1	0.002	0.002	0.22	0.641
	Disease Status:Disease Class:Water:Crop	1	0.052	0.052	6.05	0.022
	Residual	24	0.205	0.009	1.05	
sqrt(SQdiff)	Disease Status (Healthy vs Infected)	1	0.118	0.118	12.66	0.002
	Water (Watered vs Water stressed)	1	0.001	0.001	0.07	0.799
	Crop (Barley vs Wheat)	1	0.071	0.071	7.61	0.011
	Disease Status:Disease Class (Fusarium vs Yellow rust)	1	0.310	0.310	33.29	<.001
	Disease Status:Water	1	0.000	0.000	0.05	0.827
	Disease Status:Crop	1	0.013	0.013	1.42	0.246
	Water:Crop	1	0.001	0.001	0.14	0.708
	Disease Status:Disease Class:Water	1	0.016	0.016	1.67	0.209
	Disease Status:Disease Class:Crop	1	0.092	0.092	9.88	0.004
	Disease Status:Water:Crop	1	0.012	0.012	1.31	0.264
	Disease Status:Disease Class:Water:Crop	1	0.013	0.013	1.34	0.258
	Residual	24	0.224	0.009	5.08	

### 5.3.2 Model performance for yellow rust and fusarium head blight detection

The collected spectral data and field observations were subjected to PLSR with on-leave-out cross-validation. For the predicted results, this is data that was not included in the cross-validation (20% of the calibration data sets size), (Figure 26). The PLSR results for yellow

rust detection in cross-validation and prediction are shown in Table 21. The cross-validation results indicate good model performance for yellow rust % cover and yellow rust scale in wheat with  $R^2$  values of 0.82 and 0.88 (significance level of  $<0.01$ ), respectively, whereas model performance for barley is less successful ( $R^2 = 0.72$  and  $0.80$ , respectively), with a significance level of  $<0.01$ . This is also indicated by a smaller root mean square error of cross-validation (RMSECV) calculated for wheat % cover (6.04) and a slightly larger RMSECV of 0.54 for yellow rust scale, as compared to barley (7.88 and 0.37, respectively). Yellow rust is a foliar disease, the reduction in prediction performance for barley may be attributed to the crop having smaller leaves, causing a smaller foliar area to be captured by the hyperspectral imager.

Yellow rust % cover was also applied to the PLSR regressions after undergoing LOGIT transformation. The LOGIT transformation resulted in the cross-validation results in wheat being of  $0.68 R^2$ , which is lower than both the yellow rust percent and the yellow rust scale. However, using the LOGIT transformation in the percent yellow rust coverage in barley, allowed for a slightly higher  $R^2$  of  $0.74$ , as compared to the yellow rust coverage, though it was still lower than the yellow rust scale.

The PLSR result for FHB assessments in both wheat and barley are poor. However, much better results can be observed in cross-validation ( $R^2 = 0.67$  for wheat and  $0.54$  for barley) (Table 21). Prediction results in Table 21 demonstrate the reliability of the PLSR models when data independent from the models creation is applied (Figure 26). The yellow rust model performance in prediction showed a similar performance to that in cross-validation (Table 21 and Figure 26).

**Table 21:** Summary of model prediction performance of yellow rust and barley in cross-validation and prediction showing the  $R^2$ , root mean square error of the prediction (RMSEP) and cross validation (RMSECV), and the ratio of prediction deviation (RPD). Results are shown for yellow rust coverage (aa % coverage and the LOGIT transformation), yellow rust scale a class of 0 to 5 with 0 being healthy and 5 being >50% covered leaf area), and fusarium head blight (FHB) severity (severity and ratio of infected ears to healthy, 0 being healthy and 2 being >50%).

		<b>Wheat</b>				<b>Barley</b>			
		Yellow rust coverage	Yellow rust coverage Logit	Yellow rust scale	FHB severity	Yellow rust coverage	Yellow rust coverage Logit	Yellow rust scale	FHB severity
<b>Cross-validation</b>	$R^2$	0.82	0.68	0.88	0.67	0.72	0.74	0.80	0.54
	RMSECV	6.04	0.60	0.54	0.50	7.88	0.52	0.37	0.56
<b>Prediction</b>	$R^2$	0.77	0.43	0.80	0.57	0.69	0.79	0.77	0.5
	RMSEP	4.84	9.76	0.6	0.54	9.49	13.7	0.48	0.68
	RPD	2.04	1.2	2.25	1.50	1.80	1.4	1.97	1.36

RMSECV is root mean square error of cross validation; RMSEP is root mean square error of prediction; RPD is ratio of prediction deviation = standard deviation / RMSEP; The  $R^2$  report significance level of <0.01 for each regression.

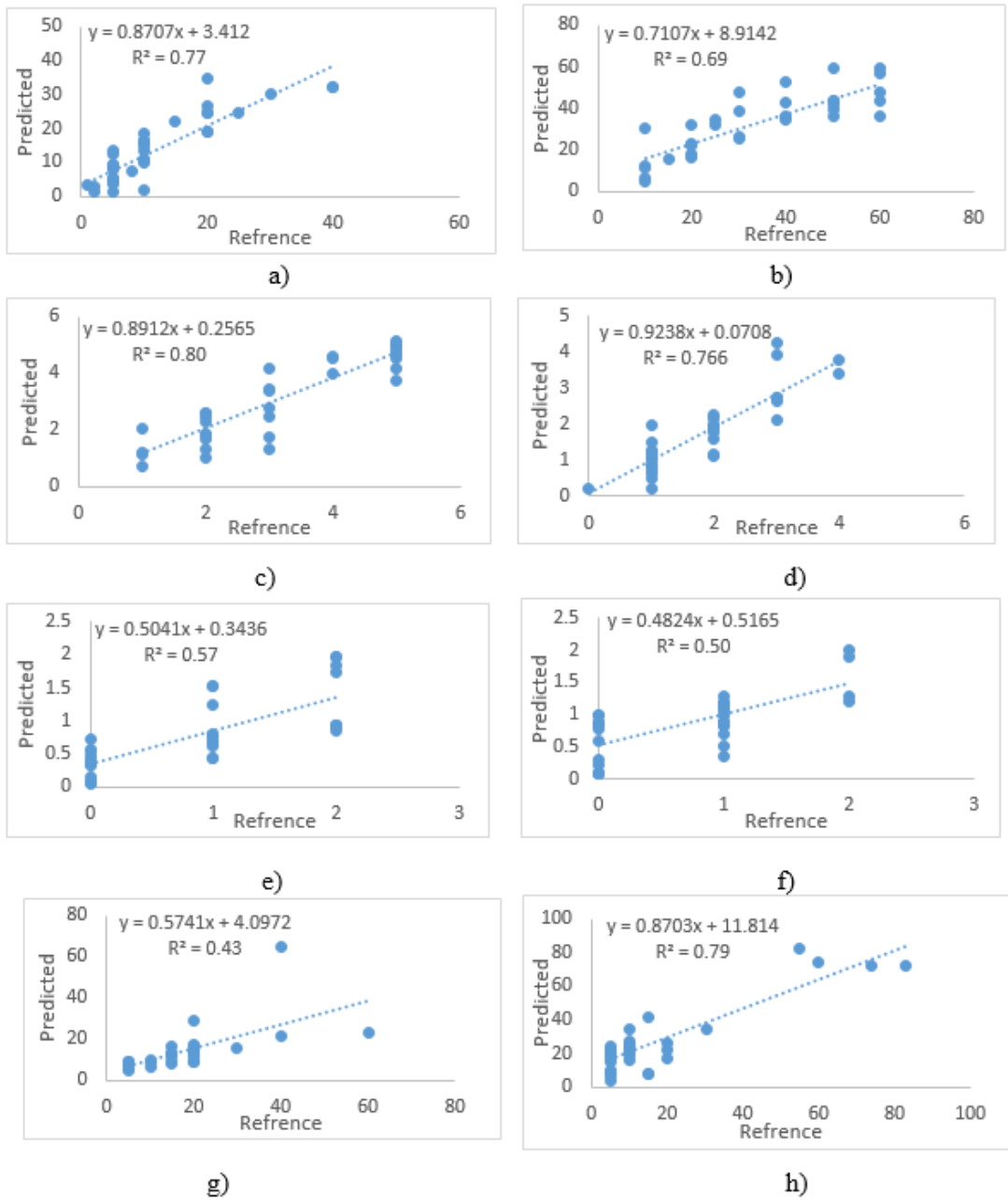


**Figure 26:** Scatter plots of predicted versus reference measured (based on 20% prediction set) yellow rust coverage in wheat (a), yellow rust coverage in barley (b), yellow rust scale in wheat (c), yellow rust scale in barley (d), fusarium head blight (FHB) severity in wheat (e), FHB severity in barley (f), wheat yellow rust logit (g), barley yellow rust logit (h). The  $R^2$  report significance level of  $<0.01$  for each regression.

To compare between the performances of different models, RPD was used in this work. According to the RPD classes proposed in the current work (Table 21), the prediction of both the yellow rust coverage (RPD = 2.04;  $R^2=0.77$  and yellow rust scale (RPD = 2.25;  $R^2=0.8$ ) is of good performance in wheat. These models again suffered deterioration in prediction performance in barley, where moderate prediction performances are recorded (RPD = 1.80 and 1.97, and  $R^2= 0.69$  and  $0.77$ , respectively). The  $R^2$  and RPD have declined for yellow rust coverage in wheat by applying the LOGIT function with an  $R^2$  of 0.68 for cross validation and in prediction to an  $R^2$  of 0.43 and RPD of 1.2. The barley results for the LOGIT transformation of yellow rust coverage have increased using the LOGIT for cross validation and predictions with  $R^2$  of 0.74 and 0.79 respectively. However, the RPD calculated for prediction has declined to 1.4, indicating that the LOGIT function was only able to distinguish between high and low yellow rust infections. The FHB prediction accuracy based on RPD values was again of a poor result of 1.5 ( $R^2=0.57$ ) for wheat and 1.36 ( $R^2=0.5$ ) for barley, suggesting the performance to be classified as moderately accurate and able to useful to distinguish between high and low infection (Table 18).

## **5.4 Discussion**

### **5.4.1 Crop canopy spectra**

The spectra shown in Figure 23 are to clearly demonstrate the shape of the spectral signature. The reflectance intensity between wheat and barley was witnessed to be similar through the scans, which is also described by Wilson *et al.* (2014), with only minor variations being seen in the NIR spectrum attributed to growth stage (rate of senescence) and the physical structure of the ears. Wilson *et al.* (2014) also discuss that growth stages 67–73 are best for making this separation. Within the visible range of 400–550 nm, there is a low reflectance due to a larger absorption of the light, attributed to the photosynthetic pigments of

the plants leaves, governed by the abundance of chlorophyll, absorbing most of the light radiation (Gates *et al.*, 1965; Thomas and Gausman, 1977). Both plant chlorophylls and carotenoids have strong absorption at 480 nm, the waveband associated with blue colour (Hunt *et al.*, 2013). Another interesting band around 670 nm, is linked with Chlorophyll a absorption (Hunt *et al.*, 2013), the latter wavelength is designated as the green leaf reflectance (Buscaglia and Varco, 2002 and Zhao *et al.*, 2005). A small absorption appears at the red edge around 715 nm, with deeper absorption in a barley spectrum than in wheat. Raper and Varco (2015) found that the strongest wavelength correlations with leaf nitrogen concentration, lint yield and plant total nitrogen content to be near 700 nm. Further analysis of these bands, as linked with crop diseases studied, is discussed below.

In Figure 24 generally all spectra are similar, although slight differences can be observed by close examining of individual plots (Figure 24, b and c). The water-stressed spectra are less reflective than watered spectra, particularly for the yellow rust (Figure 24 b). Slight differences in shape of the reflectance spectrum can be observed in the healthy canopy (a) than in the water-stressed canopy, which is in line with the findings from Earl and Davis (2003) who attributed these differences to alterations in leaf internal structure, variations in leaf angle (due to wilting) and leaf area index. Smaller reflectance at the green edge (500-570 nm) and red edge (670-750 nm) can be attributed to the water stress. However, these slight differences may indicate that water-stress has only slight influence on crop canopy reflectance, hence, on the performance of PLSR models in predicting yellow rust and FHB. The influence of water stress on the yellow rust infected crop canopy was more obvious, where the water stressed spectrum is consistently of lower reflectance (higher absorption) than the watered spectrum throughout the entire waveband (Figure 24 b). This indicates that water stress may have a considerable influence on yellow rust prediction. However, spectra

pre-processing e.g., maximum normalisation used in this study will eliminate differences in reflectance e.g., due to scattering, as all spectra will be scaled between 0-1. However, only a negligible deviation is observed between FHB infected spectra (Figure 24 c), indicating negligible effect of water stress on FHB prediction.

Figure 24 d shows spectra of each category (healthy, yellow rust, and FHB infected) for watered crops. The healthy spectrum is of a lower reflectance than both infected spectra in the range between 400 to 700 nm. The yellow rust infected crop spectra has the highest increase between 400 and 700 nm, whilst FHB infected crop spectra has a flatter (linear) curve in the 500 to 650 nm area.

The lower reflectance of the healthy canopy can be attributed to larger absorption by photosynthetic pigments of the plants associated with chlorophyll (Gates *et al.*, 1965; Thomas and Gausman, 1977). Cibula and Carter (1992) reported larger reflectance in infected leaves than healthy leaves, which is in line with findings of the current study. Indeed, after crop infection by foliar pathogens such as yellow rust, noteworthy visual symptoms can usually be observed. Early symptoms such as chlorosis, associated with a reduction in chlorophyll results in increasing reflectance due to a reduction in light absorption (Lorenzen and Jensen, 1989). Therefore, the sharpest increase in reflectance from 650 to 700 nm takes place in the healthy plant reflection spectrum.

Figure 25 compares between the average spectra of healthy, yellow rust and FHB infected barley canopy at growth stage 72. The water-stressed canopy spectrum shows more reflection or less absorption than the watered canopy spectrum for the healthy canopy in Figure 25a. This may reflect the darker (greener) canopy of the watered canopy resulting in larger absorption of light. This is in line with findings of other researchers, who have attributed the increased reflectance of the healthy canopy to early senescence caused by drought, and a

reduction in chlorophyll absorption (Jamieson *et al.*, 1995; Hunt *et al.*, 2013). With the yellow rust infected canopy (Figure 25b), the opposite trend can be observed, where higher reflectance is shown for the water-stressed canopy. This trend is observed in both the wheat (Figure 24b) and barley (Figure 25b) canopies, indicating a larger influence of yellow rust on crop canopy when combined with water stress, compared to FHB (Figures 24c and 25c), where the differences between watered and water-stressed are minimal. As for the wheat canopy, the yellow rust infected canopy has again the highest reflectance, compared to those of FHB and healthy canopies (Figure 25d). The % coverages of yellow rust and FHB is larger in wheat than in barley. In wheat, the yellow rust watered canopy had an average infection of 42%, yellow rust water stressed averaged 45%, Yellow rust watered averaged 63%, and FHB water stressed canopies averaged 66% infection, whereas, in barley, these were 36%, 33%, 48% and 52%, respectively.

Moshou *et al.* (2004) recommended the use of a wavelength range between 460 and 900 nm for successful yellow rust detection. Bauriegel *et al.* (2011) recommends spectral analysis using the range intervals of 500–533 nm (green), 560–675 nm (yellow to red), 682–733 nm (red edge) and 927–931 nm (far red) for recognition of FHB infection (in growth stages 71–85, according to Zadoks scale). Krishna *et al.* (2014), suggested particularly useful spectra wavelengths of 428, 672, and 1399, for quantitative detection of yellow rust from a healthy crop.

Table 19 refers to two indices, SD and SQdiff. SD refers to the standard deviation of each of the wavelengths between 500 and 650nm. SQdiff refers to the squared difference between 650 and 700nm wavelengths. These two proposed indices show clear differences in response both in the different crops and the different treatments. The largest differences were observed between infection type, observing a significant F statistic of  $F_{1,24}=1199$  ( $p<0.001$ ) and  $F_{1,24}=33$



( $p < 0.001$ ) for the comparison between FHB infection and yellow rust infection, for index SD and SQdiff, respectively. Analysis of the index SD revealed significant differences in response in barley and wheat ( $F_{1,24}=94.59$ ,  $p < 0.001$ ) and big differences between healthy and diseased trays ( $F_{1,24}=874.11$ ,  $p < 0.001$ ). The largest differences were observed between FHB infection and yellow rust infection ( $F_{1,24}=1199.23$ ,  $p < 0.001$ ). In contrast, there was no evidence of a significant effect of water stress ( $F_{1,24}= 1.79$ ,  $p=0.193$ ), meaning that on average (over all disease types and crops) there is no evidence of a difference in the SD index for watered and water stressed trays. However, analysis of the index SD does demonstrate a significantly different response to water stress both within different crops and under different disease infections (full ANOVA table is given in Table 20), i.e. the response to water stress is not the same in the different conditions. Analysis of the index SQdiff revealed significant differences between healthy and diseased trays ( $F_{1,24}=12.66$ ,  $p=0.002$ ) and also significant differences between FHB infection and yellow rust infection ( $F_{1,24}=33.29$ ,  $p < 0.001$ ). Moreover, different responses in the different crops were observed ( $F_{1,24}=7.61$ ,  $p=0.011$ ) with a significant interaction between crop type and disease type indicating the index SQdiff responds differently to disease type in the different crops ( $F_{1,24}=9.88$ ,  $p=0.004$ ). There was no evidence to suggest a differing response to water treatment ( $F_{1,24}=0.07$ ,  $p=0.799$ ).

Although the largest SD in reflectance between 650 and 700 nm was observed for the healthy canopy (both watered and water-stressed), the smallest SD was observed for yellow rust (Table 19). For the barley canopy, the largest SD and SQdiff can be observed for FHB infected canopies, indicating that these proposed two indices respond differently for different crops (Table 19). Consequently, the two indices adopted in the current work highlight a distinguishable difference between the yellow rust, FHB and healthy wheat and barley crop canopies. It is important to mention that whilst these indices have worked in

establishing a difference between yellow rust, FHB and a healthy canopy at growth stage 72 in this work, it may be specific to the method and equipment used. Further work should be undertaken to assess the reliability of such indices, if captured at different growth stages, under different circumstances, with alternative equipment.

#### **5.4.2 Model performance for yellow rust and fusarium head blight detection**

It is well known in spectral analysis that successful measurement of a concentration, be it soil properties or other, depends on presence of variability of that said concentration. For example, Kuang and Mouazen (2011) reported that although larger  $R^2$  and RPD values can be obtained with larger variability in soil analysis, larger RMSEP is to be expected. The RMSEP values in wheat were smaller for yellow rust coverage and larger for yellow rust scale detection, as compared to the corresponding RMSEP for barley. However, RMSEP is a valuable index for assessing individual model performance, but is not recommended to compare between models (e.g., those for wheat and barley), due to the different data range. A data set with a small variability, could result in a weak or even no correlation being established with PLSR, so that no models could be developed. However, this could be improved with the incorporation of extra data, with a larger variability. Having said that, we believe that the scale of variability in yellow rust is small (Table 17), although a reasonably high infection was recorded, this occurrence was infrequent, and the average was weighted by a few heavily infected trays. The small variability may be possibly due to the experiment being run in trays under rather controlled conditions, where only water is varied artificially. These controlled conditions may well lead to rather small variability in yellow rust (Table 17). FHB's result might be due to the full line scan being used, while the ear of the crop is captured only by a small section of the line image, compared to the foliage of the crop, which was used more successfully for yellow rust modelling and detection. This may suggest the

need to isolate segments in the line image that capture fusarium as the disease appears mainly in heads (Impey, 2012). This can be potentially implemented by splitting the crop canopy spectra into 10 cm increments, similar to the approach mentioned in Broge and Mortensen (2002) for canopy chlorophyll density, or that of Moshou *et al.* (2005), for disease detection with a data fusion technique. The few classes used for the FHB infection in the current work (Table 17) may have also contributed to lower detection accuracy. The FHB classes were no infection, mild infection (describing FHB symptoms on up to 50 % of the ears) and heavy infection (describing FHB infection in over 50% of the ears with the majority showing early senescence). The scale for FHB was classified in this manner because most ears became infected through the inoculation process. Another reason believed to have influenced the FHB model performance is the smaller number of data points considered in the PLSR cross-validation modelling, as compared to yellow rust (Table 17). Fusarium symptoms appear on crop heads at a late stage in the crop growing season (normally only after anthesis, but potentially at head emergence), allowing for a limited number of scans to be collected.

Bauriegel *et al.* (2010) claimed that *FHB* can be detected by spectral analysis in the spectral range of 400–1000 nm, with an identification accuracy of 87%. These authors advised that the ideal timing for measurement was at the medium milk stage (growth stage 75), though the scans were based on the crop ears against a black background. The scans conducted in this study, for FHB, were taken from anthesis at growth stage 61, to grain hardening at growth stage 90. Delwiche *et al.* (2011) successfully differentiated between healthy kernels from FHB infected, reporting a 95% classification accuracy between 8 groups, containing approximately 60 seeds each.

The percentage of disease coverage, a method discussed by Chiarappa (1981) and defined as “disease severity”, is the amount of expressed disease tissue of a plant. This method can be

objective, but is not free of subjectivity. In the current study, all assessments were made by just one individual, which increases subjectivity and potentially RMSEP for both yellow rust and FHB detection. The more spectral wavelength indices captured and accounted for, the greater understanding of the object (Gilchrist, 2006). However, for noisy spectra there is a need to minimise noise in the signal, by adopting an optimised measurement configuration (Whetton *et al.*, 2016b) and suitable spectra pre-processing.

Furthermore, stresses in the field are combined and might include water stress, nitrogen stress, disease stress, and other stresses that are mainly reflected on crop canopy as a yellowing of the leaves. In the current work, we have combined water stress and yellow rust infection in the tray experiments, to evaluate the prediction accuracy of the yellow rust models. The result obtained is satisfactory (RPD > 2.0 for wheat and > 1.8 for barley) to encourage exploring the goal of the current study, which is on-line measurement of yellow rust in the field using the hyperspectral imager (400 – 750 nm). However, additional affecting parameters exist in the field on top of the water stress accounted for in the current study, which should also be evaluated. Using wheat trays under glass house controlled conditions, Moshou *et al.* (2014) reported successful discrimination of water-stressed from healthy plants with 99% accuracy. Their approach was based on a combination of hyperspectral (460–900 nm) and fluorescence imagery and least squares support vectors machine learning models, for automated recognition of different biotic and abiotic stresses, of crop canopies under greenhouse conditions.

The early success in field studies for hyperspectral imager's detection of yellow rust disease such as Moshou *et al.* (2004) and Bravo *et al.* (2003), focused on the presence of yellow rust in the field, not necessarily the severity. Commonly, disease recognition attempts with hyperspectral and multispectral imagery are targeted to leaves rather than the canopy (Bock

*et al.*, 2010). Whilst recent attempts such as Zhou *et al.* (2015) studying wheat resistance, have used RGB images for quantification of disease, which is of lower cost but with larger error margins. Compared to other studies, the current work achieved good to very good accuracy based only on a relatively cost-effective hyperspectral camera in the visible and the NIR range. In addition, in the current work, the effect of water stress was also taken into consideration in the experimental trial, hence, this effect was accounted for in the PLSR models

This study used triplicate trays of each of the considered crops, disease, and conditions, with 9 scans captured across 3 locations of each tray, through multiple growth stages. The observations discussed in this paper for the development of FHB models, suggest the need for a larger dataset to be accounted for in the PLSR analysis and to explore new methods of data analysis based on machine learning and/or image processing. It is also suggested to adopt a data fusion approach of both spectra and images, which is expected to provide improved model prediction performance. Ideally the requirement is a method which incorporates not just the percentage of fusarium infected heads to healthy heads, but the coverage of the plot by the ear. A method such as a camera image with a 100-point dot grid overlay of the assessment area, discussed by Knight *et al.* (2006), could be a potential method, and should be further assessed.

## **5.5 Summary conclusions**

A hyperspectral line image camera was implemented successfully under laboratory conditions for the measurement of yellow rust and FHB in wheat and barley. The standard deviation (SD) of the wavelength range from 500 to 650 nm and the squared difference between 650 nm and 700 nm are of interest in discrimination between healthy, and yellow rust or FHB infection in a wheat or barley canopy. Yellow rust prediction models performed

more accurately than FHB models. Further work needs to consider a larger dataset in the PLSR analysis, and the exploration of new methods of data analysis based on machine learning and/or image processing, particularly for FHB detection.

## **6 Hyperspectral measurements of yellow rust and fusarium head blight in cereal crops: Part 2: on-line field measurement**

### **Chapter Synopsis;**

This chapter investigates the applicability of the optimal hyperspectral imaging configuration reached in Chapter 4 for on-line measurement of yellow rust and fusarium head blight (FHB) using PLSR analysis in three fields of winter wheat and one field with winter barley.

### **Abstract**

This study implemented a hyperspectral line imager (spectrograph) for on-line measurement of yellow rust and fusarium head blight (FHB) in wheat and barley fields. On-line measurements were carried out in four arable fields in Bedfordshire, the UK. Disease recognition consisted of visual field assessments and photo interpretation based on 100-point grid overlaid on RGB images. The spectral data and disease assessments were subjected to partial least squares regression (PLSR) analysis with leave-one-out cross-validation using calibration sets, consisting of 70% of samples. The developed recognition models were then validated with a non-mobile (25%) and mobile (5%) prediction data sets.

Results showed that yellow rust can be measured with an on-line hyperspectral imagery system with better accuracy than FHB, and that the performance was better in wheat, as compared to barley. It was found that photo interpretation was most applicable and accurate for the on-line measurement of FHB, where it was classified as a good prediction accuracy in wheat (ratio of prediction deviation (RPD) and  $R^2$  values of 2.27, and 0.82, respectively) and a moderately accurate in barley (RPD of 1.56 and an  $R^2$  of 0.61). However, visual scale analysis was most suitable for yellow rust based models, where model performance was

classified as moderately accurate in barley (RPD = 1.82; R<sup>2</sup>=0.72) and good in wheat (RPD = 2.5; R<sup>2</sup>=0.81). It was recommended to adopt the proposed on-line measurement technique coupled with PLSR to map the spatial variability in yellow rust and FHB in wheat and barley, although further analyses that include advanced image processing or machine learning techniques may further improve the current results.

## **Keywords**

On-line measurement, Yellow rust, fusarium head blight, wheat, barley, mapping, and partial least squares regression.

## **6.1 Introduction**

Fungal disease control is a large task for the successful production of cereals worldwide. For example, yellow rust (*Puccinia striiformis*) is a foliar disease, common in cool climates, one of the most devastating diseases of wheat worldwide, and reported to reduce crop yields by up to up to 7 t ha<sup>-1</sup> in severe epidemics (Ma *et al.*, 2001; Bravo *et al.*, 2003). In 2009, yellow rust mutations have enabled the disease to attack several widely grown genetically resistant cereal crop varieties, including Solstice (Milus *et al.*, 2009). Another important fungal disease that attacks cereal crops is fusarium head blight (FHB), which is caused by multiple species. *Fusarium graminearum* is a highly aggressive and prevalent species. *Fusarium graminearum* along with other fusarium species can cause mycotoxin production in grain (Rotter *et al.*, 1996; Brennan *et al.*, 2005; Desjardin, 2006; Leslie and Summerell, 2006). Fusarium predominantly affecting the ear of the crop, causing FHB. FHB is one of the most important pre-harvest diseases worldwide. Like yellow rust, FHB also causes reduction in yield quantity and quality and when producing mycotoxins, it becomes a significant threat to both humans and animals. FHB is a sporadic disease, that is dependent on warm humid weather conditions



(Rossi *et al.*, 2001; Xu, 2003), causing variability of disease presence and level of infection across regions, and years (Jelinek *et al.*, 1989). Both yellow rust and fusarium species can survive in soil and weeds occurring in the hedgerows and borders of a field, fusarium also survives within plant residues even after 2 years, acting as a source of inoculum (Jenkinson and Parry, 1994; Champeil *et al.*, 2004; Imathiu *et al.*, 2013). Therefore, control of mycotoxins caused by fusarium fungi is required to prevent toxic contamination reaching the food chain either in milling grain (for human consumption) or as cattle feed (Magan *et al.*, 2002).

Traditionally, disease detection is carried out manually by human experts using visual assessments of disease coverage throughout the field, a process that may be lengthy, subjective and tiresome (Schmale and Bergstrom, 2003; Bock *et al.*, 2010). These methods are limited in providing high sampling resolution data on spatial variability of crop disease. Therefore, on-line mobile systems are necessary to inform site specific application of fungicides.

It has been stated that optical technologies are available for development into suitable disease detection systems, but with many challengers still required to be overcome (West *et al.*, 2003). Although on-line applications are still rather limited, optical techniques have the potential to be integrated with agricultural vehicles. Optical (both remote and proximal) methods provide non-invasive and high sampling resolution data necessary for monitoring and mapping of crop diseases. Among optical sensing methods, hyperspectral and multispectral imaging techniques are the best candidates as they acquire high resolution data, at multiple points simultaneously, and have already been used in disease and stress monitoring (Hahn, 2009). Non-mobile (off-line) field and laboratory methods for disease classification and plant growing conditions have been studied and demonstrated (Roggo *et*

*al.*, 2003; Wu *et al.*, 2008). The early success in field studies for a hyperspectral imager's detection of yellow rust, focused on the presence of yellow rust in the field, not necessarily the severity. Moshou *et al.* (2005) implemented a data fusion approach of a hyperspectral (450-900 nm) and fluorescence (550-690 nm) imaging for yellow rust detection in winter wheat reporting 94.5% accuracy. Other common attempts with hyperspectral and multispectral imagery are targeted to leaves rather than the canopy (Bock *et al.*, 2010). Huang *et al.* (2015) successfully provided quantitative assessment of yellow rust in winter wheat, by hyperspectral measurement of individual infected leaves. Zhou *et al.* (2015) used low cost RGB images for quantification of yellow rust, reporting 74% and 81% detection accuracy. Zhao *et al.* (2016) focused on two sensitive bands (558 nm and 856 nm) in the wavelength ranges of 550-680 nm and 750-1300 nm to detect yellow rust with 90.6% accuracy. Krishna *et al.* (2014) used remote hyperspectral data in 350 to 2500 nm range for quantitative identification of yellow rust. Whilst mobile techniques have been successfully applied, these were instruments attached to hand moved frames. On-line here is defined as attached to an agriculture vehicle, where measurement is being taken on the move. Moshou *et al.*, in 2011 looked at a wheat crop, for both yellow rust and septoria, using an on-line method with a multi-spectral camera. To the best of our knowledge, there are few reports in the literature of on-line (mobile, using agricultural vehicles) application of proximally captured hyperspectral imagery, for simultaneous recognition and mapping of yellow rust and FHB in both wheat and barley.

A hyperspectral imager was applied to winter wheat and barley plants, grown in trays under laboratory conditions in Part 1 of this study (Whetton *et al.*, 2016c). Plants were subjected to variable water stress, and inoculated with yellow rust and FHB, these diseases were selected as their presence had been reliably witnessed in previous years. Results confirmed that

reliable models for yellow rust detection could be produced, but highlighted an alternative technique and modelling approach should be applied for FHB disease detection. However, the Part 1 of this study suggested exploring the potential of this approach for on-line field measurement. The aim of this paper is to implement a hyperspectral imager for on-line measurement of yellow rust and FHB in wheat and barley grown commercially outdoors in fields.

## **6.2 Materials and methods**

### **6.2.1 Field sites**

Field measurements were conducted in four different field sites through the 2015 cropping season. These sites were located at Duck End farm, Wilstead, Bedfordshire, UK (52°05'46.3"N 0°26'41.4"W), with an average annual rainfall of 598 mm. The farm has a three year crop rotation of oilseed rape, winter wheat and winter barley. Fields varied in size between 12 ha, 10 ha, 7 ha and 4 ha (Table 20), to allow for pattern identification of diseases with different field size. This is because yellow rust and FHB occurrence in the field often begins nearer the hedgerows, and the spread pattern throughout the growing season may well depend on the shape and size of the field. Winter wheat was grown in three fields, whereas winter barley was grown in the 10 ha field only. The largest and smallest winter wheat fields were scanned at two different intervals. Timing and growth stage of measurement in each field is shown in Table 22. Growth stage in this study refers to the Zadok's scale (Zadoks *et al.*, 1974). The dominant soil texture types in the fields are shown in Table 22, with sand fractions due to underlying gravel deposits.

**Table 22:** Experimental fields, scanning time and growth stage identified according to the Zadok's scale (Zadoks *et al.*, 1974). The soil type is presented for northern (N), southern (S) or eastern (E) and western (W) parts of a field.

Field Number	Field area (ha)	Crop	Soil type	Date of scanning	Crop stage
1	4	Winter wheat	Sandy clay	04/06/2015	booting (43)
		Solstice Variety		30/06/2015	anthesis (61)
2	10	Winter barley	N: Clay	27/05/2015	anthesis (61)
		Carat Variety	S: Sandy clay		
3	12	Winter wheat	E: Clay	22/05/2015	booting (43)
		Solstice Variety	W: Sandy clay loam	01/07/2015	milk (70)
4	7	Winter wheat	E: Clay loam	01/07/2015	milk (70)
		Solstice Variety	W: Sandy clay loam		

### 6.2.2 Hyperspectral on-line data capture

A push broom hyperspectral imager (spectrograph) (HS spectral camera model from Gilden Photonics Ltd., UK) and light source were mounted on a tractor by means of a metal frame (Figure 27). Optimal hyperspectral measurement configurations set by Whetton *et al.* (2016b) were considered in the design and manufacturing of this on-line measurement system of crop canopy. These include an integration time of 50 ms, a camera height of 0.3 m and light height and distance of 1.2 m and a camera angle of 10°. The on-line measurements were carried out at a travel speed of approximately 4 km h<sup>-1</sup>. The hyperspectral imager's line capture occurs at 1 second intervals, which is subsequently logged and geo-located with a sub-meter accuracy, using a differential global positioning system (DGPS) (EZ-Guide 250, Trimble, California, USA). The direction and angle of the imager was kept consistent, and a day with uniformly overcast weather was selected, which helped prevent issues of moving shadows from lateral sun movement on the data (West *et al.*, 2003).

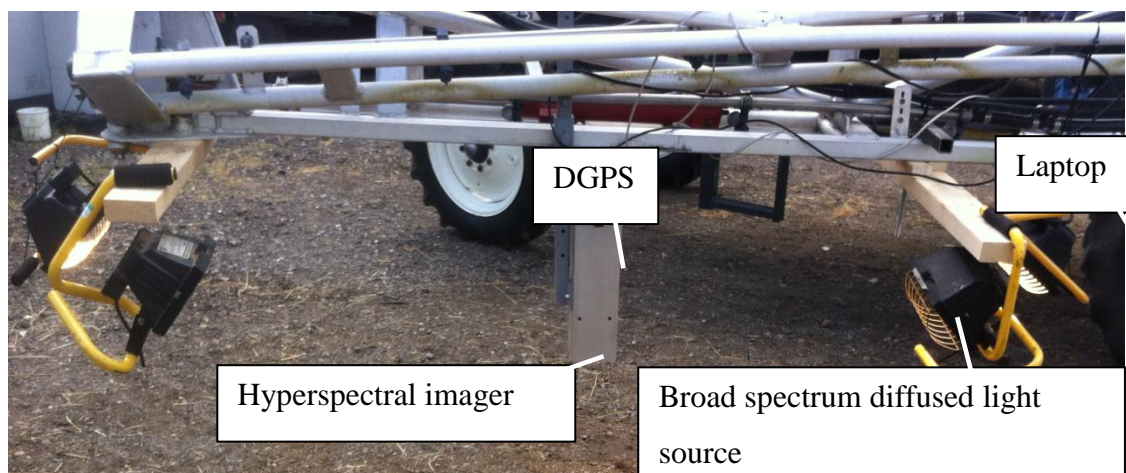


**Figure 27:** Hyperspectral imagery system mounted on a metal frame attached to the side of a tractor, ready for on-line canopy measurement.

The same hyperspectral imager used in Part 1 of this study was used for on-line field measurement, along with two external halogen lamps (Figure 27). It consists of 1608 pixels, with a spectral range of 400 - 1000 nm. More details about the hyperspectral imager's properties can be found in Whetton *et al.* (2016b). A schematic showing an overview of the methodology can be seen in Figure 28.

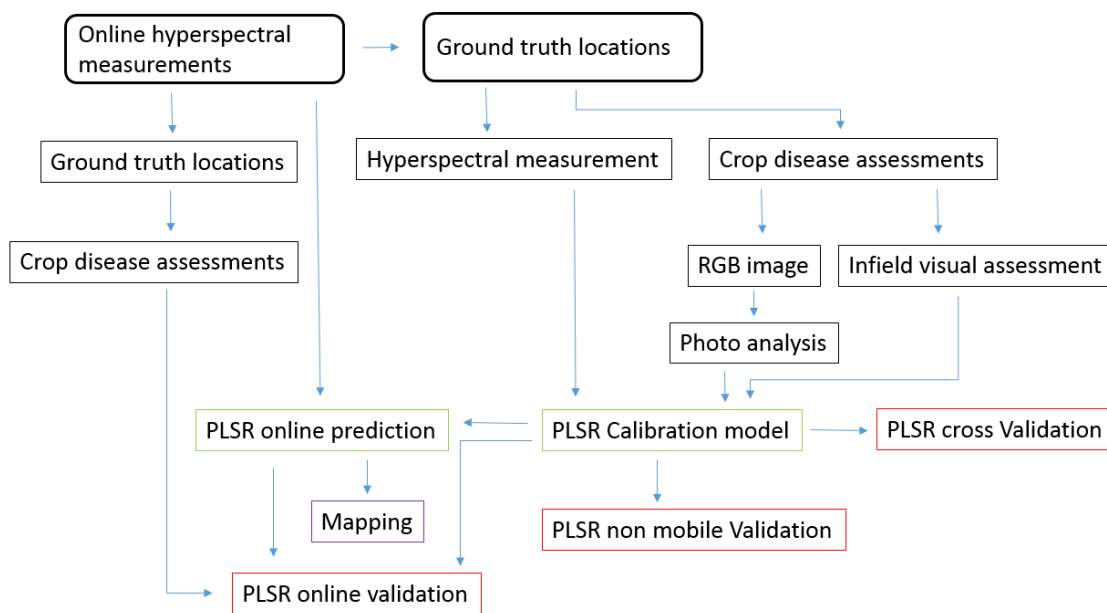


**Figure 28:** Schematic of work flow from data capture to production of PLSR models, validation, and on-line prediction for production of maps

In order to compile a full image from a set of line imagery, a steady moving platform is needed to sweep across the target object to capture every line (Gilden Photonics Ltd, Glasgow, UK). However, due to practical constraints of applying a consistent moving platform, the spectraSENS v3.3 software (Gilden Photonics Ltd, Glasgow, UK) was adapted to record a single line array. Before data capture, measurements from a white and dark reference were collected, and subsequently repeated at 10 minute intervals until the scanning

was completed. The white reference used, was a commercially available Spectralon Teflon white reflectance panel with 99.9% white reflectance value. The collected on-line data, was corrected by the white and dark scans after data collection was complete, providing the relative reflectance.

### **6.2.3 Moisture content measurement**

An on-line visible and near infrared (vis-NIR) spectroscopy soil sensor developed by Mouazen (2006) was used in this study to measure gravimetric soil moisture content (MC) in field 4, with the objective of studying the influence of MC on crop disease spatial distribution. This data was collected at beginning of the growing season in September 2014. Although MC may change daily, the distribution pattern through the field will remain consistent through the multiple seasons (Vachaud *et al.*, 1985; Mouazen *et al.*, 2005). The system consists of a subsoiler, opening a smooth trench at 15 cm depth (Mouazen *et al.*, 2005). The sensor was mounted on a three-point linkage of a tractor travelling at a speed of 3 km h<sup>-1</sup> and collecting spectral soil data at 10 m parallel intervals. In order to measure soil spectra, an AgroSpec mobile, fibre type, vis-NIR spectrophotometer (Tec5 Technology for Spectroscopy, Oberursel, Germany), with a measurement range of 305–2200 nm and a light source of 20W tungsten halogen lamp were used (Kuang and Mouazen, 2013). A differential global positioning system (DGPS) (EZ-Guide 250, Trimble, California, USA) recorded the position of the on-line spectra with sub-meter accuracy. The collection of soil spectra and DGPS readings took place at 1 sec sampling resolution using AgroSpec software (Tec5 Technology for Spectroscopy, Oberursel, Germany). A previously developed MC model (Halcro *et al.*, 2013) was used to predict MC based on on-line collected spectra in the field.

#### **6.2.4 Disease recognition in the field**

During field scanning with the hyperspectral imager, ground truth spots were selected randomly, at a rate of five samples per hectare (Figure 29), and a series of five hyperspectral images were collected per ground truth location, each covering 1 m<sup>2</sup>.

The measurement position was recorded with a DGPS. The disease assessment was assigned to each of the five scans. In order to assist in disease and crop health assessments a photograph was collected at each position using a RGB, 5 megapixel camera with a 3.85 mm f/2.8 lens at the same time of hyperspectral image capture. The 1 m<sup>2</sup> ground truth spots were used for disease recognition.



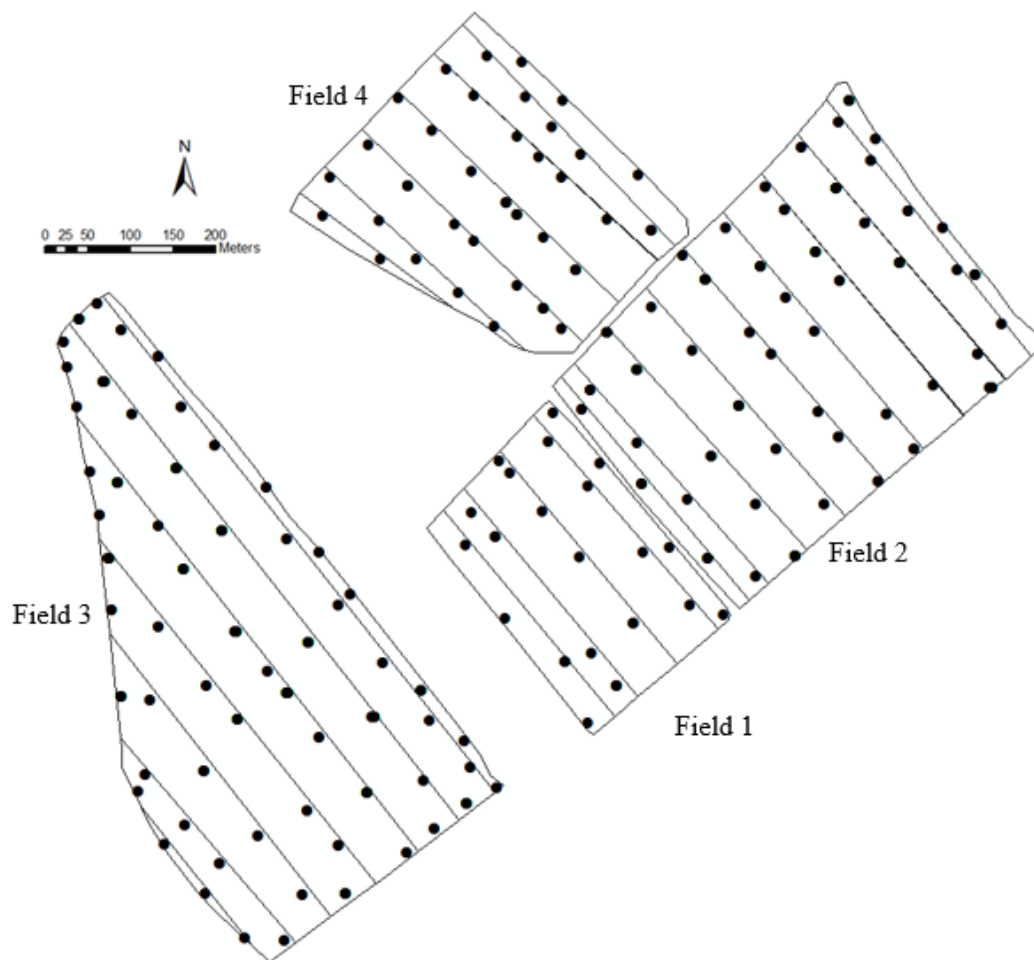


**Figure 29:** on-line hyperspectral measurement lines and position of ground truth plots, collected at five samples per ha, in the four fields. Fields 1 and 4 were validated at the same locations at two time intervals.

Disease assessments were based on the following two methods:

1- photo interpretation: Photos collected from the ground truth plots were used in this photo interpretation to assess crop disease coverage (severity), and incidence of disease, defined by Chiarappa (1981) as the percentage cover of disease, and the occurrence of disease in a field, respectively. Images were overlaid with a 100-point grid at equal spacing as illustrated in Figure 30, adopting a similar approach to that proposed by Knight *et al.* (2006). At the centre

of each point, the object and health status were recorded and used to calculate the percent coverage of infection, or incidence of disease. This approach was adopted for both the yellow rust and FHB assessment.

2- Visual assessment: Although visual assessment of crop diseases was deemed to be subjective, it is the most common and adopted by partitions. Visual assessment of both diseases at the ground truth plots were made at four levels, namely, the head (when present), at the flag leaves, at 2<sup>nd</sup> and 3<sup>rd</sup> leaves (mid canopy), and at the lower canopy. Details on this method can be found in Part 1 of this study (Whetton *et al.*, 2016c). Depending on the disease, two visual assessment approaches were considered in the current work. The assessment for FHB considered both early and later symptoms on heads, and were assessed as either a 0 for no infection, 1 for less than 5% individual infected heads, 2 for up to 10%, 3 for up to 30%, 4 for up to 50%, and 5 being a heavy infection over 50% infected heads, dependent on the ratio of FHB infected to healthy crops. For yellow rust, two different quantitative assessments were recorded, one for the percent cover on the leaves and one recorded as a 0-5 scale, which is explained by Oberti *et al.*(2014). The scale between 0 and 5 (from less to more affected plots) was given the same ratio as that for FHB. For example, 0 is given when no disease is present, 1 for up to 5% cover, 2 for up to 10%, 3 for up to 30%, 4 for up to 50% and 5 for >50%.



**Figure 30:** Example of photo interpretation to assess yellow rust and fusarium head blight (FHB) coverage based on a 100-point grid.

## 6.3 Data analyses

### 6.3.1 Crop canopy spectral data pre-processing

The first step of spectra pre-processing included removing noisy wavelengths larger than 750 nm. Following the suggestion made in Whetton *et al.* (2016b), the first and last 320 pixels were removed from each line scan. Noise removal was followed successively by reducing the number of variables by averaging three neighbouring wavelengths, maximum normalisation, first derivative and smoothing. The first derivative was used to eliminate the effect of the roughness of soil surface on the spectrums absorption (Shibusawa *et al.*, 2000; Waiser *et al.*, 2007). All spectra pre-processing was carried out using Unscrambler 10 software (Camo Inc.; Oslo, Norway). Although pre-processing of spectral data includes techniques such as smoothing, if the process of cleaning the data is intensive due to noisy spectra, it can lead to

the loss of important spectral features, and thus impact on the success of analysis (Dasu and Johnson, 2003). Therefore, a gentle smoothing of 2:2 was implemented during the first derivative and smoothing using the Savitzky–Golay algorithm (Savitzky and Golay 1964). Detailed information about the spectra pre-processing steps can be found in Martens and Naes (1989).

### **6.3.2 Evaluation of model performance**

For yellow rust analysis, the data from the five scans from the three wheat fields and the one scan from the barley field was considered (Table 22). However, FHB models were developed based on the one later data capture of each field. This is because FHB only occurs at a later crop growth stage, when the ear emerges (growth stage 51, according to Zadok's scale) (Zadoks *et al.*, 1974). The potential infections can occur when the plants are booting (growth stage 43) by washing into the sheath (Anand *et al.*, 2003). Five models were developed and validated in cross-validation, non-mobile validation and on-line (mobile) validation. The validation methods are summarised in Table 23, and the models produced are summarised in table 24.

**Table 23:** Explanation of validation sets in cross-validation, non-mobile and on-line, along with the datasets included and the methods for each.

Validation	Dataset	Method
Cross-validation	70% ground truth locations, empirical and spectral data.	Cross-validation is included with the PLSR models, which is trained on all the data except for one point each time, and the average errors from those calculations, evaluates the models.
Non-mobile validation	PLSR models. 25% (model excluded) ground truth locations, empirical and spectral data.	The non-mobile validation refers to the application of excluded data to the model, where the empirical values are compared to the predicted.
On-line (mobile) validation	PLSR model predicted on-line data. 5% (model excluded) empirical ground truth locations.	On-line (mobile) validation refers to the use of the on-line predicted data, (where on-line data was applied to the models) and compared by location to the empirical values of the remaining model excluded data.

**Table 24:** Summary of the models produced for the yellow rust and fusarium head blight (FHB) models. Showing the datasets used, the achieved outcomes and validations.

Model	Dataset	Outcome	Validations
Yellow rust Visual coverage analysis (%)	Yellow rust visual assessments, as % of disease spread on the leaves.  Spectral data from ground truth plots  On-line spectral data	Offline and on-line PLSR model for predicting % cover of yellow rust	Wheat Cross validation.  Wheat non-mobile validation.  Barley and wheat on-line validation
Yellow rust scale (0-5)	Yellow rust visual assessments, on a 0 to 5 scale of disease severity on the leaves.  Spectral data from ground truth plots  On-line spectral data	Offline and on-line PLSR model for predicting 0-5 scale cover of yellow rust	Wheat Cross validation.  Wheat non-mobile validation.  Barley and wheat on-line validation
Yellow rust photo interpretation (%)	Yellow rust assessments, from photo interpretation for disease severity on the leaves %.  Spectral data from ground truth plots  On-line spectral data	Offline and on-line PLSR model for predicting 0-5 scale cover of yellow rust	Wheat Cross validation.  Wheat non-mobile validation.  Barley and wheat on-line validation
FHB Visual coverage analysis (%)	Yellow rust visual assessments, as % of disease spread on the leaves.  Spectral data from ground truth plots  On-line spectral data	Offline and on-line PLSR model for predicting % cover of FHB	Wheat Cross validation.  Wheat non-mobile validation.  Barley and wheat on-line validation.
FHB photo interpretation (%)	Yellow rust assessments, from photo interpretation for disease severity on the leaves %.  Spectral data from ground truth plots  On-line spectral data	Offline and on-line PLSR model for predicting 0-5 scale cover of FHB	Wheat Cross validation.  Wheat non-mobile validation.

Statistics of samples used for yellow rust and FHB modelling and validation in wheat is shown in Table 25 and Table 26, respectively. However, sample statistics of on-line dataset in barley is shown in Table 27. Before running the analysis, each yellow rust dataset was divided into calibration (70%, e.g., 940 samples), non-mobile validation (25%, e.g., 235 samples) and on-line validation (5%, e.g., 47 samples) sets. A Similar division of samples was done for FHB data, although fewer samples were available, due to FHB only occurring at a later growth stage, hence, only fewer late scans were collected (Table 26). Partial least squares regression (PLSR) analysis with leave-one-out cross-validation was carried on calibration datasets. The input variables to PLSR were wavelengths (400-750 nm) and disease, assessed as coverage and category scale, as per five models described above. As for spectra pre-processing, PLSR analyses were carried out using Unscrambler 10 software (Camo Inc.; Oslo, Norway). Outliers were detected, and removed to a maximum of 5% of the total input data. These outliers were recognised by being distant from the other observations, either due to variability in the measurements or an error in data capture (e.g. missed in data cleaning). The wheat data was used to establish the PLSR calibration models and underwent both cross-validation and independent validations (both non-mobile and on-line). Although as mentioned, no barley data was considered in the cross-validation, on-line predictions in barley data were carried out using the wheat models (Table 27).

**Table 25:** Statistics of samples used for the assessment of yellow rust in wheat by partial least squares (PLSR) regression analysis. Data is shown in cross-validation, non-mobile and on-line predictions.

Item	Visual coverage analysis			Visual scale analysis			Photo interpretation (%)		
	Cross-val (%)	Non-mobile	On-line	Cross-val (0-5)	Non-mobile	On-line	Cross-val	Non-mobile	On-line
<b>Nr</b>	940	235	47	940	235	47	940	235	47
<b>Max</b>	90	65	50	5	4	5	60	65	50
<b>Min</b>	0	2	2	0	0	0	0	2	2
<b>Mean</b>	15	20	20	2	1.9	2.2	7	10	10
<b>SD</b>	17	18	13.4	1.3	1.4	1.5	14	12	16

SD is standard deviation

The performance of PLSR models were validated using the remaining 20% samples, which were not considered in the cross-validation stage. Validation was done using non-mobile collected spectra and the on-line collected data in the field using the mounted hyperspectral imager. For the on-line validation, predicted and assessed values were overlaid at the same or a very close position. However, the position of the on-line data did not always perfectly align to the ground truth spot position, due to the capture rate of the hyperspectral imager, and the accuracy of the DPGS system. Therefore, for validating the on-line predictions, a scanned area of 5 m<sup>2</sup> was considered, and the ground truth spot was located in the middle. This meant that for some ground truth points there was up to 3 on-line predicted values, where we select the point providing the greatest match. This was done with ArcGIS 10 software (ESRI, California, USA).



**Table 26:** Statistics of samples for the assessment of fusarium head blight (FHB) in wheat used in the partial least squares (PLSR) regression analysis. Data is shown for cross-validation, non-mobile and on-line predictions.

	Visual cover analysis (%)			Photo interpretation (%)		
	Cross-val	Non-mobile	On-line	Cross-val	Non-mobile	On-line
<b>Nr</b>	620	155	31	620	155	31
<b>Max</b>	5	3	5	3	2	3
<b>Min</b>	0	0	0	0	0	0
<b>Mean</b>	0.9	0.5	0.6	0.7	0.5	0.6
<b>SD</b>	1.7	0.9	1.4	1.3	0.7	1.4

**Table 27:** Statistics of samples used for on-line prediction of yellow rust and fusarium head blight (FHB) in barley by partial least squares (PLSR) regression analysis. Data is shown in on-line predictions.

	FHB		Yellow rust		
	Visual coverage analysis (%)	Photo interpretation (%)	Visual coverage analysis (%)	Visual scale analysis (0-5)	Photo interpretation (%)
<b>Nr</b>	50	50	50	50	50
<b>Max</b>	5	3	40	4	58
<b>Min</b>	2	1	0	0	3
<b>Mean</b>	2.6	1.9	5	1.9	20
<b>SD</b>	1.3	1.5	9	1.3	13

SD is standard deviation

The model performance was evaluated in cross-validation, non-mobile validation and on-line validation by means of  $R^2$ , root mean square error of prediction (RMSEP) and ratio of prediction deviation (RPD), which is the standard deviation divided by RMSEP. In order to compare between the performances of different models developed we used the classification scale proposed by Whetton *et al.* (2016c) for crop disease analysis (Table 28).

**Table 28:** Ranges of the ratio of prediction deviation (RPD) and their suitability for predicting yellow rust and fusarium head blight (FHB) in cereal crops, proposed by which was proposed in Whetton *et al.* (2016c), and is based on the classifications from Rossel *et al.* (2006).

RPD range	Class and prediction capability
< 1	Poor model predictions - not useful.
1-1.5	Possibility to discriminate between low and high values
1.5-2.0	Moderate prediction capability
2.0-2.5	Good prediction capability
2.5-3.0	Very good prediction capability
>3.0	Excellent prediction capability

### 6.3.3 Mapping

Maps for the on-line predicted yellow rust and FHB were developed with ArcGIS 10 software (ESRI, California, USA). Kriging was used to develop maps from the data collected from the tramlines illustrated in Figure 29, assuming that the distance or direction between sample points reflects a spatial correlation that can be used to explain spatial variations. To distinguish these spatial variations, semi-variograms were developed in Rstudios (RStudio,

Boston, MA) and then applied to the kriging by utilising the advanced parameters option in ArcGIS 10 software (ESRI, California, USA).

## **6.4 Results**

### **6.4.1 Crop canopy spectra analysis**

Figure 31 and Figure 32 show typical spectra collected at early (booting) and late (milk) growth stages of wheat and barley, respectively, comparing on-line and non-mobile (off-line, in the field) spectra. In Figure 31, the early on-line spectra had the lowest reflectance through the spectral signature, whilst the late non-mobile had the highest reflectance through the spectral signature apart from that at 710nm for the early non-mobile spectra, which has the second highest absorption at the rest of spectra. Late on-line spectra closely resemble late non-mobile spectral signature apart from having a slightly lower reflectance between 580 and 650. The spectra of a barley canopy are shown at the anthesis growth stage for on-line and non-mobile measurement (Figure 32), the similarity is clear although slight differences in reflection can be observed at 520 – 550 nm and at 670 - 750 nm spectral ranges.

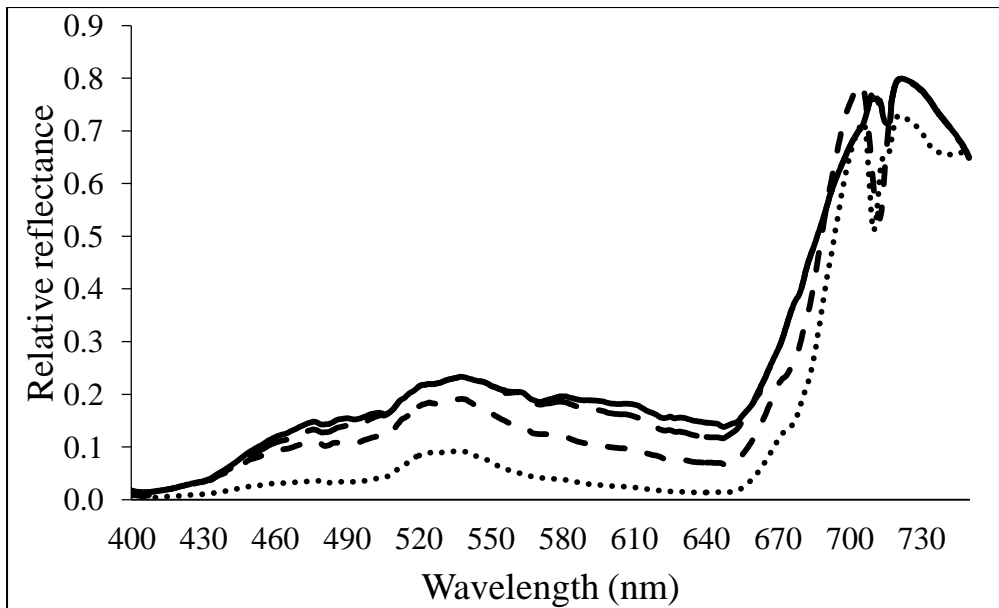


**Figure 31:** Indicative spectra of wheat canopy collected at early (booting) and late (milk) growth stages, comparing on-line and non-mobile (off-line ground truth) spectra as: (-) late non-mobile (---) early non-mobile (...) early on-line, and ( \_ \_ ) late on-line.

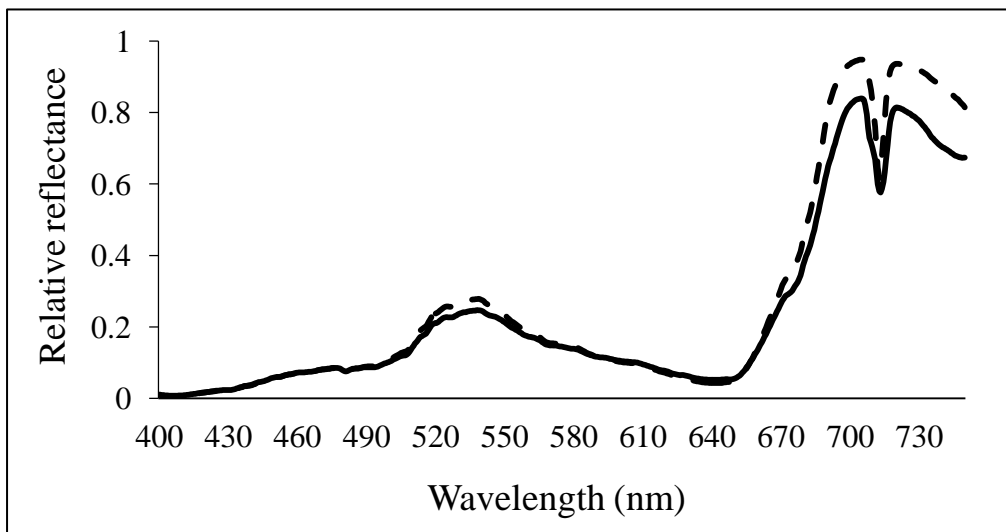


**Figure 32:** Indicative spectra of barley canopy collected at anthesis growth stage, comparing between on-line (--) and non-mobile (-) spectra.

#### **6.4.2 Evaluation of model performance**

The cross-validation results (Table 29) indicate accurate predictions, with high  $R^2$  values (above 0.74), with FHB models appearing slightly higher than yellow rust, with photo interpretation for FHB being the marginal highest at 0.87  $R^2$ , and visual scale being the highest for yellow rust at 0.82  $R^2$ . The independent validation based on non-mobile collected spectra (Table 29) in the field indicates an opposite trend to cross-validation, where measurement of yellow rust (RPD = 1.3, 2.14, 2.55 and  $R^2$  = 0.005, 0.78 and 0.82 for photo interpretation, visual coverage in %, and visual scale, respectively) is more successful than FHB (RPD = 1.4 ( $R^2=0.71$ ) and 2.31 ( $R^2=0.85$ ) for visual coverage in %, and image scale analysis, respectively). The independent (non-mobile) models based on visual scale analyses, provide improved prediction performance (RPD = 2.55,  $R^2=0.82$ ) for yellow rust, as compared to the % coverage model (RPD = 2.14,  $R^2=0.78$ ). The image scale analysis is the worst performing in yellow rust prediction (RPD = 1.30,  $R^2=0.005$ ), whereas the opposite is true for FHB (RPD = 2.31,  $R^2=0.85$ ).

**Table 29:** Summary of model prediction performance of yellow rust and fusarium head blight (FHB) in wheat in cross-validation and non-mobile independent validation. Models were developed with the five on-line scanning occasions in three wheat fields. The five models are; FHB visual cover analysis (%), FHB photo interpretation (%), Yellow rust visual coverage analysis (%), Yellow rust visual scale analysis (0-5) Yellow rust photo interpretation (%).

		FHB		Yellow rust		
		Visual scale analysis	photo interpretation	Visual coverage analysis	Visual scale analysis	photo interpretation
<b>Cross validation</b>	R <sup>2</sup>	0.86	0.87	0.79	0.82	0.74
	RMSECV	0.51	0.25	8.19	0.59	8.21
<b>Non-mobile validation</b>	R <sup>2</sup>	0.71	0.85	0.78	0.82	0.005
	RMSEP	0.5	0.39	8.2	0.55	9.2
	RPD	1.4	2.31	2.14	2.55	1.3

The R<sup>2</sup> are significant to <0.01. RMSECV is root mean square error of cross validation; RMSEP is root mean square error of prediction; RPD is ratio of prediction deviation = standard deviation / RMSEP

Scatter plots of on-line predicted versus reference assessed (both % coverage and scale) yellow rust and FHB (photo interpretation) are shown in Figure 33. Photo interpretation for yellow rust and visual analysis for FHB were excluded from Figure 33, due to their poor results, however, their results are summarised in Table 30. Table 30 also shows the PLSR results for on-line prediction, where R<sup>2</sup>, RPD, and RMSEP are provided for wheat and barley for each model. The photo interpretation provides very poor on-line predictions of yellow rust, as compared to those for FHB in both barley and wheat fields. The visual scale analysis is again (like in cross-validation and non-mobile validation) more accurate for on-line yellow

rust prediction, which can be classified as good for wheat (RPD = 2.5,  $R^2=0.81$ ) and a moderate for barley (RPD = 1.82,  $R^2=0.72$ ). The visual analysis of FHB is very poor (RPD = 0.47 ( $R^2=0.09$ ) and 0.75 ( $R^2=0.04$ ) for barley and wheat, respectively). The photo interpretation model offers an improvement of model prediction performance, which can be classified as good for wheat (RPD = 2.27,  $R^2=0.82$ ) and moderate for barley (RPD = 1.56,  $R^2=0.61$ ). For both non-mobile and on-line validation scenarios, yellow rust models based on visual coverage analyses outperformed the corresponding FHB models (Table 29 and Table 30). The photo interpretation is more accurate for FHB prediction, whereas both the visual analyses are more efficient for yellow rust prediction.

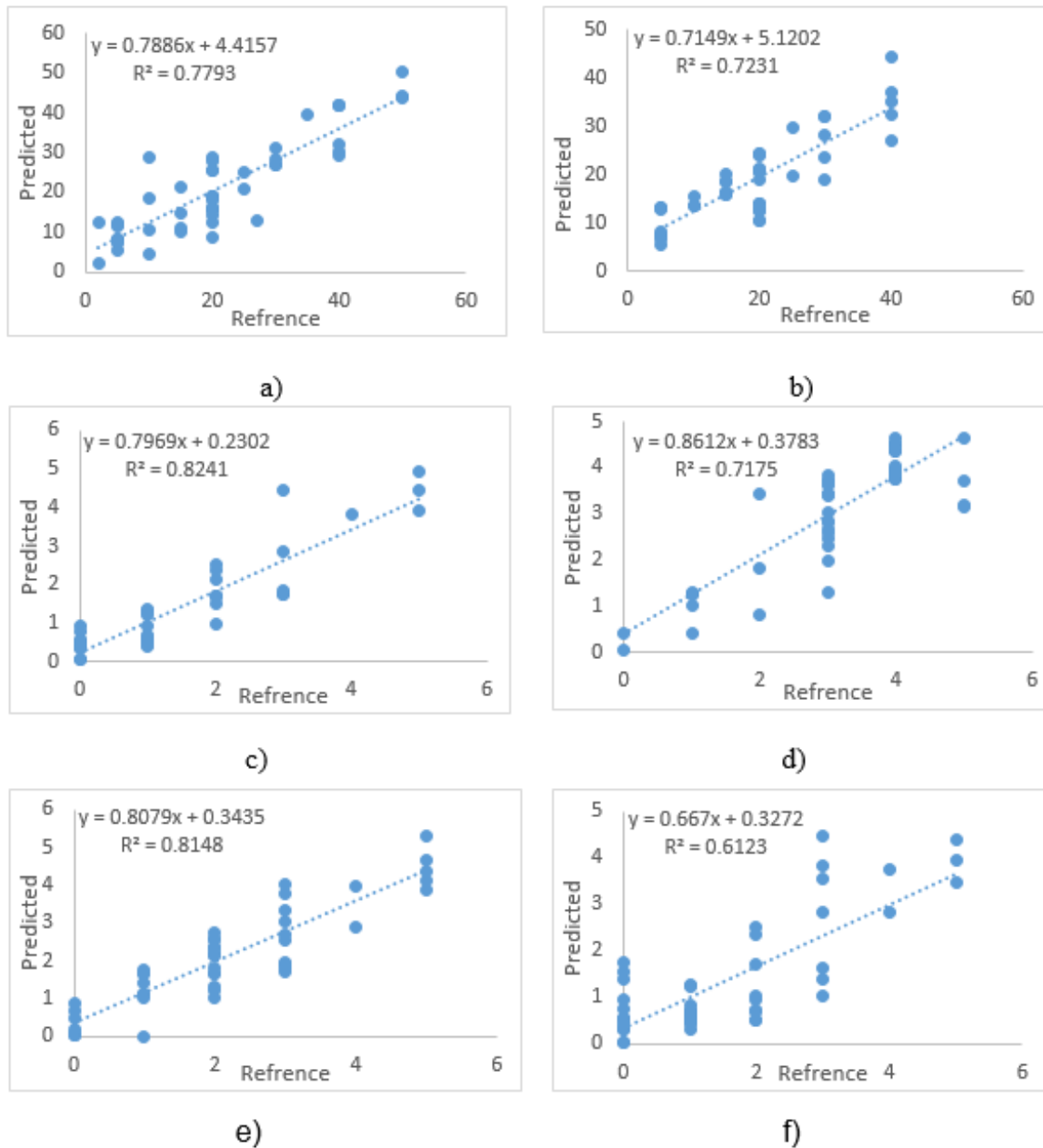


**Figure 33:** Scatter plots for the on-line predicted versus reference assessed diseases. On-line predictions was based on partial least squares regression model developed, based on visual yellow rust coverage in wheat (a), visual yellow rust coverage in barley (b), visual yellow rust scale in wheat (c), visual yellow rust scale in barley (d), image fusarium head blight (FHB) scale in wheat (e) and image FHB scale in barley (f).



**Table 30:** On-line validation results based on–line spectral data collected from three wheat fields and one barley field. The five models are; Fusarium head blight (FHB) visual cover analysis (%), FHB photo interpretation (%), Yellow rust visual coverage analysis (%), Yellow rust visual scale analysis (0-5) and Yellow rust photo interpretation (%).

		FHB		Yellow rust		
		Visual coverage analysis	Photo interpretation	Visual coverage analysis	Visual scale analysis	Photo interpretation
<b>Wheat</b>	R <sup>2</sup>	0.04	0.82	0.78	0.81	0.06
	RMSEP	1.93	0.63	6.13	0.59	22.88
	RPD	0.75	2.27	2.19	2.5	0.7
<b>Barley</b>	R <sup>2</sup>	0.09	0.61	0.72	0.72	0.045
	RMSEP	2.69	0.93	5.39	0.69	26.59
	RPD	0.47	1.56	1.67	1.82	0.49

RMSEP is root mean square error of prediction; RPD is ratio of prediction deviation = standard deviation / RMSEP the R<sup>2</sup> are significant to <0.01

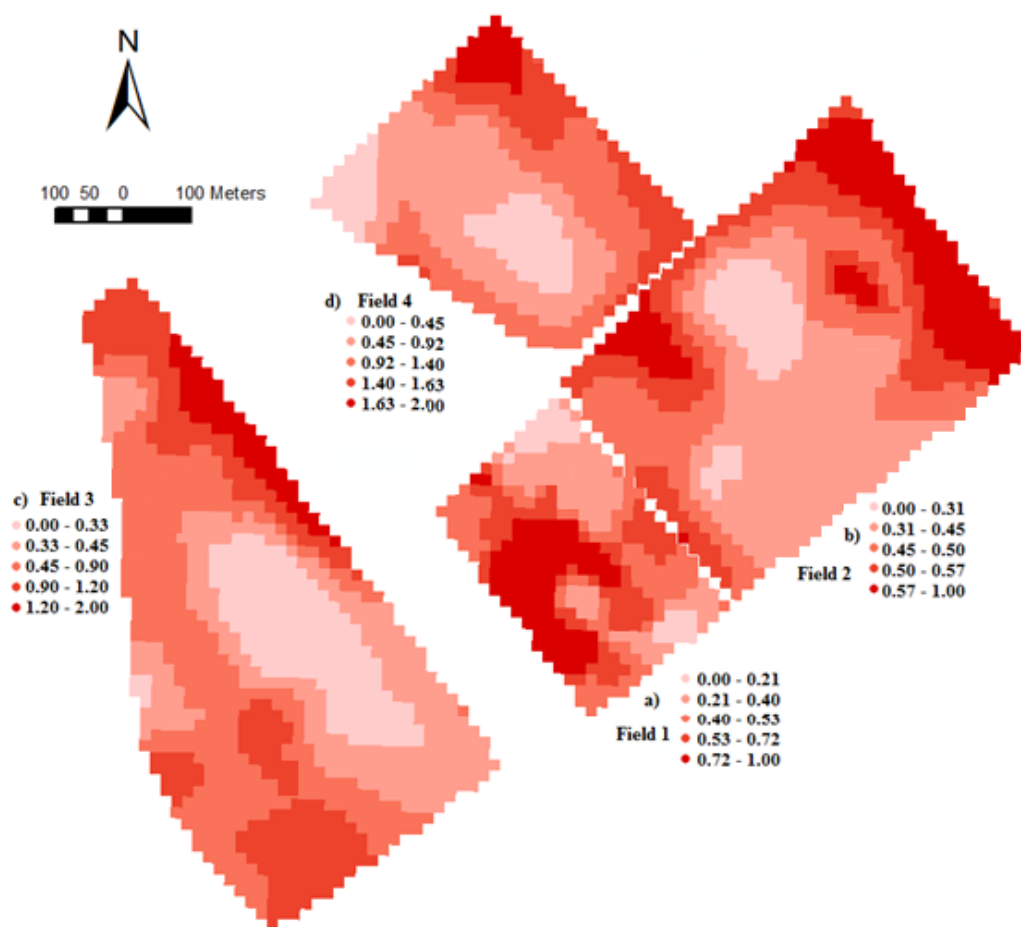
### 6.4.3 Maps

Table 31 Summarises the mapped ground truth data for each field, for FHB the photo interpretation is shown and for yellow rust the visual scale analysis is shown. The ground truth data were interpolated through Inverse distance weighting, and extracted at a 10m by 10m resolution, and are presented as maps in Figure 34 for FHB and Figure 35 for yellow rust. The maps use different scales to highlight the change in disease levels through the field. If they all used the same scale, the distribution pattern would be masked. Figure 34 shows the highest FHB infection towards the edges of the field for all fields, apart from Field 1, which is the smallest at only 4 ha, where FHB appears towards the centre and west side. The highest infection levels are seen in field 4 and field 3 in the NE corner.

The yellow rust maps are shown for the four studied 4 fields, with early scans shown for fields 1 and 3 (Figure 34). Field 4 shows heavy yellow rust infection in the centre and west side of the field. All other yellow rust field maps show heavy disease spread towards the edges of the fields.

**Table 31:** Summary statistics of the ground truth assessments of fusarium head blight (FHB) by photo interpretation and early and late yellow rust by yellow rust scale coverage.

		<b>Early yellow rust</b>	<b>Late yellow rust</b>	<b>FHB</b>
<b>Field 1</b>	Max	3.00	5.00	1.00
	Min	0.00	1.00	0.00
	Average	2.29	3.24	0.48
	SD	0.46	0.82	0.31
<b>Field 2</b>	Max	NA	4.00	1.00
	Min	NA	1.00	0.00
	Average	NA	3.02	0.40
	SD	NA	0.71	0.30
<b>Field 3</b>	Max	3.00	5.00	2.00
	Min	0.00	1.00	0.00
	Average	2.04	2.72	0.57
	SD	0.66	0.65	0.35
<b>Field 4</b>	Max	NA	4.00	3.00
	Min	NA	1.00	0.00
	Average	NA	2.2	1.23
	SD	NA	0.76	0.67



**Figure 34:** Maps of % disease cover of fusarium head blight (FHB) of ground truth data obtained with photo interpretation at a 10 by 10 m resolution. Maps are shown for the four experimental fields; Field 1 with wheat (a) (4 ha anthesis), field 2 with barley (b) (10 ha anthesis), field 3 with wheat (c) (12 ha Milk), and field 4 with wheat (d) (7 ha Milk).

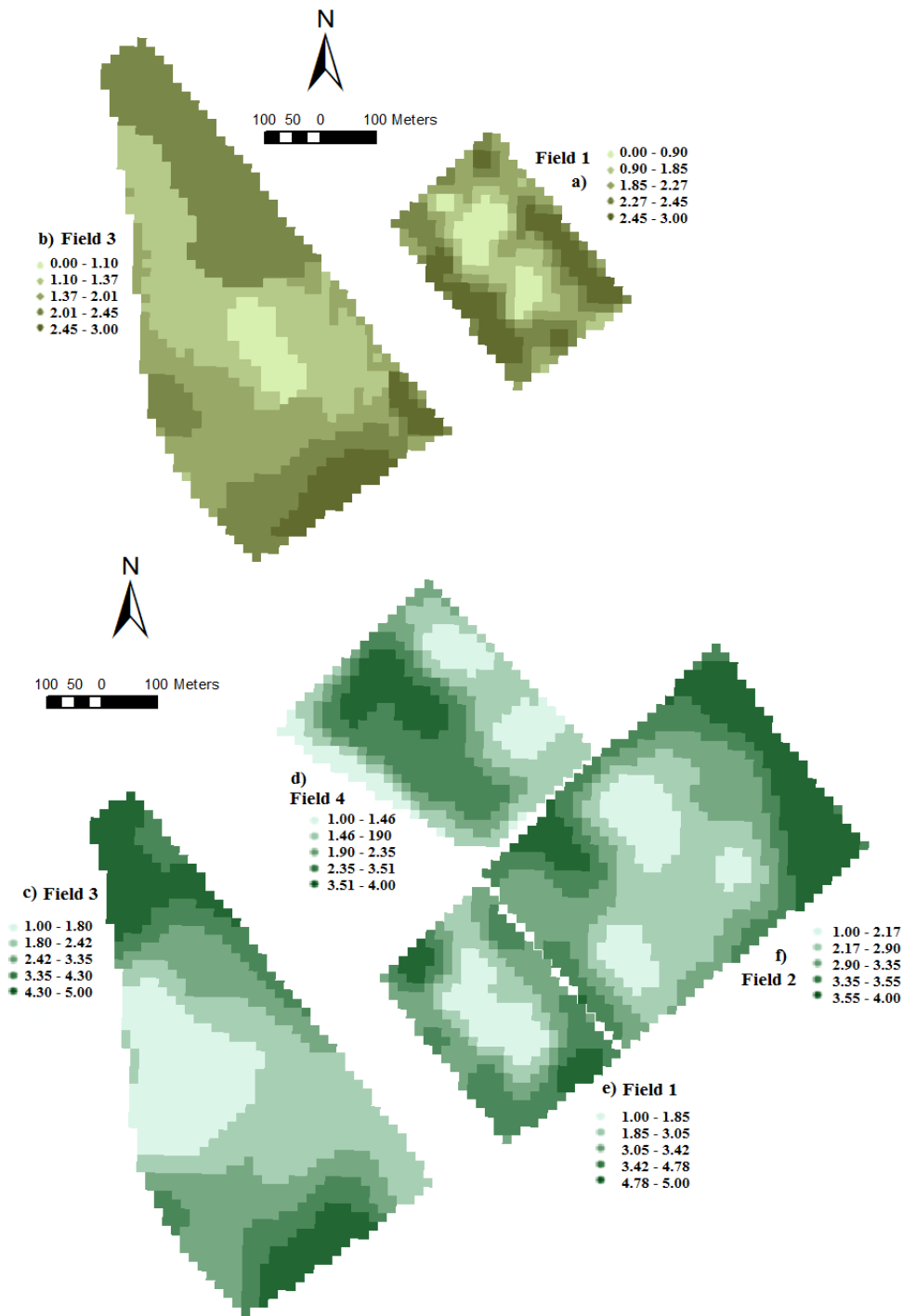


**Figure 35:** Maps of yellow rust classed in the 0-5 scale of ground truth data at a 10 by 10 m resolution. Maps are shown in the four experimental fields: (a and b) refer to maps of early stage scans in field 1 with wheat (4 ha booting) and field 3 with wheat (12 ha booting), respectively. Maps of late stage scans are shown by (c) for field 3 with wheat (12 ha Milk), (d) for field 4 with wheat (7 ha Milk) (e) for field 1 with wheat (4 ha anthesis) and (f) field 2 with barley (10 ha anthesis).

The best on-line PLSR models (e.g., photo interpretation for FHB and visual analysis for yellow rust) were selected and used to develop corresponding maps. The best fit of the spatial data for both diseases in all fields was obtained with spherical semi-variograms, whose parameters are shown in Table 32.

**Table 32:** Semi-variogram model parameters of each mapped disease in the four fields. The best fit was achieved with spherical models. Yellow rust early and late and fusarium head blight (FHB), showing nugget ( $c_0$ ), sill ( $c$ ), range ( $r$  m), proportion ( $C_0/C$  %), and the sum of square error (SSE)

		Semi-variogram parameters				
		$c_0$	$r$ (m)	$C$	$(c_0/c)$ (%)	SSE
<b>FHB</b>	Field 1	0.12	86.39	0.71	5.51	2.95
	Field 2	0.37	99.46	0.83	1.70	1.41
	Field 3	0.11	97.02	0.89	8.02	3.32
	Field 4	0.04	75.62	0.77	18.98	0.01
<b>Yellow rust early</b>	Field 1	0.001	77.75	0.002	1.001	3.383
	Field 2	0.001	68.1	0.003	2.002	8.029
	Field 3	0.0001	78.34	0.001	9.0009	2.56
	Field 4	0.02	76.63	0.043	1.173	0.0021
<b>Yellow rust late</b>	Field 1	0.01	77.75	0.022	1.212	2.11
	Field 3	0.01	92.57	0.039	2.929	1.534
<b>MC</b>	Field 4	2.02	65.01	3.52	0.57	5.29

$c_0$  is nugget variance,  $c$  is sill,  $r$  is range,  $c_0/c$  is proportion, and SSE is sum of squared error.

The semi-variogram represents the spatial correlation of empirical values from sample points. The empirical values of each point were plotted into lag points, and a spherical model was fitted to them. The nugget value is attributed to small sampling intervals or measurement errors. The sill represents the semi-variance value of when the model first flattens out. The range reports when this sill occurs and gives the variance in meters, anything beyond the range is not spatially correlated (Bohling, 2005). This translates into the maps shown in Figures 36 and 37 for on-line FHB and yellow rust, respectively, where the on-line predicted data from the hyperspectral imager is interpolated using kriging, from the spatial parameters (nugget, range and sill) based on the semi-variogram data (Table 32).

On-line maps of FHB and yellow rust are shown in Figure 36 and Figure 37. FHB Figures shows a clear spatial pattern of high disease towards the edge of the fields in fields 2, 3, and 4 (Figure 36). In the earlier scans of yellow rust (Figure 37), high infection along the edges of the fields 1 and 3 is also recorded. This pattern of disease distribution is also noticed in field 2 in the later yellow rust scans. The late scans also show higher concentrations of yellow rust, specifically in fields 1, 3 and 4. In fields 1 and 3 it's possible to see the change in distribution from the early infection, which is towards the edge of the field, and the later infection which covers a larger area. However, this disease distribution pattern is not necessarily the case for the smallest field 1 with four ha area, as in this field, significantly lower spatial variability in disease pressure was observed, with high levels of the disease appear within the middle parts (Figures 36 and 37).

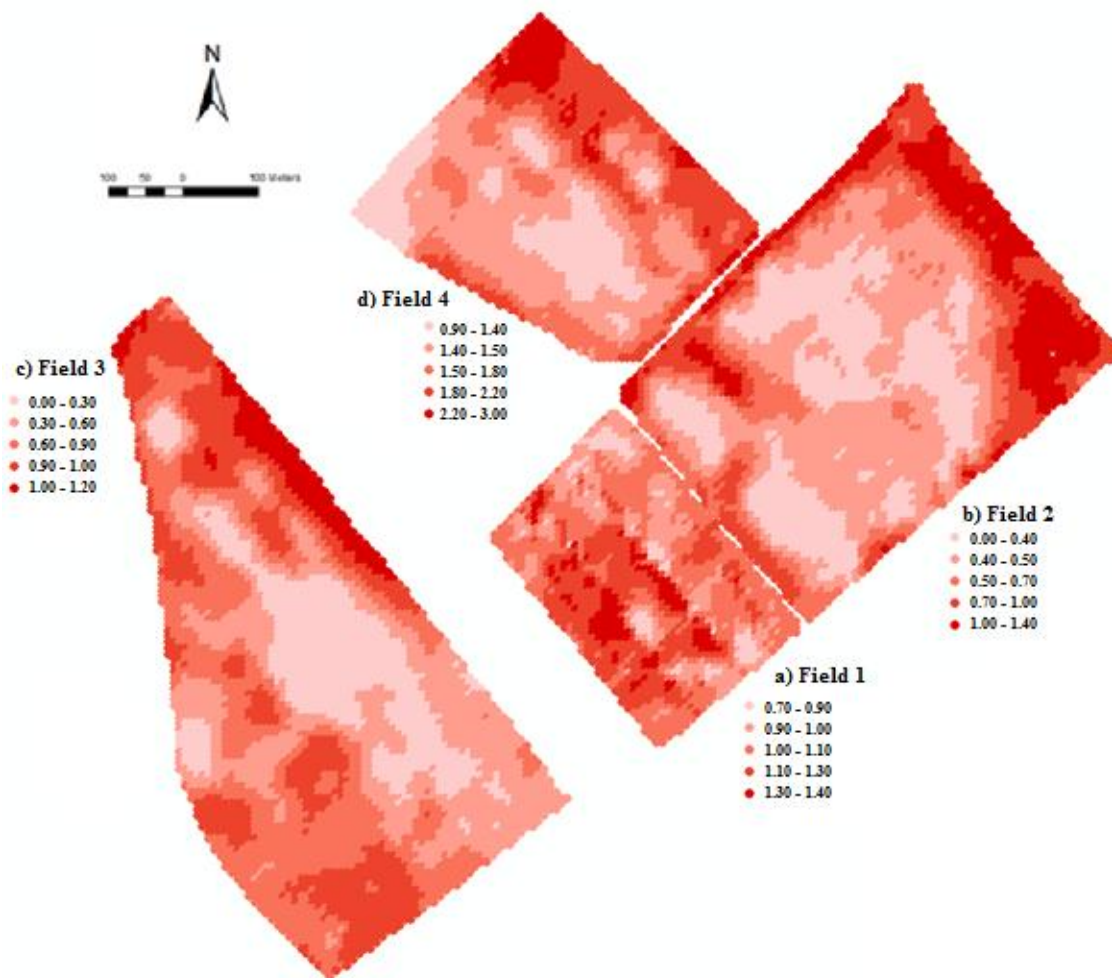


**Figure 36:** On-line measured % infection of fusarium head blight (FHB) maps using photo interpretation in the four experimental fields; Field 1 with wheat (a) (4 ha anthesis), field 2 with barley (b) (10 ha anthesis), field 3 with wheat (c) (12 ha Milk), and field 4 with wheat (d) (7 ha Milk).

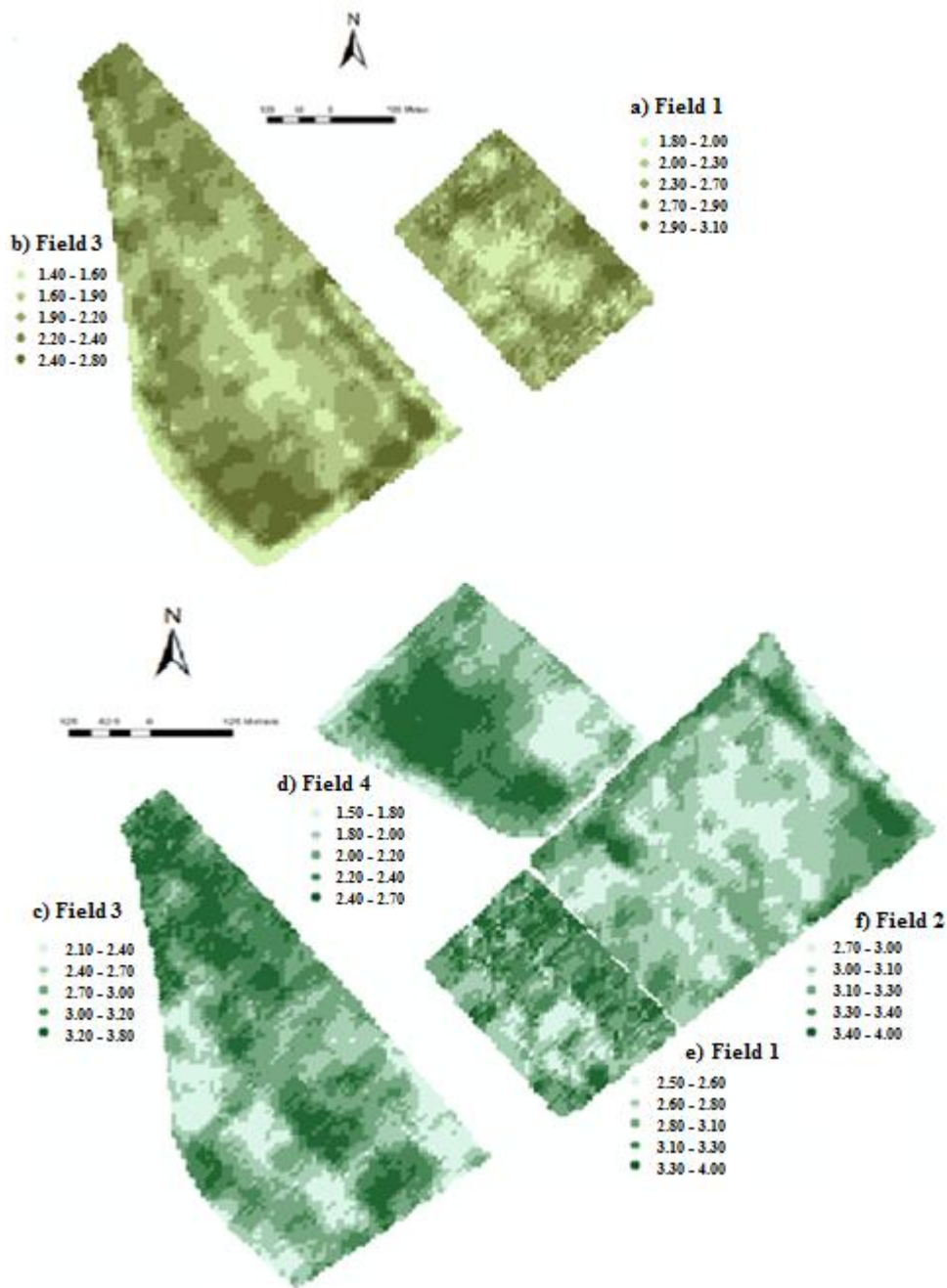


**Figure 37:** On-line measured yellow rust maps, classed in the 0-5 scale (0 is given when no disease is present, 1 for up to 5% cover, 2 for up to 10%, 3 for up to 30%, 4 for up to 50% and 5 for >50%) in the four experimental fields: (a and b) refer to maps of early stage scans in field 1 with wheat (4 ha booting) and field 3 with wheat (12 ha booting), respectively. Maps of late stage scans are shown by (c) for field 3 with wheat (12 ha Milk), (d) for field 4 with wheat (7 ha Milk) (e) for field 1 with wheat (4 ha anthesis) and (f) field 2 with barley (10 ha anthesis).



Figures 34 and 35, and Figures 36 and 37 show maps of ground truth data, and on-line predictions, each for FHB and yellow rust, respectively. In general, good spatial similarities can be observed between measured (ground truth) and on-line predicted corresponding maps. However, the spatial resolution of the ground truth maps shown in Figures 34 and 35 are of much lower spatial resolution. The good spatial similarity is particularly true for FHB, showing a very good comparison of high and low areas. However, the level of disease does not match well, as the model tends to over predict FHB observations, apart from field 3, where it was under predicted. The range of prediction to the reference values can be seen for the online data in figure 33. The yellow rust maps also show a good similarity, with the main difference is the central area of field 1, which seems to be healthier in the ground truth maps. Again, different classes are used for each field and map, a decision that was attributed to the need to show and compare the spatial variation of disease between measured and on-line predicted maps. If all maps were on the same scale much of this detail would have been lost.

The largest yellow rust infection can be observed on the SW part of the field (Figures 35 and 37), whereas FHB spatial distribution follows an opposite trend (Figures 34 and 36), where the highest infection is observed on the NE part of the field. The MC map in field 4 shows higher MC in the NE part of the field compared to the SW part. The MC spatial distribution in this field matches that of FHB. Although moisture content values will vary from day to day, the spatial distribution pattern will remain almost constant (Vachaud *et al.*, 1985; Mouazen *et al.*, 2005).

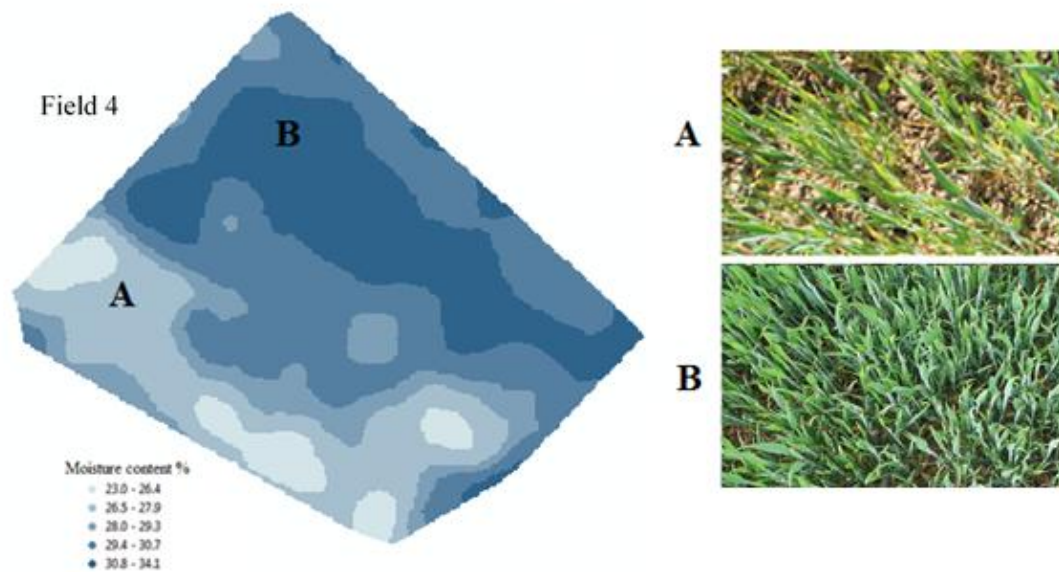


**Figure 38:** Soil moisture content map and images of measured with the on-line visible and near infrared spectroscopy sensor (Mouazen, 2006) in field 4.

## 6.5 Discussion

### 6.5.1 Crop canopy spectra analysis

Figures 31 and 32 both showed similar spectral features to those reported by Whetton *et al.* (2016c) under laboratory scanning conditions. However, the difference between 650 and 700 (nm) in field spectra is much larger than that in the laboratory spectra (in part 1 of the study), which may indicate larger absorption in the 400-650 nm range by the darker canopy colour associated with larger intensity of Chlorophyll in leaves. This large absorption in the 400-650nm wavelength range is linked to absorbance from chlorophyll a (Hunt *et al.*, 2013).

Zhang and Zhang (2016) recommend the use of the spectral range of 470 to 800 nm, which chlorophyll is sensitive to, to monitor crop diseases. Reduced absorption can be observed for a late stage captured spectra, as compared to an early stage, which may be attributed to a reduction in leaf area due to increased yellow rust infection or as Xavier *et al.* (2006) suggest

it's attributed to the increase of senescent leaves. Furthermore, both on-line and non-mobile spectra captured late in the growing season were more similar to each other than they were to the early spectra (Figure 31). The early spectra both on-line and non-mobile show a very similar pattern through the spectral signature. However, a more noticeable difference in relative reflectance can be seen from 670nm onwards. This difference could be due to the individual plant, or the amount of foliage being captured by a moving platform, as from 700nm onwards greater foliage has a greater reflectance. This large similarity in spectra (Figure 31) is a first indication of a good quality canopy spectra collected in this study under mobile conditions. The high similarity between the on-line and non-mobile spectra seen in the barley canopy (Figure 32) is a good indication of the hyperspectral system stability in providing high quality spectra to enable modelling yellow rust and FHB with desirable accuracy, to be evaluated in the following section. There was a slightly lower reflectance recorded for both (early and late) non-mobile wheat spectra, however, the barley has a slightly higher reflectance for the non-mobile spectra. The differences between the on-line and non-mobile spectra are attributed to the moving platform. As the on-line captures are steadily moving and thus capturing an average over a small distance, as opposed to capturing just a small area (a line) like the non-mobile spectra. The spectra between wheat and barley appears similar in Figures 31 and 32. Wilson *et al.* (2014), found only minor differences in the spectra of wheat and barley and attributed these small differences to the physical structure of the ears.

### 6.5.2 Evaluation of model performance

The highest independent validation of yellow rust obtained with the visual scale assessment (RPD = 2.55,  $R^2=0.82$ ) can be classified as very good prediction performance, whereas the highest performance for FHB was obtained with image scale analysis (RPD = 2.31,  $R^2=0.85$ ), which can also be classified as good prediction ability (Table 28). The implication of this is that both an image and visual assessments should be collected for accurate disease models. An RGB image might not capture yellow rust in the low canopy layers. This is the reason why Zhao *et al.* (2016) recommended investigating the disease development for different leaf layers. FHB seems to be better captured in the RGB image than yellow rust as the disease appears on heads that present at the top of the crop canopy; hence, FHB disease is unlikely to be obscured like yellow rust, allowing for an accurate count and representation to be made with the photo interpretation. The photo interpretation also removes the potential of subjectivity between assessments. Due to yellow rust being a foliar disease and leaf overlapping occurring in a canopy, the level of disease could be hidden in an RGB image. Whilst it's arguable that the RGB photograph would be representing the same area seen by the hyperspectral imager, the latter may pick up alterations in the crop's reflectance due to yellow rust, which can be captured by the spectral data.

Huang *et al.* (2015) successfully assessed yellow rust in winter wheat, reporting a high  $R^2$  value of 0.88, based on hyperspectral measurements of individual infected leaves, which is of limited use as compared to canopy measurement adopted in the current work. Peteinatos *et al.* (2016) measured spectral reflectance using two hand-held passive spectrometers and one fluorometer, and concluded that early detection of yellow rust was possible. Adopting a data fusion approach of hyperspectral data (450 – 900 nm) and fluorescence data (550 – 690 nm), Moshou *et al.* (2005), reported a high accuracy (94.5 %) of detecting yellow rust in winter

wheat. They needed two detection technologies to achieve this accuracy, increasing the cost for field application. Similar reliable results for quantitative identification of yellow rust in winter wheat have been demonstrated by Krishna *et al.* (2014), achieving high  $R^2$  and RPD values of 0.90 of 3.8, respectively. However, they have to include the entire visible and near infrared range (e.g., visible and near infrared (VNIR) and short wavelength infrared (SWIR) of 350 to 2500 nm) to reach this accuracy, whereas the current work achieved good (RPD = 2.14,  $R^2=0.78$ ) to very good (RPD = 2.55,  $R^2=0.82$ ) prediction accuracy, based on a mobile relatively cost-effective hyperspectral camera, in the visible range only.

There is limited literature for FHB detection in the field, which may be attributed to the difficult detection of symptoms appearing on ears. Polder *et al.* (2005) reported successful detection of fusarium in single kernels, by using both spectroscopy and imaging. Similarly, Delwiche and Kim (2000) successfully used a hyperspectral imager at 435 – 860 nm and machine learning for fusarium detection in wheat kernels. Bauriegel *et al.* (2011) utilised a hyperspectral imager, based on wavelength range intervals of 500–533 nm (green), 560–675 nm (yellow to red), 682–733 nm (red edge) and 927–931 nm (NIR), to identify the percent coverage of fusarium disease in ears, achieving average recognition accuracy of 67% and as high as 87%. Oerke and Steiner (2010) utilised an infrared thermography method for *in-situ* detection of FHB symptoms at a canopy level, by detecting a significantly higher temperature in infected ears.

The non-mobile independent validation results (Table 29) were better than those of the on-line validation (Table 30), particularly for yellow rust. This is expected as during on-line measurement, uncontrollable external conditions such as vibrations and variations in camera and light source heights and angles, negatively affect the measurement accuracy. Since fusarium infects the ear as opposed to the foliage, the impact of fusarium symptoms on

spectra in less pronounced in early growing stages (Rossi *et al.*, 2001; Xu, 2003), hence, can only be applied to the data collected later in the season. Prediction of FHB infection in wheat (Table 30) is more accurate than in the barley, as the wheat data for the FHB models were collected at milk (70) in field 1 and 2 and at anthesis (61) in field 4 for wheat, compared to just anthesis (61) for barley (Table 22). Though FHB was only detected later in the season, its recognition can still be useful for selective harvest (see next Chapter), and perhaps for the last fungicide application, which is usually targeted towards maintaining the health of the crops ear (Pillinger *et al.*, 2004).

The improved models performance is in line with the findings of Part 1 of this study (Whetton *et al.*,(2016c), and could be attributed to the reduction in the subjectivity effect on the assessments, by grouping readings within 5 different groups of infections detailed above. The on-line prediction performance of percent coverage, obtained with the visual analysis of FHB is very poor (RPD = 0.47 ( $R^2=0.09$ ) and 0.75 ( $R^2=0.04$ ) for barley and wheat respectively). There is very limited literature about on-line measurement of cereal disease, particularly for FHB. Examining the on-line validation in Table 30 suggests that FHB should be detected by the RGB photo interpretation, whereas yellow rust by the visual analyses, both the percent coverage and scale. This is true for both wheat and barley. On-line predictions in wheat were better than those in the barley field, which is expected as models were created using data from wheat fields and then applied to predict disease presence in the barley field to test robustness.

### 6.5.3 Maps

From the maps developed, it can be generally observed that higher disease is located towards the edges of the fields, where hedgerows and borders of a field act as a source of inoculum of yellow rust and fusarium species (Jenkinson and Parry, 1994; Champeil *et al.*, 2004; Imathiu *et al.*, 2013). Initial infections of soil-borne pathogens, commonly result from infected plant residues left over from the previous year's harvest. Fusarium fungi survive over winter on plant residues (as mycelium), which can produce ascospores that infect the flag shoot (Sutton, 1982; Oberti *et al.*, 2014). The late (second) scans of the 10 and 4 ha fields (Figure 37) show the yellow rust spreads further towards the centre of the field. Figure 39 shows yellow rust and FHB infection from the RGB images captured in the late scans.

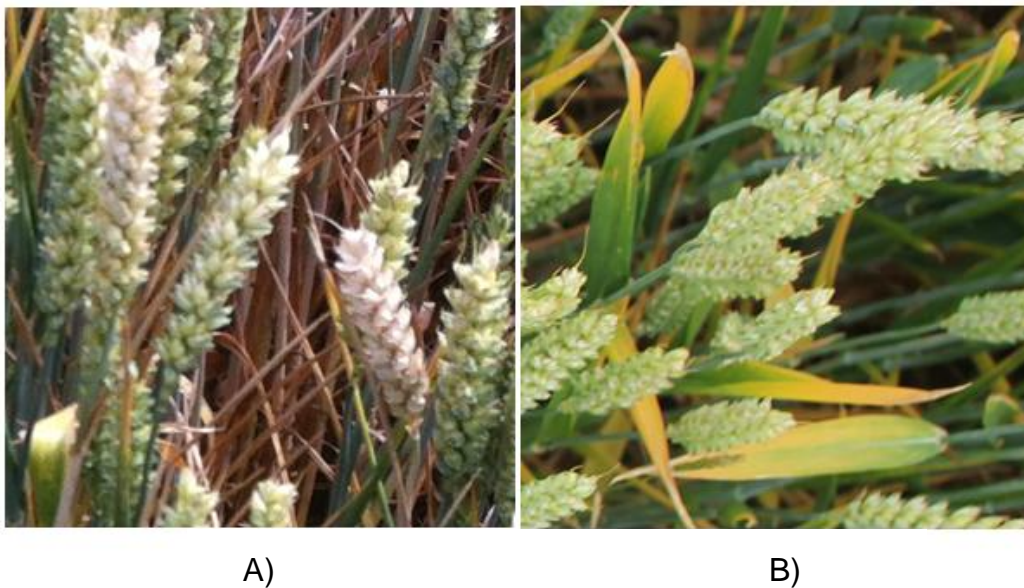


**Figure 39:** Images of wheat crop at the field site in Bedfordshire, UK. Wheat was at growth stage 72 (Milk). Part A) Fusarium head blight infection (FHB), and part B) Yellow rust infection.

Fields 1 and 2 (Figure 36) were classed at anthesis growth stage. FHB infection can occur at the booting growth stage. However, it's unlikely to see symptoms until after anthesis (Anand *et al.*, 2003; Reis *et al.*, 2016). Development of crop is heavily affected by temperature, which can vary through a field due to microclimate. The majority of the crop in field 1 and 2 was at the anthesis growth stage however, there are areas in the field that were further developed. The infection witnessed in field 1 and 2 were the first symptoms of FHB, being a pink tint in some of the ears. The majority of field 2 had a very low infection, particularly towards the centre of the field. Field 1 however, had a more homogenous distribution of FHB. (Dammer, 2003; Saiyed *et al.*, 2009; AHDB 2015).

It is important to point out here that the 7 ha field 4 can be split according to soil type into almost two halves, with the NE half being of a heavier soil (clay loam), whilst the other SW half being of a much lighter soil (sandy clay loam). This field was only scanned in one occasion at the milk (grain filling) stage on 1<sup>st</sup> July, 2015, which is quite late in the season. The largest yellow rust infection can be observed on the SW part of the field (Figure 35), whereas FHB spatial distribution follows an opposite trend, where the highest infection is observed on the NE part of the field (Figure 34). Due to the dry but warm conditions of 2015 spring, FHB infection was low in general. It is of interest to mention that May according to the UK metrological office was particularly dry, and record breaking temperatures had been reached later on in the season. This resulted in half of the field being under substantially more water stress (SW) than the other wetter half (NE), due to the difference in the soil type and its ability to retain soil moisture. Subsequently, this soil type and moisture retention differences between the two halves affected the crop canopy, and substantially impacted on the microclimate conditions of the crop. It was reported that a variation in soil texture can lead to variations in soil properties.



For example, an increase in nitrogen will increase the duration and green area index of the canopy, which further affects the microclimate conditions (Stokes *et al.*, 1997; Sylvester-Bradley and Kindred, 2009). The underlying spatial distribution of moisture content in field 4 (Figure 38) confirms the NE part to have a larger moisture content than the SW part. This is resulted as plants in the NE part being a denser, thicker and greener canopy (Part B in Figure 38), than plants in the dryer SW part (Part A in Figure 38). Whilst moisture content will vary quickly, the underlying spatial distribution pattern of water presence will remain similar through the season (Vachaud *et al.*, 1985).

Local climate and weather conditions are considered the most influential factor regarding the distribution and severity of fungal infections in a crop stand. Under clear weather conditions in spring and summer, areas of the field with a lower crop density will warm up and cool down faster than those with dense canopies. Temperature in a wheat field's microclimate could have an inter-canopy variation of up to 7.5°C (Dammer, 2003), depending on crop canopy density and soil moisture content. Therefore, different soil texture type and subsequently moisture content encountered in this study may have affected crop canopy density and humidity and crop health under the exceptionally dry conditions in the spring of 2015, which led to the different disease spread pattern in among the two parts of the Field 4.

Literature demonstrates that epidemics of fungal diseases are strongly influenced by the local environment, persistence and adaption of the pathogen and the crop's variety and physiological condition (Dammer, 2003). Therefore, variation in one of more of these will possibly affect disease distribution, which we believe to be the case in the 7 ha, field 4. The conidial fusarium spores are commonly transported by rain drop splashes, though this depends on the species (Parry *et al.*, 1995). Variability of disease presence is common for FHB. This is due to infection being dependent on warm humid weather conditions, which

may explain why the NE part of field 4 had higher fusarium disease ranges than the dryer SW part (Jelinek *et al.*, 1989; Rossi *et al.*, 2001; Xu, 2003). In the NE part, the crop canopy was denser due to heavier texture and larger MC which resulted in a higher humidity. However, the higher infection with yellow rust in the dryer SW part of this field can be attributed to the fact that yellow rust spores are predominantly dispersed by wind but require moisture to infect the crops leaves. The less dense canopy of the SW part, as compared to the NE part (Figure 38) may have allowed for better penetration of yellow rust spores by wind, hence increase infection rates in this part. This is an interesting point to consider in plant protection against yellow rust and FHB, although further investigations are necessary.

Examining the spatial distribution of the on-line FHB (Figure 36) and yellow rust (Figure 37) maps, one can observe the high infection concentrated at the hedgerows and borders of fields. This suggests the need for site specific application of fungicides that should target these highly infected edge parts, and that application should take place at earlier growing stages. This will prevent or at least reduce the possibility of diseases to expand towards the inner parts. The on-line measured disease maps become more important at late growing stages once diseases spread over the field, and site specific spraying becomes more important to adopt. Further work will need to use these maps for site specific fungicide applications, followed by cost-benefit and life cycle analysis to evaluate the economic and environmental benefits as compared to the traditional homogeneous applications adopted by majority of farmers today.

## **6.6 Summary conclusions**

This Chapter introduces the work related to the on-line measurement of yellow rust and fusarium in four fields using the optimal measurement set up of the hyperspectral line image camera, obtained in Chapter 4. The results from this study show that on-line hyperspectral measurement and mapping of yellow rust (using visual assessments) and FHB (using image interpretation) is possible, with moderate accuracy in barley and good accuracy in wheat. The spatial distribution of yellow rust, and FHB, were impacted by both soil texture and moisture content. This will allow for future work to be carried out on on-line measurement for both crop diseases to guide site specific fungicide application or selective harvest, to be discussed in the next Chapter.

## **7 Management zone maps for variable fungicide application and selective harvest**

### **Chapter Synopsis;**

This chapter focuses on data fusion of disease data (yellow rust and fusarium head blight (FHB)), along with canopy and soil properties, to produce management zones (MZ) in winter wheat. The chapter introduces theoretical MZ methods of selective harvest (SH) (so grain can be separated in relation to quality) and variable fungicide application (VRFA) of application rates dependent on the severity of disease. The MZ approaches are compared to conventional methods by means of virtual cost-benefit analyses, under certain assumptions. The data is collected through the methods introduced and discussed in chapters 3, 4, 5, and 6.

### **Abstract**

Currently the majority of crop protection approaches are based on homogeneous application of fungicides over the entire field area. With the increasing pressures on fungicide applications, associated with increased environmental impact and cost, an alternative approach based on site specific fungicide application and selective harvest (SH) is needed. But, to achieve this goal high resolution data on the affecting factors in the system is needed to allow accounting for the within field variability in the analysis. High sampling resolution data on crop growth and diseases, soil properties and yield were subjected to k-mean cluster analysis to develop management zone (MZ) maps for one experimental field in Bedfordshire, UK. Cost-benefit analyses for variable rate fungicide application (VRFA) and SH were performed at T1, T2 and T3 growth stages of wheat. Results showed that with VRFA, when compared to homogeneous rate fungicide application (HRFA), reductions in fungicide application of 22.24% at T1 and T2 and 25.93% at T3 are expected. SH reduced the risk of market rejection due to low quality and high mycotoxin content. Total profit of combining

SH and VRFA was £83.35 per hectare, divided into £48.04 ha<sup>-1</sup> for SH, £17.6 ha<sup>-1</sup> for each VRFA at T1 and T2 growth stages and £17.7 ha<sup>-1</sup> at T3. We recommend adopting this MZ concept for VRFA and SH, as economic and environment viability is feasible.

## **Keywords**

Yellow rust, Fusarium head blight, Hyperspectral imager, Management zones, Cost-benefit analysis, Selective harvest, Variable rate fungicide application, Canopy humidity, canopy temperature, k-mean clustering.

## **7.1 Introduction**

Ideally, high crop yields would need to be produced with minimal impact on the environment (Pimentel *et al.*, 1997; Tilman, 1999). Although intensive conventional agriculture based on unsustainable management of external inputs has led to increasing yields, it has posed severe environmental problems (Pimentel *et al.*, 1995; Hole *et al.*, 2005). But, varieties with high productivity are associated with higher sensitivity to disease leading to yield loss, which necessitates a sustainable approach for managing farm external inputs in a site specific way. In order to achieve this goal, data on all affecting factors in the system should be collected at high sampling resolution. This is possible today for specific diseases, crop canopy and soil properties, using on-line crop and soil sensors (Kuang *et al.*, 2012; Kuang and Mouazen, 2013; Whetton *et al.*, 2016a). Fusing these different layers of information is a main requirement for creating management zones (MZ), to explore the potential of VRFA and SH.

A balanced availability of soil nutrition contributes to disease resistance and susceptibility. Nitrogen and phosphorus are the main soil macro nutrients affecting the severity of fungal diseases, whilst micronutrients (e.g. Ca, Mg, Zn, B, Mn, Mo, Ni, Cu, Fe, S, and Si) are also known to affect various diseases in plants (Engelhard, 1989; Fageria and Baligar, 1997;

Graham and Webb, 1991; Huber, 1980). For example, high potassium in crops reduces the incidence of diseases (Perrenoud 1990; Prabhu *et al.*, 2007). When considering a method for disease control, it is important to acknowledge its interaction with nitrogen. Increases in nitrogen will increase the green area index and duration of the canopy, which in turn affects the microclimate of the crop and increases the likelihood of infection (Stokes *et al.*, 1997; Sylvester-Bradley and Kindred, 2009). Therefore, information about key soil properties and their effect on crop disease spread is essential for site specific plant protection.

Fusarium head blight (FHB) is a sporadic disease, causing variability of disease presence and level of infection across regions, and years (Jelinek *et al.*, 1989). FHB can result in yield losses, leading to both direct and indirect economic losses and negative influences on human and animal health (Paul *et al.*, 2005). The direct economic loss is attributed to reduced grain quantity and size, whereas the indirect loss is due to mycotoxin contamination (a secondary metabolite of the fusarium mould), associated with market rejection or downgrading of grain quality (Parry *et al.*, 1995). Yellow rust is a foliar fungal disease that is also linked with a long history of yield loss. The loss due to yellow rust is mostly attributed to a reduction in the number of grains per ear, and weight of the individual grains (Herrera-Foessel *et al.* 2006). Across the globe, yield losses due to yellow rust are reported to be between 10 and 70% (Chen, 2005). Doodson *et al.* (1964) reported yield losses of 64.5% in individual severely infected plants. Doling and Doodson (1968) also remarked substantial yield loss, but with a maximum of 30% reduction, which was attributed to the extensive cultivation of resistant spring and winter wheat varieties. Singh *et al.* (2012) witnessed severe epidemics of yellow rust infection in various cultivars that were formerly protected by resistance genes. It is still a major contributor to yield loss, with large variations in yield reduction observed between susceptible and resistant varieties, often being >50% (Safavi, 2015).

Fungicides can be organic (contain carbon atoms) or inorganic (do not contain carbon). Some of the oldest fungicides were inorganic and based on heavy metals. Fungicides can be contact or systemic. Contact fungicides (protectants) work on the surface of the plant, whereas systemic (penetrants) are absorbed. Fungicides damage the cell membranes of fungi, or interfere with processes (by inactivating enzymes, or prevent energy production or respiration). Fungicides can also be grouped as narrow spectrum - affecting only a few related pathogens and are often systemic, or broad spectrum - affecting a wide range of pathogens and often contact based. Contacts are generally applied as preventatives, while systemic fungicides can be applied as both preventive and curative. Contacts are often reapplied to protect new growth of the plant. Depending on the type of fungicide, and the targeted disease, the timings and number of fungicide applications will vary. Typically, there are up to four timings of fungicide application to control foliar diseases of wheat, with the fourth application also being aimed at ear diseases. T0 (Timing 0) is applied between growth stage 25 and 30 (Zadoks scale). Its application is usually a preventative in historically problematic fields, or if early disease is observed. T1 (GS 31-33) and T2 (GS 37-39) are applied to keep the third, second and flag leaves healthy, as these heavily influence yield in wheat. The T3 application (GS 52-60) can also be an “ear wash”, and is usually applied to preserve the quality of the grain. T2 is commonly considered the most crucial application and is the most frequently followed, due to the importance of maintaining flag leaf health. T1 is considered secondary in importance followed by T3 and then T0 (HGCA 2008; Clark, 2016). In some regions of Europe, there have been trials to reduce the number of fungicide applications. The fungicide applications are applied after growth stage 31, but only if infection levels reach a defined threshold (Verreet *et al.*, 2000; Falisse and Meeus 2002).

Therefore, information about crop disease in the field, collected at high sampling resolution, is another essential step towards site specific plant protection. But sole information about crop disease is not sufficient for an integrated decision support system, due to the influence of other factors e.g., relevant soil properties, microclimate conditions and crop canopy characteristics (Huber, 1980; Engelhard, 1989; Graham and Webb, 1991; Fageria and Baligar, 1997; Stokes *et al.*, 1997; Sylvester-Bradley and Kindred, 2009).

The aim of this paper is to propose and implement a multi-sensor and data fusion approach for the delineation of management zone (MZ) maps. The MZ map will be used for creating recommendations for VRFA and SH. A cost-benefit analysis will evaluate whether this approach has economic benefits. To our best knowledge, no reports have been produced for assessing the environmental and economic benefits of VRFA and SH based on data fusion of high sampling resolution spectral data, collected with on-line soil and crop sensors. This study focuses on the potential economic benefits of non-homogenous fungicide applications and selective harvest based on high sample data, compared to a conventional practice. However, the study will not ask the question about when and which fungicide should be applied.

## **7.2 Materials and methods**

### **7.2.1 Field site**

One study field of 10.8 ha with cereal crop production was selected for this study. It is located at Duck End Farm, a commercial family farm in Wilstead, Bedfordshire, UK (52°05'46.3"N 0°26'41.4"W), with an average annual rainfall of 598 mm. The fields N part is of a clay soil, whereas the S part is of a sandy clay soil. The farmer uses a 3-year crop rotation of barley, wheat and oilseed rape. The experiment was carried out in 2015, when the crop grown was winter wheat (solstice variety). Yellow rust and FHB were observed in the



field, and blackgrass presented in small patches in the NE of the field. Dates of measurement of soil, crop canopy, diseases, micro-climate conditions, and yield in relation with growth stages are shown in Table 33 Detailed information about the collection of each dataset is described below.

**Table 33:** Date of different measurement as related to crop growth stages according to the zadok's scale (Zadoks *et al.*, 1974).

Parameter	Date of measurement	Growth stage
Yield	September, 2015	NA
NDVI and LAI	May, 2015	43
Soil properties (MC, TN, OC, CEC)	September, 2014	NA
Yellow rust early	May, 2015	43
Yellow rust late	July, 2015	70
Fusarium head blight	July, 2015	70
Canopy data (humidity, temperature)	May, 2015	43

NDVI is normalised difference vegetation index; LAI is leaf area index; MC is moisture content; TN: is total nitrogen; CEC is cation exchange capacity; OC is organic carbon

### 7.2.2 Disease and canopy property data collection

A push broom hyperspectral imager (spectrograph) (HS spectral camera model from Gilden Photonics Ltd., UK) with a spectral range between 400 and 750 nm, and a halogen light source were mounted on a tractor by means of a metal frame for on-line measurement of yellow rust and FHB (Whetton *et al.*, 2016a). Measurement was carried out at a forward travel speed of approximately 4 km h<sup>-1</sup>, and line images were captured at 1 sec frequency, which was subsequently logged and geo-located with a sub-meter accuracy, using a differential global positioning system (DGPS) (EZ-Guide 250, Trimble, California, USA). The methodology followed the optimal configurations discussed in Whetton *et al.* (2016b). These include an integration time of 50 ms, a camera height of 0.3 m and light height and distance of 1.2 m and a camera angle of 10°.

At 5 locations per hectare, ground truth plots were selected (Figure 40), where manual disease assessment and recognition of yellow rust and FHB were made according to methods discussed in detail by Whetton *et al.* (2016a and 2016c). The assessment for FHB considered both early and late symptoms on heads, and were assessed as either a 0 for no infection, 1 for less than 5% individual infected heads, 2 for up to 10%, 3 for up to 30%, 4 for up to 50%, and 5 being a heavy infection over 50% infected heads, dependent on the ratio of FHB infected to healthy crops. Similarly, for yellow rust, a 0-5 scale was applied, similar to the approach adopted by Oberti *et al.* (2014). A scale between 0 and 5 (from less to more affected plots) was given the same ratio as that for FHB.

At the same ground truth locations, data of leaf area index (LAI) was collected with use of a Sunscan (V1, Delta-T devices, Cambridge, UK) sensor, whereas air humidity and temperature were measured with a hand held device (Testo 610, Hampshire, UK), positioning the sensor just under the flag leaf. Yield was measured with on-board yield sensor of the farmer's combine harvester (New Holland, CX8070 model), whereas normalised differential vegetation index (NDVI) was measured with a Crop Circle sensor (Crop Circle ACS 470, Holland Scientific, Lincoln, NE USA).

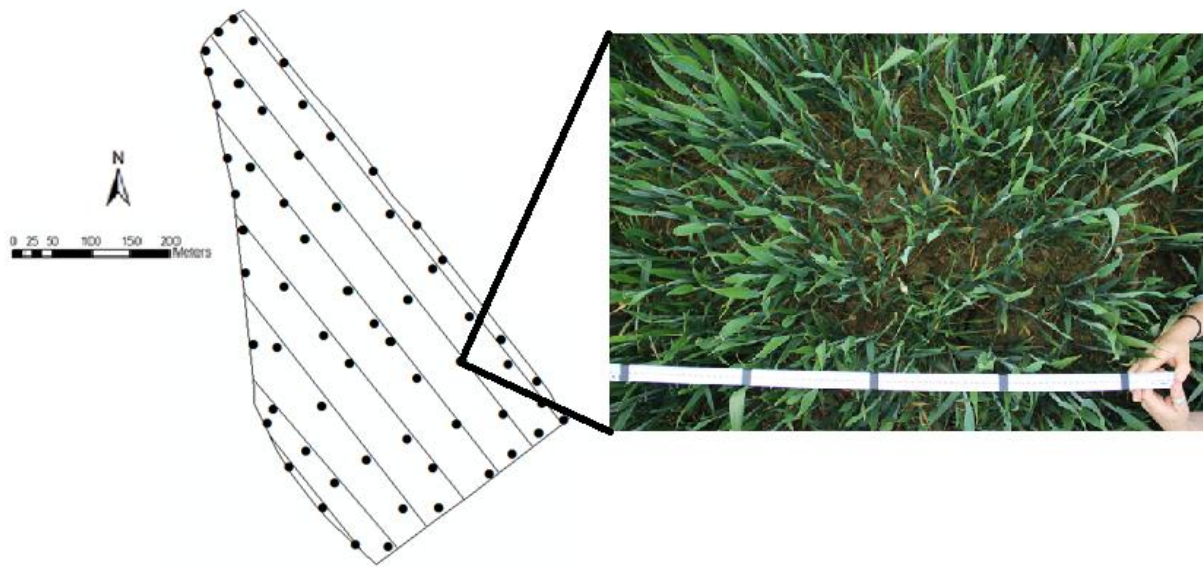


**Figure 40:** Map of the experimental field where ground sample locations (5 per hectare, n=60) are shown.

### **7.2.3 On-line soil measurement**

An on-line visible and near infrared (vis-NIR) spectroscopy sensor (Mouazen, 2006) was used for the measurement of soil total nitrogen (TN), organic carbon (OC), moisture content (MC) and cation exchange capacity (CEC). It consists of a mobile, fibre type, AgroSpec visible and near infrared (vis-NIR) spectrophotometer (tec5 Technology for Spectroscopy, Germany) with a measurement range of 305-2200 nm, and a differential global positioning system (DGPS) (EZ-Guide 250, Trimble, California, USA) to record the position of the on-line measured spectra with sub-metre accuracy. The spectrophotometer is linked to an optical probe by means of two optical fibres. The optical probe is attached to the back side of a subsoiler that penetrated the soil and opened a smooth trench, which is illuminated by a 20 W light source, while diffuse reflected spectra is collected at 1 sec frequency. A detailed description of the system can be found in Kuang, and Mouazen, (2013). On-line measurement was carried out in 2014, after the harvest of the previous crop at parallel transects of about 10 m apart and at 2 km forward speed, setting the sensor at 15 cm depth.

### **7.2.4 Spectral modelling of disease and soil properties**

The pre-processing of the soil and canopy spectral data was carried out following an approach outlined in Mouazen *et al.* (2006). The first step was to remove noisy wavelengths at the two far edges of spectra, before they underwent averaging of neighbouring wavebands, maximum normalisation, first derivative calculation and smoothing, successively. All spectra pre-processing was carried out using Unscrambler 10 software (Camo Inc.; Oslo, Norway).

The hyperspectral imager data set was randomly divided into two sets of 80% and 20%, representing the calibration and validation data sets, respectively. The pre-processed canopy spectra and manual assessments of disease were subjected to partial least squares regression

(PLSR) analysis with full-cross validation using the calibration set (80%). PLSR analyses were carried out using Unscrambler 10 software (Camo Inc.; Oslo, Norway). The models' performance was evaluated using the on-line validation set (20%). More detailed information about the calibration and validation of the FHB and yellow rust models can be found in Whetton *et al.* (2016a). The same approach was used for the calibration and validation of models to predict soil properties (e.g., MC, OC, TN and CEC). More detailed information about the calibration and validation of these models can be found in Halcro *et al.* (2013) for TN, OC and MC and Marin-González *et al.* (2013) for CEC.

The calibration models for FHB and yellow rust were used to predict these two diseases using on-line collected hyperspectral data in 2015 (Table 33). Yellow rust prediction was made twice for early scanning (May, 2015) and late scanning (July 2015), whereas FHB was measured at the late scanning only, as this disease affects the crop heads, at a late growing stage. The calibration models developed earlier for OC, TN and MC (Halcro *et al.*, 2013) and CEC (Marin-González *et al.*, 2013) were used to predict soil properties using the on-line measured soil spectra after crop harvest in September, 2014 (Table 33).

Since the canopy properties apart from NDVI, including LAI, humidity and temperature were measured only at 60 locations shown in Figure 40; these limited data were used for further analysis. However, a much larger number of data points was obtained of the on-line predicted crop yellow rust and FHB, on-line predicted TN, OC, MC and CEC, measured NDVI and yield.

### **7.2.5 Mapping**

Maps for the measured NDVI and yield and the on-line predicted yellow rust, FHB, soil TN, OC, MC and CEC were developed using ArcGIS 10 software (ESRI, California, USA). The first step in the development of maps was the creation of semi-variograms in R-studio (RStudio, Boston, MA). After an optimal semi-variogram (smallest sum of square error) was established for a given property, kriging was applied to develop a full point map using ArcGIS 10 software (ESRI, California, USA). A different number of data points was considered in the semi-variogram development and kriging, hence, the quality of maps differs among different maps, although the best fit was found with spherical semi-variogram models for all properties investigated.

### **7.2.6 Management zone maps**

The on-line predicted soil properties and crop diseases, measured canopy and yield and microclimate conditions were pulled into one matrix by means of Statistica software (StatSoft inc., Oklahoma USA), before running k-means clustering. The k-mean cluster analyses were performed for the following applications to produce three different MZ maps, with a different number of MZ, depending on variability resulting from the different input data used:

- 1) Selective harvest: In this case, only the on-line predicted FHB and late yellow rust data were included in the k-mean clustering to produce a MZ map for SH.
- 2) T1 and T2 variable fungicide applications: The k-means cluster analysis here aimed at producing MZ maps for VRFA at growth stages 31 to 39, applied as a foliar disease preventative. In this case, the on-line predicted early yellow rust and soil properties (MC, OC, TN and CEC) and canopy properties (NDVI, LAI, canopy humidity and temperature) were included in the analysis.

3) T3 variable rate fungicide applications: The k-means cluster analysis produced a MZ map for the growth stage 52-60, where fungicides are usually applied to preserve the grain quality. Input data included the on-line predicted FHB and soil properties (MC, OC, TN, and CEC), canopy properties (NDVI, LAI, canopy humidity and temperature).

### **7.2.7 Eventual calculation of cost-benefit analysis**

The following assumptions were made in this study for the cost-benefit analyses;

- 1) The cost of implementing the different sensing technologies and data mining was not taken into consideration.
- 2) FHB presence is directly linked to mycotoxin presence, which is in line with Paul *et al.* (2005) who reported a mean correlation of  $R^2$  of 0.73 between deoxynivalenol (DON) level and fusarium observed in 163 studies in the USA. Turner and Jennings (1997) reported the occurrence of mycotoxins in UK cereals was lower than expected due to *M. nivale* (*Microdochium* species which hold no mycotoxin risk), which suppressed the infection of *Fusarium* species. However, a correlation was still observed.
- 3) VRFAs would not reduce the efficiency of disease control obtained with homogeneous applications, an assumption supported by a practical note that reduced doses of fungicide should be applied in low disease pressure areas (FRAC, 2010) and vice versa.
- 4) Wheat grain would be sold at a lower price due to fusarium contamination of mycotoxins. This assumption is supported by the European commission imposed upper limits of the DON mycotoxin in cereal grain for human consumption.

- 5) A uniform application of fungicide was proposed for the T0 growing stage, as it is usually a preventive treatment and at this early growth stage disease sensing would be difficult, as the canopy is sparse.

Two fungicides commonly used in fungicide control were selected in this study (chemical labels are available in Appendix C). Adexar (epoxicoazole) is suitable for the treatment of many fungal disease infections and is particularly common for FHB treatment. It is used at a maximum of 2 litres per hectare ( $\text{lha}^{-1}$ ), with a maximum of 2 applications per annum for wheat in Europe. The current price is £34 per litre. Proline 275 (prothioconazole), is suitable for many fungal disease infections but it is particularly used for treatment of early yellow rust. It is applied at a maximum of  $0.72 \text{ lha}^{-1}$  per dosage, with a max total of  $2.16 \text{ lha}^{-1}$  per year for wheat treatment in Europe. The current price is between £52.5 and £59 per litre<sup>1</sup>. The following two cost-benefit analyses were carried out for the VRFA and SH;

- 1- The cost-benefit for the variable fungicide treatments (T1, T2 and T3) was applied using ArcGIS 10 software (ESRI, California, USA), by dividing the field area into high infection risk (HIR) and low infection risk (LIR) zones, taking into consideration the boom width relative to the position of tramlines. Zones of HIR were virtually subjected to a full application rate, whereas the LIR zones were given a 50% application rate. For T3 the medium infection zones (MIF) were subjected to 75% dosage rate. All MZ were considered in the analysis, and the amount of fungicide per area was calculated. The overall applied amount of fungicide was then compared to that of a conventional full homogenous application, and the potential savings or losses were calculated.



2- The cost-benefit analysis for SH was calculated in a similar manner to that of VRFA using ArcGIS 10 software (ESRI, California, USA). MZ were classified into HIR and LIR. This was made by proposing separate harvest of the HIR (low quality) from that of the LIR (high quality) zones. All MZ were considered in the analysis, and their corresponding area was calculated, so as the average yield per zone could be calculated. The total prices of wheat grain obtained from Farmer's Weekly (FWI 2016) were £145 and £135 per tonne, for the high-quality and low-quality yield, respectively. The SH was compared with the homogeneous harvest of the entire field area, sold at the lower price of £135.

## **7.3 Results and discussion**

### **7.3.1 Spatial variability of different properties**

The analysis for semi-variogram of different soil and crop properties indicated that the best approximation can be achieved with spherical models, whose properties can be found in Table 34. The largest sum of square error is calculated for TN followed by MC. The small values of the proportion between the nugget (attributed to small sampling intervals, or measurement errors) to sill variation (less pairs of points separated by far distances) indicate the autocorrelation between different properties studied, because this proportion is an important parameter to quantify short-distance autocorrelation or the degree of spatial dependency for a variable (Cambardella *et al.*, 1994; Chang *et al.*, 2014). Cambardella *et al.* (1994) defined three categories of spatial dependency of high, moderate, and weak with ratios of less than 25%, between 25% and 75%, and greater than 75%, respectively. Ranges of spatial dependency are wider than the sampling interval of on-line soil measurement (10 m), disease, LAI, humidity and NDVI (24 m), and yield (12 m), confirming the effectiveness of geostatistical analysis adopted in this study (Chang *et al.*, 2014). The only exception is for the NDVI measurement (Table 34.).

**Table 34:** Properties of the spherical semi-variogram obtained for yellow rust early (YR early) and late (YR late) scans, fusarium head blight (FHB), soil moisture content (MC), organic carbon (OC), total nitrogen (TN), cation exchange capacity (CEC), leaf area index (LAI) and normalised difference vegetation index (NDVI), crop humidity and temperature. Showing nugget ( $c_0$ ), sill ( $c$ ), range ( $r$  m), proportion ( $C_0/C$  %), and the sum of square error (SSE)

<b>Property</b>	<b><math>c_0</math></b>	<b><math>r</math> (m)</b>	<b><math>c</math></b>	<b><math>c_0/c</math> (%)</b>	<b>SSE</b>
<b>FHB</b>	0.11	97.02	0.89	8.02	3.32
<b>YR early</b>	0.00	78.34	0.02	9.00	2.56
<b>YR late</b>	0.01	92.57	0.04	2.93	1.53
<b>OC</b>	0.00	9.60	0.01	9.55	2.65
<b>TN</b>	0.00	23.04	0.01	3.00	12.46
<b>MC</b>	4.43	15.52	5.09	0.81	6.23
<b>CEC</b>	0.73	24.71	1.48	1.78	4.20
<b>NDVI</b>	0.061	4.45	0.21	2.6	2.15
<b>Yield</b>	3.24	98.36	6.49	4.25	1.68
<b>LAI</b>	1.08	68.04	2.07	1.9	3.06
<b>Humidity</b>	0.17	102.96	1.07	6.19	0.57
<b>Temperature</b>	0.1	83.09	1.06	10.05	0.51

$c_0$  is nugget variance,  $c$  is sill,  $r$  is range,  $c_0/c$  is proportion, and SSE is sum of squared error.

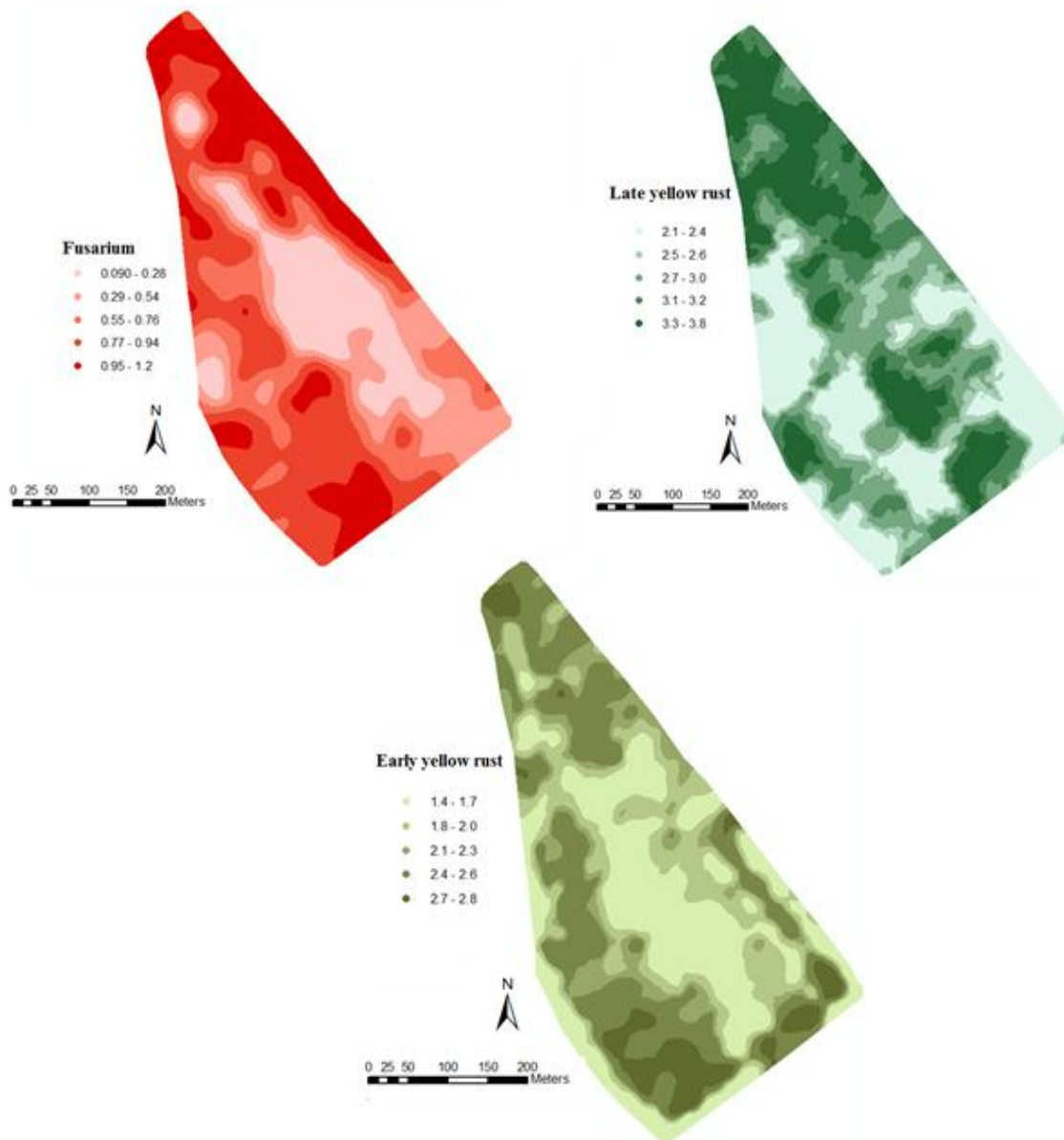
Figure 41 shows the spatial distribution of FHB, early scanned and late scanned yellow rust. As a general observation, the crop was healthier towards the centre of the field. This was particularly evident in the early yellow rust map, whereas the late yellow rust map is more heavily infected towards the centre of the field. This is an expected spatial pattern, as yellow rust and fusarium spores are both wind borne, and can survive in soil and weeds occurring in the borders of a field, acting as a source of inoculum for the next cropping season (Jenkinson

and Parry, 1994; Champeil *et al.*, 2004; Imathiu *et al.*, 2013). Between the early and late scan of yellow rust, some areas have increased in yellow rust severity whilst other areas have decreased, such as the SE of the field. This reduction in disease severity could be due to additional crop growth, from later tillers and secondary tillers, and in damaged crop regrowth (McCormick *et al.*, 2014; Livingston *et al.*, 2016).

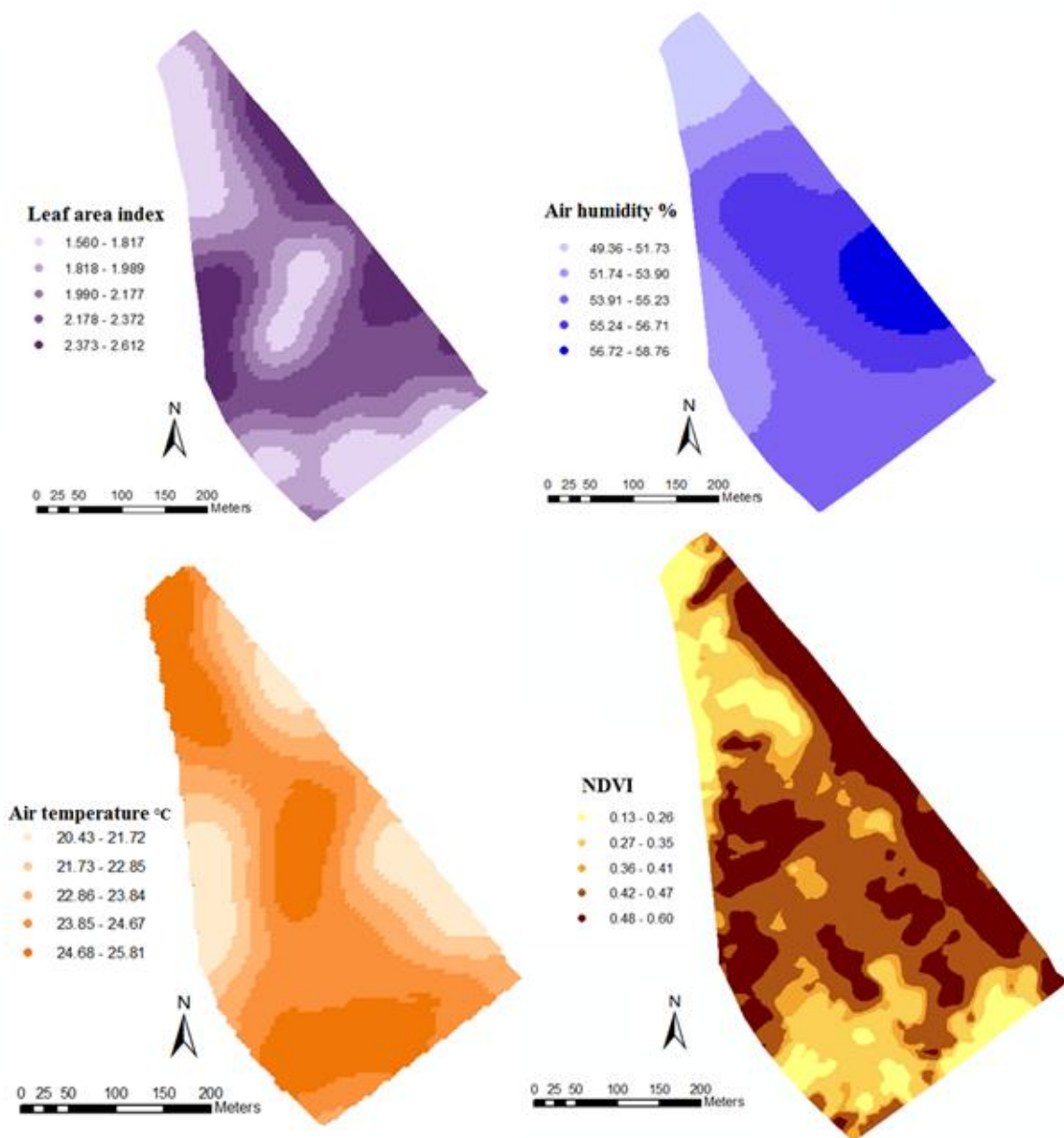
Figure 42 shows maps of canopy properties (collected in May), measured at high sampling resolution (e.g., NDVI), and low (60) sampling resolution (e.g., humidity, temperature and LAI). The NE edge of the field has large values of both NDVI and LAI. Similar observation for NDVI and LAI can be made through the field (Figure 42). The central part of the field is of low LAI, which coincides well with low concentrations of both FHB and early yellow rust spatial distribution pattern in the field (Figure 41). Visually, LAI and temperature appear to have similar spatial distribution pattern, but of inverse magnitude. The same is true for NDVI (Figure 42). NDVI and LAI is related to canopy density that affects a canopies temperature. Areas of the field with a lower crop density will warm up and cool down faster than those with dense canopies (Dammer, 2003). Differences in a wheat field's canopy temperature could have an inter-canopy variation of up to 7.5°C (Dammer, 2003), a variation of 5.4°C (at canopy level) was recorded during the field scan in May. The lower temperatures were found in denser canopies, highlighting the differences in microclimate through the field.

Figure 43 shows the spatial distribution of the four on-line predicted soil properties (CEC, TN, MC and OC), indicating small spatial variability, hence, might not have effect on crop diseases, an assumption to be tested further below. Clear similarity between crop yield (Figure 44) and NDVI (Figure 42) can be observed. The highest yield is recorded in the middle part of the field, which coincides with the NDVI map. This is in line with other

studies, reporting that NDVI of previous years can be used as an indicator for yield in the following years (Mkhabela *et al.*, 2011).



**Figure 41:** Disease severity; On-line predicted maps of fusarium head blight (FHB) measured at milk growth stage 72 (july 2015), early yellow rust measured at booting growth stage 43 (may 2015), and late yellow rust measured at milk growth stage 72 (july 2015). The disease is classified on a 0 to 5 scale, where 0 indicates low disease presence and 5 indicates high disease.



**Figure 42:** Properties attributed to the canopy; On-line measured normalised difference vegetation index (NDVI), along with the 60 samples based developed maps for leaf area index (LAI), canopy air temperature and humidity. These data were all collected at the booting growth stage 43, in May 2015.

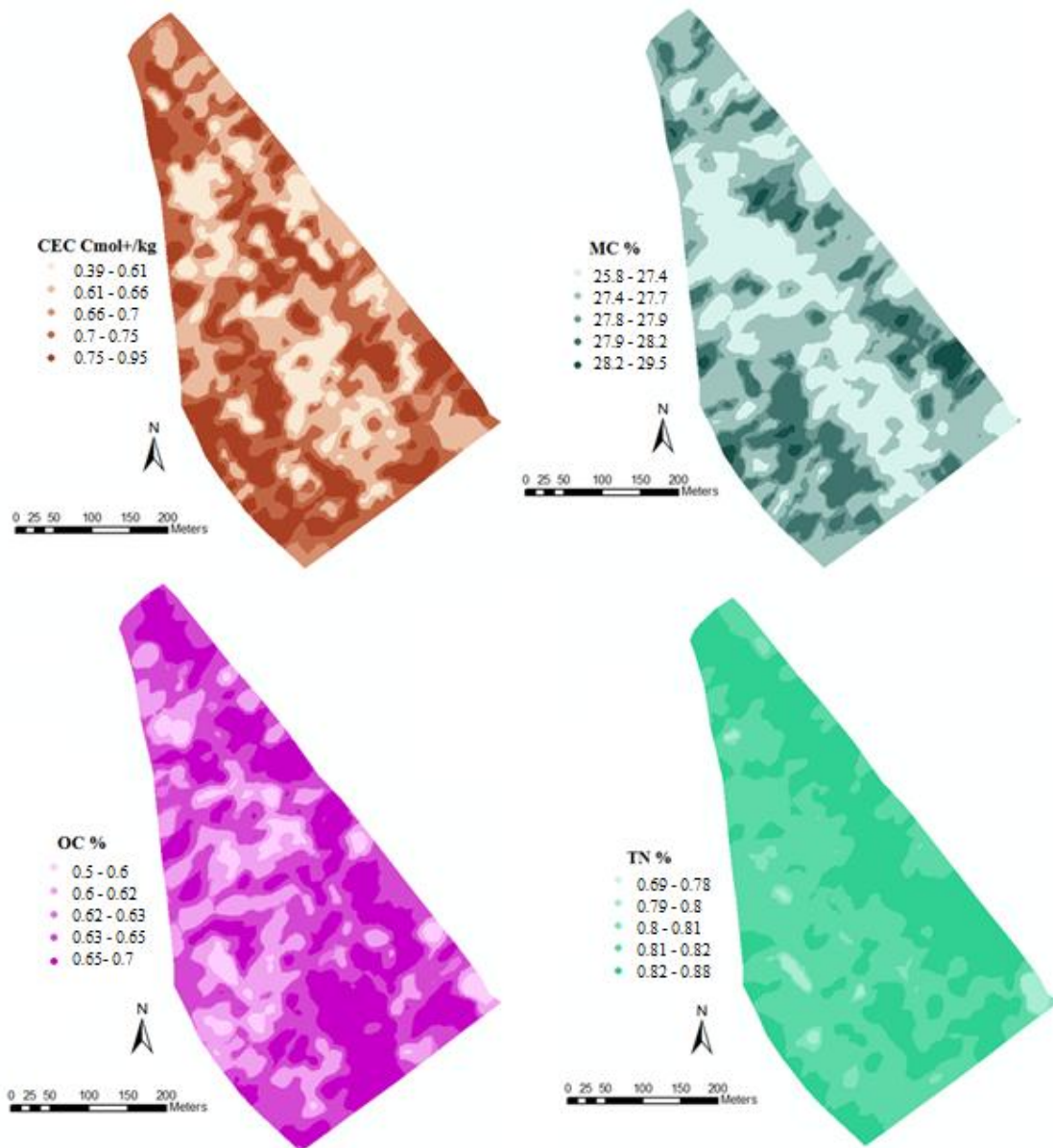


**Figure 43:** Soil properties; On-line predicted soil cation exchange capacity (CEC in Cmol/kg), total nitrogen (TN in %), moisture content (MC in %) and organic carbon (OC in %). The soil properties were collected before the seed was drilled in September 2014.

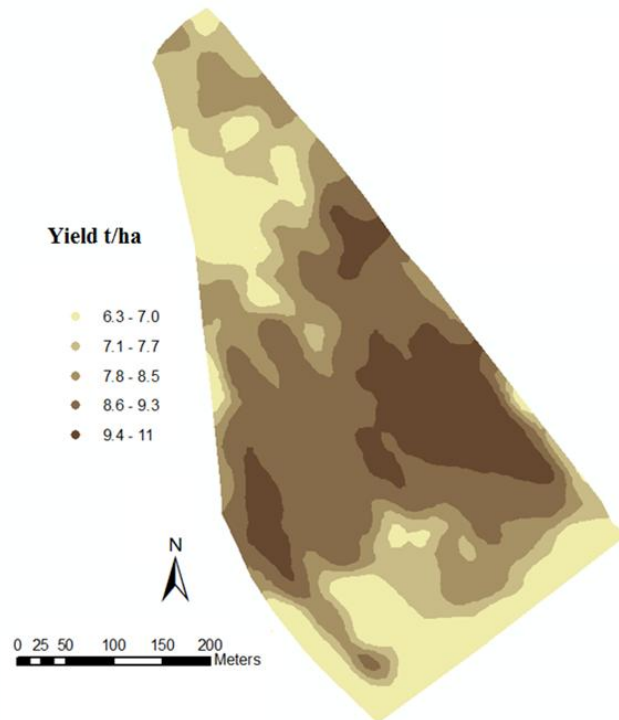


**Figure 44:** Yield map of wheat measured in September 2015.

Blackgrass (*Alopecurus myosuroides*) is a widespread perennial weed, which is notoriously difficult pest in temperate cereal crops. Blackgrass was noted in small patches within the field, specifically in the north part of the field, corresponding to areas of low quantity grain (Figure 44) and high LAI (Figure 42). In severe epidemics, blackgrass can cause up to 50% yield losses in winter wheat (Moss, 2013)

### 7.3.2 K-means clusters

A k-means cluster is an unsupervised learning algorithm, which partitions multiple observations into a suitable number of clusters, and a data point is classified into a cluster point based on the cluster with the nearest mean (MacQueen, 1967), which allowed MZ based on multiple properties to be delineated, for VRFA and SH.

The K-mean clustering carried out for 1) SH, (Figure 45) 2) T1 and T2 variable fungicide applications (Figure 46) and 3) T3 variable fungicide application resulted in different numbers of clusters (Figure 47). For SH, where on-line predicted FHB and late yellow rust were included in the analysis, the k-mean clustering resulted in two classes (Figure 45). Cluster 1 (Figure 45) demonstrated high normalised means associated with high yellow rust and FHB spread, whereas cluster 2 associated with lower spread of both diseases. Therefore, it is a straightforward decision to be made for classifying the wheat yield into high quality and low quality, associated with the cluster 2 and cluster 1, respectively. This classification is made assuming that FHB presence relates to mycotoxin accumulation and can cause downgrading of grain on the market, causing economical loss (Parry *et al.*, 1995). Yellow rust was included in the classification, as infection reduces quantity but also affects grain filling. Yield losses in wheat from *yellow rust* infections are usually the result of reduced kernel number per ear and low weight (Prescott *et al.*, 1986). Small grains are associated with low flour extraction rates (during milling), and low energy contents for livestock feed (Gooding and Davies 1997; Rose *et al.*, 2001). Grain protein content is often reduced with infection by rust (Dimmock and Gooding, 2002). A higher protein content in the grain can fetch higher prices (Devadas *et al.*, 2014)



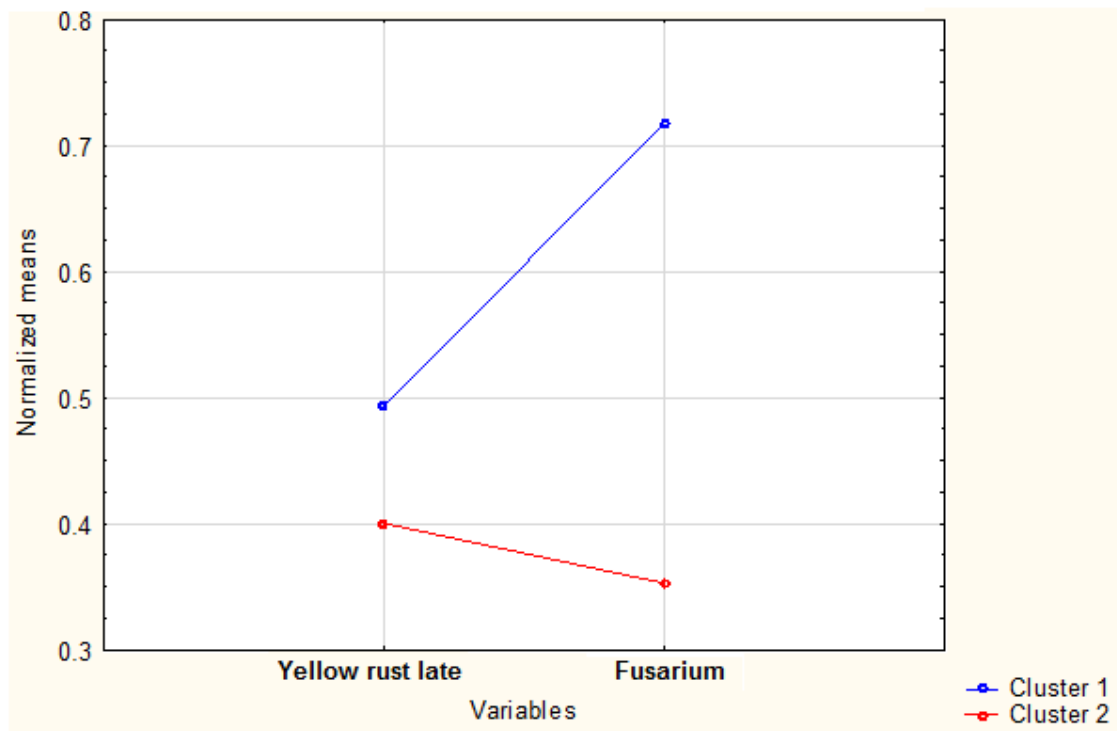


**Figure 45:** K-means cluster analysis based on the on-line predicted late yellow rust and fusarium head blight (FHB) showing two classes to be adopted for the selective harvest (SH).

The k-mean cluster analysis for T1 and T2 variable fungicide applications using on-line predicted early yellow rust, and the four soil properties, NDVI, LAI, temperature and humidity has resulted in two clusters (Figure 46). It was necessary to rank these two clusters into highly and poorly infected. In cluster 1, high yellow rust is associated with low NDVI and LAI, indicating degraded crop growth (Figure 46). A smaller crop density (smaller LAI and NDVI) could permit a greater penetration and distribution of the yellow rust spores (Whetton *et al.*, 2016d). However, moisture is essential for yellow rust infection. Yellow rust is most likely to occur in areas with a cool and moist environment during the growing season, with the optimum temperature for urediniospore germination being between 7 and 12°C (Schröder and Hassebrauk, 1964; Chen *et al.*, 2014). A denser canopy is more likely to

maintain a higher humidity, but to heat up and cool down slower compared to a sparse canopy (Dammer, 2003). The cluster analysis demonstrates no influences of the on-line predicted soil properties, as no clear differences in the normalised mean values for the four soil properties can be observed between the two clusters. This is expected due to the small variability measured throughout the field area. Only minor differences can be attributed to MC and CEC. Due to the higher yellow rust spread of cluster 1, a high fungicide application rate would be proposed, whereas a low application rate would be proposed for cluster 2.

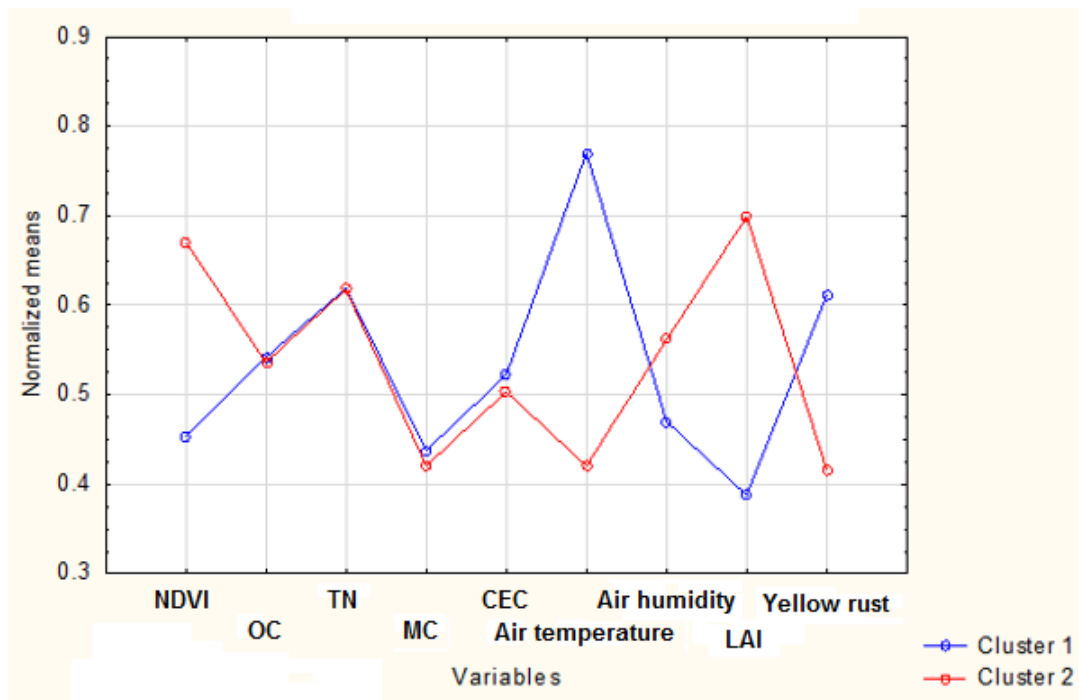


**Figure 46:** K-means cluster analysis for variable rate fungicide application (VRFA) at the T1 and T2 growing stages. Input data were measured normalised difference vegetation index (NDVI), air temperature, air humidity, leaf area index (LAI), on-line predicted soil organic carbon (OC), total nitrogen (TN), moisture content (MC) and cation exchange capacity (CEC), and on-line predicted early yellow rust disease.

The K-mean cluster analysis for T3 variable fungicide application results in three clusters (Figure 47). Similar to that for T1 and T2 growing stages and due to the small spatial variability range, the effect of on-line predicted soil properties on FHB spread is negligible, although minor differences in normalised means can be observed for MC and CEC. Again lower LAI and NDVI (lower crop density) of cluster 1 associate with higher air temperature and lower air humidity than those of clusters 2 and 3. This has resulted in cluster 1 having the largest FHB pressure, and has negatively affected the crop growth indicated as low NDVI and LAI. The clear majority of cluster 2 areas are along the edge of the field, where it is understood that there is a higher risk of inoculation, due to the hedgerow (Jenkinson and Parry, 1994; Champeil *et al.*, 2004; Imathiu *et al.*, 2013). Due to the degree of FHB pressure, clusters, 1, 2 and 3 have been classified at the highest, medium and lowest risks for FHB severity. Whilst soil properties have little influence on crop disease severity in this study field, it is suggested to continue accounting for them in future, particularly in fields with high variability in soil properties.

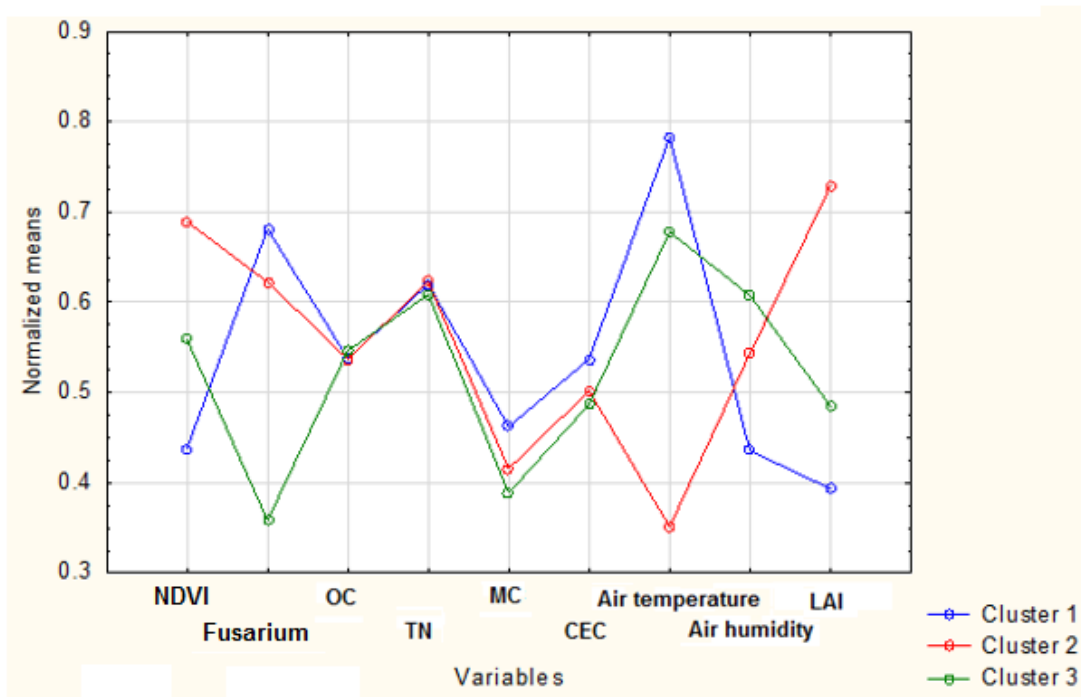


**Figure 47:** K-means cluster analysis for variable rate fungicide application (VRFA) at the T3 growing stage. Input data were measured normalised difference vegetation index (NDVI), air temperature, air humidity, leaf area index (LAI), on-line predicted soil organic carbon (OC), total nitrogen (TN), moisture content (MC) and cation exchange capacity (CEC), and on-line predicted fusarium head blight (FHB) disease.

### 7.3.3 Treatment maps

MZ maps for the SH developed by k-mean cluster analysis using on-line predicted late yellow rust and FHB show two distinctive MZs (Figure 45 and Figure 48). Based on this MZ map, the field was divided into experimental plots of 12 m width to match the width of the cutting head of a combine harvester, which would be used for performing SH. The owner of the Duck End Farm (the study farm) claimed that in recent years increasing levels of mycotoxin have been witnessed. Therefore, a variable harvest will enable reducing the economic loss and increase efficiency by separating the harvested wheat grain into two categories of high and low quality and selling it separately. This SH would also reduce the

mycotoxin levels in grain and toxic influences on human health. MZ1(Figure 48) associated with cluster 1 in Figure 45 is with high FHB presence and high risk for mycotoxin presence and toxic effects on human health, whereas MZ 2 associated with cluster 2 is of low risk of mycotoxin presence and the grain can be sold at a higher price than that in MZ1.

Figure 49 and Figure 50 illustrate spatial distribution MZs and the division of the field area into 24 m width plots, responding to a fungicide sprayer boom width of 12 m either side of a tramline. West *et al.* (2003) discussed the highest benefit to variable fungicide applications is in diseases, which make a small number of large areas, with a boom containing separately controllable sections. However, at the commercial farm this technology was not available, so the VRFA maps are based on 24m widths (with the standard being 12m on either side). MZ 2 in Figure 49, associates with cluster 2 in Figure 46 indicates low disease in the centre, whereas MZ 1 at the field hedges linked with cluster 1 refers to high yellow rust. It's proposed that this MZ map is adopted for VRFA for T1 and T2 growing stages. The MZ map (Figure 50) for VRFA for the T3 application stage shows three MZs of high (northern and southern edge areas), medium (east and west edge areas) and low (central areas) FHB spread, associated with cluster 1, cluster 2 and cluster 3, respectively (Figure 47). The general shape of the MZ map here (Figure 43) is similar to that of the one developed for yellow rust for T1 and T2 application times (Figure 46), but the former is divided into three MZs not two as for the latter map.

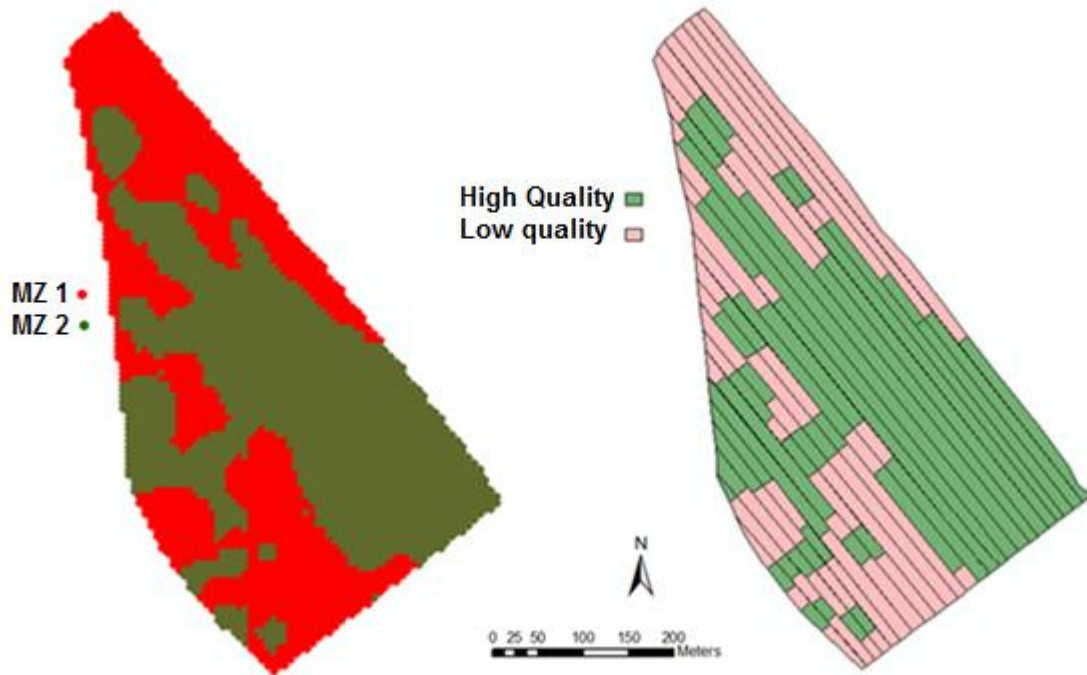


**Figure 48:** Management zone (MZ) maps for selective harvest (SH), The map on the left shows high disease infection (MZ 1) and low disease infection (MZ 2) which is obtained by k-means clustering that included on-line predicted fusarium head blight (FHB) and late yellow rust. With the right map showing high and low infection zones on the right, with the field being split into plots of 12 m (due to the combine harvest cutting head).

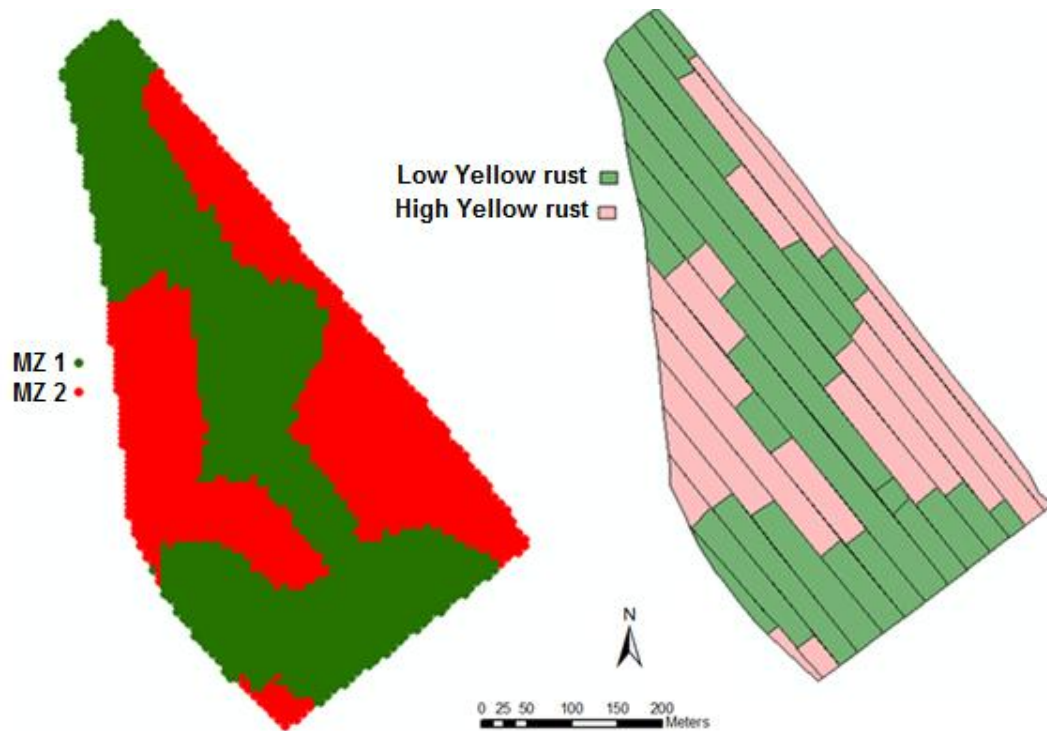


**Figure 49:** Management zone (MZ) maps for variable rate fungicide application (VRFA) at the T1 and T2 growing stages. The map on the left show low yellow rust (MZ 1) and high yellow rust (MZ 2), which is obtained by k-means clustering that included, measured canopy properties (normalised difference vegetation index (NDVI), air temperature, air humidity, and leaf area index (LAI)), on-line predicted soil (organic carbon (OC), total nitrogen (TN), moisture content (MC) and cation exchange capacity (CEC)), and on-line predicted early yellow rust disease. With the right map showing high and low infection zones on the right, with the field being split into plots of 24 m (due to the boom width).

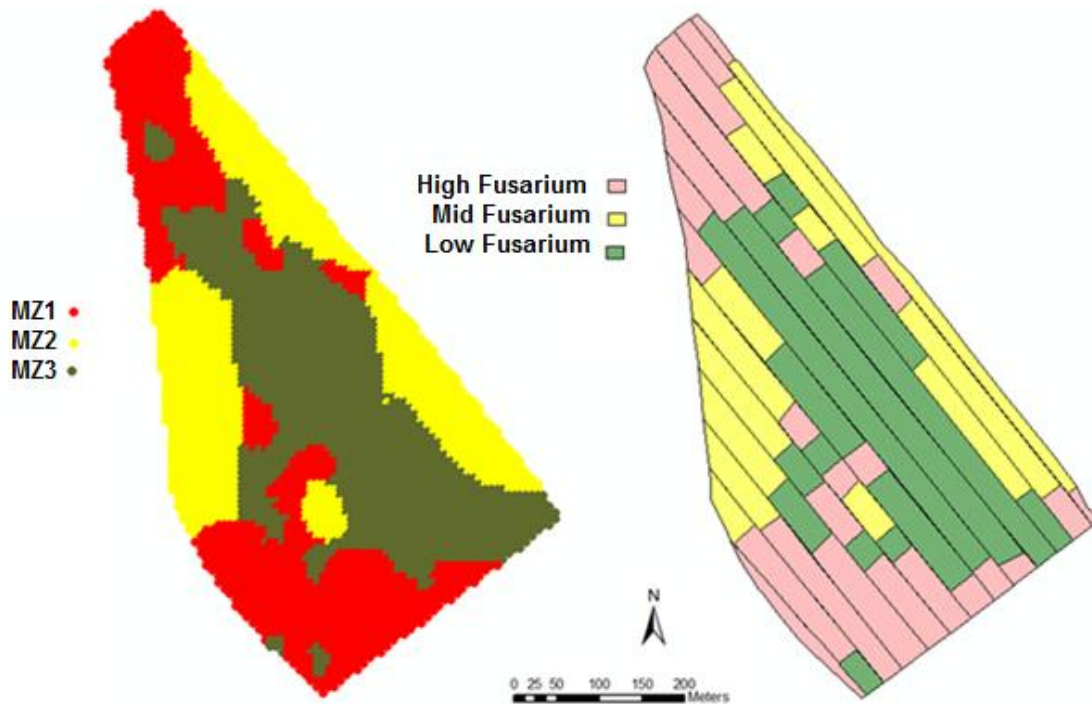


**Figure 50:** Management zone (MZ) maps for variable rate fungicide application (VRFA) at the T3 growing stages, The map on the left show high fusarium head blight (FHB) (MZ 1) and medium FHB (MZ 2), and high FHB (MZ3), which is obtained by k-means clustering that included, measured canopy properties (normalised difference vegetation index (NDVI), air temperature, air humidity, and leaf area index (LAI)), on-line predicted soil (organic carbon (OC), total nitrogen (TN), moisture content (MC) and cation exchange capacity (CEC)), and on-line predicted FHB. With the right map showing high and low infection zones on the right, with the field being split into plots of 24 m (due to the boom width).

Grain is commonly tested for mycotoxin content at or post-harvest, where time consuming and expensive laboratory tests are needed (HPLC, serological rapid tests, Fast-DON-ELISA-test) (Thate *et al.*, 2008). Fusarium damaged wheat grains can be detected by hyperspectral imaging with an accuracy of up to 95%. Mycotoxin content detection depended on important wavelengths in the NIR range of 1204, 1365 and 1700 nm, whereas spectral differences in the ranges between 1425 to 1440 nm and 1915 to 1930 nm are



important for the detection of mycotoxin DON in the grain (Delwiche 2003; Singh *et al.*, 2007; Peiris *et al.*, 2009). However, it is uncertain to how well different fungi may be distinguished using NIR (Peiris *et al.*, 2009).

The downgrading of grain can be in response to a percentage of the harvested grain, which reduces the quality or surpasses mycotoxin health limits. However, the BoMill TriQ (Bowmill AB, Sweden) was studied and showed the capability in bulk separating good quality wheat grain from downgraded fusarium infected grain, using crude protein content (Kautzman *et al.*, 2015). With the increased awareness of food security, and the knowledge that one third of food is currently lost or wasted, innovative studies are needed to maximise yields reaching the market (Gustavsson *et al.*, 2011).

#### **7.3.4 Economic benefits**

Table 35 summarises the yield and average disease development in each MZ. For SH, the MZ 2 (low disease pressure shown in Figure 48 and Figure 45) associates with a higher average yield (8.2  $\text{tha}^{-1}$ ) and lower average late yellow rust (1.9) and FHB (0.54), as compared to MZ 1 (6.9  $\text{tha}^{-1}$ , 2.9 and 0.87, respectively). Similarly, for VRFA at T1 and T2 growing stages, MZ 2 (lower early yellow rust pressure shown in Figure 46 and Figure 49) is associated with higher average yield (8.3  $\text{tha}^{-1}$ ) and lower early yellow rust pressure (1.2), as compared to MZ 1 (6.7  $\text{tha}^{-1}$  and 2.2, respectively). For the variable fungicide application at the T3 growing stage, the MZ 3 (lowest FHB pressure as shown in Figure 47 and Figure 50) has the highest average yield (8.3  $\text{tha}^{-1}$ ) and lowest FHB (0.54), followed by MZ 2 and MZ 1, respectively (Table 35). The consistent link between the yield and disease pressure in the three studied

cases proves the correct classification of the field area into proposed MZs, so that MZs with high disease pressure associate with low yield and vice versa.

**Table 35:** Statistics of yield and disease pressure (fusarium head blight (FHB), early and late yellow rust (YR)) of each management zone (MZ), for the variable rate fungicide applications (VRFA) at growing stage T1 and T2 (which consider soil properties, canopy properties and early yellow rust); at growing stage T3 (which consider soil properties, canopy properties, and FHB); for the selective harvest (SH) (late yellow rust and FHB). For the VR T1 and T2 applications two MZ are considered; MZ1 (high yellow rust disease) and MZ2 (low yellow rust disease). For the VR T3 applications three MZ are considered; MZ1 (high FHB disease) and MZ2 (medium FHB disease) MZ3 (low FHB disease). SH considers two MZ; MZ1 (lower quality crop) and MZ2 (higher quality crop).

	MZ	Total cluster area, ha	Total yield, t	Average Yield, $\text{tha}^{-1}$	Average early YR	Average late YR	Average FHB
<b>SH</b>	MZ1	4.5	33.2	6.9	NA	2.9	0.87
	MZ2	6.3	51.9	8.2	NA	1.9	0.54
<b>VR T1 and T2</b>	MZ1	4.8	36.5	7.6	2.2	NA	NA
	MZ2	6	49.8	8.3	1.2	NA	NA
<b>VR T3</b>	MZ1	3.6	26.3	7.3	NA	NA	0.8
	MZ2	3.2	25.9	8.1	NA	NA	0.71
	MZ3	4	33.2	8.3	NA	NA	0.54

The cost-benefit analysis of SH based on two MZs proposed in this work (Table 36) reveals that a total saving of £519 per field (£48.05 ha<sup>-1</sup>) would be gained, as compared to the homogeneous harvest of the entire field area. This is because of the higher price that the SH could provide for almost 59% of the field area with high quality of grains (FWI, 2016) harvested from MZ2 with low FHB spread or low mycotoxin concentration.

**Table 36:** Cost-benefit analysis results comparing the selective harvest (SH) with the homogeneous harvest (HH), based on on-line available prices of grain (FWI, 2016). Management zone (MZ) 2 being of high quality grain (low fusarium head blight (FHB) spread and low mycotoxin concentration) and MZ1 being of low quality grain (high FHB spread and high mycotoxin concentration).

Harvest type	MZ	Total area, ha	Total yield, t	Price, £/t	Price per MZ, £	Total field price, £	Difference (HH – SH) for field, £	Difference (HH – SH), per ha, £
<b>SH</b>	MZ1	4.55	33.2	135	4482	12007.5	519	48.05
	MZ2	6.35	51.9	145	7525.5			
<b>HH</b>	All field	10.8	85.1	135	11488.5	11488.5		

VRFA at the T1 and T2 growth stages aimed at protecting the third, second, and flag leaves from foliar diseases, such as yellow rust. In this study, VRFA is split into two areas of high and low disease pressure as compared to a homogenous rate application applied as the full dose. The calculated potential benefit of the VRFA at the T1 and T2 was £95.04 per application for this field (£190.08 for the T1 and T2 applications), with an average saving of £8.8 per ha per application (or £17.6 for two applications) (Table 37), compared with the homogeneous application. This is based on the assumption that yellow rust has a direct link

with grain yield, and that a lower dose would not have significant negative impacts. The homogenous rate would consume 7.776 L Proline 275 per application for the 10.8 ha field, whereas the variable rate would need 6.048 L, suggesting a potential reduction of 1.73 L per application (or 3.46 L for the two applications). This reduction would sum up to a 22.24% reduction in fungicide application by adopting the variable application method, as compared to the homogeneous application.

The VRFA at the T3 application stage is usually an ear wash aimed at preserving grain quality from diseases such as FHB. This application in the study field would be based on 3 rates according to the three MZ delineated by the k-mean clustering (Figure 47 and Table 37). Treatments proposed are of full dose for the heavily infected MZ1, 75% dose for the medium infected MZ2 and 50% dose for the low infected MZ3, compared to the full dose rate for the homogenous application proposed for the entire field area. The per field potential saving of the VRFA at the T3 growth stage is £191.2, with an average saving of £17.7 ha<sup>-1</sup> (Table 37). The homogenous rate would consume 21.6 l Adexar per 10.8 ha total field area, whereas the VRFA would consume 16 l, with a potential reduction of 5.6 l per application, or 25.93% to be expected by adopting the VRFA, as compared to the uniform application.

**Table 37:** Cost-benefit analysis results for variable rate fungicide application (VRFA) at T1 and T2 growth stages, and at T3 growth stage, as compared to homogeneous application (HA). Management zones (MZs) 1, 2 and 3 refer to high dosage rate, medium rate and low rate, respectively. Fungicide used is Proline 275 (£34 per litre) for T1 and T2 application and Adexar (£55 per litre) for T3 application.

		Total area, ha	Total yield	Application rate, lha <sup>-1</sup>	Price of chemical l <sup>-1</sup> , £	Price of chemical ha <sup>-1</sup> , £	Cost per treatment, £	Difference (HA – VR) for field, £	Difference (HA – VR), ha <sup>-1</sup> , £
<b>T1andT2</b>	MZ1 high	6	46	0.72	55	39.6	237.6	95.04	8.8
	MZ2 low	4.8	39.8	0.36		19.8	95.04		
	HA	10.8	85.8	0.72		39.6	427.68		
<b>T3</b>	MZ1 high	3.6	26.3	2	34	68	244	191.2	17.7
	MZ2 mid	3.2	25.9	1.5		51	163.2		
	MZ3 low	4	33.2	1		34	136		
	HA	10.8	85.4	2		68	734.4		

By combining the SH with the VRFA at T1 and T2 and at T3 application times, a potential saving of £900.18 is expected for this field, which is an average of £83.35 per ha. It is possible to consider both methods as a combined economic benefit as the SH is considering the savings from preventing down grading of the grain, if the full field were to be collected homogeneously, whilst the variable fungicide applications consider the savings from fungicide costs compared to a full homogeneous rate. VRFA are here assumed to maintain the grain

quality and quantity by applying higher rates on needed areas, compared to a full rate, and not improve the quality. VRFA would only be assumed to improve grain quantity and quality if compared to a homogenous reduced or half rate. Thus, SH would still be required to separate the higher quality grain from the lower quality areas. The current technology of fungal disease treatment based on the CROP-meter offers economic benefits by just reducing fungicide input, but does not necessarily increase crop quality or quantity (Ehlert *et al.*, 2003). The suggested methodology in the current work may lead to not only economic, but environmental and social benefits. The potential reduction in the amount of fungicide applied (Table 37) would lead not only to reducing the environmental impact due to reduced soil and water contamination, but improve the quality of grain harvest, by targeting areas of risk to fungicide pressure with the larger fungicide concentrations. The social benefit is associated with less mycotoxin concentration in human consumed grain obtained with SH. This could be considered from the other perspective, that if a field has generally a low disease spread, and the farmer or agronomist would otherwise prescribe a half dose for the field, they can add a full dose in the areas recognised to be at risk. The reason this is of interest is better control of the disease (by applying higher rates on risk areas than lower rates homogeneously), and lowering the chance of the efficacy of the fungicide product being reduced in the long term, as fungal strains adapt and develop increased immunity (FRAC, 2010).

There is a need to recognise the current work's proposed method of SH and VRFA. However, before the current work can be adopted in practice, further work is needed to account for cost-benefit analysis, which includes the cost of data collection and application of the process. The costs of implementing both SH and VRFA have not been discussed. It is important to acknowledge that initially extra costs would be incurred in fuel consumption and grain storage. However, if such methods prove to be beneficial, agricultural equipment could

be modified or developed to accommodate both methods, eliminating the need for additional driving and grain storage trailers. Purchasing the equipment would have an initial cost, which will vary depending on the specifications of the imager (size, wavebands, resolution, etc.), with a low spatial and spectral resolution camera being more affordable. As the field develops, options of leasing equipment are also increasing. Details on hyperspectral imager costs are by request and vary between suppliers. For an imager with similar spec to the one used in this study costs of around £10,000 should be expected. Whilst the cost of the hyperspectral equipment has not been included in this study, through further work we aim to investigate if the economic and environmental benefits would support the expense. However, many of the issues that West *et al.* (2003) highlighted with predicting economic benefit are still relevant today, with limitations of farming equipment being common i.e., boom length and variable section control. Furthermore, costs of fungicide and prices of grain continue to vary (FWI 2016). Predicting economic benefit becomes further taxing when considering the increasing legislation on the choice of fungicides, mutations of fungicide resistant disease, and the impacts of climate change, the efficacy of disease control, and the response to fungicide treatment (Sung and Cook, 1981; De Vallavieille-Pope *et al.*, 1995; Rossi *et al.*, 2001; Xu, 2003; Dufault *et al.*, 2006; FRAC, 2010; Mielecki, 2011).

The current work assesses the use of high spatial resolution data to compare the economic and environmental benefit of a VRFA and a SH to a conventional homogenous practice. Whilst the study found initial economic savings of £83.35 per ha, the results are specific to this field, crop and year. For a decision tool that would recommend a time of spraying and VRFA, further components would need to be considered such as the use of air sampling for the detection of airborne pathogens. West *et al.* (2008) combined air sampling with polymerase chain reaction analysis, for the quantitative identification of Pathogens. A process

based model including climate data would create a robust decision tool, where parameters could be considered relating to fungicide applications. In conventional farming, fungicides are often applied in response to agronomists' visual assessments. An example of prescribed fungicides can be found in Appendix D. This study has highlighted the potential economic benefit of the disease mapping methodology for VRFA and SH, compared to conventional methods. However, further work should consider a combination of disease mapping, pathogen sensor technologies, and temporal data (such as plant growth, and climate data) in a process based model, for production of a robust decision tool.

#### **7.4 Summary conclusions**

The study explores the virtual cost-benefit analysis results of variable rate fungicide applications for yellow rust, compared to the conventional method of homogenous full rate application. This analysis has also included selective harvest against homogeneous harvest when fusarium head blight disease protection concerned. The virtual total calculated profit of combining selective harvest and variable rate fungicide application is £83.35 per hectare and an environmental benefit of fungicide reduction of was found to be around 25%. Air sampling for pathogens should also be considered in future work for a dynamic decision tool of disease site specific management.



## 8 Conclusions and further work

### Chapter Synopsis;

This chapter includes a short discussion about some recent publications, revisits the hypotheses, aims, and objectives of the thesis, and discusses and highlights the previous chapter's conclusions and further work. Drawing attention to the recognised gaps in knowledge, and how the thesis has tried to address them. Discussing the potential further work which could take the data introduced and discussed in this thesis, to further develop and full fill the gaps in knowledge.

### 8.1 Recent publications

Bhattacharai *et al.* (2017) used Multivariate and cluster analysis in distinguishing soil limiting factors and grouping types of coffee farms. Where they attempted to understand variations and yield gaps from farm resources. Highlighting multiple farm variations influencing yield variations, soil properties were one of the major contributors in yield variability, specifically noting the  $(Ca + Mg)/K$  ratio, and soil Fe content. However, Chenu *et al.* (2017), encourages the use of process based models for understanding crop growth and yield gaps, which should be based on worldwide climate data, soil properties and characteristics, cropping practices and local conditions. Supporting that the studies on yield limiting factors (in chapter 3), whilst interesting for the field studied to understand field level yield variations, process based models are required for a more global application.

Pantazi *et al.* (2017) were capable of distinguishing between yellow rust and nitrogen stress at canopy level with an accuracy of over 95% for three techniques of hierarchical self-organizing classifiers. Which highlights the importance of distinguishing between biotic and abiotic factors and the potential of a hyperspectral imager to do so. Masri *et al.* (2017) found

the use of thermography was useful in detecting the advancement of FHB after inoculation. Finding that air temperature to fusarium infected ears was negatively correlated. This would be an interesting aspect to involve and improve FHB detection which was investigated in this thesis (chapters 5, 6 and 7).

A review by Mahlein (2016), discusses the use of optical sensors for the recognition of crop disease. Thermography and chlorophyll fluorescence is sensitive to early stress symptoms in plants, however, they are not alone capable of being used for specific disease detection. Suggesting a data fusion and combined use with RGB images and hyperspectral techniques, highlighting the development process that the imaging technologies need to undergo. This is a subject touched upon through the thesis, particularly chapter 4, which focuses on the current limitations of applying on-line a proximal hyperspectral imager, to a cereal crop canopy.

Mahlein (2016) encourages future use of data fusion, from different sensors in the understanding of the plant-pathogen systems. Whilst this thesis attempted the use of multiple sources of data, and the fusion of data (chapter 7) for a greater understanding of disease management, there are still many more technologies that could be incorporated in future work. It also highlights the potential use of different platforms of data, which could be utilised to overcome some of the current limitations.

## **8.2 Objectives and chapter conclusions**

The Introduction in Chapter 1 brings attention to areas of particular interest, which have limited published knowledge, they are discussed further in chapter 2. This chapter aims to summarise the conclusions found in the previous chapters and how they fulfil the highlighted objectives.

The aim of this study;

To apply a hyperspectral imager on-line application to cereal crop disease recognition, critically appraising the existing technology. It also investigates a novel modelling approach for quantifying the crop yield limiting factors. The key aim is to produce management zone maps for variable rate fungicide application and selective harvest, in response to crop disease pressures, soil characteristics and micro-climatic conditions.

Yellow rust and fusarium head blight (FHB) was selected to be the two diseases studied through the thesis, as they have a history of occurrence at the studied farm. The selection also meant that both a significant foliar disease (yellow rust) and a significant ear disease (FHB) could be included in the study.

This aim has been broken into five objectives, which are stated and discussed below;

### **8.2.1 Objective 1:**

“To critically appraise different approaches, and identify the best configuration for the hyperspectral imaging systems for *in-situ* and on-line field measurement of crop disease.”

Conclusions of Chapter 4;

Whilst progress has been made in disease recognition in the field, there are few on-line (*in-situ* and applied with a moving platform, e.g. an agricultural vehicle) yellow rust specific identification systems and none for fusarium head blight (FHB). Objective 1 was designed to address this observation in literature. And is addressed within the literature review and further assessed in chapter 4; “optimising the configuration of a hyperspectral imager for on-line measurement of wheat canopy”. The literature review summarises the current approaches and developments in on-line spectroscopy and hyperspectral imaging. Chapter 4 focuses specifically on hyperspectral imaging and evaluates the individual and interaction effects of

the system, and the parameters that are of interest. Resulting in an optimal configuration for a high quality spectra assessed by signal-to-noise ratio (SNR) for an on-line hyperspectral imager, the influence of on-line measured soil moisture content (MC) and total nitrogen (TN) on SNR was also evaluated. This allowed for the following conclusions to be drawn:

- 1) The integration time followed by the camera height and camera angle appeared to have the largest influence on the SNR. As integration, increased SNR increased, however a long integration time (>50 ms) was of a negligible influence and only slightly increased the SNR, but result in spectral saturation, hence should be avoided. An increase in camera angle benefitted SNR, however a decrease in camera height benefitted SNR.
- 2) The PCA similarity map showed that the light height and distance have a strong correlation with each other but a minimal influence on SNR.
- 3) Both on-line measured MC and TN were found to have significant effects on the SNR of the wheat canopy spectra at 95% confidence. The on-line soil measurements revealed stronger spatial similarity between the hyperspectral SNR and MC maps (kappa value = 0.75), which was attributed to soil deformation below the tractor tyre.
- 4) The variable reflected light intensity captured by the different pixels across the line imagery is an interesting factor to take into account, due to the impact of varying camera height during the on-line measurement. Whilst the solution suggested here is appropriate, it is camera specific.

Further work is planned to overcome variation in SNR associated with camera height changes (vibration, bounce in the boom, and soil deformation during the on-line measurement) by the further investigation in spectra pre-processing. It is also planned to implement these

hyperspectral measurement configurations for on-line measurements of crop canopy for detection of crop health and disease presence, which is approached in chapters 5 and 6.

### **8.2.2 Objective 2:**

“To evaluate the individual and interaction effects of parameters limiting crop growth and yield”.

Conclusions of chapter 3;

To the best of our knowledge, no previous studies have utilised high sampling resolution data on multi-soil properties collected with a vis-NIRS on-line sensor to quantify crop yield limiting soil factors using a VNRX model. Assessing the contribution of disease collected through high resolution hyperspectral imaging, in comparison with nutrient factors collected through high resolution vis-NIR as a yield limiting factor has not yet been approached in literature. Whilst studies have been undertaken to assess yield limiting factors, few have used high resolution spectroscopy. Studies in the area have historically used sub plots within a field, as (Sylvester-Bradley and Kindred, 2009). An alternative to this would be to consider the entire field, this, however, requires a higher sampling resolution of environmental parameters, crop disease, and yield mapping. This is partially addressed by Objective 2, approached in chapter 3, yield limiting factors. This chapter is presented in two parts. Part 1 “A new non-linear parametric modelling method to quantify influence of soil properties on crop yields - Methodology”, which focused towards the quantification of soil related yield limiting factors. This was based on a parametric modelling technique of a Volterra non-linear regressive with eXogenous inputs (VNRX) technique which was applied and compared with a random forest technique through two cropping seasons of 2013 and 2014. And Part 2 “A new non-linear parametric modelling method to quantify influence of soil properties on crop yields - Application to on-line soil data” where the parametric modelling technique of a

Volterra non-linear regressive with eXogenous inputs (VNRX) technique was applied to NIR-Vis on-line collected soil data.

Concluding that;

- 1) The results of VNRX-LN model accounting for both linear and non-linear interactions explained 52.2% and 50.7% of yield variation in 2013 and 2014 respectively, which were much higher than those obtained with VNRX-L (total contributions of 19.15% and 8.5% in 2013 and 2014, respectively), accounting for the linear interaction only.
- 2) The contribution of the RF model produced the highest contribution of 55.6% in 2013, which dropped down considerably to 45.8% in 2014.
- 3) The VNRX-LN model indicated that P, CEC and OC are the highest contributors to oilseed rape yield variability in 2013 and P, Na and OC to wheat yield variability in 2014. TN was surprisingly a small contributor particularly in 2013. It was observed that P and OC are consistently the highest contributors to yield variability through all VNRX models. Light, N, P, and K are the main factors affecting crop yield, the results in this chapter are specific to the yield variability and were attributed to the properties being more limited in the field, it did not measure for factors that were not limiting (such as N which was applied as fertiliser).
- 4) The RF analysis presented OC and TN to be the highest contributors to yield in both studied cropping seasons.
- 5) The RF and VNRX-LN models were comparable in predicting contribution of soil properties to yield variation, with VNRX-LN being slightly higher, however the RF model provided a higher consistency for individual soil property importance.
- 6) Yield variability for the VNRX-LN model showed a higher variability contribution from P and K and Na than the RF model, whilst P and K contribute to yield (P has a

direct link with crop yield), Na can have negative effects on moisture uptake, and can inhibit enzyme activities.

The RF model is an established method, whilst the application of the VNRX-LN was a novel approach introduced in this thesis. It's for these reasons that we will conduct further studies in quantifying yield variability with the new VNRX-LN method.

The further work highlighted in the first part of this subchapter included the use of high resolution data on soil chemical properties, which is addressed in part two of the chapter; which further explores the objective of yield limiting factors within the field, drawing the following conclusions:

1. The VNRX-LN model can be successfully used to quantify the influence of multi-soil properties, collected at high sampling resolution with an on-line soil sensor, on crop yield.
2. The effect of soil properties on crop yield varied with soil property, with the largest contribution observed for CEC, Mg and TN, with error reduction ratio contribution (ERRC) values of 14.6%, 4.69% and 1%, respectively.
3. The overall contribution of the eight soil properties sums up to an ERRC value of 23.21%. This value was found to be surprisingly low, a large part of the studied field suffers from a drainage problem, and this is thought to have masked some of the effects of soil properties on crop yield, and contributed to the low value.

The application of a VNRX to soil property, yield and NDVI data has been applied in chapter 3 part 1 and 2. Showing there is still a significant variability in yield and NDVI, that has not been accounted for, the further work is to apply the method to more study sites and include other variables. Sites of variable Nitrogen should also be considered, as the model is limited to detecting the influence of limited and variable properties on the yield. This is believed to

be the main reason for the impact on yield variability from Mg. Appendix A demonstrates the initial results of disease (late yellow rust and FHB) contribution to yield and NDVI prediction, which is the same 10 ha field considered in chapter 7. Though in this model, soil properties were reduced to just 4 properties (OC, TN, MC, CEC) and had little impact on the yield and NDVI predictions, this is understandable as in chapter 7 the same properties are reviewed and had little variation through the field. Reinforcing that variable/precision agriculture is only appropriate for non-homogenous crop stands.

### **8.2.3 Objective 3:**

“To create a spectral library using hyperspectral data to identify and quantify specific crop diseases (yellow rust and fusarium head blight) independent from water stresses”.

Conclusions of Chapter 5;

The monitoring and detection of stress and diseases in plants is vital for sustainable agriculture practice. This observation was considered best approached by first developing a technique for disease recognition independent of water stress, and is captured by objective 3 “Chapter 5; Hyperspectral measurements of yellow rust and FHB in cereal crops: Part 1: Laboratory study”, addresses this objective by exploring the potential of a hyperspectral line imager (400-750 nm) with the use of linear partial least squares regression (PLSR) analysis, concluding 5 main points:

- 1) The standard deviation (SD) of the wavelength range from 500 to 650 nm and the squared difference between 650 nm and 700 nm are of particular interest in discrimination between healthy, and yellow rust or FHB infected sites in a wheat and barley canopy. With the lowest 500-650 nm SD, and highest 650-700 nm squared difference being attributed to healthy crop, a noticeably lower 650-700 nm squared



difference attributed to yellow rust infected crop, and a noticeably higher 500-650 nm SD attributed to FHB infected crop.

- 2) Yellow rust models performed more accurately than FHB models, which was attributed to the fact that yellow rust is a foliar disease, which has larger chance to be captured by the hyperspectral line image, as compared to FHB being head disease that appear late in the growing season.
- 3) Scale-based assessment of yellow rust, based on 0-5 classes, produced a marginally more reliable model performance than the percent coverage data set.
- 4) Modelling of yellow rust in wheat is rather more accurate than in barley, which is possibly due to wheat having larger leaves. Prediction results indicated moderate prediction accuracy for barley (RPD = 1.80 - 1.97;  $R^2 = 0.69 - 0.77$ ) and good accuracy for wheat (RPD = 2.04 - 2.25;  $R^2 = 0.77 - 0.80$ ). Therefore, it can be concluded that yellow rust can be detected with appreciable accuracy and reliability in both wheat and barley. Whilst the Logit scale applied for yellow rust for wheat and barley was able to distinguish between high and low (RPD = 1.2 and  $R^2 = 0.43$ , and RPD = 1.4 and  $R^2 = 0.79$ , respectively)
- 5) Results for FHB prediction were of moderate accuracy for wheat (RPD = 1.5;  $R^2 = 0.57$ ) and able to distinguish between high and low values (RPD = 1.36;  $R^2 = 0.5$ ) for barley, suggesting the need for a more effective measurement and modelling approaches for barley. FHB models were able to predict FHB infection severity, to an accuracy of low and high infection. Further work should be done to enable assessment of % FHB coverage.

The laboratory trials in this study have been designed to emulate a field. The data used in the models was all collected from the wheat and barley trays, designed to simulate a field

canopy, so the variance of reflectance due to canopy is included in the models. Whilst other properties such as illumination angle, view positions, shadows, plant species, maturity and phenology can be controlled under the laboratory conditions, these parameters will have considerable influences under field conditions. Their on-line application is considered in chapter 6 which is the second part of this study.

#### **8.2.4 Objective 4:**

“To implement the hyperspectral imager for on-line detection and mapping of the spatial distribution of yellow rust and fusarium head blight in winter wheat and barley”.

Conclusions of chapter 6;

To the best of our knowledge, there are few on-line spectral recognition systems, which are capable of being disease specific for yellow rust, and none for FHB. Presenting a gap in knowledge for an on-line hyperspectral recognition system, capable of differentiating between water stressed, yellow rust and FHB infected crops. In addition to the necessity of an on-line disease recognition system, it has been reported that a greater occurrence of fungal diseases is observed in denser canopies, although a conclusive regression has not been obtained. This was approached in chapter 6 “Hyperspectral measurements of yellow rust and FHB in cereal crops: Part 2: on-line field measurement” to obtain objective 4. The chapter considers the potential of a hyperspectral line imager (400-750 nm) for the on-line measurement and mapping of yellow rust and FHB in wheat and barley, and discusses the impact of soil moisture and crop density on the disease distributions. Results reported allowed the following conclusions to be made;

1. On-line hyperspectral measurement and mapping of yellow rust and FHB is possible with moderate accuracy in barley and good accuracy in wheat.

2. Yellow rust is more accurately measured, based on models developed with visual disease assessment, whereas assessment of FHB required photo interpretation to provide more accurate measurement. This is believed to be due to fusarium symptoms on ears being better captured in an RGB image, than yellow rust attacking the foliage.
3. Photo interpretation-based on-line measurement of FHB was classified as good in wheat (RPD = 2.27;  $R^2= 0.82$ ) to moderately accurate in barley (RPD = 1.56;  $R^2= 0.61$ ), whereas good (RPD = 2.5;  $R^2=0.81$  in wheat) and moderate (RPD = 1.82;  $R^2= 0.72$  in barley) measurement accuracy was achieved for yellow rust by means of visual scale assessment.
4. On-line maps developed in this study support that in large fields, disease concentration is higher at the edges of the field and then expand towards the inner parts through the growing season. However, the findings suggest that disease pressures in the smaller field were more evenly distributed across the entire field area, than the larger fields.
5. A PLSR model developed for recognition of FHB and yellow rust in wheat, can be applied to barley with a slight reduction in accuracy.
6. Soil texture and moisture content affect and canopy density and subsequently humidity, which in turn affect FHB and yellow rust spatial pattern.

The suggested further work highlighted by this chapter, is approached in chapter 7 “Management zone maps for variable fungicide application and selective harvest”. The suggestions being; to evaluate the impact of on-line maps of yellow rust and FHB on site specific recommendations of fungicides, and to adopt a management-zone concept for site specific applications and selective harvest.

### 8.2.5 Objective 5:

“To adopt a data-fusion approach for delineation of management zones for variable rate fungicide application and selective harvest.”

Conclusions of chapter 7;

Diseases such as yellow rust can vary considerably in very short distances and reduce yields by up to 7  $\text{tha}^{-1}$  (Bravo *et al.*, 2003). The crop density could reflect multi-stresses occurring at the same time e.g. water, nutrients, temperature, disease etc. crop density is also dependent upon the climatic conditions each year and associated crop variety. The CROP-meter optimizes fungicide control by reducing fungicide input and maintains control, but does not increase crop quality or quantity, highlighting an un-met demand where quality and quantity of yield is improved by considering environmental parameters. To the best of our knowledge there are no proposed methods of precise management of fungal diseases, which takes into account a high spectral sampling resolution, of disease pressure and canopy and soil properties. This was approached in chapter 7 “Management zone maps for variable fungicide application and selective harvest” to obtain objective 5.

The study proposed the delineation of management zone maps for variable rate fungicide application and selective harvest in one field with wheat subjected to yellow rust and FHB spread. A k-mean cluster analysis was explored to divide the experimental field into separated clusters (zones) based on on-line predicted FHB and yellow rust (measured with a hyperspectral imager), on-line predicted soil total nitrogen (TN), organic carbon (OC), moisture content (MC) and cation exchange capacity (CEC) (using an on-line visible and near infrared (vis-NIR) spectroscopy sensor), measured crop canopy normalised difference vegetation index (NDVI) and leaf area index (LAI), yield, and air humidity and temperature. The main findings highlight the following conclusions:

- 1) The field was divided into a different number of management zones depending on the input data layers used for the k-mean cluster analysis. Management zones with high disease pressure associated with low NDVI and LAI, and high air temperature and vice versa for low disease pressure management zones.
- 2) Average overall reductions in fungicide of 22.24% (for T1 and T2 growth stages applications) and 25.93% (for T3 growth stage application) were calculated for the entire field area of 10.8 ha for variable rate fungicide application as compared to homogeneous application.
- 3) The selective harvest of high quality grain from low quality grain would result in less risk of mycotoxins affecting human health.
- 4) The virtually total calculated profit of combining selective harvest and variable rate fungicide application is £900.18 per field or £83.35 per hectare, divided into selective harvest of £48.04 ha<sup>-1</sup>, variable rate fungicide application at T1 and T2 growth stages of £17.6 ha<sup>-1</sup> each and; T3 £17.7 ha<sup>-1</sup>).

Future work should focus on the implementation of the proposed methodology in the field, to allow actual cost-benefit analysis to be carried out. The cost of collecting the multi-layer data on crop and soil characteristics and microclimatic conditions and yield responses should be accounted for in the cost-benefit analysis. Additional sensors could be involved, to produce a more robust decision support tool, and additional vegetation indices could be considered.

### **8.3 Hypothesis consideration**

The thesis suggested two hypotheses;

“Proximal hyperspectral imagery is capable of detecting specific crop diseases (e.g. Fusarium head blight and yellow rust) and applied on-line can be used to quantify their distribution pattern.”

And;

“Multi-sensor and data fusion of crop disease, and canopy and soil properties collected at high sampling resolutions, contribute to the quantification of the yield limiting factors, which can be utilised in variable management zones.”

The first hypothesis has been proven true for the detection of only two diseases. To fully understand if the disease recognition is specific further diseases such as septoria should be considered. This would allow the current system to be tested on its capability to distinguish specific diseases, not just on the presence of a particular symptom, as septoria disease can also cause similar chlorosis symptoms to that of yellow rust. Chapters 5 and 6 show that with suitable disease assessments and PLS regressions, with hyperspectral data collected at an optimal configuration (chapter4), a good accuracy of prediction can be obtained for yellow rust infection and a moderate accuracy for FHB infection on-line.

The second hypothesis has also been found true (though some variability still needs to be accounted for, such as disease and pest presence) through chapter 3, where VNRX modelling was utilised on soil properties to predict Yield (and further explored in the data provided in Appendix A), and the production of management zones through K-means clustering in chapter 7, where the potential cost benefits of applying the selective harvests and variable fungicide applications are discussed.

## 8.4 Contributions to knowledge

Methods of yield variability have been assessed and found a possibility of attributing 55.6% (through VNRX modelling) and 52% (from RF modelling) of yield variability, from soil properties alone, both having a significance level of  $<0.01$ . The further work for this is to include disease data. Initial findings for this are provided in Appendix A, where they show a significant contribution of yield and predictions based on NDVI can be attributed to late yellow rust and FHB presence. A yield gap exists between current production and the maximum yield potential of a crop. Further work with detecting and mapping the crop and soil qualities, could help towards better management of crop limiting factors, to reduce the current yield gap.

An optimal configuration for the application of a push broom hyperspectral imager to a cereal crop canopy has been suggested. With configurations of 0.3 m, 1.2 m, 1.2 m and  $10^\circ$  values of camera height, light height, light distance and camera angle, respectively. The optimum integration time for on-line field measurement was 50 ms.

A hyperspectral technique coupled with PLSR can be successfully used for the estimation of yellow rust in winter wheat and barley canopy. At tray level ratio of prediction deviation (RPD) values of 2.25 ( $R^2= 0.80$ ) and 1.97 ( $R^2=0.77$ ) were calculated for wheat and barley based on scale measurement, and 2.04 ( $R^2=0.77$ ) and 1.80 ( $R^2=0.69$ ) for percentage coverage, respectively, which were classified as good accuracy in wheat and as moderately accurate in barley. FHB detection, results were less successful RPD = 1.5 ( $R^2=0.57$ ) (just at the edge of moderately accurate) in wheat and RPD= 1.36 ( $R^2=0.5$ ) (differentiate between high and low values) in barley). However, the disease recognition needs further applications to establish its reliability in the presence of additional crop diseases, such as septoria. Currently, it was trialled upon yellow rust (a foliage disease) and FHB (an ear disease), further applications

should be made on detecting these whilst other diseases are known to be present. i.e. detection of yellow rust in a yellow rust and septoria affected crop stands. This would allow greater understanding if the system is capable of being disease specific.

It was found that photo interpretation was the most applicable and accurate for on-line measurement of FHB, which was classified as a good to moderately accurate recognition method, since the ratio of prediction deviation (RPD) values were 2.27 ( $R^2=0.82$ ) for wheat and 1.56 ( $R^2=0.61$ ) for barley. For yellow rust significantly improved results for the PLSR models were obtained when the ground truths were based on visual scale assessment, where model performance was classified as moderately accurate in barley (RPD = 1.82;  $R^2=0.72$ ) and good in wheat (RPD = 2.5;  $R^2=0.81$ ).

A method of selective harvest has been suggested, with potential cost benefits (under certain assumptions) with Financial savings of £900.18 for the 10.8 ha field, with an average of £83.35 per hectare (harvest = £48.05 ha<sup>-1</sup>; T1 and T2 = £8.8 ha<sup>-1</sup> each and; T3 £17.70 ha<sup>-1</sup>)

## **8.5 Further work**

The chapters have addressed the objectives, and aimed towards contributing to the current gaps in knowledge. However, each chapter has highlighted further work, which would contribute to knowledge. These have not been obtained in this thesis due to either being outside of the study's focus, or due to time restraints. The recommended further work is summarised in 3 parts; yield limiting factors, hyperspectral imaging of disease, and management zones.

### **8.5.1 Yield limiting factors**

Further work is suggested to validate the concept of Volterra Non-linear Regressive with eXogenous inputs (VNRX) models to study and quantify the effect of soil properties on crop



yield, on a larger number of fields. Where other affecting parameters such as, crop diseases (from the methods highlighted in Chapter 5), environmental factors (e.g., pests, topography, microclimate conditions), and soil physical properties (e.g., soil compaction, hydraulic conductivity, etc), should be considered in the analysis, to take into account the full picture of yield limiting factors.

### **8.5.2 Hyperspectral imaging of disease**

Further work is planned to overcome variation in SNR associated with camera height changes (vibration, bounce in the boom, and soil deformation during the on-line measurement) by investigating further the variations of spectra pre-processing.

### **8.5.3 Management zones**

This chapter suggests theoretical methods of selective harvest and fungicide application, using collected data from soil and canopy properties, and disease data compared to harvest data. Suggesting potential economic and environmental benefits under certain assumptions. The further work will be focused on applying these methods in practice. Air sampling for pathogens should also be considered for a dynamic decision tool, for disease management.

## **8.6 Concluding remarks**

The homogenous application of chemicals throughout a field to control crop disease has been in practice in agriculture for nearly a century. There is an ever-growing demand for food. As the population growth continues to escalate, and the competition for agricultural land for alternative use rises, the pressure for maximizing yield increases. Fungicides are being removed from the market due to environmental concerns, they, along with disease resistant strains of crop, are succumbing to mutating fungal strains. It has become imperative to move away from conventional farming methods, and find a more sustainable approach. Whilst

research into alternative methods, such as precision agriculture is becoming more of a focus, there are still limitations, gaps in knowledge, and the application of this knowledge. Whilst it's been recognised for a while that optical technologies are suitable for disease detection systems, no sensor-based technologies for disease detection commercially exist, that are directly related to a diseases presence within a field. This thesis has focused towards moving the technology to the field, to understand the yield limiting factors at high sample rates, recognise disease (yellow rust and FHB) in cereal crops (winter wheat and winter barley) and apply the technology on-line. This has been combined into approaches of variable fungicide applications and a selective harvest approach, which will hopefully contribute towards confidence in variable applications, and quantify the potential environmental and economic benefits.

## REFERENCES

- Agegehu, G., Nelson, P., and Bird, M. (2016). Crop yield, plant nutrient uptake and soil physicochemical properties under organic soil amendments and nitrogen fertilization on Nitisols. *Soil and Tillage Research*, 160, pp. 1–13.
- Agrios, G.N., (1997). *Plant Pathology Academic Press San Diego. California, USA, 390.*
- AHDB, 2016, Fungicide performance in oilseed rape, Agriculture and Horticulture Development Board publications
- Al Masri, A., Hau, B., Dehne, H.W., Mahlein, A.K. and Oerke, E.C., (2017). Impact of primary infection site of *Fusarium* species on head blight development in wheat ears evaluated by IR-thermography. *European Journal of Plant Pathology*, 147(4), pp.855-868.
- Ali M.A., Hussain M., Khan M.I., Ali Z., Zulkiffal M., Anwar J., Sabir W., Zeeshan M. (2010). Source-sink relationship between photosynthetic organs and grain yield attributes during grain filling stage in spring wheat (*Triticum aestivum*). *International Journal of Agriculture and Biology*, 12: pp. 509–515.
- Alvarez, A.M., 2004. Integrated approaches for detection of plant pathogenic bacteria and diagnosis of bacterial diseases. *Annual Review of Plant Pathology* 42, 339–366.
- Anand, A., Zhou, T., Trick, H.N., Gill, B.S., Bockus, W.W. and Muthukrishnan, S. (2003). Greenhouse and field testing of transgenic wheat plants stably expressing genes for thaumatin-like protein, chitinase and glucanase against *Fusarium graminearum*. *Journal of Experimental Botany*, 54(384), pp.1101-1111.
- Andersen AL. (1948). The development of *Gibberella zeae* head blight of wheat. *Phytopathology* 38, pp.595–611.
- Asner, G. P. (1998). Biophysical and biochemical sources of variability in canopy reflectance. *Remote sensing of Environment*, 64(3), pp.234-253.
- Backhouse, D., (2014). Global distribution of *Fusarium graminearum*, *F. asiaticum* and *F. boothii* from wheat in relation to climate. *European journal of plant pathology*, 139(1), pp.161-173.
- Bai G, Shaner G (1994) Scab of wheat: prospects for control. *Plant Dis* 78: pp.760–766
- Baligar, V., Fageria, N., and He, Z. (2001). Nutrient use efficiency in plants. *Communications in Soil Science and Plant Analysis*, 32(7-8), pp. 921-950.
- Barbedo, J. G., Tibola, C. S., and Fernandes, J. M. (2015). Detecting *Fusarium* head blight in wheat kernels using hyperspectral imaging. *Biosystems Engineering*, 131, pp. 65-76.
- Bauriegel, E., Giebel, A., Geyer, M., Schmidt, U. and Herppich, W.B. (2011). Early detection of *Fusarium* infection in wheat using hyper-spectral imaging. *Computers and Electronics in Agriculture*, 75(2), pp. 304-312.
- Bekele, G.T., (2002). *Wheat diseases and pests: a guide for field identification.*
- Bélanger M.C., Roger J.M., Cartolaro P., Viau A.A., Bellon-Maurel V., (2008), Detection of powdery mildew in grapevine using remotely sensed UV-induced fluorescence, *Int. J. Remote Sens.*, 29 pp. 1707–172
- Belasque, L., Gasparoto, M.C.G., Marcassa, L.G., (2008). Detection of mechanical and disease stresses in citrus plants by fluorescence spectroscopy. *Applied Optics* 47
- Bergamin Filho A. and Amorim, L. (1996). *Doenças de plantas tropicais: epidemiologia e controle econômico.* São Paulo: Editora Agronômica Ceres Ltda.
- Bergaya, F., and Vayer, M. (1997). CEC of clays: measurement by absorption of a copper ethylenediamine complex. *Applied clay science*, 12(3), pp. 275-280.

- Bhattarai, S., Alvarez, S., Gary, C., Rossing, W., Tittonell, P. and Rapidel, B., (2017). Combining farm typology and yield gap analysis to identify major variables limiting yields in the highland coffee systems of Llano Bonito, Costa Rica. *Agriculture, Ecosystems and Environment*, 243, pp.132-142.
- Bieri, S., Potrykus, I. and Futterer, J. (2000) Expression of active barley seed ribosome-inactivating protein in transgenic wheat. *Theor. Appl. Genet.* 100, 755–763.
- Bigg, G. R., Wei, H. L., Wilton, D. J., Zhao, Y., Billings, S. A., Hanna, E., and Kadirkamanathan, V. (2014). A century of variation in the dependence of Greenland iceberg calving on ice sheet surface mass balance and regional climate change. *Proceedings of the Royal Society A: Mathematical, Physical and Engineering Sciences*, 470(2166), pp. 20130662.
- Billings, S. A. (2013). *Non-linear system identification: NARMAX methods in the time, frequency, and spatio-temporal domains*. London: John Wiley and Sons.
- Billings, S., Chen, S., and Korenberg, M. J. (1989). Identification of MIMO non-linear systems using a forward regression orthogonal estimator. *International Journal of Control*, 49, pp. 2157–2189.
- Bilsborrow, P., Cooper, J., Tétard-Jones, C., Średnicka-Tober, D., Barański, M., Eyre, M. and Wilcockson, S. (2013). The effect of organic and conventional management on the yield and quality of wheat grown in a long-term field trial. *European Journal of Agronomy*, 51, 71-80.
- Bisby, G.R., (1943). Geographical distribution of fungi. *The Botanical Review*, 9(7), pp.466-482
- Bliffeld, M., Mundy, J., Potrykus, I. and Futterer, J. (1999) Genetic engineering of wheat for increased resistance to powdery mildew disease. *Theor. Appl. Genet.* 98, 1079–1086
- Bock, C. H., Graham, J. H., Gottwald, T. R., Cook, A. Z., and Parker, P. E. (2010). Wind speed effects on the quantity of *Xanthomonas citri* subsp. *citri* dispersed downwind from canopies of grapefruit trees infected with citrus canker. *Plant Disease*, 94(6), pp. 725-736.
- Bock, C.H., Poole, G.H., Parker, P.E. and Gottwald, T.R. (2010a). Plant disease severity estimated visually, by digital photography and image analysis, and by hyperspectral imaging. *Critical Reviews in Plant Sciences*, 29(2), pp. 59-107
- Bohling, G., 2005. *Introduction to geostatistics and variogram analysis*. Kansas geological survey, pp.1-20.
- Boone, L., De Meester, S., Vandecasteele, B., Muylle, H., Roldán-Ruiz, I., Nemecek, T., and Dewulf, J. (2016). Environmental life cycle assessment of grain maize production: An analysis of factors causing variability. *Science of The Total Environment*, 553, pp. 551-564.
- Borlaug, N. E. and C. R. Doswell. (1994). Feeding a human population that increasingly crowds a fragile planet 15th World Cong. of Soil Sci. Acapulco, Mexico. Supplement to Trans. pp.10
- Boyer, J. (1982). Plant productivity and environment. *Science*, 218, pp. 443–448.
- Bravo, C., Moshou, D., Orberti, R., West, J., McCartney, A., Bodria, L. and Ramon, H. (2004). Foliar disease detection in the field using optical sensor fusion. *Agricultural Engineering International: CIGR Journal of Scientific Research and Development*. Manuscript FP 04 008. Vol.6, pp. 14.
- Bravo, C., Moshou, D., West, J., McCartney, A., and Ramon, H. (2003). Early disease detection in wheat fields using spectral reflectance. *Biosystems Engineering*, 84(2), pp. 137-145.
- Breiman, L. (2001). Random forests. *Machine learning*, 45(1), pp. 5-32.
- Breiman, L. (2002). *Manual on setting up, using, and understanding random forests v3. 1*. CA, USA: Statistics Department University of California Berkeley.
- Brennan, J.M., Egan, D., Cooke, B.M, Doohan, F.M. (2005). Effect of temperature on head blight of wheat caused by *Fusarium culmorum* and *F. graminearum*. *Plant Pathology* 54, pp. 156.

- Broge, N.H. and Mortensen, J.V. (2002). Deriving green crop area index and canopy chlorophyll density of winter wheat from spectral reflectance data. *Remote sensing of environment*, 81(1), pp.45-57.
- Broschius, S.C., Frank, J.A., and Frederick, J.R. (1985). Influence of winter wheat management practices on the severity of powdery mildew and Septoria blotch in Pennsylvania. *Phytopathology*, pp. 75, pp. 538–542.
- Brown, J.K. and Hovmøller, M.S., (2002). Aerial dispersal of pathogens on the global and continental scales and its impact on plant disease. *Science*, 297(5581), pp.537-541.
- Bruulsema, T. (2015). *Plant Nutrition TODAY*. Georgia USA: International Plant Nutrition Institute (IPNI).
- Bryson, R., Paveley, N., Clark, W., Sylvester-Bradley, R., and Scott, R. (1997). Use of in-field measurements of green leaf area and incident radiation to estimate the effects of yellow rust epidemics on the yield of winter wheat. *European Journal of Agronomy*, 7, pp. 53-62.
- BSI. (1995). Determination of organic and total carbon after dry combustion (elementary analysis), BSI 389. Chiswick High Road, London W4 4AL, UK.: British Standard Institute (BSI).
- BSI. (2007). Soil improvers and growing media: BS EN 13040:2007. Sample preparation for chemical and physical tests, determination of dry matter content, moisture content and laboratory compacted bulk density. UK: British Standards Institution.
- Buckee, G. K. (1994). Determination of total nitrogen in barley, malt and beer by Kjeldahl procedures and the Dumas combustion method — Collaborative trial. *Journal of the Institute of Brewing* 1994, 100 (2), pp. 57–64.
- Burth, U., Hartleb, W., Hartmann, W., and Hamann, W. (1990). Zur variablen, situationsbezogenen Bemessung der Aufwandmenge bei der Applikation von Pflanzenschutzmitteln (Variable situation based adaptation of the application rate of pesticides). *Nachrichtenblatt für den Pflanzenschutzdienst in der DDR*, 44, 194–196.
- Buscaglia, H. J., and Varco, J. J. (2002). Early detection of cotton leaf nitrogen status using leaf reflectance. *Journal of Plant Nutrition*, 25, pp. 2067–2080.
- Calcante, A. Mena, F. Mazzetto Evaluation of “ground sensing” optical sensors for diagnosis of *Plasmopara viticola* on vines Spanish *J. Agric. Res.*, 10 (2012), pp. 619–630
- Calderón, R., Montes-Borrego, M., Landa, B.B., Navas-Cortés, J.A. and Zarco-Tejada, P.J., (2014). Detection of downy mildew of opium poppy using high-resolution multi-spectral and thermal imagery acquired with an unmanned aerial vehicle. *Precision Agriculture*, 15(6), pp.639-661.
- Calderón, R., Navas-Cortés, J.A., Lucena, C. and Zarco-Tejada, P.J., (2013). High-resolution airborne hyperspectral and thermal imagery for early detection of *Verticillium* wilt of olive using fluorescence, temperature and narrow-band spectral indices. *Remote Sensing of Environment*, 139, pp.231-245.
- Cambardella, C.A., Moorman, T.B., Parkin, T.B., Karlen, D.L., Novak, J.M., Turco, R.F. and Konopka, A.E. (1994). Field-Scale Variability of Soil Properties in Central Iowa. *Soil Science Society of America Journal* 58, pp.1501–1511.
- Cameron, R. J. (1970). Light intensity and the growth of Eucalyptus seedlings: II. The effect of cuticular waxes on light absorption in leaves of Eucalyptus species. *Australian Journal of Botany*, 18: pp. 275 – 284.
- Campbell KAG, Lipps PE (1998) Allocation of resources: sources of variation in *Fusarium* head blight screening nurseries. *Phytopathology* 88: pp.1078–1086
- Campbell, J., and Norman, M. (1998). *An Introduction to Environmental Biophysics*. American: Springer-Verlag, 97-97.
- Carlyle, J. (1993). Carbon in forested sandy soils: properties, processes, and the impact of forest management. *New Zealand Journal of Forestry Science*, 23(3), pp. 390-402.
- Chaerle, L., Lenk, S., Hagenbeek, D., Buschmann, C., Van Der Straeten, D., (2007). Multicolor fluorescence imaging for early detection of the hypersensitive reaction to tobacco mosaic virus. *Journal of Plant Physiology* 164 (3), 253–262.

- Champeil, A., Dore, T. and Fourbet, J.F. (2004). Fusarium head blight: epidemiological origin of the effects of cultural practices on head blight attacks and the production of mycotoxins by Fusarium in wheat grains. *Plant science*, 166(6), pp. 1389-1415.
- Chandler, D., (2008). The consequences of the 'cut off' criteria for pesticides: alternative methods of cultivation, [http://www.europarl.europa.eu/RegData/etudes/note/agri/2008/408962/IPOL-AGRI\\_NT%282008%29408962\\_EN.pdf](http://www.europarl.europa.eu/RegData/etudes/note/agri/2008/408962/IPOL-AGRI_NT%282008%29408962_EN.pdf) [accessed: 15.12.12].
- Chang, D., Zhang, J., Zhu, L., Ge, S.-H., Li, P.-Y. and Liu, G.-S. (2014). Delineation of management zones using an active canopy sensor for a tobacco field. *Computers and Electronics in Agriculture*, 109, pp. 172–178.
- Chen, S., and Billings, S. A. (1989). Representation of non-linear systems: the NARMAX model. *International Journal of Control*, 49, pp. 1013-1032.
- Change, I.P.O.C., 2007. Climate change 2007: The physical science basis. *Agenda*, 6(07), p.333.
- Chen, S. and Billings, S.A., (1989). Recursive prediction error parameter estimator for non-linear models. *International Journal of Control*, 49(2), pp.569-594.
- Chen, X. M. (2005). Epidemiology and control of stripe rust (*Puccinia striiformis* f. sp. *tritici*) on wheat. *Canadian Pathology*, 27, pp. 314-337.
- Chen, X. W., Post, W. M., Norby, R. J., and Classen, A. T. (2011). Modeling soil respiration and variations in source components using a multi-factor global climate change experiment. *Climatic Change*, 107(3), pp. 459-480.
- Chen, W., Wellings, C., Chen, X., Kang, Z. and Liu, T., (2014). Wheat stripe (yellow) rust caused by *Puccinia striiformis* f. sp. *tritici*. *Molecular plant pathology*, 15(5), pp.433-446.
- Chenu, K., Porter, J.R., Martre, P., Basso, B., Chapman, S.C., Ewert, F., Bindi, M. and Asseng, S., (2017). Contribution of Crop Models to Adaptation in Wheat. *Trends in Plant Science*.
- Chiarappa L., ed. (1981). *Crop Loss Assessment Methods — Supplement 3*. Wallingford; CAB International
- Christy, C. (2008). Real-time measurement of soil attributes using on-the-go near infrared reflectance spectroscopy. *Computers and Electronics in Agriculture*, 61, pp. 10-19.
- Cibula WG, Carter GA. (1992). Identification of a far-red reflectance response to ectomycorrhizae in slash pine. *International Journal of Remote Sensing*, 13, pp. 925–32.
- Clark, B., (2016) Fungicide management: timings, Farmers Academy, <http://www.fwi.co.uk/academy/lesson/fungicide-management-timings>.
- Clausen, M., Krauter, R., Schachermayr, G., Potrykus, I. and Sautter, C. (2000) Antifungal activity of a virally encoded gene in transgenic wheat. *Nat. Biotechnol.* 18, 446–449
- Cohen, J., (1960). Kappa: Coefficient of concordance. *Educational Psychologist, Measurement*, 20, pp. 37
- Condon, A., and Giunta, F. (2003). Yield response of restricted-tillering wheat to transient waterlogging on duplex soils. *Australian Journal of Agricultural Research*, 54(10), pp. 957-967.
- Contribution of Crop Models to Adaptation in Wheat. *Trends in Plant Science*.
- Coops, N. C., Smith, M. L., Martin, M. E., and Ollinger, S. V. (2003). Prediction of eucalypt foliage nitrogen content from satellite-derived hyperspectral data. *IEEE Transactions on Geoscience and Remote Sensing*, 41(6), pp. 1338-1346.
- Corwin, D., Lesch, S., Shouse, P., Soppe, R., and Ayars, J. (2003). Identifying soil properties that influence cotton yield using soil sampling directed by apparent soil electrical conductivity. *Agronomy Journal*, 95(2), pp. 352-364.
- Crous, P.W., (2013). Sizing up septoria. *Studies in Mycology*, 75, pp.307-390.

- Cuculeanu, V., Tuinea, P. and Bălteanu, D., (2002). Climate change impacts in Romania: Vulnerability and adaptation options. *GeoJournal*, 57(3), pp.203-209.
- Cunniffe, N. J., Koskella, B., Metcalf, C. J. E., Parnell, S., Gottwald, T. R., and Gilligan, C. A. (2015). Thirteen challenges in modelling plant diseases. *Epidemics*, 10, pp. 6-10.
- Curran, P.J. and Dungan, J.L., (1989). Estimation of signal-to-noise: a new procedure applied to AVIRIS data. *IEEE Transactions on Geoscience and Remote Sensing*, 27(5): pp. 620-628.
- D'Hose, T., Cougnon, M., De Vlieghe, A., Vandecasteele, B., Viaene, N., Cornelis, W., Reheul, D. (2014). The positive relationship between soil quality and crop production: A case study on the effect of farm compost application. *Applied Soil Ecology*, 75, pp. 189-198.
- Dammer, K. H., and Ehlert, D. (2006). Variable-rate fungicide spraying in cereals using a plant cover sensor. *Precision Agriculture*, 7(2), pp. 137-148.
- Dammer, K.-H. (1999). Analyse und Darstellung der Dispersion von Schaderregern sowie Möglichkeiten der Stichprobennahme bei aggregiertem Auftreten (Analysis and dispersion maps of pests and sampling design under their aggregated pattern). Germany: Kropstaedt.
- Dammer, K.-H. (2003). In: Investigations into the dynamic of climatic parameters and infections with fungi diseases in heterogeneous cereal stands, Potsdam, Germany: Jahresbericht des ATB. pp. 23.
- Dammer, K.H., Wollny, J. and Giebel, A., (2008). Estimation of the Leaf Area Index in cereal crops for variable rate fungicide spraying. *European Journal of Agronomy*, 28(3), pp. 351-360
- Das, A.K., (2004). Rapid detection of *Candidatus Liberibacter asiaticus*, the bacterium associated with citrus Huanglongbing (Greening) disease using PCR. *Current Science* 87 (9), pp. 1183–1185.
- Dasu, T., and Johnson, T. (2003). *Exploratory data mining and data cleaning* (Vol. 479). John Wiley and Sons.
- Daumard, F., Champagne, S., Fournier, A., Goulas, Y., Ounis, A., Hanocq, J.F. and Moya, I., (2010). A field platform for continuous measurement of canopy fluorescence. *IEEE Transactions on Geoscience and Remote Sensing*, 48(9), pp.3358-3368.
- De Vallavieille-Pope, C., Ali, S., Leconte, M., Enjalbert, J., Delos, M. and Rouzet, J. (2012). Virulence dynamics and regional structuring of *Puccinia striiformis* f. sp. *tritici* in France between 1984 and 2009. *Plant Disease*, 96, pp. 131-140
- De Vallavieille-Pope, C., Huber, L., Leconte, M. and Goyeau, H. (1995). Comparative effects of temperature and interrupted wet periods on germination, penetration, and infection of *Puccinia recondita* f. sp. *tritici* and *P. striiformis* on wheat seedlings. *Phytopathology*, 85(4), pp. 409-415
- DEFRA. (2010). *The analysis of agriculture materials*. Reference book 427. Stationary office, London.
- Del Ponte EM, Fernandes JMC, Bergstrom GC. (2007) Influence of growth stage on fusarium head blight and deoxynivalenol production in wheat. *J Phytopathol* 155, pp.577–581.
- Dell'Endice, F. (2008). Improving the Performance of Hyperspectral Pushbroom Imaging Spectrometers for Specific Science Applications. In *ISPRS 2008: Proceedings of the XXI Congress: Silk Road for Information from Imagery: The International Society for Photogrammetry and Remote Sensing* pp. 215-220.
- Delwiche, S.R. and Kim, M.S., (2000), December. Hyperspectral imaging for detection of scab in wheat. In *Environmental and Industrial Sensing* pp. 13-20. International Society for Optics and Photonics
- Delwiche, S.R., (2003). Classification of scab–and other mold–damaged wheat kernels by near–infrared reflectance spectroscopy. *Transactions of the ASAE*, 46(3), p.731.
- Delwiche, S.R., Graybosch, R.A., (2002). Identification of waxy wheat by near-infrared reflectance spectroscopy. *Journal of Cereal Science* 35 (1), pp. 29–38.

- Delwiche, S.R., Kim, M.S. and Dong, Y. (2011). Fusarium damage assessment in wheat kernels by Vis/NIR hyperspectral imaging. *Sensing and instrumentation for food quality and safety*, 5(2): pp. 63-71.
- Demetriades-Shah, T.H., Steven, M.D. and Clark, J.A., (1990). High resolution derivative spectra in remote sensing. *Remote Sensing of Environment*, 33(1): pp.55-64.
- Desjardin, A.E. (2006). *Fusarium mycotoxins. Chemistry, Genetics, and Biology*. APS Press, St. Paul, MN.
- Devadas, R., Simpfendorfer, S., Backhouse, D. and Lamb, D.W., (2014). Effect of stripe rust on the yield response of wheat to nitrogen. *The Crop Journal*, 2(4), pp.201-206.
- Dhillon, N., Samra, J., Sadana, U., and Nielson, D. (1994). Spatial variability of soil test values in a typical Ustochrept. *Soil Technology*, 7, pp. 163–171.
- Di Gennaro, S.F., Battiston, E., Di Marco, S., Facini, O., Matese, A., Nocentini, M., Palliotti, A. and Mugnai, L., (2016). Unmanned Aerial Vehicle (UAV)-based remote sensing to monitor grapevine leaf stripe disease within a vineyard affected by esca complex. *Phytopathologia Mediterranea*, 55(2), p.262.
- Dill-Macky, R. and Jones, R.K., (2000). The effect of previous crop residues and tillage on Fusarium head blight of wheat. *Plant disease*, 84(1), pp.71-76
- Dimmock, J.P.R.E. and Gooding, M.J., (2002). The influence of foliar diseases, and their control by fungicides, on the protein concentration in wheat grain: a review. *The Journal of Agricultural Science*, 138(04), pp.349-366
- Doling, D.A. and Doodson, J.K., (1968). The effect of yellow rust on the yield of spring and winter wheat. *Transactions of the British Mycological Society*, 51(3), pp. 427-434
- Doodson, J.K., Manners, J.G. and Myers, A., (1964). Some effects of yellow rust (*Puccinia striiformis*) on the growth and yield of a spring wheat. *Annals of Botany*, 28(3), pp. 459-472.
- Dufault, N.S., DeWolf, E.D., Lipps, P.E., Madden, L.V., (2006). Role of temperature and moisture in the production and maturation of *Gibberella zeae* perithecia. *Plant Disease* 90, pp. 637–644
- Dytham, C. (2011). *Choosing and using statistics: a biologist's guide*. John Wiley and Sons.
- Earl, H.J. and Davis, R.F. (2003). Effect of drought stress on leaf and whole canopy radiation use efficiency and yield of maize. *Agronomy journal*, 95(3), pp. 688-696.
- Eberhart, S., and Russell, W. (1966). Stability parameters for comparing varieties. *Crop science*, 6(1), pp. 36-40.
- Eby, W.H. (1996). "Soybean cultivar 1572432." U.S. Patent 5,569,815, issued October 29.
- Edwards SG. (2007) Investigation of fusarium mycotoxins in UK barley and oat production. HGCA Project Report No. 415. HGCA, London.
- Ehlert, D., Hammen, V., and Adamek, R. (2003). on-line sensor pendulum-meter for determination of plant mass. *Precision Agriculture*, 4, pp. 139–148.
- Engelhard, A. W. (ed.). (1989). *Soil borne. Plant Pathogens. Management of Diseases with Macro-and Microelements*. The American Phytopathological Society Press. St. Paul, MN.
- Epstein, E., (1972). *Mineral nutrition of plants: principles and perspectives*.
- Eyal, Z., (1987). *The Septoria diseases of wheat: concepts and methods of disease management*. Cimmyt.
- Eyal, Z., Amiri, Z. and Wahl, I., (1973). Physiologic specialization of *Septoria tritici*. *Phytopathology*.
- Fageria, N. K., and V. C. Baligar. (1997). Phosphorous—use efficiency by corn genotypes. *J. Plant Nutr.* 20: pp. 1267–1277.
- Fan, M., Cao, J., Wei, W., Zhang, F., and Su, Y. (2013). Managing soil organic carbon for advancing food security and strengthening ecosystem services in China. In R. Lal, K. Lorenz, H. R.F., B. Schneider, and J. Von



- Braun (Eds.), *Ecosystem Services and Carbon Sequestration in the Biosphere* pp. 419–429. Netherlands: Springer.
- Falisse A, Meeus P. (2002). Froment d'hiver. In *Fumure et Protection Phytosanitaire des Cereales*, ed. A Falisse, P Meeus, Gembloux. Belgium: FUSAGx and CRAGx. 60 pp.
- Färe, R., Grabowski, R., Grosskopf, S., and Kraft, S. (1997). Efficiency of a fixed but allocatable input: A non-parametric approach. *Economics Letters*, 56(2), pp. 187-193.
- Fischer, R. A., Byerlee D., AND Edmeades G. O. (2014). *Crop Yields and Global Food Security: Will Yield Increase Continue to Feed the World?* ACIAR Monograph No. 158. Canberra, Australia: Australian Centre for International Agricultural Research.
- Fleischer, S. J., Blom, P. E., and Weisz, R. (1999). Sampling in precision IPM: When the objective is a map. *phytopathology*, 89, pp. 1112–1118.
- Fones, H. and Gurr, S., (2015). The impact of *Septoria tritici* Blotch disease on wheat: an EU perspective. *Fungal Genetics and Biology*, 79, pp.3-7.
- Fourcaud, T., Zhang, X. P., Stokes, A., Lambers, H., and Körner, C. (2008). Plant Growth Modelling and Applications: The Increasing Importance of Plant Architecture in Growth Models. *Annals of Botany*, 101(8), pp.1053–1063.
- Frogbrook, Z. L., and Oliver, M. A. (2007). Identifying management zones in agricultural fields using spatially constrained classification of soil and ancillary data. *Soil Use and Management*, 23(1), pp. 40-51.
- Fungicide Resistance Action Committee, (2010). *FRAC Recommendations for Fungicide Mixtures Designed to Delay Resistance Evolution*.
- FWI (2016) Market prices Arable, Available at: <http://www.fwi.co.uk/business/prices-trends/> (Accessed: 10th November 2016).
- Gates, D.M., Keegan, H.J., Schleiter, J.C. and Weidner, V.R. (1965). Spectral properties of plants. *Applied optics*, 4(1), pp.11-20.
- Geis, J.P., (2014). Application and timing effects of QoI and DMI fungicides and a foliar fertilizer on overall plant health and grain yield in corn.
- Genuer, R., Poggi, J.-M., and Tuleau, C. (2008). Random Forests: Some Methodological Insights. Research Report 6729. Institut National de Recherche en Informatique et en Automatique.
- Gilbert J, Tekauz A (2000) Review: recent developments in research on *Fusarium* head blight of wheat in Canada. *Can J Plant Pathol* 22 pp.1–8
- Gilchrist J. R. (2006). Gilchrist Photonics Ltd and Timo Hyvärinen, Spectral Imaging Ltd. *Hyperspectral Imaging Spectroscopy: A Look at Real-Life Applications*. Photonics.com. [On-line].
- Gnyp, M.L., Miao, Y., Yuan, F., Ustin, S.L., Yu, K., Yao, Y., Huang, S. and Bareth, G. (2014). Hyperspectral canopy sensing of paddy rice aboveground biomass at different growth stages. *Field Crops Research*, 155: pp. 42-55.
- Godfray, H.C.J., Beddington, J.R., Crute, I.R., Haddad, L., Lawrence, D., Muir, J.F., Pretty, J., Robinson, S., Thomas, S.M. and Toulmin, C., (2010). Food security: the challenge of feeding 9 billion people. *science*, 327(5967), pp. 812-818.
- Godoy, C.V., Koga, L.J. and Canteri, M.G. (2006). Diagrammatic scale for assessment of soybean rust severity. *Fitopatologia Brasileira*, 31(1), pp. 63-68.
- Gómez-Casero, M.T., Castillejo-González, I., García-Ferrer, A., Peña-Barragán, J.M., Jurado-Expósito, M., García-Torres, L. and López-Granados, F. (2010). Spectral discrimination of wild oat and canary grass in wheat fields for less herbicide application. *Agronomy for Sustainable Development*, 30(3), pp. 689-699.

- Gooding, M.J. and Davies, W.P., (1997). Wheat production and utilization: systems, quality and the environment. CAB international.
- Goswami RS, Kistler HC. (2004). Heading for disaster: *Fusarium graminearum* on cereal crops. *Mol Plant Pathol* 5, pp. 515–525
- Gowen, A.A., O'Donnell, C.P., Cullen, P.J., Downey, G., Frias, J.M., 2007. Hyperspectral imaging—an emerging process analytical tool for food quality and safety control. *Trends in Food Science and Technology* 18 (12), pp. 590–598
- Graham, R. D. and M. J. Webb. (1991). Micronutrients and disease resistance and tolerance in plants. pp. 329–370. In J. J. Mortvadt, F. R. Cox, L. M. Shuman and R. M. Welch (eds.), *Micronutrients in Agriculture*. 2nd ed. Soil Science Society American Book series no. 4, Madison, WI.
- Griffin, M.K. and Burke, H.H.K., (2003). Compensation of hyperspectral data for atmospheric effects. *Lincoln Laboratory Journal*, 14(1), pp.29-54.
- Grömping, U. (2009). Variable importance assessment in regression: Linear regression versus random forest. *The American Statistician*, 63(4), pp. 308–319.
- Guo, T.T., Guo, L., Wang, X.H., Li, M., (2009). Application of NIR spectroscopy in classification of plant species. In: *International Workshop on Education Technology and Computer Science*, Wuhan, Hubei, China, vol. 3, pp. 879–883.
- Gustavsson, J., Cederberg, C., Sonesson, U., Van Otterdijk, R. and Meybeck, A., (2011). *Global food losses and food waste* (pp. 1-38). Rome: FAO.
- Hahn, F., (2009). Actual pathogen detection: Sensors and algorithms—a review. *Algorithms* 2, pp. 301–338.
- Halcro, G., Corstanje, R., and Mouazen, A. (2013). Site-specific land management of cereal crops based on management zone delineation by proximal soil sensing. In: J. Stafford (Ed.), *Precision Agriculture* pp. 475-481. Wageningen, Netherlands: Wageningen Academic Publishers.
- Harmsen, K., Matar, A., Saxena, M., and Silim, S. (2001). Yield response to phosphorus fertilizer in a wheat-lentil rotation in a Mediterranean environment. *NJAS-Wageningen Journal of Life Sciences*, 49(4), pp. 385-403.
- Hazelton, P. A., and Murphy, B. W. (2007). *Interpreting soil test results: what do all the numbers mean* Australia. Australia: CSIRO publisher.
- Henson, J.M., French, R., (1993). The polymerase chain reaction and plant disease diagnosis. *Annual Review of Plant Pathology* 31, 81–109
- Herrera-Foessel, S.A., Singh, R.P., Huerta-Espino, J., Crossa, J., Yuen, J. and Djurle, A., (2006). Effect of leaf rust on grain yield and yield traits of durum wheats with race-specific and slow-rusting resistance to leaf rust. *Plant Disease*, 90(8), pp.1065-1072.
- Herrmann, I., Shapira, U., Kinast, S., Karnieli, A. and Bonfil, D.J., (2013). Ground-level hyperspectral imagery for detecting weeds in wheat fields. *Precision agriculture*, 14(6): pp. 637-659.
- Hillocks, R.J., (2012). Farming with fewer pesticides: EU pesticide review and resulting challenges for UK agriculture. *Crop Protection* 31 (1), pp. 85–93.
- Hole, D., Perkins, A., Wilson, J. D., Alexander, I. H., Grice, P. V., and Evans, A. (2005). Does organic farming benefit biodiversity? *Biological Conservation*, 122, pp. 113–130.
- Holmes, M.R.J., (1962). The magnesium requirements of arable crops. *Journal of the Science of Food and Agriculture*, 13(11), pp.553-556.
- Home Grown Cereal Authority (HGCA) (2008). *The spring wheat disease management guide*. Warwickshire: Home Grown Cereals Authority (HGCA Publication).

- Home Grown Cereal Authority HGCA (2010) foliar disease. Agriculture and Horticulture Development Board. Warwickshire: Home Grown Cereals Authority (HGCA Publication).
- Home Grown Cereal Authority HGCA (2012) septoria tritici in winter wheat. Agriculture and Horticulture Development Board. Warwickshire: Home Grown Cereals Authority (HGCA Publication).
- Home Grown Cereal Authority HGCA. (2014). Oilseed rape guide. Agriculture and Horticulture Development Board. Warwickshire: Home Grown Cereals Authority (HGCA Publication).
- Huadong, G. (2001). Applications of Radar Remote Sensing in China. New York: Taylor and Francis inc. 56.
- Huang, J., Wang, X., Li, X., Tian, H., and Pan, Z. (2013). Remotely sensed rice yield prediction using multi-temporal NDVI data derived from NOAA's-AVHRR. *PloS one*, 8(8), e70816.
- Huang, L.S., Ju, S.C., Zhao, J.L., Zhang, D.Y., Teng, L. and Yang, F. (2015). Hyperspectral Measurements for Estimating Vertical Infection of Yellow Rust on Winter Wheat Plant. *International Journal of Agriculture and Biology*, 17(6), pp. 1234-1241.
- Huang, M.Y., Huang, W.H., Liu, L.Y., Huang, Y.D., Wang, J.H., Zhao, C.H., Wan, A.M., (2004). Spectral reflectance feature of winter wheat single leaf infested with stripe rust and severity level inversion. *Transactions of the CSAE* 20 (1), pp. 176– 180
- Huang, W., Lamb, D.W., Niu, Z., Zhang, Y., Liu, L. and Wang, J. (2007). Identification of yellow rust in wheat using in-situ spectral reflectance measurements and airborne hyperspectral imaging. *Precision Agriculture*, 8(4-5), pp. 187-197.
- Huber, D. M. (1980). The role of mineral nutrition in defense. pp. 381– 406. In: J. G. Horsfall and E. B. Cowling (eds.), *Plant Pathology An Advanced Treatise*. Academic Press, New York, NY.
- Huete, A. R. (1988). A soil vegetation adjusted index (SAVI). *Remote Sensing of Environment*, 25: pp. 295 – 309.
- Hunt J., and Poole N. (2010). Simulating leaf area duration to predict yield response to foliar fungicide in wheat and barley. In: Dove H, Culvenor RA, editors. *Food security from sustainable agriculture*. Proceedings of 15th Agronomy Conference; 2010 Nov; Lincoln, New Zealand.
- Hunt, E.R., Doraiswamy, P.C., McMurtrey, J.E., Daughtry, C.S., Perry, E.M. and Akhmedov, B., (2013). A visible band index for remote sensing leaf chlorophyll content at the canopy scale. *International Journal of Applied Earth Observation and Geoinformation*, 21, pp.103-112
- Imathiu SM. (2008) *Fusarium langsethiae* infection and mycotoxin production in oats. Harper Adams University College, UK. PhD Thesis
- Imathiu, S.M., Edwards, S.G., Ray, R.V. and Back, M.A. (2013). *Fusarium langsethiae*—a HT-2 and T-2 Toxin Producer that Needs More Attention. *Journal of Phytopathology*, 161(1), pp.1-10
- Impey, L. (2012). *Fusarium* found on wheat leaves in western England. Available: <http://www.fwi.co.uk/articles/19/07/2012/134000/fusarium-found-on-wheat-leaves-in-western-england.htm>. Last accessed 14/10/2013
- Ines, A.V., Das, N.N., Hansen, J.W. and Njoku, E.G., (2013). Assimilation of remotely sensed soil moisture and vegetation with a crop simulation model for maize yield prediction. *Remote Sensing of Environment*, 138, pp.149-164.
- Ishikawa, S., Hare, M.C., Kettikewell, P.S., (2012). Effects of strobilurin fungicide programmes and fertiliser nitrogen rates on winter wheat: severity of *Septoria tritici*, leaf senescence and yield. *Journal of Agriculture Science* 150, pp. 411–426.
- Ishwaran, H. (2007). Variable Importance in Binary Regression Trees and Forests. *Electronic Journal of Statistics*, 1, pp. 519–537.

- Jebbouj R, El Yousfi B (2006) Effet comparé de l'inoculation par *Pyrenophora teres* f. *Maculate* et/ou la défoliation simultanée des quatre feuilles supérieures, sur le rendement grain de l'orge. *Al Awamia*. 120:50-71.
- Jebbouj R, El Yousfi B (2009) Barely yield losses due to defoliation of upper three leaves either healthy or infected at boot stage by *Pyrenophora teres* f. *teref.teres*. *Eur J Plant Pathol*. 125:303-315.
- Jelinek CF, Pohland AE, Wood GE. (1989) Worldwide occurrence of mycotoxins in foods and feeds-An update. *J AOAC Int*, 72, pp. 223–230.
- Jenkinson, P. and Parry, D.W. (1994). Splash dispersal of conidia of *Fusarium culmorum* and *Fusarium avenaceum*. *Mycological Research*, 98(5), pp.506-510.
- Jones, H. G., and Vaughan, R. A. (2010). *Remote sensing of vegetation: principles, techniques, and applications*. Oxford, UK: Oxford university press.
- Kautzman, M.E., Wickstrom, M.L. and Scott, T.A., (2015). The use of near infrared transmittance kernel sorting technology to salvage high quality grain from grain downgraded due to *Fusarium* damage. *Animal Nutrition*, 1(1), pp.41-46.
- Khonga, E.B. and Sutton, J.C., (1988). Inoculum production and survival of *Gibberella zeae* in maize and wheat residues. *Canadian Journal of Plant Pathology*, 10(3), pp.232-239.
- Khosla, R., Inman, D., Westfall, D. G., Reich, R. M., Frasier, M., Mzuku, M., Hornung, A. (2008). A synthesis of multi-disciplinary research in precision agriculture: site-specific management zones in the semi-arid Western Great Plains of the USA. *Precision Agriculture*, 9, pp. 85-100.
- Kipp, S., Mistele, B., and Schmidhalter, U. (2014). The performance of active spectral reflectance sensors as influenced by measuring distance, device temperature and light intensity. *Computers and Electronics in Agriculture*, 100, pp. 24–33.
- Knight, J.F., Lunetta, R.S., Ediriwickrema, J. and Khorram, S. (2006). Regional scale land cover characterization using MODIS-NDVI 250 m multi-temporal imagery: A phenology-based approach. *GIScience and Remote Sensing*, 43(1), pp.1-23.
- Kodaira, M., and Shibusawa, S. (2013). Using a mobile real-time soil visible-near infrared sensor for high resolution soil property mapping. *Geoderma*, 199, pp. 64-79.
- Kravchenko, A., and Bullock, D. (2000). Correlation of corn and soybean grain yield with topography and soil properties. *Agronomy Journal*, 92(1), pp. 75-83.
- Krishna, G., Sahoo, R.N., Pargal, S., Gupta, V.K., Sinha, P., Bhagat, S., Saharan, M.S., Singh, R. and Chattopadhyay, C. (2014). Assessing wheat yellow rust disease through hyperspectral remote sensing. *The International Archives of Photogrammetry, Remote Sensing and Spatial Information Sciences*, 40(8), pp.1413.
- Kuang, and Mouazen, A. M. (2013). Non-biased prediction of soil organic carbon and total nitrogen with vis-NIR spectroscopy, as affected by soil moisture content and texture. *Biosystems Engineering*, 114(3), pp. 249-258.
- Kuang, B., and Mouazen, A. (2011). Calibration of a visible and near infrared spectroscopy for soil analysis at field scales across three European farms. *European Journal of Soil Science*, 62(4), pp. 629-636.
- Kuang, B., Mahmood, H.S., Quraishi, M.Z., Hoogmoed, W.B., Mouazen, A.M. and van Henten, E.J., (2012). 4 Sensing Soil Properties in the Laboratory, In Situ, and On-Line: A Review. *Advances in Agronomy*, 114(1), pp.155-223
- Kuang, B., Tekin, Y., Mouazen, A.M., (2015). Comparison between artificial neural network and partial least squares for on-line visible and near infrared spectroscopy measurement of soil organic carbon, pH and clay content. *Soil and Tillage Research*, 146(Part B), pp. 243-252.
- Kweon, G., Lund, E., and Maxton, C. (2013). Soil organic matter and cation-exchange capacity sensing with on-the-go electrical conductivity and optical sensors. *Geoderma*, 199, pp. 80-89.
- Lacey J, Bateman GL, Mirocha CJ. (1999). Effects of infection time and moisture on the development of ear blight and deoxynivalenol production by *Fusarium* species in wheat. *Ann Appl Biol* 134, pp. 277–283.

- Lal, R. (2011). Sequestering carbon in soils of agro-ecosystems. *Food Policy*, 36, pp. 33-39.
- Landis, J. R., and Koch, G. G. (1977). The measurement of observer agreement for categorical data. *Biometrics*, 33, pp. 159-174.
- Larsolle, A., Muhammed, H.H., (2007). Measuring crop status using multivariate analysis of hyperspectral field reflectance with application to disease severity and plant density. *Precision Agriculture* 8 (1–2), pp. 37–47.
- Leach, C. M. (1967). Interaction of near-ultraviolet light and temperature on sporulation of the fungi *Alternaria*, *Cercospora*, *Fusarium*, *Helminthosporium*, and *Stemphylium*. *Canadian Journal of Botany*, 45(11), pp. 1999-2016.
- Lee, J. B., Woodhyatt, S., and Berman, M. (1990). Enhancement of high spectral resolution remote-sensing data by a noise-adjusted principal components transform. *IEEE Transactions on Geoscience and Remote Sensing*, 28: pp. 295–304
- Lee, K.J., Kang, S., Kim, M.S., Noh, S.H., (2005). Hyperspectral imaging for detecting defect on apples. ASABE Paper No. 053075, 2005 ASAE Annual International Meeting, Tampa, FL, 17–20 July, 2005.
- Leitch, M.H., Jenkins, P.D., (1995). Influence of nitrogen on the development of *Septoria* epidemics in winter wheat. *The Journal of Agricultural Science Cambridge* 124, pp. 361–368
- Lenk, S. and Buschmann, C., (2006). Distribution of UV-shielding of the epidermis of sun and shade leaves of the beech (*Fagus sylvatica* L.) as monitored by multi-colour fluorescence imaging. *Journal of Plant Physiology*, 163(12), pp.1273-1283.
- Lenk, S., Chaerle, L., Pfündel, E.E., Langsdorf, G., Hagenbeek, D., Lichtenthaler, H.K., Van Der Straeten, D., and Buschmann, C., (2007). Multispectral fluorescence and reflectance imaging at the leaf level and its possible applications. *Journal of Experimental Botany* 58 (4), pp. 807–814.
- Leslie, J.F., Summerell, B.A. (2006). *The Fusarium Laboratory Manual*. Blackwell Publishing, Ames, IA
- Liaw, A., and Wiener, M. (2015). Breiman and Cutler's Random Forests for Classification and Regression. R package version n 4.6-12. Retrieved from <https://cran.r-project.org/web/packages/randomForest/randomForest.pdf>
- Lobell, D. B. (2013). The use of satellite data for crop yield gap analysis. *Field Crops Research*, 143, 56–64.
- Lobell, D. B., Roberts, M. J., Schlenker, W., Braun, N., Little, B. B., Rejesus, R. M., and Hammer, G. L. (2014). Greater Sensitivity to Drought Accompanies Maize Yield Increase in the U.S. Midwest. *Science*, 344(6183), pp. 516–519.
- López, M.M., Bertolini, E., Olmos, A., Caruso, P., Gorris, M.T., Llop, P., Penyalver, R., and Cambra, M., (2003). Innovative tools for detection of plant pathogenic viruses and bacteria. *International Microbiology* 6, pp. 233–243.
- Lorenz, K., Lal, R., Preston, C., and Nierop, K. (2007). Strengthening the soil organic carbon pool by increasing contributions from recalcitrant aliphatic bio (macro) molecules. *Geoderma*, pp. 142, 1-10.
- Lorenzen, B. and Jensen, A., (1989). Changes in leaf spectral properties induced in barley by cereal powdery mildew. *Remote Sensing of Environment*, 27(2), pp. 201-209.
- Lowenberg-DeBoer, J., and Aghib, A. (1999). Average return and risk characteristics of site specific P and K management: eastern Corn Belt on-farm trial results. *Journal of Production Agriculture*, 12, pp. 276–282.
- Ma, J., Zhou, R., Dong, Y., Wang, L., Wang, X. and Jia, J., (2001). Molecular mapping and detection of the yellow rust resistance gene *Yr26* in wheat transferred from *Triticum turgidum* L. using microsatellite markers. *Euphytica*, 120(2), pp.219-226
- MacQueen, J., (1967), June. Some methods for classification and analysis of multivariate observations. In *Proceedings of the fifth Berkeley symposium on mathematical statistics and probability* (Vol. 1, No. 14, pp. 281-297).

- Mader, P., Fliessbach, A., Dubois, D., Gunst, L., Fried, P., Niggli, U., (2002). Soil fertility and biodiversity in organic farming. *Science* 296, pp. 1694–1697.
- Magan, N., and Evans, P. (2000). Volatiles as an indicator of fungal activity and differentiation between species, and the potential use of electronic nose technology for early detection of grain spoilage. *Journal of Stored Products Research*, 36(4), pp. 319-340.
- Magan, N., Hope, R., Colleate, A., and Baxter, E. S. (2002). Relationship between Growth and Mycotoxin Production by *Fusarium* species, Biocides and Environment. *European Journal of Plant Pathology*, 108(7), pp. 685-690.
- Mahesh, S., Manickavasagan, A., Jayas, D.S., Paliwal, J., White, N.D.G., (2008). Feasibility of near-infrared hyperspectral imaging to differentiate Canadian wheat classes. *Biosystems Engineering* 101 (1), pp. 50–57
- Mahlein, A.K., (2016). Plant disease detection by imaging sensors—parallels and specific demands for precision agriculture and plant phenotyping. *Plant Disease*, 100(2), pp.241-251.
- Mahlein, A.K., Steiner, U., Dehne, H.W. and Oerke, E.C., (2010). Spectral signatures of sugar beet leaves for the detection and differentiation of diseases. *Precision Agriculture*, 11(4), pp.413-431.
- Maleki, M., Mouazen, A., De Keterlaere, B., Ramon, H., and De Baerdemaeker, J. (2008). On-the-go variable-rate phosphorus fertilisation based on a visible and near infrared soil sensor. *Biosystems Engineering*, 99(1), pp. 35-46.
- Maleki, M.R., Mouazen, A.M., Ramon, H. and De Baerdemaeker, J., (2007). Optimisation of soil VIS–NIR sensor-based variable rate application system of soil phosphorus. *Soil and Tillage Research*, 94(1), pp. 239-250.
- Malo, D., Logsdon, S., Clay, D., Moore, D., and Tsegaye, T. (2008). Measuring nutrient removal, calculating nutrient budgets. In S. Logsdon, D. Clay, D. Moore, and T. Tsegaye (Eds.), *Soil Science Step-by-Step Field Analysis* (pp. 158–182). Madison, USA: Soil Science Society of America.
- Malthus, T.J., Madeira, A.C., (1993). High resolution spectroradiometry: spectral reflectance of field bean leaves infected by *Botrytis fabae*. *Remote Sensing of Environment* 45, pp. 107–116.
- Marin-González, O., Kuang, B., Quraishi, M., Munoz-Garcia, M., and Mouazen, A. (2013). on-line measurement of soil properties without direct spectral response in near infrared spectral range. *Soil and Tillage Research*, 132, pp. 21-29.
- Martens, H. and Naes, T. (1989). Assessment, validation and choice of calibration method. *Multivariate calibration*, pp. 237-266
- Matheron, G. (1963). Principles of geostatistics. *Economic Geology*, 58, pp. 1246–1266.
- McElhaney, R., Alvarez, A.M. and Kado, C.I., (1998). Nitrogen limits *Xanthomonas campestris* sp. *campestris* invasion of the host xylem. *Physiological and molecular plant pathology*, 52(1), pp.15-24.
- McMullen MP, Jones R, Gallenberg G (1997). Scab of wheat and barley: a re-emerging disease of devastating impact. *Plant Dis* 81, pp. 1340–1348
- Mehl, P.M., Chen, Y.R., Kim, M.S., Chan, D.E., (2004). Development of hyperspectral imaging technique for the detection of apple surface defects and contaminations. *Journal of Food Engineering* 61 (1), pp. 67–81.
- Mielecki, R.V. (2011). *Agricultural Dialogue* 14 BASF the chemical company. Available: [http://www.agro.basf.com/agr/AP-Internet/en\\_GB/function/conversions:/publish/upload/news\\_room/agricultural\\_dialogue/BASF\\_newsletter\\_ENG\\_low.pdf](http://www.agro.basf.com/agr/AP-Internet/en_GB/function/conversions:/publish/upload/news_room/agricultural_dialogue/BASF_newsletter_ENG_low.pdf). Last accessed 10th november 2013.
- Milus, E.A., Kristensen, K., and Hovmøller, M.S. (2009). Evidence for increased aggressiveness in a recent widespread strain of *Puccinia striiformis* f. sp. *tritici* causing stripe rust of wheat. *Phytopathology*, 99(1), pp. 89-94.

- Mkhabela, M., Bullock, P., Raj, S., Wang, S., and Yang, Y. (2011). Crop yield forecasting on the Canadian Prairies using MODIS NDVI data. *Agricultural and Forest Meteorology*, 151(3), pp. 385-393.
- Monteith, J.L. and Unsworth, M.H., (2008). Microclimatology of radiation (iii) interception by plants and animals. *Principles of Environmental Physics*, pp.116-133.
- Moshou, D., Bravo, C., West, J., Wahlen, S., McCartney, A., Ramon, H. (2004). Automatic detection of 'yellow rust' in wheat using reflectance measurements and neural networks. *Computers and Electronics in Agriculture* 44 (3), pp. 173–188.
- Moshou, D., Bravo, C., Oberti, R., West, J., Bodria, L., McCartney, A. and Ramon, H. (2005). Plant disease detection based on data fusion of hyper-spectral and multi-spectral fluorescence imaging using Kohonen maps. *Real-Time Imaging*, 11(2), pp.75-83.
- Moshou, D., Pantazi, X.E., Kateris, D. and Gravalos, I., (2014). Water stress detection based on optical multisensor fusion with a least squares support vector machine classifier. *Biosystems Engineering*, 117, pp. 15-22.
- Moshou, D, Bravo, C, Oberti, R, West, J.S, Ramon H., Vougioukas S., Bochtis D., (2011). Intelligent multi-sensor system for the detection and treatment of fungal diseases in arable crops, *Biosyst. Eng.*, 108, pp. 311–32
- Moss, S., (2013). Black-grass (*Alopecurus myosuroides*). A Rothamsted Research technical publication
- Mouazen, A. M. (2006). Soil Survey Device. International publication published under the patent cooperation treaty (PCT). World Intellectual Property Organization, International Bureau. International Publication Number: WO2006/015463; PCT/BE2005/000129; IPC: G01N21/00; G01N21/00.
- Mouazen, A., and Kuang, B. (2016). on-line visible and near infrared spectroscopy for in-field phosphorous management. *Soil and Tillage Research*, 156, pp. 471-477.
- Mouazen, A., De Baerdemaeker, J., and Ramon, H. (2005). Towards development of on-line soil moisture content sensor using a fibre-type NIR spectrophotometer. *Soil and Tillage Research*, 80(1-2), pp. 171-183.
- Mouazen, A., De Baerdemaeker, J., and Ramon, H. (2006). Effect of wavelength range on the measurement accuracy of some selected soil constituents using visual-near infrared spectroscopy. *Journal of Near Infrared Spectroscopy*, 14, pp. 189–199.
- Mouazen, A.M., Anthonis, J., and Ramon, H., (2005). An automatic depth control system for on-line measurement of spatial variation in soil compaction, Part 4: improvement of compaction maps by using a proportional integrative derivative depth controller. *Biosystems Engineering*, 90(4), pp. 409-418.
- Muhammed, H.H., (2002). Using hyperspectral reflectance data for discrimination between healthy and diseased plants, and determination of damage-level in diseased plants. In: *IEEE: Proceedings of the 31st Applied Imagery Pattern Recognition Workshop*, pp. 49–54.
- Muhammed, H.H., (2005). Hyperspectral crop reflectance data for characterizing and estimating fungal disease severity in wheat. *Biosystems Engineering* 91 (1), pp. 9–20.
- Mulla, D. (2013). Twenty Five Years of Remote Sensing in Precision Agriculture: Key Advances and Remaining Knowledge Gaps. *Biosystems Engineering*, 114, pp. 358-371.
- Murray, G. M., Ellison, P. J., Watson, A., and Cullis, B. R. (1994). The relationship between wheat yield and stripe rust as affected by length of epidemic and temperature at the grain development stage of crop growth. *Plant Pathology*, 43, pp. 397–405.
- Mzuku, M., Khosla, R., Reich, R., Inman, D., Smith, F., and MacDonald, L. (2005). Spatial variability of measured soil properties across site-specific management zones. *Soil Science Society of America Journal*, 69, pp. 1572-1579.
- Naidu, R.A., Perry, E.M., Pierce, F.J., Mekuria, T., (2009). The potential of spectral reflectance technique for the detection of Grapevine leafroll-associated virus-3 in two red-berried wine grape cultivars. *Computers and Electronics in Agriculture* 66, pp. 38–45.

- Oberti, R., Marchi, M., Tirelli, P., Calcante, A., Iriti, M., and Borghese, A. N. (2014). Automatic detection of powdery mildew on grapevine leaves by image analysis: Optimal view-angle range to increase the sensitivity. *Computers and Electronics in Agriculture*, 104, pp. 1-8.
- Oerke, E.C. and Steiner, U., (2010). Potential of digital thermography for disease control. In *Precision Crop Protection-the Challenge and Use of Heterogeneity* Springer Netherlands, pp. 167-182.
- Oerke, E.C., (2006). Crop losses to pests. *The Journal of Agricultural Science*, 144(1), pp.31-43.
- Oerke, E.C., (2006). Crop losses to pests. *The Journal of Agricultural Science*, 144(01), pp.31-43
- Okamoto, H. and Lee, W.S. (2009). Green citrus detection using hyperspectral imaging. *Computers and Electronics in Agriculture*, 66(2): pp.201-208.
- Olsen, S.R., (1954). Estimation of available phosphorus in soils by extraction with sodium bicarbonate. United States Department Of Agriculture; Washington
- OMAFRA Staff (2009) Cereals: Planting and Crop Development, Available at: <http://www.omafra.gov.on.ca/english/crops/pub811/4planting.htm> (Accessed: 30th November 2016).
- Osborne L.E. and J.M. Stein, (2007). Epidemiology of Fusarium head blight on small-grain cereals. *International Journal of Food Microbiology* 119 (1–2), pp. 103–108.
- Palm, R. (1997). Les modèles de prévision statistique: cas du modèle Eurostat-Agromet. In B. Tychon, and V. Tonnard (Eds.), *Estimation de la production agricole à une échelle régionale Luxembourg: Official Publications of the EU*. pp. 85-108.
- Pantazi, X.-E., Moshou, D., Alexandridis, T., Whetton, R., and Mouazen, A. (2016). Wheat yield prediction using machine learning and advanced sensing technologies. *Computers and Electronics in Agriculture*, 121, pp. 57-65.
- Pantazi, X.E., Moshou, D., Oberti, R., West, J., Mouazen, A.M. and Bochtis, D., 2017. Detection of biotic and abiotic stresses in crops by using hierarchical self organizing classifiers. *Precision Agriculture*, 18(3), pp.383-393
- Parikka P, Hietaniemi V, Ram S, Jalli H. (2007) The effect of cultivation practices on Fusarium langsethiae infection of oats and barley. *Proceedings of the COST SUSVAR Fusarium Workshop –Fusarium Diseases in Cereals*. pp 15–18.
- Park, R. F., Ash, G. J., and Rees, R. G. (1992). Effect of temperature on the response of some Australian wheat cultivars to *Puccinia striiformis* f. sp. *tritici*. *Mycological Research*, 96, pp. 166–170
- Parker, S.R., Shaw, M.W. and Royle, D.J. (1995). The reliability of visual estimates of disease severity on cereal leaves. *Plant Pathology*, 44(5), pp. 856-864.
- Parry DW, Jenkinson P, McLead L. (1995). Fusarium ear blight (scab) in small grain cereals—a review. *Plant Pathol* 44, pp. 207–238
- Parry, D.W., Jenkinson, P. and McLeod, L., (1995). Fusarium ear blight (scab) in small grain cereals—a review. *Plant pathology*, 44(2), pp.207-238.
- Paul, P.A., El-Allaf, S.M., Lipps, P.E. and Madden, L.V., (2004). Rain splash dispersal of *Gibberella zeae* within wheat canopies in Ohio. *Phytopathology*, 94(12), pp.1342-1349.
- Paul, P.A., Lipps, P.E. and Madden, L.V., (2005). Relationship between visual estimates of Fusarium head blight intensity and deoxynivalenol accumulation in harvested wheat grain: A meta-analysis. *Phytopathology*, 95(10), pp. 1225-1236.
- Paveley, N., Blake, J., Gladders, P., and Cockerell, V. (2012). *Wheat disease management guide*. HGCA.
- Peiris, K.H., Pumphrey, M.O. and Dowell, F.E., (2009). NIR absorbance characteristics of deoxynivalenol and of sound and Fusarium-damaged wheat kernels. *Journal of Near Infrared Spectroscopy*, 17(4), pp.213-221.



- Pereyra, S.A. and Dill-Macky, R., (2008). Colonization of the residues of diverse plant species by *Gibberella zeae* and their contribution to *Fusarium* head blight inoculum. *Plant Disease*, 92(5), pp.800-807. Perrenoud S (1990) Potassium and plant health. IPI-Research Topics No. 3, 2nd edn. International Potash Institute, Basel, pp. 365
- Peteinatos, G.G., Korsath, A., Berge, T.W. and Gerhards, R. (2016). Using Optical Sensors to Identify Water Deprivation, Nitrogen Shortage, Weed Presence and Fungal Infection in Wheat. *Agriculture*, 6(2), pp. 24.
- Pillinger, C., Evans, E.J., Whaley, J.M., Knight, S.M. and Poole, N., 2004. Managing early-drilled winter wheat: seed rates, varieties and disease control. HGCA Project Report
- Pimentel, D., Harvey, C., Resosudarmo, P., Sinclair, K., Kurz, D., McNair, M., Crist, S., Shpritz, L., Fitton, L., Saffouri, R. and Blair, R., (1995). Environmental and economic costs of soil erosion and conservation benefits. *Science-AAAS-Weekly Paper Edition*, 267(5201), pp.1117-1122.
- Pimentel, D., Wilson, C., McCullum, C., Huang, R., Dwen, P., Flack, J., Tran, Q., Saltman, T. and Cliff, B., (1997). Economic and environmental benefits of biodiversity. *BioScience*, 47(11), pp.747-757.
- Pinter, JR, P.J. and Jackson, R.D. (1985). Sun-angle and canopy-architecture effects on the spectral reflectance of six wheat cultivars. *INT. J. REMOTE SENSING*, 6(12): pp. 1813-1825.
- Pisek, J., Chen, J.M., Miller, J.R., Freemantle, J.R., Peltoniemi, J.I. and Simic, A., (2010). Mapping forest background reflectance in a boreal region using multiangle compact airborne spectrographic imager data. *IEEE Transactions on Geoscience and Remote Sensing*, 48(1), pp.499-510. Polder, G., Van Der Heijden, G.W.A.M., Waalwijk, C. and Young, I.T., (2005). Detection of *Fusarium* in single wheat kernels using spectral imaging. *Seed Science and Technology*, 33(3), pp. 655-668.
- Polischuk, V.P., Shadchina, T.M., Kompanetz, T.I., Budzanivskaya, I.G., Sozinov, A., (1997). Changes in reflectance spectrum characteristic of *Nicotiana debneyi* plant under the influence of viral infection. *Archives of Phytopathology and Plant Protection* 31 (1), pp. 115–119.
- Polischuk, V.P., Shadchina, T.M., Kompanetz, T.I., Budzanivskaya, I.G., Sozinov, A., (1997). Changes in reflectance spectrum characteristic of *Nicotiana debneyi* plant under the influence of viral infection. *Archives of Phytopathology and Plant Protection* 31 (1), pp. 115–119.
- Pontius, J., Hallett, R., Martin, M., (2005). Assessing hemlock decline using visible and near-infrared spectroscopy: indices comparison and algorithm development. *Applied Spectroscopy* 59 (6), pp. 836–843.
- Poutaraud, A., Latouche, G., Martins, S., Meyer, S., Merdinoglu, D. and Cerovic, Z.G., (2007). Fast and local assessment of stilbene content in grapevine leaf by in vivo fluorometry. *Journal of agricultural and food chemistry*, 55(13), pp.4913-4920.
- Prabhu AS, Fageria NK, Huber DM, Rodrigues FA (2007) Potassium and plant disease. In: Datnoff LE, Elmer WH, Huber DM (eds) Mineral nutrition and plant disease. The American Phytopathological Soc Press, Saint Paul, pp. 57– 78
- Pradhan, B., Chaudhari, A., Adinarayana, J., and Buchroithner, M. (2012). Soil erosion assessment and its correlation with landslide events using remote sensing data and GIS: a case study at Penang Island, Malaysia. *Environmental monitoring and assessment*, 184(2), pp. 715-727.
- Prescott, J.M., Burnett, P.A., Saari, E.E., Ransom, J.K., Bowman, J., De Milliano, W.A.J., Singh, R.P. and
- Prithviraj, B., Vikram, A., Kushalappa, A.C., Yaylayam, V., (2004). Volatile metabolite profiling for the discrimination of onion bulbs infected by *Erwinia carotovora* ssp. *carotovora*, *Fusarium oxysporum* and *Botrytis allii*. *European Journal of Plant Physiology* 110, pp. 371–377.
- Quaedvlieg, W., Verkley, G.J.M., Shin, H.D., Barreto, R.W., Alfenas, A.C., Swart, W.J., Groenewald, J.Z. and
- Ramamurthy, R., Canning, C. F., Scheetz, J. P., and Farman, A. G. (2004). Impact of ambient lighting intensity and duration on the signal-to-noise ratio of images from photostimulable phosphor plates processed using DenOptix® and ScanX® systems. *Dentomaxillofac Radiol*, 33(5), pp. 307-11

- Ramon, H., Anthonis, J., Vrindts, E., Delen, R., Reumers, J., Moshou, D., Deprez, K., De Baerdemaeker, J., Feyaerts, F., Van Gool, L., DeWinne, R., Van den Bulcke, R., (2002). Development of a weed activated spraying machine for targeted application of herbicides. *Aspects of Applied Biology* 66, pp. 147–164.
- Raper T. B. and Varco J. J. (2015) Canopy-scale wavelength and vegetative index sensitivities to cotton growth parameters and nitrogen status. *Precision Agriculture*, 16(1), pp. 62–76
- Raun, W., Soile, J., Johnson, G., Stone, M., Whitney, R., Lees, H., Philips, S. (1998). Microvariability in soil test, plant nutrient and yield parameters in Bermudagrass. *Soil Science Society of America Journal*, 62, pp. 683–690.
- Rauner, J. L. (1976). Deciduous forests. *Vegetation and the Atmosphere*, 2, pp. 241-264.
- Rautiainen, M., Lang, M., Mõttus, M., Kuusk, A., Nilson, T., Kuusk, J. and Lükk, T., (2008). Multi-angular reflectance properties of a hemiboreal forest: An analysis using CHRIS PROBA data. *Remote Sensing of Environment*, 112 (5), pp. 2627-2642
- Ray, M., Ray, A., Dash, S., Mishra, A., Achary, K.G., Nayak, S. and Singh, S., (2017). Fungal disease detection in plants: Traditional assays, novel diagnostic techniques and biosensors. *Biosensors and Bioelectronics*, 87, pp.708-723.
- Reeves, D. (1997). The role of soil organic matter in maintaining soil quality in continuous cropping systems. *Soil and Tillage Research*, 43, pp. 131–167.
- Reis, E.M., Boareto, C., Danelli, A.L.D. and Zoldan, S.M., (2016). Anthesis, the infectious process and disease progress curves for fusarium head blight in wheat. *Summa Phytopathologica*, 42(2), pp.134-139.
- Rengasamy, P., Greene, R.S.B. and Ford, G.W., (1986). Influence of magnesium on aggregate stability in sodic red-brown earths. *Soil Research*, 24(2), pp.229-237.
- Renouf, M., Wegener, M., and Pagan, R. (2010). Life cycle assessment of Australian sugarcane production with a focus on sugarcane growing. *The International Journal of Life Cycle Assessment*, 15(9), pp. 927–937.
- Reynolds M., Foules M.J., Slafer G.A., Berry P., Parry M.A., Snape J.W., Angus W.J. (2009). Raising wheat potential. *Journal of Experimental Botany*. 60: pp. 1899–1918.
- Rijks, D., Rembold, F., Nègre, T., Gommès, R., and Cherlet, M. (2003). Crop and rangeland monitoring in eastern Africa for early warning and food security. Nairobi (Kenya): International Workshop on Crop Rangeland Monitoring in Eastern Africa for Early Warning and Food Security.
- Roberts, M.R. and Paul, N.D., (2006). Seduced by the dark side: integrating molecular and ecological perspectives on the influence of light on plant defence against pests and pathogens. *New Phytologist*, 170(4), pp.677-699.
- Roberts, M., Schlenker, W., and Eyer, J. (2012). Agronomic weather measures in econometric models of crop yield with implications for climate change. *American Journal of Agricultural Economics*, 95(2), pp. 236–243.
- Roggo, Y., Duponchel, L., and Huvenne, J.P. (2003). Comparison of supervised pattern recognition methods with McNemar's statistical test: application to qualitative analysis of sugar beet by near-infrared spectroscopy. *Analytica Chimica Acta*, 477(2), pp. 187–200.
- Rose, S.P., Pirgozliev, V.R., McCracken, K.J., McNab, J.M. and Miller, H.M., (2001). Specific weight and quality measurements on the nutritional value of four wheat cultivars for broiler chickens. *ASPECTS OF APPLIED BIOLOGY*, 64, pp.85-86.
- Rossel, R.V., Walvoort, D.J.J., McBratney, A.B., Janik, L.J. and Skjemstad, J.O., (2006). Visible, near infrared, mid infrared or combined diffuse reflectance spectroscopy for simultaneous assessment of various soil properties. *Geoderma*, 131(1), pp.59-75.
- Rossi V, Ravanetti A, Patteri E, Giosue S. (2001) Influence of temperature and humidity on the infection of wheat spikes by some fungi causing fusarium head blight. *J Plant Pathol* 83, pp.189–198.

- Rossi V, Ravanetti A, Patteri E, Giosue S. (2001) Influence of temperature and humidity on the infection of wheat spikes by some fungi causing fusarium head blight. *J Plant Pathol*, 83, pp. 189–198.
- Rotter, B.A., Prelusky, D.B., Pestka, J.J. (1996). Toxicology of deoxynivalenol (vomitoxin). *Journal of Toxicology and Environmental Health* 48, pp. 1–34.
- Rozalski, K., Pudelko, J., and Skrzypczak, G. (1998). Disease incidence in winter wheat and spring triticale as influenced by crop protection and nitrogen. *Progress in Plant Protection*, 38, pp. S.551–S.554.
- Ruiz-Ruiz, S., Ambrós, S., Carmen Vives, M., Navarro, L., Moreno, P., Guerri, J., (2009). Detection and quantification of Citrus leaf blotch virus by TaqMan real-time RTPCR. *Journal of Virological Methods* 160 (1–2), pp. 57–62.
- Sache, I., (2000). Short-distance dispersal of wheat rust spores. *Agronomie*,20(7), pp.757-767.
- Safavi, S.A., (2015). Effects of yellow rust on yield of race-specific and slow rusting resistant wheat genotypes. *Journal of Crop Protection*, 4(3), pp. 395-408.
- Saiyed, I.M., Bullock, P.R., Sapirstein, H.D., Finlay, G.J. and Jarvis, C.K., (2009). Thermal time models for estimating wheat phenological development and weather-based relationships to wheat quality. *Canadian Journal of Plant Science*, 89(3), pp.429-439.
- Salas B., B.J. Steffenson, H.H. Casper, B. Tacke, L.K. Prom, T.G. Fetch Jr. and P.B. Swhwarz, (1999). Fusarium species pathogenic to barley and their associated mycotoxins. *Plant Disease* 83, pp. 667–674.
- Sankaran, S., Mishra, A., Ehsani, R., and Davis, C. (2010). A review of advanced techniques for detecting plant diseases. *Computers and Electronics in Agriculture*, 72(1), pp. 1-13.
- Saponari, M., Manjunath, K., Yokomi, R.K., (2008). Quantitative detection of Citrus tristeza virus in citrus and aphids by real-time reverse transcription-PCR (TaqMan®). *Journal of Virological Methods* 147 (1), pp. 43–53.
- Sarrigiannis, P. G., Zhao, Y., Wei, H.-L., Billings, S. A., Fotheringham, J., and Hadjivassiliou, M. (2014). Quantitative EEG analysis using error reduction ratio-causality test; validation on simulated and real EEG data. *Clinical Neurophysiology*, 125(1), pp. 32–46.
- Savitzky, A. and Golay, M.J., (1964). Smoothing and differentiation of data by simplified least squares procedures. *Analytical chemistry*, 36(8), pp.1627-1639.
- Schaad, N.W., Frederick, R.D., (2002). Real-time PCR and its application for rapid plant disease diagnostics. *Canadian Journal of Plant Pathology* 24 (3), pp. 250–258.
- Schmale, D. G., III, and Bergstrom, G. C. (2003). Fusarium head blight in wheat. *The Plant Health Instructor*. <http://dx.doi.org/10.1094/PHI-I-2003-0612-01>.
- Schröder, J., (1964). Untersuchungen über die Keimung der Uredosporen des Gelbrostes (*Puccinia striiformis* West.). Technische Hochschule Carolo-Wilhelmina zu Braunschweig.
- Schuh, W., (1990). Influence of tillage systems on disease intensity and spatial pattern of Septoria leaf blotch. *Phytopathology*, 80(12), pp.1337-1340.
- Sentelhas, P.C., Pedro, M.J., and Felicio, J.C. (1993). Effects of different conditions of irrigation and crop density on microclimate and occurrence of spot blotch and powdery mildew. *Bragantia*, 52, pp. 45–52.
- Sharma, K., Grace, J., Mandal, U., Gajbhiye, P., Srinivas, K., Korwar, G., Yadav, S. (2008). Evaluation of long-term soil management practices using key indicators and soil quality indices in semi-arid tropical Alfisol. *Soil research*, 46, pp. 368–377.
- Shearman, V.J., Sylvester-Bradley, R., Scott, R.K. and Foulkes, M.J., (2005). Physiological processes associated with wheat yield progress in the UK. *Crop Science*, 45(1), pp.175-185

- Shibusawa, S., Imade Anom, S., Sato, S., Sasao, A., and Hirako, S. (2001). Soil mapping using the real-time soil spectrophotometer. In G. Grenier, and S. Blackmore, Third European Conference on Precision Agriculture (Vol. 1, pp. 497–508). Montpellier, France: ECPA.
- Shibusawa, S., Sato, H., Sasao, A., Hirako, S. and Otomo, A., (2000). A revised soil spectrophotometer. IFAC Proceedings Volumes, 33(29), pp.231-236.
- Shier, N.W., Kelman, J., Dunson, J.W., (1984). A comparison of crude protein, moisture, ash and crop yield between organic and conventionally grown wheat. *Nutrition Reports International* 30, pp. 71–76.
- Shukla, M., Lal, R., and Ebinger, M. (2006). Determining soil quality indicators by factoranalysis. *Soil and Tillage Research*, 87, pp. 194–204.
- Sighicelli, M., Colao, F., Lai, A., Patsaeva, S., (2009). Monitoring post-harvest orange fruit disease by fluorescence and reflectance hyperspectral imaging. *ISHS Acta Horticulturae* 817, pp. 277–284.
- Singh, C.B., Jayas, D.S., Paliwal, J. and White, N.D.G., (2007). Fungal detection in wheat using near-infrared hyperspectral imaging. *Transactions of the ASABE*, 50(6), pp.2171-2176.
- Singh, R.P., Duveiller, E. and Huerta-Espino, J., (2012). Virulence to yellow rust resistance gene Yr27: a new threat to stable wheat production in Asia. In *Meeting the Challenge of Yellow Rust in Cereal Crops* pp. 25.
- Smith, S. W. (1999). *The Scientist and Engineer's Guide to Digital Signal Processing*. 2nd ed. San Diego: California Technical Publishing, Chapter 2, pp. 13-16).
- Snoeiijers, S.S., Pérez-García, A., Joosten, M.H. and De Wit, P.J., (2000). The effect of nitrogen on disease development and gene expression in bacterial and fungal plant pathogens. *European Journal of Plant Pathology*, 106(6), pp.493-506.
- Sohne, W., (1958). Fundamentals of pressure distribution and soil compaction under tractor tires. *Agricultural Engineering*, 39, p.290.
- Spinelli, F., Noferini, M., Costa, G., (2006). Near infrared spectroscopy (NIRs): Perspective of fire blight detection in asymptomatic plant material. *Proceeding of 10th International Workshop on Fire Blight. Acta Horticulturae* 704, pp. 87–90.
- Stenberg, B., Rossel, R.A.V., Mouazen, A.M. and Wetterlind, J., 2010. Chapter five-visible and near infrared spectroscopy in soil science. *Advances in agronomy*, 107, pp.163-215.
- Stokes, D.T., Sylvester-Bradley, R., Clare, R., Scott, R.K., Hopkinson, J., Milford, G.F.J. and Salmon, S.E., 1998. An integrated approach to nitrogen nutrition for wheat. *HGCA Project Report (United Kingdom)*.
- Strobl, C., Boulesteix, A., Kneib, T., Augustin, T., and Zeileis, A. (2008). Conditional Variable Importance for Random Forests. *BMC Bioinformatics*, 9, pp. 307.
- Suffert, F., Sache, I. and Lannou, C., (2011). Early stages of septoria tritici blotch epidemics of winter wheat: build-up, overseasoning, and release of primary inoculum. *Plant Pathology*, 60(2), pp.166-177.
- Sundaram, J., Kandala, C.V., Butts, C.L., (2009). Application of near infrared (NIR) spectroscopy to peanut grading and quality analysis: Overview. *Sensing and Instrumentation for Food Quality and Safety* 3 (3), pp. 156–164
- sung, J.-M., Cook, R.G., (1981). Effect of water potential on reproduction and spore germination by *Fusarium roseum* ‘Graminearum’, ‘Culmorum’, and ‘Avenaceum’. *Phytopathology* 71, pp. 499–504.
- Sutton, J.C. (1982). Epidemiology of wheat head blight and maize ear rot caused by *Fusarium graminearum*. *Canadian Journal of Plant Pathology*, 4, pp. 195.
- Sylvester-Bradley R., Kindred D. (2009). Analysing nitrogen responses of cereals to prioritise routes to the improvement of nitrogen use efficiency. *Journal of Experimental Botany*, 60, pp. 1939–51.

- Sylvester-Bradley, R., Lord, E., Sparkes, D.L., Scott, R.K., Wiltshire, J.J.J. and Orson, J., (1999). An analysis of the potential of precision farming in Northern Europe. *Soil use and management*, 15(1), pp.1-8.
- Tallada, J.G., Nagata, M., Kobayashi, T., (2006). Detection of bruises in strawberries by hyperspectral Imaging. ASABE Paper No. 063014, 2006 ASABE Annual International Meeting, Portland, Oregon, 9–12 July 2006.
- Teich, A.H. and Hamilton, J.R., (1985). Effect of cultural practices, soil phosphorus, potassium, and pH on the incidence of *Fusarium* head blight and deoxynivalenol levels in wheat. *Applied and environmental microbiology*,49(6), pp.1429-1431
- Tekin, Y., Kuang, B., and Mouazen, A. M. (2013). Potential of on-line visible and near infrared spectroscopy for measurement of pH for deriving variable rate lime recommendations. *Sensors*, 13(8), pp. 10177-10190.
- Thate, A., Schumann, S., Hanschmann, G. and Urban, Y., (2008). Auftreten von Ährenfusariosen und Mykotoxinen in Sachsen und Ergebnisse der Vor-und Nachernteuntersuchungen von Winterweizen 2007. *Nachrichtenbl. Dtsch. Pflanzenschutzdienst*, 60, p.117.
- Thomas, J.R. and Gausman, H.W. (1977). Leaf reflectance vs. leaf chlorophyll and carotenoid concentrations for eight crops. *Agronomy journal*,69(5), pp. 799-802
- Thomas, S., Wahabzada, M., Kuska, M.T., Rascher, U. and Mahlein, A.K., (2017). Observation of plant–pathogen interaction by simultaneous hyperspectral imaging reflection and transmission measurements. *Functional Plant Biology*, 44(1), pp.23-34.
- Thorp, K. R., Ale, S., Bange, M. P., Barnes, E. M., Hoogenboom, G., Lascano, R. J., White, J. W. (2014). Development and Application of Process-based Simulation Models for Cotton Production: A Review of Past, Present, and Future Directions. *The Journal of Cotton Science*, 18, pp. 10–47.
- Tiessen, H., Cuevas, E., and Chacon, P. (1994). The role of soil organic matter in sustaining soil fertility. *Nature*, 371, pp. 783–785.
- Tilman, D., (1999). Global environmental impacts of agricultural expansion: the need for sustainable and efficient practices. *Proceedings of the National Academy of Sciences*, 96(11), pp. 5995-6000
- Timlin, D., Williams, R., Ahuja, L., and Heathman, G. (2004). Simple parametric methods to estimate soil water retention and hydraulic conductivity. *Developments in Soil Science*, 30, pp. 71–93.
- Tiwari, A.N., Nawale, V.P., Tambe, J.A. and Satyakumar, Y., (2010). Variation in calcium and magnesium ratio with increasing electrical conductivity of groundwater from shallow basaltic aquifers of Maharashtra (India). *Journal of environmental science and engineering*, 52(4), pp.311-314.
- Tothill, I.E., (2001). Biosensors developments and potential applications in the agricultural diagnosis sector. *Computers and Electronics in Agriculture*,30(1), pp.205-218.
- Vachaud, G., Passerat de Silans, A., Balabanis, P. and Vauclin, M., (1985). Temporal stability of spatially measured soil water probability density function. *Soil Science Society of America Journal*, 49(4), pp .822-828
- Van Beek, J., Tits, L., Somers, B., and Coppin, P. (2013). Stem water potential monitoring in pear orchards through WorldView-2 multispectral imagery. *Remote Sensing*, 5(12), pp. 6647-6666.
- Van der Meer, F. and De Jong, S.M., (2000). Improving the results of spectral unmixing of Landsat Thematic Mapper imagery by enhancing the orthogonality of end-members. *International Journal of Remote Sensing*,21(15): pp. 2781-2797.
- Verreet JA, Klink H, Hoffmann GM. (2000). Regional monitoring for disease prediction and optimization of plant protection measures: the IPM wheat model. *Plant Dis*. 84:816–26
- von Tiedemann, A., (1996). Single and combined effects of nitrogen fertilization and ozone on fungal leaf diseases on wheat. *Zeitschriftfur Pflanzenkrankheiten und Planzenschutz* 103, pp. 409–419.

- Vrindts, E., Reyniers, M., Darius, P., Gilot, M., Sadaoui, Y., Frankinet, M., Hanquet, B. and Destain, M.F., 2003. Analysis of soil and crop properties for precision agriculture for winter wheat. *Biosystems engineering*, 85(2), pp.141-152.
- Waiser, T.H., Morgan, C.L., Brown, D.J. and Hallmark, C.T., (2007). In situ characterization of soil clay content with visible near-infrared diffuse reflectance spectroscopy. *Soil Science Society of America Journal*, 71(2), pp.389-396.
- Wakeel, A., (2013). Potassium–sodium interactions in soil and plant under saline-sodic conditions. *Journal of Plant Nutrition and Soil Science*, 176(3), pp.344-354.
- Wang, X., Zhao, C., Guo, N., Li, Y., Jian, S. and Yu, K., (2015). Determining the canopy water stress for spring wheat using canopy hyperspectral reflectance data in loess plateau semiarid regions. *Spectroscopy Letters*, 48(7), pp.492-498.
- Wang, Y.P. and Shen, Y., 2015. Identifying and characterizing yield limiting soil factors with the aid of remote sensing and data mining techniques. *Precision agriculture*, 16(1), pp.99-118.
- Webster, R. (2007). Analysis of variance, inference, multiple comparisons and sampling effects in soil research. *European Journal of Soil Science*, 58(1), pp. 74-82.
- Wei, H., Billings, S., and Liu, J. (2004). *International Journal of Control*. Term and variable selection for non-linear system identification, 77, pp. 86-110.
- Wellings, C.R., (2011). Global status of stripe rust: a review of historical and current threats. *Euphytica*, 179(1), pp.129-141.
- West, J.S., Bravo, C., Oberti, R., Lemaire, D., Moshou, D. and McCartney, H.A., (2003). The potential of optical canopy measurement for targeted control of field crop diseases. *Annual review of Phytopathology*, 41(1), pp.593-614.
- West, J.S., Atkins, S.D., Emberlin, J. and Fitt, B.D., 2008. PCR to predict risk of airborne disease. *Trends in microbiology*, 16(8), pp.380-387.
- Whetton R.L., Waive T.W. and Mouazen, A.M. (2016b). Optimising configuration of a hyperspectral imager for on-line field measurement of wheat canopy. *Biosystems engineering* (accepted).
- Whetton, R., Zhao, Y., Nawar, S., and Mouazen, A. (2016a). A new non-linear parametric modelling method to quantify influence of soil properties on crop yields. Part 1: Methodology. *Soil Research*, (Under review).
- Whetton, R.L., Waive, T.W. and Mouazen, A.M. (2016c). Hyperspectral measurements of yellow rust and fusarium in cereal crops: Part 1: Laboratory study *Biosystems engineering* (Under review).
- Whetton, R.L., Waive, T.W. and Mouazen, A.M. (2016d). Hyperspectral measurements of yellow rust and fusarium in cereal crops: Part 2: on-line field measurement *Biosystems engineering* (Under review)
- Wilson, J.H., Zhang, C. and Kovacs, J.M., (2014). Separating crop species in northeastern Ontario using hyperspectral data. *Remote Sensing*, 6(2), pp.925-945.
- Wittry, D.J. and Mallarino, A.P., (2004). Comparison of uniform-and variable-rate phosphorus fertilization for corn–soybean rotations. *Agronomy Journal*, 96(1), pp. 26-33.
- Wold, S., Esbensen, K. and Geladi, P., 1987. Principal component analysis. *Chemometrics and intelligent laboratory systems*, 2(1-3), pp.37-52.
- Wolf, T. (2016). variable-rate-spraying. [ON-LINE] Available at: <http://sprayers101.com/variable-rate-spraying/>. [Accessed 28 November 2016]
- Wolfe, M., (1985). The current status and prospects of multiline cultivars and variety mixtures for disease resistance. *Annual review of phytopathology*, 23(1), pp. 251-273.

- Wu, D., Feng, L., Zhang, C., and He, Y., (2008). Early detection of *Botrytis cinerea* on eggplant leaves based on visible and near-infrared spectroscopy. *Transactions of the ASABE* 51 (3), pp. 1133–1139.
- Xavier, A.C., Rudorff, B.F.T., Moreira, M.A., Alvarenga, B.S., Freitas, J.G.D. and Salomon, M.V., (2006). Hyperspectral field reflectance measurements to estimate wheat grain yield and plant height. *Scientia Agricola*, 63(2), pp.130-138.
- Xin, N., Gu, X.-F., Wu, H., Hu, Y.-Z., and Yang, Z.-L. (2012). Discrimination of raw and processed *Dipsacus asperoides* by near infrared spectroscopy combined with least squares-support vector machine and random forests. *Spectrochimica Acta Part A: Molecular and Biomolecular Spectroscopy*, 89, pp. 18-24.
- Xu X.M. (2003) Effects of environmental conditions on the development of fusarium ear blight. *Eur J Plant Pathol*, 109. pp. 683–689.
- Xu, H.R., Ying, Y.B., Fu, X.P., Zhu, S.P., (2007). Near-infrared spectroscopy in detecting leaf miner damage on tomato leaf. *Biosystems Engineering* 96 (4), pp. 447–454.
- Yang ZP (1994) Breeding for resistance to *Fusarium* head blight of wheat in the mid- to lower Yangtze River Valley of China. Wheat Special Report No. 27. CIMMYT, Mexico, D.F
- Yao, H., Hruska, Z., DiCrispino, K., Brabham, K., Lewis, D., Beach, J., Brown, R.L., Cleveland, T.E., (2005). Differentiation of fungi using hyperspectral imagery for food inspection. ASAE Paper No. 053127, 2005 ASAE Annual International Meeting, Tampa, FL, 17–20 July 2005.
- Yuan, L., Pu, R., Zhang, J., Wang, J. and Yang, H. (2016). Using high spatial resolution satellite imagery for mapping powdery mildew at a regional scale. *Precision Agriculture*, 17(3): pp. 332-348.
- Yvon, M., Thébaud, G., Alary, R., Labonne, G., (2009). Specific detection and quantification of the phytopathogenic agent ‘*Candidatus Phytoplasma prunorum*’. *Molecular and Cellular Probes* 23 (5), 227–234.
- Zadoks, J.C., Chang, T.T. and Konzak, C.F., (1974). A decimal code for the growth stages of cereals. *Weed research*, 14(6), pp.415-421.
- Zhang, C., Shen, Y., Chen, J., Xiao, P., Bao, J., (2008). Nondestructive prediction of total phenolics, flavonoid contents, and antioxidant capacity of rice grain using near-infrared spectroscopy. *Journal of Agricultural and Food Chemistry* 56 (18), 8268–8272.
- Zhang, H., Hu, H. and Zhang, H. (2016). Monitoring Methods of Crop Diseases and Pests Based on Hyperspectral Technology. *International Journal of Simulation--Systems, Science and Technology*, 17(11), pp.2.1-2.5.
- Zhang, X., Xu, M., Sun, N., Xiong, W., Huang, S., and Wu, L. (2016). Modelling and predicting crop yield, soil carbon and nitrogen stocks under climate change scenarios with fertiliser management in the North China Plain. *Geoderma*, 265, pp. 176-186.
- Zhao, D., Reddy, K. R., Kakani, V. G., Read, J. J., and Koti, S. (2005). Selection of optimum reflectance ratios for estimating leaf nitrogen and chlorophyll concentrations of field-grown cotton. *Agronomy Journal*, 97, pp. 89–98.
- Zhao, J., Zhang, D., Huang, L., Zhang, Q., Liu, W. and Yang, H. (2016). Vertical features of yellow rust infestation on winter wheat using hyperspectral imaging measurements. In *Agro-Geoinformatics (Agro-Geoinformatics)*, 2016 Fifth International Conference on (pp. 1-4). IEEE.
- Zhao, Y., Bigg, G. R., Billings, S. A., Hanna, E., Sole, A. J., Wei, H., and Wilton, D. J. (2016a). Inferring the variation of climatic and glaciological contributions to West Greenland iceberg discharge in the twentieth century. *Cold Regions Science and Technology*, 121, pp. 167–178.
- Zhao, Y., Billings, S. A., Wei, H., and Sarrigiannis, P. (2012). Tracking time-varying causality and directionality of information flow using an error reduction ratio test with applications to electroencephalography data. *Physical Review E*, 86, pp. 051919.

Zhao, Y., Billings, S. A., Wei, H., He, F., and Sarrigiannis, P. G. (2013). A new NARX-based Granger linear and non-linear casual influence detection method with applications to EEG data. *Journal of Neuroscience Methods*, 212(1), pp. 79–86.

Zhao, Y., Mehnen, J., Sirikham, A., and Roy, R. (2017). A novel defect depth measurement method based on Non-linear System Identification for pulsed thermographic inspection. *Mechanical Systems and Signal Processing*, 85, pp. 382–395.

Zhong, C., Ding, Y., and Fu, J. (2011). Image Forward Motion Compensation Method for Some Aerial Reconnaissance Camera Based on Neural Network Predictive Control. *Advanced Research on Computer Science and Information Engineering*. 152 (1), pp. 237-244.

Zhou, B., Elazab, A., Bort, J., Vergara, O., Serret, M.D. and Araus, J.L. (2015). Low-cost assessment of wheat resistance to yellow rust through conventional RGB images. *Computers and Electronics in Agriculture*, 116, pp. 20-29.



## APPENDICES

### Appendix A; yield limiting factors

	Yield	NDVI
Soil properties	9.99%	10.09%
Soil properties and fusarium	28.24%	21.30%
Soil properties and yellow rust	26.80%	26.65%
Soil properties and fusarium and yellow rust	39.43%	40.26%

Figure A: NARMARX model results, for soil properties and disease, for percentage contribution to yield and NDVI.

### Appendix B; ANOVA results

	Df	Sum Sq	Mean Sq	F value	Pr(>F)	
light_h	1	1	1	2.81E+01	1.14E-07	***
light_d	1	1706	1706	6.76E+04	< 2e-16	***
camera_h	1	726	726	2.87E+04	< 2e-16	***
camera_angle	1	1037	1037	4.11E+05	< 2e-16	***
integration_time	1	1688	1688	6.69E+06	< 2e-16	***
light_h:light_d	1	587	587	2.33E+04	< 2e-16	***
light_h:camera_h	1	1	1	5.81E+01	2.48E-14	***
light_d:camera_h	1	1	1	2.63E+01	2.97E-07	***
light_h:camera_angle	1	1889	1889	7.48E+04	< 2e-16	***
light_d:camera_angle	1	477	477	1.89E+04	< 2e-16	***
camera_h:camera_angle	1	21	21	8.39E+02	< 2e-16	***
light_h:integration_time	1	30	30	1.19E+03	< 2e-16	***
light_d:integration_time	1	0	0	7.87E+00	0.00502	**
camera_h:integration_time	1	126	126	5.00E+00	< 2e-16	***

					03	16	
camera_angle:integration_time		1	893	893	3.54E+04	< 2e-16	***
light_h:light_d:camera_h		1	43	43	1.70E+03	< 2e-16	***
light_h:light_d:camera_angle		1	325	325	1.29E+04	< 2e-16	***
light_h:camera_h:camera_angle		1	50	50	1.98E+03	< 2e-16	***
light_d:camera_h:camera_angle		1	8	8	3.11E+02	< 2e-16	***
light_h:light_d:integration_time		1	87	87	3.45E+03	< 2e-16	***
light_h:camera_h:integration_time		1	10	10	3.80E+02	< 2e-16	***
light_d:camera_h:integration_time		1	0	0	4.66E+00	0.0308	*
light_h:camera_angle:integration_time		1	316	316	1.25E+04	< 2e-16	***
light_d:camera_angle:integration_time		1	120	120	4.75E+03	< 2e-16	***
camera_h:camera_angle:integration_time		1	20	20	7.92E+02	< 2e-16	***
light_h:light_d:camera_h:camera_angle		1	94	94	3.72E+03	< 2e-16	***
light_h:light_d:camera_h:integration_time		1	1	1	4.89E+01	2.69E-12	***
light_h:light_d:camera_angle:integration_time	me	1	73	73	2.89E+03	< 2e-16	***
light_h:camera_h:camera_angle:integration_time	ime	1	28	28	1.12E+03	< 2e-16	***
light_d:camera_h:camera_angle:integration_time	ime	1	14	14	5.59E+02	< 2e-16	***
light_h:light_d:camera_h:camera_angle:integration_time	rati o	1	2	2	7.14E+01	< 2e-16	***
Residuals		13892 10	3506 9	0			

Figure B: ANOVA results, considering parameters of light height and distance, integration time, camera height and angle, for optimal configurations. Showing the significance of each parameter and their interactions.

### Appendix C: Chemical labels



Figure C-1: Proline 275 chemical label part 1

**DISEASES CONTROLLED (Cont'd)**

**Barley**  
Eyespot, powdery mildew, yellow rust, brown rust, ear disease complex – *Fusarium* ear blight\* and reduction of sooty moulds, *Rhynchosporium* and net blotch

**Rye**  
Eyespot, powdery mildew, brown rust and *Rhynchosporium*

**Oats**  
Eyespot, crown rust and mildew

**Winter oilseed rape**  
Light leaf spot\*, *Phoma* leaf spot and stem canker and *Sclerotinia* stem rot.

\*Proline<sup>275</sup> will provide moderate control of these diseases

**CEREALS**

**Eyespot (*Tapesia* spp.)**  
Spray in the spring at the first sign of disease, from when the leaf sheaths begin to become erect until the 2nd node is detectable (GS 30-32).

**Septoria Leaf Blotch and Glume Blotch (*Septoria tritici* and *Stagonospora nodorum*)**

Apply before disease is established in the crop. To protect the upper leaves and ear apply Proline<sup>275</sup> at full flag leaf emergence (GS 37) up to mid-flowering (GS 65). Where disease pressure remains high application may be repeated. Applications to upper leaves where *S. tritici* symptoms are present are likely to be less effective.

Proline<sup>275</sup> contains a DMI fungicide. Resistance to some DMI fungicides has been identified in *Septoria* leaf blotch (*Mycosphaerella graminicola*) which may seriously affect the performance of some products. For further advice on resistance management in DMI's contact your agronomist or specialist advisor, and visit the FRAG-UK website.

**Powdery Mildew (*Blumeria graminis*)**

Apply Proline<sup>275</sup> at the first signs of disease. Where disease pressure remains high application may be repeated.

**Yellow Rust (*Puccinia striiformis*)**

Apply Proline<sup>275</sup> at the first signs of disease. Proline<sup>275</sup> controls yellow rust in wheat and winter barley. A second application may be made 2-3 weeks later if re-infection occurs. Applications made to established infections are likely to be less effective.

**Brown Rust**

Apply Proline<sup>275</sup> at the first signs of disease. Proline<sup>275</sup> controls brown rust in barley (*Puccinia hordei*) and rye (*P. recondita*) and will give moderate control of brown rust in wheat (*P. recondita*).

A second application may be made 2-3 weeks later if re-infection occurs. Applications made to established infections are likely to be less effective.

**Crown Rust (*Puccinia coronata*)**

Apply Proline<sup>275</sup> at the first signs of disease. Proline<sup>275</sup> controls crown rust in winter and spring oats. A second application may be made 2-3 weeks later if re-infection occurs. Applications made to established infections are likely to be less effective.

**Tan Spot (*Pyrenophora tritici-repentis*)**

Apply Proline<sup>275</sup> at the first signs of disease in spring/early summer. Proline<sup>275</sup> will give moderate control of tan spot in winter wheat. Where disease pressure remains high application may be repeated.

**Ear Disease Complex**

Apply Proline<sup>275</sup> soon after ear emergence until the end of flowering (GS 59-69) for moderate control of *Fusarium* ear blight and reduction of sooty moulds. Control of ear diseases can result in cleaner, brighter ears. Through the reduction of ear blight, Proline<sup>275</sup> effectively reduces the level of the *Fusarium* mycotoxin deoxynivalenol (DON) in wheat grain. However, where *Fusarium* levels are high, the reduction achieved may not always be sufficient to ensure that DON levels fall below the statutory limit.

**Leaf Blotch (*Rhynchosporium secalis*)**

Proline<sup>275</sup> gives high levels of *Rhynchosporium* control. Apply Proline<sup>275</sup> in spring at the first signs of disease. For severe infections a second application may be necessary 2-3 weeks later.

**Net Blotch (*Pyrenophora teres*)**

Apply Proline<sup>275</sup> at the first signs of disease in spring/early summer. For severe infections, a second application 2-3 weeks later will give most effective control when conditions remain favourable for disease development.

**WINTER OILSEED RAPE**

**Light Leaf Spot**

Apply Proline<sup>275</sup> in autumn/winter (usually late October to early December) protectively. Follow up spray(s) may be required in early spring from the onset of stem elongation, depending on disease development.

**Phoma Leaf spot/Stem Canker**

Apply Proline<sup>275</sup> in autumn at the first sign of disease. Repeat application in late autumn/winter, if disease symptoms reoccur.

**Sclerotinia stem rot (*Sclerotinia sclerotiorum*)**

Apply Proline<sup>275</sup> at early to full flower.

**Spring oilseed rape (QUALIFIED MINOR USE RECOMMENDATION)**

Proline<sup>275</sup> can also be used on varieties of spring oilseed rape but crop safety has not been fully established.

**SAFETY PRECAUTIONS**

**Operator Protection**

Engineering control of operator exposure must be used where reasonably practicable in addition to the following personal protective equipment:

WEAR SUITABLE PROTECTIVE CLOTHING (COVERALLS) AND SUITABLE PROTECTIVE GLOVES AND FACE PROTECTION (FACESHIELD) when handling the concentrate.

WEAR SUITABLE PROTECTIVE CLOTHING (COVERALLS) when applying the product

WEAR SUITABLE PROTECTIVE CLOTHING (COVERALLS) AND SUITABLE PROTECTIVE GLOVES when handling contaminated surfaces.

However, engineering controls may replace personal protective equipment if a COSHH assessment shows they provide an equal or higher standard of protection.

WHEN USING DO NOT EAT DRINK OR SMOKE.

WASH ANY CONTAMINATION from eyes immediately.

IF YOU FEEL UNWELL, seek medical advice (show label where possible).

WASH HANDS AND EXPOSED SKIN before eating and drinking and after work.

**Environmental Protection**

Do not contaminate water with the product or its container. (Do not clean application equipment near surface water. Avoid



contamination via drains from farmyards and roads). DO NOT ALLOW DIRECT SPRAY from horizontal boom sprayers to fall within 5 m of the top of the bank of a static or flowing water body.

unless a Local Environmental Risk Assessment for Pesticides (LERAP) permits a narrower buffer zone, or within 1 m of the top of a ditch which is dry at the time of application.

Aim spray away from water.

This product qualifies for inclusion within the Local Environment Risk Assessment for Pesticides (LERAP) scheme. Before each spraying operation from a horizontal boom sprayer, either a LERAP must be carried out in accordance with CRD's published guidance or the statutory buffer zone must be maintained.

The results of the LERAP must be recorded and kept available for three years.

**Storage and Disposal**

KEEP AWAY FROM FOOD, DRINK AND ANIMAL FEEDINGSTUFFS.

KEEP IN ORIGINAL CONTAINER tightly closed in a safe place.

WASH OUT CONTAINER THOROUGHLY, empty washings into spray tank and dispose of safely.

DO NOT RE-USE CONTAINER for any purpose. PROTECT FROM FROST

**RESISTANCE**

Repeated application of Proline<sup>275</sup> alone should not be used on the same crop against a high risk pathogen such as cereal powdery mildew. Tank-mixtures or alternation with fungicides having a different mode of action (e.g. morpholines) have been shown to protect against the development of resistant forms of disease. The possible development of disease strains resistant to Proline<sup>275</sup> cannot be excluded or predicted. Where such resistant strains occur, Proline<sup>275</sup> is unlikely to give satisfactory control.

Strains of light leaf spot resistant to azole fungicides are known to exist. To avoid development of resistance apply product protectively in response to disease forecasts. Where possible, when light leaf spot is present, avoid the use of azole based fungicides when targeting other diseases such as *Sclerotinia* at mid flowering stage.

**CROP SPECIFIC INFORMATION**

**Cereals**

Apply Proline<sup>275</sup> at 0.72 L/ha in 100-300 L water/ha.

Apply as a MEDIUM spray quality (as defined by BCPC). A spray pressure of 2-3 bar is recommended. Maximum total dose per crop is 1.44 L/ha for barley and oats and 2.16 L/ha for wheat and rye. Proline<sup>275</sup> may be applied at any stage before grain milky ripe stage (GS 71) in winter wheat and winter rye and up to beginning of flowering in barley and oats.

**Winter Oilseed Rape**

Apply Proline<sup>275</sup> at 0.63 L/ha in 100-300 L water/ha.

Apply as a MEDIUM spray quality (as defined by BCPC). A spray pressure of 2-3 bar is recommended. Maximum total dose per crop is 1.26 L/ha. Proline<sup>275</sup> may be applied at any stage up to a pre harvest interval of 56 days.

Apply Proline<sup>275</sup> in 100 to 300 litres of water per hectare. The higher spray volumes are recommended where the crop is dense or disease pressure / risk is high to ensure good penetration to the lower leaves and stem bases. Disease control may be compromised by reducing water volumes, where good spray coverage is difficult to achieve.

**MIXING AND SPRAYING**

Thoroughly shake the pack before use. Add the required quantity of Proline<sup>275</sup> to the half-filled spray tank with the agitation system in operation and then fill to the required level. Continue agitation at all times during spraying and stoppages until the tank is completely empty. Spray immediately after mixing. Sprayers should be thoroughly cleaned before use, and filters and jets checked for damage and blockages. Boom height should be adjusted to ensure even coverage of the crop, particularly at later growth stages. The correct height is one at which the spray from alternate nozzles meets just above the crop. In dense crops, at later growth stages, higher water volumes should be used. Spray equipment should be thoroughly cleaned with detergent after use.

© Proline is a registered Trade Mark of Bayer  
© Bayer CropScience 2016

Figure C-2: Proline 275 chemical label part 2

# Adexar®



**MAPP 17109**

An emulsifiable concentrate containing 62.5 g/litre (6% w/w) epoxiconazole and 62.5 g/litre (6% w/w) fluxapyroxad. A systemic fungicide for use in winter wheat, spring wheat, durum wheat, winter barley, spring barley, triticale, rye and oats.

The (COSHH) Control of Substances Hazardous to Health Regulations may apply to the use of this product at work.

**SAFETY PRECAUTIONS**

**Operator protection**

Engineering control of operator exposure must be used where reasonably practicable in addition to the following personal protective equipment:

WEAR SUITABLE PROTECTIVE CLOTHING (COVERALLS), SUITABLE PROTECTIVE GLOVES AND FACE PROTECTION (FACESHIELD) when handling the concentrate. WEAR SUITABLE PROTECTIVE CLOTHING (COVERALLS) AND SUITABLE PROTECTIVE GLOVES when handling contaminated surfaces.

WEAR SUITABLE PROTECTIVE CLOTHING (COVERALLS) during application. However, engineering controls may replace personal protective equipment if a COSHH assessment shows they provide an equal or higher standard of protection.

WHEN USING DO NOT EAT, DRINK OR SMOKE. WASH HANDS AND EXPOSED SKIN before meals and after work.

**Environmental protection**

Do not contaminate water with the product or its container. Do not clean application equipment near surface water. Avoid contamination via drains from farmyards and roads.

To protect aquatic organisms respect an unsprayed buffer zone to surface water bodies in line with LERAP requirements.

DO NOT ALLOW DIRECT SPRAY from horizontal boom sprayers to fall within 5m of the top of the bank of a static or flowing waterbody, unless a Local Environment Risk Assessment for Pesticides (LERAP) permits a narrower buffer zone, or within 1m of the top of a ditch which is dry at the time of application. Aim spray away from water.

This product qualifies for inclusion within the Local Environment Risk Assessment for Pesticides (LERAP) scheme. Before each spraying operation from a horizontal boom sprayer, either a LERAP must be carried out in accordance with CRD's published guidance or the statutory buffer zone must be maintained. The results of the LERAP must be recorded and kept available for inspection for three years.

**Storage and disposal**

KEEP AWAY FROM FOOD, DRINK AND ANIMAL FEEDINGSTUFFS. KEEP OUT OF REACH OF CHILDREN. RINSE CONTAINER THOROUGHLY by using an integrated pressure rinsing device or manually rinsing three times. Add washings to sprayer at time of filling and dispose of safely. Store in a suitable pesticide store. Keep dry and protect from frost.

**10 Le**

This label is compliant with the CPA Voluntary Initiative Guidance

Supplied by:  
BASF plc  
Crop Protection  
PO Box 4, Earl Road  
Cheadle Hulme, CHEADLE  
Cheshire SK8 6QG  
Tel: 0161 485 6222  
Emergency Information:  
(24 hours freephone):  
0049 180 2273112  
Technical Enquiries:  
0845 602 2553 (office hours)



We create chemistry

® = Registered trademark of BASF

Figure C-3: Adexar chemical label part 1

# Adexar®

An emulsifiable concentrate containing 62.5 g/litre (6% w/w) epoxiconazole and 62.5 g/litre (6% w/w) fluxapyroxad. Contains propanoic acid, 2-hydroxy-, 2-ethylhexyl ester, (2S)-. May cause an allergic reaction.

**DANGER:**  
**HARMFUL IF SWALLOWED**  
**MAY CAUSE AN ALLERGIC SKIN REACTION.**  
**CAUSES SERIOUS EYE IRRITATION.**  
**SUSPECTED OF CAUSING CANCER.**  
**MAY DAMAGE THE UNBORN CHILD.**  
**SUSPECTED OF DAMAGING FERTILITY.**  
**VERY TOXIC TO AQUATIC LIFE WITH LONG LASTING EFFECTS.**

AVOID BREATHING MIST.  
WEAR PROTECTIVE GLOVES/PROTECTIVE CLOTHING/  
EYE PROTECTION/FACE PROTECTION.  
IF ON SKIN: WASH WITH PLENTY OF SOAP AND WATER.  
IF IN EYES: RINSE CAUTIOUSLY WITH WATER FOR SEVERAL MINUTES.  
REMOVE CONTACT LENSES, IF PRESENT AND EASY TO DO.  
CONTINUE RINSING.  
STORE LOCKED UP.  
DISPOSE OF CONTENTS/CONTAINER TO A LICENSED HAZARDOUS-WASTE  
DISPOSAL CONTRACTOR OR COLLECTION SITE EXCEPT FOR EMPTY CLEAN  
CONTAINERS WHICH CAN BE DISPOSED OF AS NON-HAZARDOUS WASTE.

To avoid risks to human health and the environment, comply with the instructions for use



This product is approved under the Plant Protection Products Regulation (EC) No 1107/2009

## IMPORTANT INFORMATION

FOR USE ONLY AS AN AGRICULTURAL FUNGICIDE, as directed below:

Crops	Maximum individual dose	Maximum number of treatments	Latest time of application
Winter and spring wheat, Rye, Triticale Durum wheat	2.0 litres product per hectare	2 per crop	Up to and including flowering (anthesis) just complete (GS 69)
Winter and spring Barley, Oats	2.0 litres product per hectare	2 per crop	Up to and including emergence of ear just complete (GS 59)

READ THE LABEL BEFORE USE. USING THIS PRODUCT IN A MANNER THAT IS INCONSISTENT WITH THE LABEL MAY BE AN OFFENCE. FOLLOW THE CODE OF PRACTICE FOR USING PLANT PROTECTION PRODUCTS.

Figure C-4: Adexar chemical label part 2

# Appendix D: Example of agronomists notes


H Meskell and Sons		Recommendation Plan 01020 Wheat T2 (Wilestead) Issued: 14/05/2015			Advisor: David Parish Basis / Facts: R/E:1298 F:00538 Telephone: 01234 825732 Mobile: 07702 721508 Email: david.parish@nlab.com		TAG 				
<b>Job 1</b>		Total job area: 18.4000 ha									
<i>Reason: T2 (flag leaf) fungicide. Late season Growth Regulator, low dose. Wild Oats esp for end. Occasional cleaver. Manganese and Magnesium. Comment: Apply when flag leaf is fully emerged, ie from now on. Apply before the ear starts splitting from the boot. Apply to a dry(flag) leaf, needs 1-2 hours dry.</i>											
<b>Fields</b>	Job 1	Share Rtd	Area ha	Crop	Variety	Growth Stage	LERAP	Watercourse			
Cotton End 46ac		1840.000	18.4000	Winter: Wheat	Winter: Wheat	39: Flag Leaf fully emerged, ligule visible	None				
<b>Products</b>	Job 1							Application rate: 100 L			
Earliest application: 01/03/2015, Earliest growth stage: 37; Flag leaf visible-rolled. Latest growth stage: 39; Flag Leaf fully emerged, ligule visible. Spray quality: Medium, LERAP star rating: Standard											
		Rate / ha	Required	Units	% Rate	LERAP	Total Used				
Adexar	MAPP:15474 At:Epoconazole 0.25%, Fluxapyroxad 0.25% Expires:05/10/2016	1.339	24.643	L	67	B	26.6 L				
Joules	MAPP:15730 At:Chlorothalonil 50.00% Expires:30/04/2020	1.004	18.482	L	50	B	18.4 L				
Hurler	MAPP:13458 At:Furoxypyr 20.00% Expires:30/06/2024	0.558	10.268	L	28		10.2 L				
Padawan	MAPP:15577 At:2-chloroethylphosphonic acid 48.00% Expires:31/01/2020	0.335	6.161	L	45		6 L				
Axial	MAPP:12521 At:Pinoxaden 10.00% Expires:30/11/2017	0.353	6.500	L	79		6.5 L				
Adigor		0.543	10.000	L			10 L				
Manganese Liquid (15%Mn)		1.566	28.816	L			28.8 L				
Magnesium Liquid eg Headland Promise		0.668	12.312	L			12.3 L				
<b>Operator Records</b>	Job 1	Area ha	Date	Start	Finish	Wind Speed	Direction	Weather	Temp °C	Operator	Buffer Zone (m)
Cotton End 46ac		18.4	15.5.15	pm	pm	14 kph	N/E	Cloudy	11	Parish	

Figure D: Example of Agronomy notes for the T2 application